



POLITECNICO
MILANO 1863

Doctoral Dissertation

A Periodic Design: σ -Hole Interactions at Work



PhD Student: Andrea Daolio, XXXIVth cycle

Supervisor: Prof. Cav. Giuseppe Resnati

Co-Supervisor: Dr. Andrea Pizzi

Tutor: Prof. Francesco Gilberto Gatti

On the Cover:

Green Lion devouring the Sun (colorized)

- *Rosarium Philosophorum Sive Pretiosissimum Donum Dei* (1550).

“The highest inspiration for any scholar should be the observation and the reproduction of everything Nature does.”

“What is Nature?”

“Everything that is invisible, and yet works visibly.”

- Paracelsus, hermetical writings

Table of Content:

<u>I. Abstract</u>	1
<u>II. Scope of the Research</u>	3
<u>III. Glossary and Graphical Representation</u>	4
<u>1. Introduction</u>	5
1.1. Supramolecular Chemistry: from Molecules to Materials	5
1.2. σ-Holes are a deficiency of electron density	8
1.3. The σ-Hole Family in action	13
1.4. Computational and Experimental Methods	20
References.....	24
<u>2. The Halogen Bond at Work</u>	30
2.1. Uncommon adducts between iodoperfluoroalkanes and a fluoride anion	31
References.....	41
<u>3. The Chalcogen Bond at Work</u>	43
3.1. Benzisothiazolinones as Chalcogen Bond Donors and their Structure-Functions Relationship	44
3.2. Chalcogen Bond Drives the Packing of Cyanine Crystals	54
References.....	66
<u>4. The Tetrel Bond at work</u>	69
4.1. Methonium salts as methyl-Tetrel Bond donors	70
4.2. Bis(pyridinium)methylene Salts as $-C(sp^3)H_2$-Tetrel Bond Donors	84
4.3. Chalcogen and Tetrel Bonds in Choline and Betaine derivatives	91
References.....	100
<u>5. Beyond the p-block</u>	103
5.1. Tetrachloridoaurate as an Effective Anion...Anion Coinage Bond Donor	104
5.2. Group 8 elements as electrophilic sites: The formation of osme bonded adducts	113
References.....	123
<u>6. Experimental</u>	126
<u>7. Conclusions</u>	211
7.1. Acknowledgments	213
7.2. List Of Publications	214

Declaration of Academic Achievements

The research described in this thesis is the result of the collaborative effort of students in G. Resnati group, staff, and occasional external collaborators. The contribution of the following co-workers is described:

GR – Giuseppe Resnati, full Professor at Politecnico di Milano.

GT – Giancarlo Terraneo, full Professor at Politecnico di Milano.

PP – Peter Politzer, full professor at University of New Orleans.

JM – Jane Murray, full professor at University of New Orleans.

AF – Antonio Frontera, full Professor at Universidad de las Islas Baleares.

AG – Alessandro Genoni, full Professor at University of Lorraine.

FV – Fiorenza Viani, Researcher of CNR (Consiglio Nazionale delle Ricerche).

TP – Tullio Pilati, former Researcher of Politecnico di Milano and CNR.

ND – Nicola Demitri, researcher at Elettra Synchrotron, Trieste.

SN - Susantha Nayak, former PhD student at Politecnico di Milano.

SB – Simone Bordignon, postdoctoral fellow at University of Torino.

EW – Erna Wieduwilt, postdoctoral fellow at University of Lorraine.

AP – Andrea Pizzi, postdoctoral fellow at Politecnico di Milano (RTDa).

AD – Andrea Daolio, PhD student at Politecnico di Milano author of this thesis.

MC – Miriam Calabrese, PhD student at Politecnico di Milano.

MU – Maurizio Ursini, laboratory technician at Politecnico di Milano.

CG – Christian Grassi, undergraduate student at Politecnico di Milano.

I. Abstract.

Non-covalent interactions play a major role in all recognition and self-assembly phenomena. They are thus central in supramolecular chemistry and nanotechnologies and impact fields as diverse as catalysis, biology, drug design and materials chemistry. It may be considered that the IUPAC definition of halogen bond in 2013, in rapid sequence after the IUPAC definition of the hydrogen bond in 2011, represented a milestone for noncovalent interactions development. It paved the way for the understanding and rationalization of a large number of inter- and intra-molecular forces. It was soon discovered, in fact, that halogens were not alone in the periodic table in establishing attractive interactions with nucleophiles due to the anisotropic distribution of the electron density in bonded atoms. Many other groups of the periodic table rapidly joined the “ σ -hole family”. As of 2021, the chalcogen bond too received an IUPAC definition, while noble gas bond, pnictogen bond, tetrel bond and triel bond are routinely used terms to designate interactions involving atoms of the remaining groups of the *p*-block. Lately, even some evidence highlighting the role of σ -holes in transition metal compounds are being reported.

The understanding of interactions as the result of the polarization of particular atomic species and the subsequent formation of localized areas of positive electrostatic potential on the extension of covalent bonds has come a long way too. This phenomenon was known for more than a century for hydrogen atoms, but its use for explaining the noncovalent adducts where halogen atoms attractively interact with donors of electron density (a phenomenon first reported early nineteenth century) began just thirty years ago with the studies of Peter Politzer. Once the concept of halogen bond (and σ -hole) had been established and sufficiently developed, it was recognised that group 17 was not alone in showing that behaviour, as it was found that several other atomic species show the same features. After 2010, the interest in the field grew rapidly and the geometric and energetic characteristics of the noncovalent adducts wherein the atoms of the *p*-block were acting as electrophiles was examined, clarified, and exploited. Halogen and chalcogen bond in particular have now found relevant applications in medicinal chemistry and catalysis in the same fashion of the hydrogen bond in previous years, while known natural and industrial phenomena are being “rediscovered” under the new light of σ -hole interactions. The body of work of this doctorate thesis is part of this field of study.

Namely, some adducts formed between iodoperfluoroalkanes and naked fluoride anions provides compelling evidence of the importance of effective crystal engineering design strategies to obtain uncommon halogen bonded adducts. This is an example of the ability of such interaction to impact crystal formation.

A portion of this thesis analyses some supramolecular synthons based on chalcogen bond that control the crystal packing of various benzothiazole derivatives. The ability of the synthons to affect the crystalline habits of these compounds will be considered in detail and their presence in biologically relevant systems will be examined. Specifically, the focus will be on benzoisothiazolinones and cyanines engaging concurrently in chalcogen and hydrogen bonds. The possibility to tune the interaction strength by slightly modifying the molecular scaffold, for example substituting the chalcogen atom (sulphur for selenium), is also examined.

It is known that smaller and less polarizable atoms are less prone to engage in σ -hole interactions than bigger and softer ones. Nonetheless, the ubiquitous presence of carbon in biomolecules poses the question if tetrel bond may be a factor impacting some key bioprocesses. Our work on model systems like hexamethonium and bis-pyridinium methylene provides convincing evidence of the potential of the weak tetrel bond formed by carbon to play a role in the self-assembly of crystalline adducts. The geometrical features for the distinction between tetrel bond and hydrogen bonds are discussed for both methyl ($-\text{CH}_3$) and methylene ($-\text{CH}_2-$) moieties. Thanks to a rigorous computational approach and Hirschfeld Atom Refinement (HAR) method, general geometrical distinction for the study of these moieties are provided.

The knowledge gained through the study of chalcogen and tetrel bonds is employed to analyse the interaction landscape of some biomolecules, e.g., choline derivatives. The obtained information may be helpful in understanding the biochemistry of these compounds.

The last portion of this thesis investigates the formation of σ -hole interactions by elements of the d-block of the periodic table. Specifically, the last chapter of this thesis assesses the presence of localized areas of positive electrostatic potential on the back end of various polarized bonds involving elements of the group 8 and group 11. The possibility of such areas to engage in the formation of stable noncovalent adducts is also shown. To identify the presence of σ -holes at the surface of d-block elements and to prove the ability of these holes to affect or control the attractive interactions formed by these elements may have far-reaching impacts. It may help in understanding and tuning the functional properties of the derivatives of these elements, one for all in optimizing their catalytic properties.

II. Aims of the Research.

The scope of this research is the following:

- To understand the ability of some atoms of the *p*-block of the periodic table (i.e., I, S, Se, C) to act as electrophilic sites and to attractively interact with electron rich atoms (nucleophiles).
- To extend the set of known atomic species able to engage in σ -hole interactions to some of the d-block transition metals.
- To identify the organic moieties (tectons) tailored to the formation of the pursued interactions (i.e., halogen bond, chalcogen bond, tetrel bond, coinage bond, osme bond) and to investigate the ability of said tectons to be used as tools in crystal engineering for the formation of 1D, 2D and 3D crystalline architectures.
- To highlight the key geometrical features of the formed interactions in the solid.
- To explore the role of the aforementioned interactions in solution.
- To study the cooperative and competitive actions of those interactions and their relative strength.

Several tools have been employed to pursue to scopes listed above. Surveys of the Cambridge Structural Database (CSD) - and more rarely of the Protein Data Bank (PDB) - are first employed to obtain indications on the tectons preferentially involved in the considered interactions and on the preferred geometrical features of the interactions in the solid. Obtained information instruct the design of the tectons which are then synthesized if not commercially available. Tectons self-assembly is then obtained through crystallization from solution. Whenever possible, the formed adducts are studied via single crystal X-ray analyses to assess the presence of σ -hole interactions and to establish their geometrical features. Adducts characterisation is complemented by spectroscopic investigations (e.g., IR and NMR (^1H , ^{13}C , ^{15}N)). Computational analyses were often employed in collaboration with other research groups; this allowed for gaining additional understanding of the nature of the interactions taking place in the solid state. Among the large and ever-expanding list of suitable computational tools, Quantum Theory of Atoms In Molecules (QTAIM) analysis and Noncovalent Interaction Index (NCIplot) were often the preferred ones. In order to obtain a better resolution of the position of the hydrogen atoms in X-Ray structures, Hirschfeld atom refinement (HAR) was employed in place of the widely used Independent Atom Model (IAM).

1. Introduction.

“[...] one might assert that the chemistry of the last century was largely the chemistry of covalent bonding, whereas that of the present century is more likely to be the chemistry of noncovalent binding.”

- H.-J. Schneider

1.1. Supramolecular Chemistry: from Molecules to Materials.

Supramolecular chemistry deals with the study of processes involving a distinct number of molecules, including host-guest interactions^[1], self-assembly processes^[2,3] and biological molecular recognition^[4]. This concept has offered many advantages in several and different fields, among the crystal engineering^[5], material's design^[6] and stimuli responsive devices^[7]. At the same time, supramolecular chemistry deepens our understanding of the principles governing the lock-and-key processes of enzymes^[8], pharmacological action of drugs^[9] and even chemical catalysis^[10]. The understanding of the relationships between distinct molecular entities, i.e., noncovalent interactions, has given a major contribution to supramolecular chemistry. Noncovalent interactions are often described as molecular forces between molecules wherein the sharing of electrons does not result in the formation of a covalent or coordination bond^[11]. In the last fifty years, chemists identified many different interactions between molecules, the most well-known being hydrogen bonds^[12] (known for more than a century) and π - π interaction^[13]. In recent years, the attention in noncovalent interactions grew substantially. A big number of supramolecular forces have been identified, analysed in their fundamental properties and exploited for the design of all sorts of devices. Between them, we cite: metallophilic interactions^[14], cation-^[15] and anion- π interactions^[16], σ -^[17] and π -hole^[18] interactions (Figure 1.1.1). “Dissecting the ways in which different molecular entities relate to each other, our understanding reached a point where we can see supramolecular chemistry as a sort of chemical sociology” (J.M. Lehn,^[19]).

The analysis of crystal structures is often performed through the study of intermolecular interactions and their repetitive structural units, typically small in size and composed by specific molecular functionalities, arranged in rational and periodic ways in the crystalline lattice^[20]. The identification of said arrangements, often dubbed supramolecular synthons, is particularly important as they are often associated with packing features^[21]. Schematically speaking, molecules often aggregate in supramolecular synthons, which in turn aggregate in crystalline structures (Figure 1.1.2).

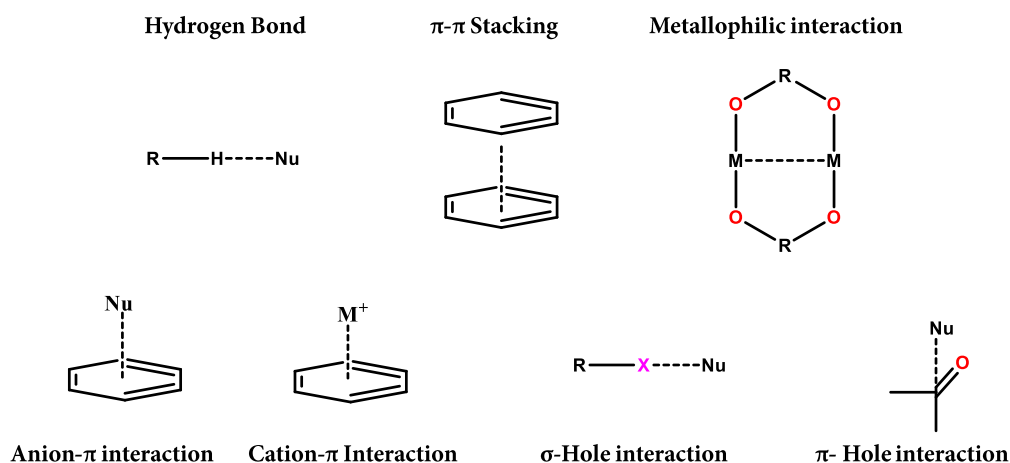


Figure 1.1.1. Some of the noncovalent interactions identified in the past years. A dashed line represents the interaction. The name of the interaction is reported near the scheme.

Resorting to a parallel between supramolecular chemistry and architecture, intermolecular interactions can be considered the mortar enabling the assembly of the bricks, namely the molecular entities, to form the supramolecular systems and the crystal packings. Since the establishment of the heuristic principle of close packing^[22], describing how molecules will tend to fill space in the most efficient way and engaging in the highest number of favourable noncovalent interactions, it was possible to design periodic systems on the basis of the interactions that the building blocks establish with each other. The occurring interactions are directly related to the shape of the molecules and the nature of

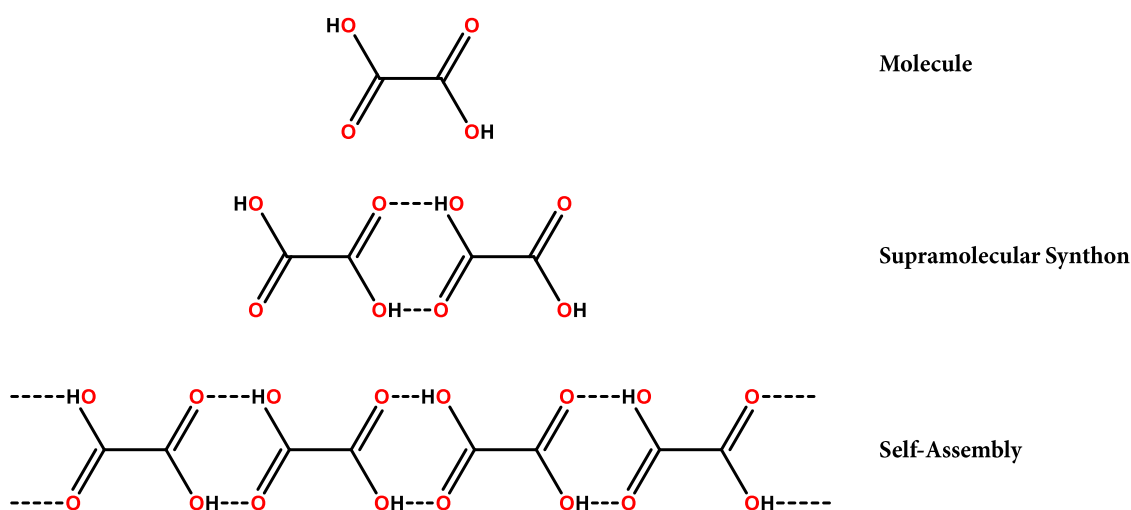


Figure 1.1.2. From molecules to self-assembly. The bottom-up approach governing supramolecular assembly is exemplified by the hydrogen bond driven self-assembly of oxalic acid.

the atoms that compose them, the molecules to be used for the assembly of supramolecular systems can be studied on the basis of their structure-function relationship, borrowing concepts from the biochemical world^[23].

The materials research of the 20th century was largely based on metals, metal oxides, and polymers and depended mostly on a 'top down' approach for the fabrication of devices^[24]. The alternative 'bottom up' approach began to be considered and used towards the end of the century when molecular materials entered the centre stage with the ultimate goal of building functional materials by controlling through design the properties associated with the component molecules and the properties resulting from their assembly^[25-27]. This shift in approaching material's development has brought to many advantages in the field, expanding the material engineering area to a cross-disciplinary field bridging together chemistry, physics, and biology. The huge number of synthetic methods now available makes possible to finely tune the molecular diversity and the resulting noncovalent interactions pattern in a material^[28]. The resulting forces can be so robust to dictate the assembly of the building blocks in highly specific conformation and geometries^[29] or be flexible enough to afford reversible and variable functional diversity^[30]. Design principles are available to control the arrangement of the molecular building blocks and synthons in the solid state, in principle it is also possible to control the properties of the resulting material^[31].

This approach has come a long way from its basic postulates. From the design of inclusion compounds like clathrates and cavities^[32], the attention has shifted to host-guest structures like cyclodextrins^[33] and calixarenes^[34] up to dendrimers^[35] and even liquid systems retaining the properties of their building blocks (like liquid crystals^[36]). One of the most interesting developments of this approach resulted in the design of molecular machines. These supramolecular systems are able to perform mechanical operations once subjected to an external stimulus such as the action of visible light^[37], usually making good use of the competitive action of two (or more) different noncovalent interactions between a mobile acceptor and different static (docking stations) donors. From their basic concepts like rotaxanes and catenanes^[38] to much more top-notch devices such as self-healing materials^[39], the design of the mentioned systems has received much attention in recent years, with its climax in the Nobel Prize Medal to J.F. Stoddart, J.-P. Sauvage and B. Feringa in 2016, for the development of molecular machines.

"When I was a student, I learned how molecules work, it is just incredible that nowadays I am able to see them dance" a dear Professor told to me after one of his lectures during my first year in academia, ultimately making me fall in love with the subject.

1.2. σ -Holes are a Deficiency of Electron Density.

The name σ -hole denotes areas of depleted electron density, frequently having a positive electrostatic potential, which are located on the back end of covalent bonds. Their origin and features will be discussed in this section. σ -Holes can serve as the binding site for a family of attractive interactions, named σ -hole interactions; formed with areas of excess electron density, frequently areas of negative electrostatic potential. Figure 1.2.1 gives a pictorial representation of the first and probably most studies of these interactions, the halogen bond.

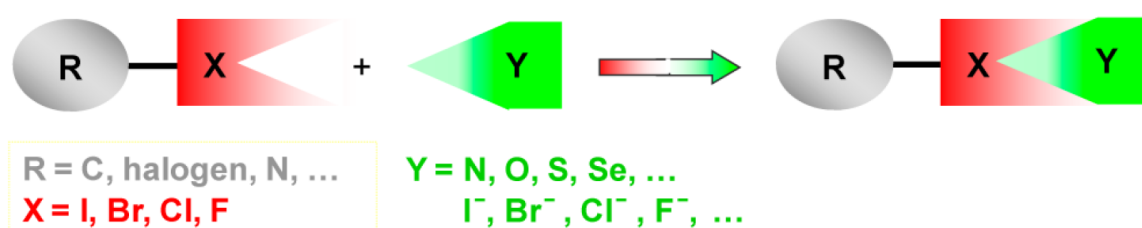


Figure 1.2.1. Schematic representation of the geometrical features of a HaB. Reprinted from *Chem. Rev.* 2016, 116, 2478–2601.

The ability of iodine and other halogens to form adducts in the liquid and solid phase was first reported in the XIXth century, when a I₂...NH₃ complex, now understood as an halogen bonded adduct^[40], was prepared in J. L. Gay-Lussac's laboratory by his colleague J. J. Colin^[41]. However, much like the ionic liquids and other phenomena and systems now of great interest, these kind of adducts have long received little attention. Two were the main concepts - introduced during the XXth century - that paved the way to the concepts of σ -hole and σ -hole interactions. First, the work of H.A. Benesi, J.H. Hildebrand and, later, R. Mulliken^[42] rationalizing the nature of many different adducts and introducing the concept of donor-acceptor complexes. Second, the work of P. Politzer on the electron density distribution of isolated molecules and its effect on molecular properties when, in the late '80s, he was working for the U.S. Army Research Office on analogues of the warfare agent Sarin^[43] and identified the key of the strong activity of the compound in the polarization of the P–F bond. During the '90s^[44] to early 2000s, Politzer developed this understanding based on polarization into concept of σ -hole, whose basis can be summarized as follows.

The electronic density $\rho(r)$ of a system of nuclei and electrons is the number of electrons in an infinitesimal volume dr at the point r . Given the rapid motion of electrons, $\rho(r)$ is commonly addressed as the average electronic density at the point r . The (molecular) electrostatic potential, instead, is related to Coulomb's law. Any point charge

Q_a generates an electrostatic potential in the surrounding space. At the distance R , the value of the electrostatic potential is $V_{(R)} = Q_a/R$ (Eq. 1.2.1) and the interacting energy between two charges is $\Delta E = Q_a Q_b / R$ (Eq. 1.2.2).

The electron density distribution around isolated atoms is anisotropic. This is a consequence of the position and orientation of atomic orbitals, the leading cause of localization of the electron density around atoms. Additionally, the fixed nucleus will have a stronger effect than the disperse electrons, so the electrostatic potential will be always positive.

In molecules, even more clearly, it is possible to see areas of depleted and increased electrostatic potential (Eq. 1.2.3.). This can be proven experimentally, via diffraction studies^[45,46], or computationally, in both cases by measuring the electron density in the surroundings of the molecules^[47]. The electrostatic potential will then display positive and negative areas that can be related to the chemical and physical properties of the molecules.

$$V(\mathbf{r}) = \sum_A \frac{Z_A}{|\mathbf{R}_A - \mathbf{r}|} - \int \frac{\rho(\mathbf{r}') d\mathbf{r}'}{|\mathbf{r}' - \mathbf{r}|}$$

Equation 1.2.3.

The molecular electrostatic potential is a physical observable that can be calculated experimentally, which makes all the following considerations somewhat easier than invoking the concept of molecular orbitals. It is nevertheless routinely computed *in silico*.

In this calculation, nuclei and electrons can be approximated as point charges and, according to the Born-Oppenheimer principle^[48], the nuclei are considered at a fixed position. In place of the moving electrons, the average electron density $\rho(\mathbf{r})$ is introduced. In Equation 1.2.3, Z_A is the charge of the nucleus A , in position \mathbf{R}_A . The denominator is, basically, the distance between the nucleus A and the point \mathbf{r} where the potential is calculated. Molecular electrostatic potential $V_{(r)}$ results from the difference between the electrostatic potential of the positive nuclei and the potential of the infinitesimal volumes dominated by the negative moving electrons, each with electronic charge $\rho(\mathbf{r}') d\mathbf{r}'$.

This approach is in strong accordance with some important theoretical concepts, among them the Hellmann-Feynman theorem^[49]. It states that, once the position of every particle of the system has been defined using the Schrödinger equation^[50] (i.e. the exact value of the electron density has been calculated) every force can be derived from classical electrodynamic concepts.

Politzer assumed to calculate $V_{(r)}$ on the molecular surface, taken at a distance from the nucleus where $\rho(r)$ is 0.001 atomic units (au, e^-/a_0^3); unless stated otherwise, this will not change in all the other proposed calculations of this dissertation and will be designated as $V_{s(r)}$. It has been demonstrated that the molecular surface encompasses most of the electronic density of any given molecules and it often lies beyond the van der Waals radius of the atoms, so it is a convenient way to evaluate noncovalent interactions.

Before considering specific examples, it is important to state that the role of polarization is usually neglected in these calculations but it plays an important role in real, experimental works^[51]. Namely, when two molecules approach each other (for example engaging in noncovalent interactions) their charge distribution undergoes some polarization as a reciprocal answer to the electrostatic potential of the other. Polarization is an intrinsic, stabilizing property of molecules and makes possible interactions that may seem sometimes prohibited.

As already stated, the electrostatic potential is positive everywhere for every spherical atomic entity^[52] but when atoms are aggregate into molecules region of lower and higher electrostatic potential appear^[53]. The calculation of $V_{s(r)}$ for CF_4 results in a surface that is almost completely negative. Replacing one of the fluorines for a chlorine atom and calculating the $V_{s(r)}$ of CF_3Cl , it is possible to see a small positive region on the extension of the C–Cl covalent bond, located on the surface of Cl, and a belt of negative potential orthogonal to the positive area^[54]. The same analysis can be also made for CF_3Br and CF_3I , that display stronger and even stronger positive regions (Figure 1.2.2). The origin of these regions, the so called σ -holes, can be found in the depletion of the electron density of the heavier (hence more polarizable) halogen atoms induced by the formation of the covalent (σ) bond. σ -Holes, when positively charged, can be approached by other nucleophiles establishing net attractive interactions visible in all states of matter. σ -Hole interactions can also be seen as $n \rightarrow \sigma^*$ interactions.

It needs to be pointed out that the same analysis performed on CH_3Cl , CH_3Br and CH_3I does not bring the same results, since these molecules display much weaker, if any, region of positive potential^[55]. This bring us the first common feature of σ -holes: the effect of substituents on the molecular backbone is of pivotal importance^[56]. The electron withdrawing effect of the fluorines on the molecular electrostatic potential in the aforementioned example plays a huge role in determining the extension of the σ -hole and its electrostatic potential. The σ -hole location brings to another key feature, i.e., directionality^[57]. σ -Hole interactions are usually particularly directional, much more than the HB. Since an electron rich molecule attractively interacts with a positive σ -hole but not with the negative belt around the σ -hole, this often results in Y–Ha...Nu angles very close to linearity with short (hence strong) interactions being much more linear than long (hence weak) ones. When Nu are lone-pair possessing molecules such as pyridines or carbonyls, the nucleophile is often positioned in such a way that its lone pair is directed

towards the σ -hole^[58,59]. The same can be said for π systems such as triple bonds or benzene rings, where the π electrons often face in the same direction^[60,61].

Both computational^[62] and experimental^[63] works proved that the atomic radius of monovalent halogen atoms opposite to the covalent bond is smaller than the one of isolated halogens, as a consequence of the depleted electron density along the bond axis; this effect is named polar flattening.

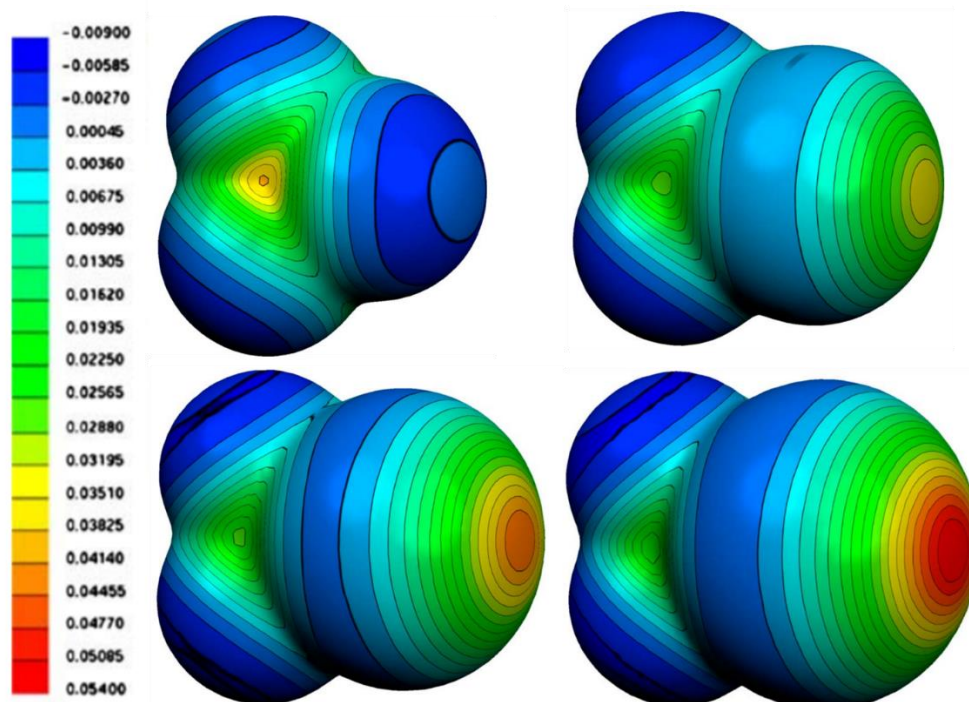


Figure 1.2.2. Molecular electrostatic potential calculated over the 0.001 au surface of CF_4 (upper left), CF_3Cl (upper right), CF_3Br (lower left) and CF_3I (lower right). Reproduced with slight modifications from *J. Mol. Model.* (2007) 13, 291–296. Correspondence between colours and potential intensities given by the leftmost scale.

σ -Holes become more extended and their electrostatic potential more positive moving from chlorine to iodine^[64]. Hence the “strength” of the σ -hole grows with the polarizability of the atom involved and decreases with its electronegativity^[65,66]. For this reason, iodine-based σ -holes are often stronger than bromine-based σ -holes, which in turn are stronger than chlorine ones. Fluorine is the halogen that displays the weakest interactions, and for long has been assumed, due to its high electronegativity, that was not possible for F to behave as a σ -hole donor. However, evidences of the ability of fluorine to develop a positive σ -hole when bound to high electronegative moieties in compounds like $\text{CF}_3\text{C}(\text{O})\text{OF}$ has been proven and the generality of the σ -hole theory confirmed^[67].

The strength of an interaction can be thus easily tuned by design, selecting the donor atom and the nature of the substituents in the surrounding of the molecule^[68,69]. Another possible strategy when working with halo-organic derivatives is changing the hybridization of the carbon atom directly bound to the halogen. The greater the s character of the carbon in the C–halogen bond, the greater is the electron withdrawing ability of carbon and the more extended and positive is the σ -hole on the halogen (as confirmed experimentally^[51] and computationally^[70,71]).

The most commonly used strategy to enhance the “strength” of a σ -hole is to substitute parts of the molecular backbone of the donor with strong electron attracting moieties, fluorine atoms and cyano groups being the most common^[72,73]. These and any other possible modification of the σ -hole strength can translate into the tunability of the interaction strength for possible applications in crystal engineering, material’s design, and biological applications making this feature of paramount importance for practical applications. Two other worth mentioning features of σ -hole interactions are their intrinsic lipophilicity^[74–76] (at least in comparison with the HB) and the higher sensibility, in respect to HB, to steric hindrance^[77], this being a consequence of the higher dimension of halogens with respect to hydrogen.

1.3. The σ -Hole Family in Action.

Halogen atoms are often considered donors of electron density. Their ability to function as electron density donors (nucleophiles) is well understood and commonly accepted. Its role in chemical reactivity is well-established but it is also known (since the 1920s) that halocarbons can establish attractive noncovalent interactions with hydrogens, alkali metal cations and other electron-poor organic moieties^[78]. But as discussed above, the electron density of halogens is anisotropically distributed, in particular when they establish covalent bonds with highly electron-attractive moieties^[79]. When the anisotropy is sufficiently pronounced, the area of depleted electron density can be positive, being able, in turn, to engage in net attractive interactions with nucleophiles and electron-rich moieties. Weak forces where the halogen atoms engage in interactions with nucleophiles have been dubbed halogen bonds (HaB). The general ability of halogen atoms to work as acceptors of electron density has been recognized and systematically exploited in the nineteen nineties^[80]. Since then a major interest in crystal engineering^[81] spawned and the HaB is now employed as a common tool in supramolecular chemistry. The IUPAC definition of HaB states “A halogen bond occurs when there is evidence of a net attractive interaction between an electrophilic region associated with a halogen atom in a molecular entity and a nucleophilic region in another, or the same, molecular entity”^[82].

Applications to the most diverse fields of science are now common. One of the first interesting report on useful HaB applications dates back to 1999, when G. Resnati and P. Metrangolo reported the ability of (-)-sparteine hydrobromide to resolve the racemic mixture of 1,2-dibromohexafluoropropane, via the formation of a crystalline complex between enantiopure sparteine and one single dibromoperfluoropropane enantiomer^[83]. This was just the first of a long series of adducts, inclusion compounds, and porous systems exploiting the HaB to build robust, often reversible, 3D frameworks for capturing specific molecules and electron rich moieties. Particular attention was given to compounds for anion capture and separation^[84,85], used also for as stationary phases in separation techniques^[86-88]. Halogen bonded adducts have been obtained also via mechanochemical techniques^[89-91] and enabled solid-state reactions^[92]. Less common but equally intriguing are the findings linking the presence of an HaB to the properties of soft materials like gel^[93] and liquid systems^[94,95] that highlight the dynamic nature of the interaction. Many groups also focused on the exploitation of the interaction in organic catalysis^[96].

The HaB has been proven useful in two of the most interesting fields of supramolecular chemistry, functional materials and pharmaceuticals. For the former we report important progresses made in the field of optoelectronics^[97], conductive light-emitting materials^[98-100] and magnetic materials^[101,102]. For the latter, an extensive

literature is present highlighting the role of HaB in biological processes and the relevance of this interaction in the activity of specific drugs^[103].

After the definition of the HaB, many other molecular systems were studied on the premise that the σ -hole model was flexible enough to be extended to atoms different from halogens^[104] (Figure 1.3.1). Analogous geometric and energetic features were, in fact, known for several other elements of the p-block of the periodic table, often in systems of biological and industrial importance^[105,106]. Some of the most important are listed in the following.

First of all, S...S contacts are common in proteins^[107-110] and they retain many similarities with the Ha...Ha close contacts that paved the way to the research on the HaB. It was known since the 1970s, in fact, that divalent sulfur could interact with both electrophiles and nucleophiles, presenting a specific interaction geometry for each case, that could well be assimilated to the two interaction modes of halogens (through the σ -hole or the negative belt). In the same fashion, contacts between PF₃ and nucleophiles were reported in 1991^[111], with the molecule being listed as a strong Lewis acid, hence anticipating the presence of areas of positive electrostatic potential on the surface of the phosphorous.

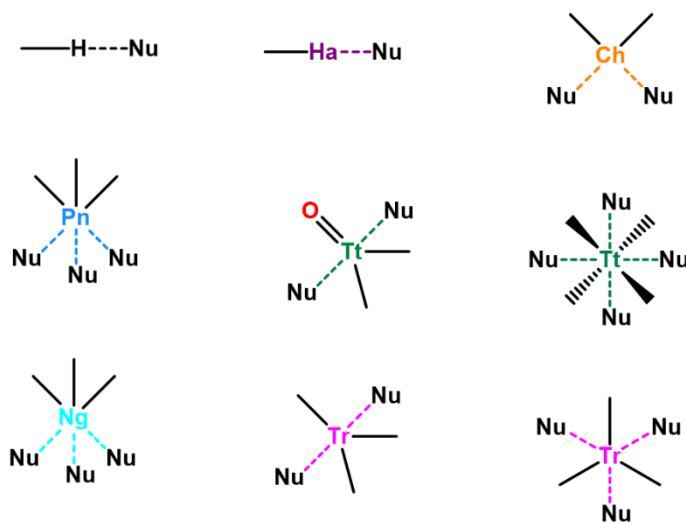


Figure 1.3.1. Bonding and σ -hole interaction patterns of different groups of the periodic table. Colour code as reported in the glossary.

Likewise, P...P, P...N and P... π contacts^[112-114] had already been observed during the 1990s and are now being studied under the light of the anisotropic distribution of the electron density around phosphorus. Si...N and Ge...N contacts were also known for a time and these contacts were known to play a role in governing unexpected geometrical features visible in the solid state, now easily explainable with the concept of σ -hole^[115,116].

Indeed, many elements of the p block, like halogens, display areas of higher and lower electrostatic potential on their surfaces, the latter being typically on the extension of the covalent bonds with highly electron attractive atoms or moieties^[117,118]. These areas can form attractive interactions with nucleophiles (e.g., lone-pair possessing atoms) and resulting adducts can be stable in the solid, liquid, and gas phases^[119]. Computational studies show that on the surface of atoms of group 16 and 15 there are, similar to halogens, also regions of excess electron density and negative electrostatic potential, thus consistent with the amphoteric behaviour of these atoms. Differently, this is not the case for elements of groups 13 and 14, consistent with the absence of lone pairs on these atoms (Figure 1.3.2).

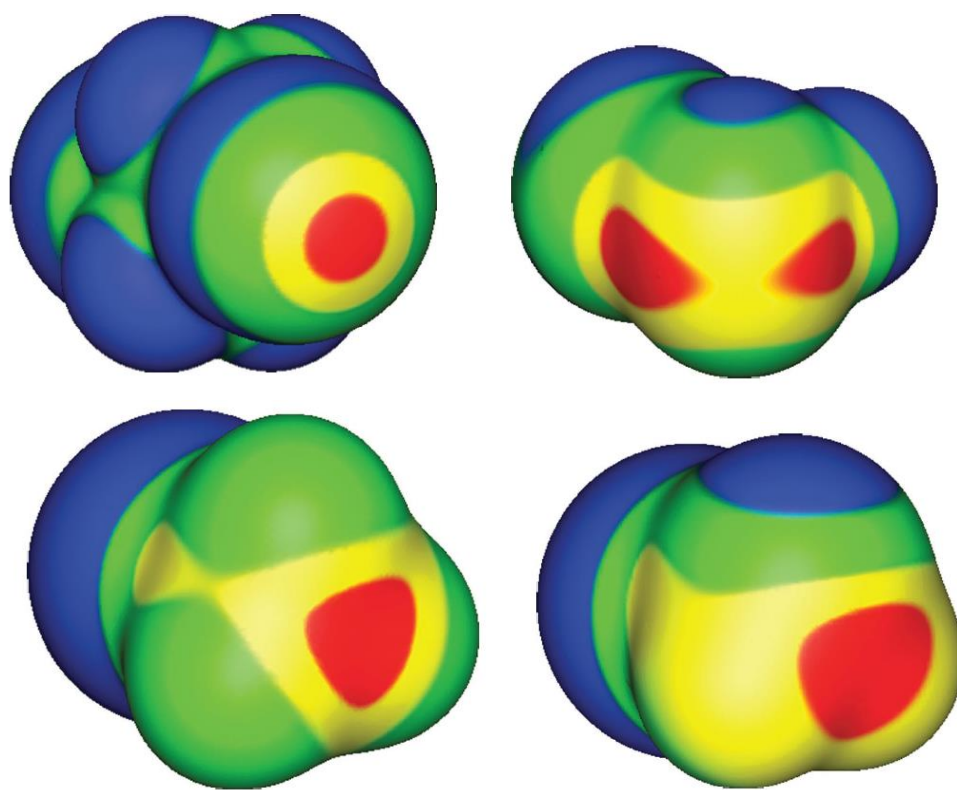


Figure 1.3.2. Molecular Electrostatic Potential of 1,2-diiodoperfluoroethane (upper left), SeFCl (upper right), GeH₃Br (lower left), PH₂Cl (lower right) computed on the 0.001 au contour of the electron density. Iodine, selenium, germanium, and phosphorous are at the front. Color ranges, in kcal·mol⁻¹, are: red, greater than 25; yellow, between 15 and 25; green, between 0 and 15; blue, less than 0 (negative). Reproduced from *Phys. Chem. Chem. Phys.*, (2013), 15, 11178.

In 2009, just two years after the seminal paper “Halogen Bonding: the σ -hole”^[54] by P. Politzer, another one, entitled “Chalcogen Bond: a sister noncovalent bond to the Halogen Bond”^[120] was published by Y. Zhang et. al. In the following years, many computational analyses were performed in rapid sequence^[18,121–124] over a huge number of

model compounds, in order to demonstrate that the amphoteric behaviour displayed by halogens was the norm across the periodic table. Experimental results confirming theoretical predictions quickly followed^[125,126].

The presence of these interactions in some systems had been observed and reported much earlier than their rationalization as a consequence of the anisotropic distribution of the electron density in bonded atoms.

In order to provide an unambiguous nomenclature of these interactions, to prevent the spreading of unclear or misleading names, and in analogy with the terms halogen bond and hydrogen bond (the parent interaction of this set), a systematic naming scheme was developed. Hence, it is now customary to refer to σ -hole interactions with the name of the group of the periodic table the electrophilic atom^[127] (the one displaying the σ -hole) belongs to. Chalcogen Bond^[128] (ChB) is the term now used to define any noncovalent interaction where a group 16 element act as an electrophile: the term was given an IUPAC definition in 2019^[129].

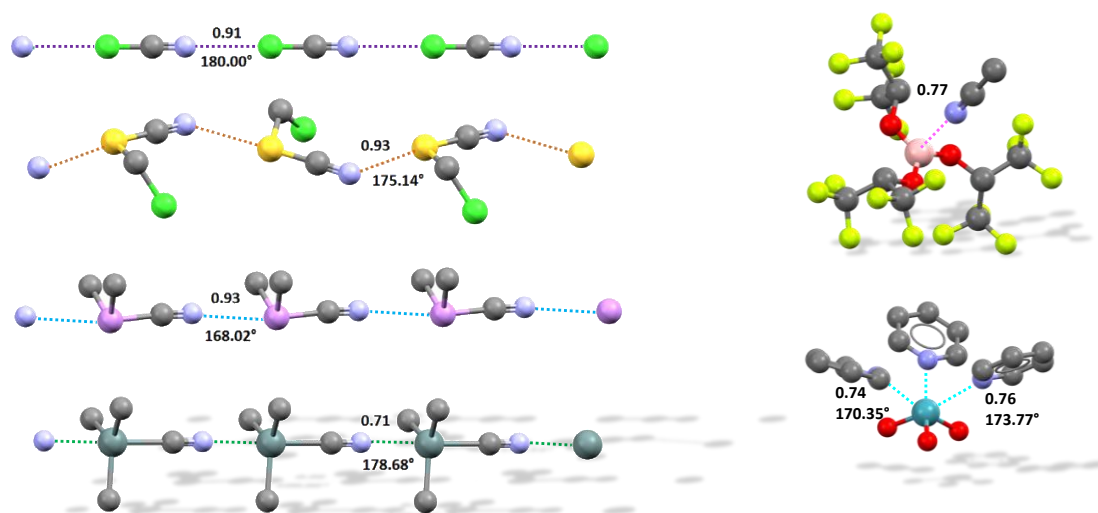


Figure 1.3.3. Different examples of σ -hole bonded chains. (left, top to bottom) cyanogen chloride^[130], chloromethylthiocyanate (Refcode, IKIQAW), cyanodimethylarsine (Refcode, CNMARS), cyanotrimethyltin (Refcode, TIMSNC01), reprinted with slight modifications from *Coordination Chemistry Reviews* 413 (2020) 213265; (right, top to bottom) triel bonded adduct of tris(1,1,1,3,3,3-Hexafluoropropan-2-yl) borate acetonitrile solvate (Refcode, FUFKAU), noble gas bonded adducts of XeO₃ (Refcode, VIFKUT). Colour code as reported in the glossary.

The terms pnictogen bond (PnB)^[131] and tetrel bond (TtB)^[132] are routinely used to denote net attractive interactions where the electrophilic moiety is an element of group 15 and 14, respectively. The terms noble gas bond (NgB, group 18)^[133] and triel bond (TrB, group 13)^[134] are also used, but these interactions have received less extensive

consideration (Figure 1.3.3). The terms alkali bond (AkB) and alkaline earth (AeB)^[127] bonds have been occasionally employed to denote interactions involving elements of the s-block of the periodic table. This classification has been proven satisfactory in describing those interactions since the Periodic Table provides information about the number of covalent bonds a specific atomic species tends to form and, consequently, the maximum number of σ -holes at that atom and resulting attractive interactions with nucleophiles.

The anisotropic electron density distribution is affected by the number and geometry of the bonds an atom can establish^[135]. So, halogen atoms usually form only one covalent bond and consequently display only one σ -hole on their outer surface. Differently, chalcogen atoms typically form two covalent bonds that determine the presence of two distinct σ -holes on their surface^[118]. Hypervalent halogen and chalcogen atoms form more than one and two covalent bonds, respectively, and the number of σ -holes on their surface changes accordingly. Analogously, pnictogen and tetrel atoms can show the presence of up to three and four σ -holes, namely they can form up to three and four σ -hole interactions. The increasing interest in the subject also brought to a second set of analogous interaction dubbed π -hole interactions^[118]. They are attractive forces where the most electrophilic area of the electrostatic potential surface of an atom does not lie of the extension of a covalent bond but rather orthogonal to it^[136]; this is the case for tetrel and triel π -hole involving moieties with a planar conformation^[137] (Figure 1.3.3).

In very recent years the study of the electron density distribution in derivatives of d-block transition metals revealed the presence, in some systems, of positive areas consistent with the concept of σ -hole interaction. In 2014 Resnati et al. observed that the mindset employed to name interactions involving atoms of group 13-16 as the electrophilic site could be expanded to transition metal elements^[127]. In 2017 T. Brink and A.C. Legon in 2018 reported the finding of attractive interactions consistent with the σ -hole modelling wherein the nucleophilic site was an element of group 11 of the periodic table. Brink identified the interaction computationally in gold nanoparticles^[138] and Legon in halides of silver and gold^[139]. The interaction has been dubbed regium bond (RgB) or coinage bond (CiB, in this thesis this latter term is used). To date, σ -holes have been identified on group 11 elements in oxidation state I and III, allowing for an easy rationalization of the geometries of the adducts formed^[140]. Various works report the presence of σ -holes also on copper, silver and gold nanoparticles^[141,142] and the presence of π -holes in gold derivatives and anion...anion^[143] and cation...cation^[144] interactions could be rationalized. Perhaps counterintuitively, an interaction where a cation is the donor of a CiB and an anion is the acceptor was even reported^[145].

During 2020, a rationalization based on σ -holes was proposed for group 12 derivatives. The proposed term to name the interaction is Spodium bond (SpB). The interaction was first found in CdBr_2L_2 and HgBr_2L_2 (L= thiourea)^[146-148]. The role of SpB

in Zn-containing proteins has also been analysed^[149]. Similar to the CiB, the interaction seems to be responsible for the formation, in the solid state, of anionic chains^[150].

In its seminal 2017 paper, Brinck group also reported the presence of σ -holes in Pt nanoparticles^[138]. To date, the analysis of group 10 elements has been extended also to Ni nanoparticles, highlighting how these forces govern the catalytic activity^[151].

Lastly, in 2021 two new interactions were proposed involving group 8 and 7 of the periodic table. The interactions were dubbed Osme Bond^[152] (OmB) and Matere Bond^[153] (MaB), respectively.

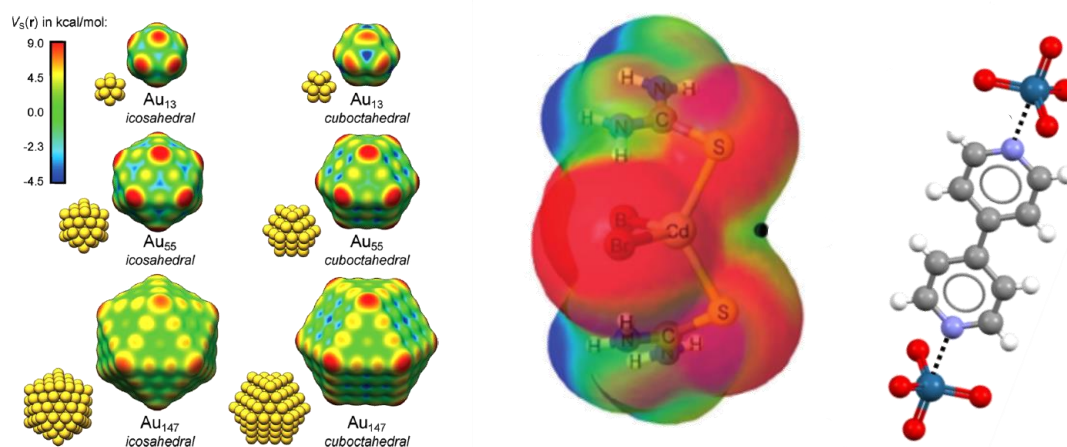


Figure 1.3.4. Examples of early findings of σ -holes in d-block transition metals are reported. Left, MEP of gold nanoparticles (reprinted from *J. Am. Chem. Soc.* **2017**, 139, 11012–11015). Middle, MEP surfaces (0.001 a.u.) of $CdBr_2L_2$ (L= thiourea), reprinted and slightly modified from *Angew. Chem. Int. Ed.* **2020**, 59, 17482–17487). Right, crystal structures of OsO_4 adduct with 4,4' dipyridyl (colour code: gray carbon, whitish hydrogen, light blue nitrogen, red oxygen, navy rhenium) (reprinted and slightly modified from *Angew. Chem. Int. Ed.* **2021**, 133, 20891–20895).

To date, most of the papers on σ -hole interactions involving d block elements as the electrophilic site are computational and theoretical^[154], with experimental findings being quite limited. The last chapter of the thesis describes some of our findings in this field (both theoretical and experimental) highlighting that the behaviour of d block elements can be in accordance with the concept of σ -hole interactions. In particular, the focus of our research was to find a number of small molecules that could serve as model compounds for the analysis of σ -hole interaction on elements of groups 11, 8, and 7.

All the interactions highlighted in this section retain many similarities and trends. Due to their high electronegativity and low polarizability, the elements of the first-row of each group does not routinely show the presence of positive σ -holes which can be located only in particularly polarized moieties^[155]. At the opposite, in compounds bearing

particularly heavy atoms, the entire atom surface may be positive, with σ -holes localized at local $V_{s,max}$. σ -Holes on any element are more positive whenever strongly electron withdrawing groups are bonded close to the element and resulting σ -hole interactions tend to be shorted and closer to linearity^[156]. The presence of lone-pair(s) on the atoms acting as electrophiles tend to decrease the linearity of σ -hole^[157].

The possibility to rationally tune the σ - and π -hole interactions formed by most atoms enabled for many fruitful exploitation in supramolecular chemistry^[158], biochemistry^[159] and material's design^[160]. In recent years chemists and material's scientists thus found new and exciting ways to tune the properties of devices^[161] and materials^[160,162] based on the principles of σ -hole, once again encompassing inclusion compounds^[163], catalysis applications^[164], anion transport^[165], self-assembly^[166,167]. In the same fashion, the rationalization enabled by the concepts first highlighted by P. Politzer has brought to an improved understanding of many already known processes. We cite, in particular, the findings suggesting that σ -holes on carbon atoms may be the key to understand the S_N2 reaction mechanism^[168].

1.4. Computational and Experimental Methods.

σ -Hole interactions are a well-defined subset of noncovalent forces that are known to impact all states of matter. In this regard, a large number of techniques are able to detect the presence or the formation of σ -hole based adducts. Considering the halogen bond, its concept lays on the counterintuitive assumption that formally nucleophilic atoms can, at times, act as electrophiles. A large body of proofs, both computational and experimental, have been used to demonstrate this behaviour. During the '90s and '00s, many studies investigated many different aspects of the interaction, not only profiling the HaB in depth, but also providing useful fingerprints for other σ -hole interactions to follow.

The main source of information came from single crystal X-Ray diffraction, even dating back to O. Hassel's experiments in the '50s^[169]. The possibility to effectively locate the positions of atoms was instrumental to afford details on how, in the solid state, atoms with complementing electronic profiles were interacting with each other. The preferential linearity of σ -hole interactions was forcefully proven, nucleophilic atoms being approximately located on the extension of polarized covalent bonds (i.e., the R–Ha...Nu angle tends to be close to 180°^[170]). Also, as in any attractive interaction, involved atoms are at a distance shorter than the sum of their van der Waals radii. A useful descriptor of this feature is the "Normalised Contact" (Nc), which is the ratio between the experimental distance of the interacting atoms and the sum of their respective van der Waals radii (or ionic radius if one of the atoms is a charged species)^[171]. While having limitations, this number can nicely complement other structure descriptors as it allows for:

- a) an intuitive way to signal the presence of an interaction (Nc < 1).
- b) a useful comparison of interactions between atoms with different Van der Waals radii.
- c) a qualitative estimate of the strength of the interaction, since usually the lower the Nc is, the stronger the interaction is.

The elongation of the R–Ha covalent bond is sometimes taken as another descriptor employed to assess the presence of the interaction.

The presence of noncovalent interactions can also be traced down with a number of other techniques. Among them, Infrared (IR) spectroscopy and Nuclear Magnetic Resonance (NMR) spectroscopy (applied over a wide number of different nuclei) are probably the most commonly used to study organic systems. The first is widely used since the presence of a specific interaction can have dramatic impact on the vibrational spectra of compounds. On formation of the generic adduct R–Sh...Y–R' (Sh is the σ -hole bond donor), it is often possible to pinpoint a shift of the bands relative to R–Sh and Y–R modes of vibration^[172,173], consistent with the weakening of the covalent bonds close to the

interacting sites and the donation of electron density from Y to Sh. Moreover, sometimes the formation of new bands can be noted, consistent with a loss of symmetry and appearance of new relaxation modes^[174,175]. In some cases, for example in cryogenic studies, complexes stoichiometries can also be derived from the change of bands intensities^[176–178]. To a lesser extent, Raman spectroscopy is also employed to observe vibrational modes with low FTIR intensity, in particular in the far-IR region^[179]. Vibrational spectroscopy has proven equally effective to identify HaB, ChB, TtB and other σ -hole interactions^[180,181].

NMR spectroscopy has been extensively employed to reveal the presence of σ -hole adducts in the solid and in solution. Differences in chemical shifts and coupling constants of adducts with respect to pure compounds are typically used^[182]. A variety of nuclei have been used, e.g., ^1H , ^{13}C , ^{19}F , ^{35}Cl , ^{77}Se , ^{31}P , ^{15}N .

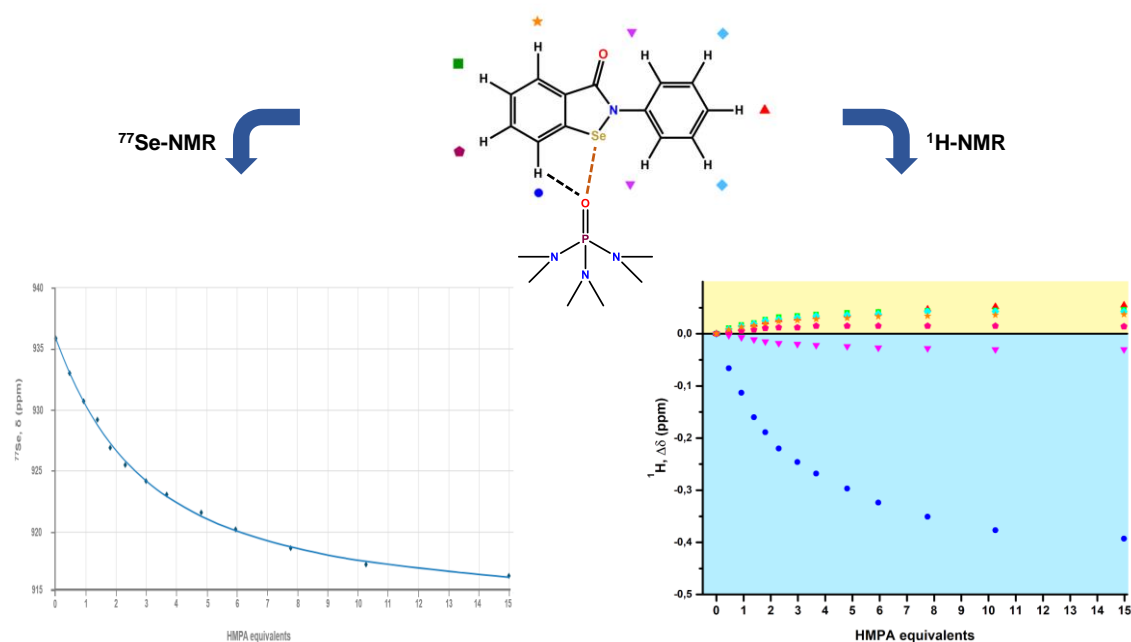


Figure 1.4.1. Schemes depicting the chemical shift of the ^{77}Se (left) and ^1H (right) NMR signals of ebselen upon incremental additions of HMPA. This is an example of the spectroscopic detection of a bifurcated synthon involving hydrogen and chalcogen bonds. Reprinted and slightly modified from *New J. Chem.*, **2020**, 44, 20697-20703.

Generally, the formation of adducts is associated with a change of the chemical shift associated with the σ -hole donor, consistent with an increase of the electron density around the atom of interest^[183]. When the atom acting as electrophilic site is not suitable for NMR analyses, other close by nuclei can be examined or changes in the NMR properties of the nucleophile atom can be fruitfully used^[184].

Other resonance techniques are sometimes employed, e.g., Nuclear Quadrupole Resonance has been used for liquid and solid systems^[185]. UV-Vis spectroscopy has been used to investigate solution systems^[186].

Microwave spectroscopy has been extensively used to reveal the presence of noncovalent interactions in the gas phase. It has been extensively employed to examine halogen bonded adducts, but it has also used for chalcogen, pnictogen, and coinage bonded systems (Figure 1.4.2)^[139].

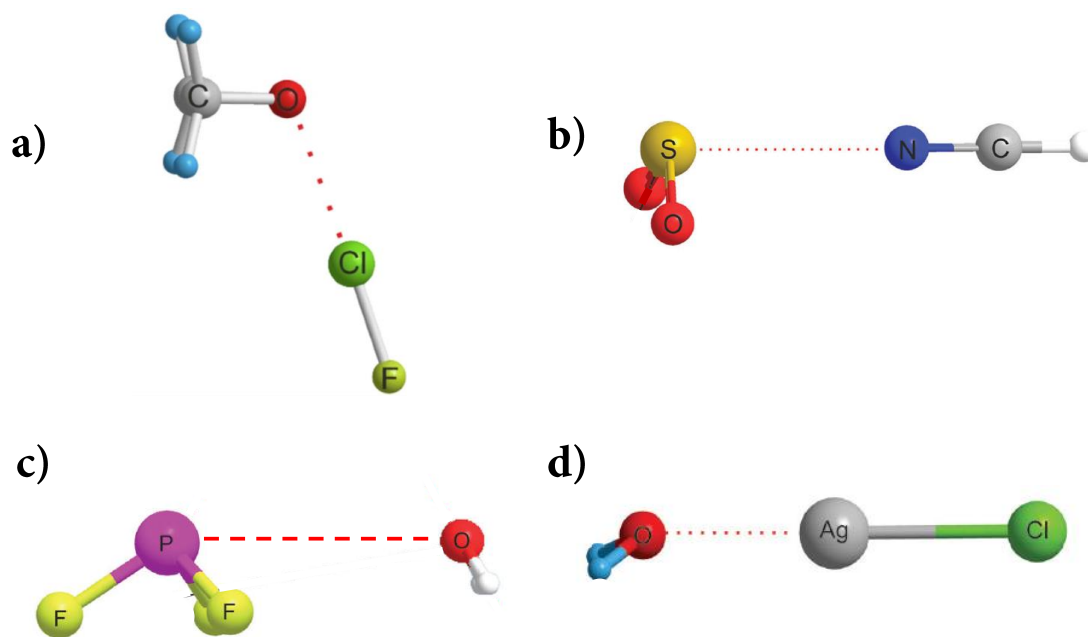


Figure 1.4.2. Ball and stick representation of some of the σ -hole bonded adducts identified over the years by microwave spectroscopy. a) FCl...Oxirane, b) O₂S...NCH, c) F₃P...OH₂ d) ClAg...OH₂. Atom names are reported on the atoms. Interactions are dashed lines. Reprinted and slightly modified from a) *J. Indian Inst. Sci.* **2020**, 1, 191-202; b) and c) *Phys. Chem. Chem. Phys.*, **2017**, 19, 14884; d) *Phys. Chem. Chem. Phys.*, **2018**, 20, 19332.

Interestingly, the techniques afford information on the charge redistribution in an adduct and intermolecular stretching forces^[187]. Two of the most used techniques are the pulsed-jet Fourier transform microwave spectroscopy and the chirped-pulse Fourier transform microwave spectroscopy. The advantage of this approach is that the expanded gas has a very low effective temperature (around 2 K) and a very low density. In these conditions it is possible to identify isolated noncovalently bonded adducts (even if the interaction is very weak) not surrounded by other molecular entities, allowing the precise measurement of many properties^[188].

In addition to the huge set of spectroscopic techniques, several computational methods and approaches were applied in the study of noncovalent interactions as a whole and σ -hole interactions specifically. As it was already discussed, the “rediscovery” of HaB came from the proposal of the σ -hole concept, which in turn arises from a number of calculations of the electrostatic potential of specific molecules^[189]. As already mentioned, while this physical observable can be obtained from diffraction studies, it is customarily calculated *in silico*. The calculation of the electrostatic potential, however, does not bring particular information about the interaction energy, which usually relies on DFT calculation. A large suite of programs is nowadays used to characterise the interactions, between them QTAIM and NCI index are probably the most frequently used to study σ -hole interactions. The first develops from Bader’s theory of atom in molecules and it is based on calculating an electron density map for all the space of a crystal (or more in general a condensed phase) locating the Critical Points (CP), *i.e.* the single points where the gradient of the electron density change sign. Representing the map on a surface instead that on a 3D space, we could notice that CPs are present on the cusp of the higher (and lower) electron density regions. When the CP is an absolute maximum it marks the position of a nucleus, when it is a saddle point takes the name of Bond Critical Point (BCP) and denotes a “path” of electron density between two atoms^[47]. While the uncritical use of this method has been strongly questioned and indeed can bring to chemically senseless results^[190], it still represent one commonly used tool for the study of noncovalent interactions, especially when paired up with other techniques^[191].

Another commonly employed tool in the analysis of weak attractive forces is the noncovalent interaction index (NCI)^[192]. This analysis is based on the empirical observation that a noncovalent interaction is associated with a reduced gradient of the electron density, which described how much the system of interest differs from an homogeneous electron gas. While QTAIM is a more rigorous tool for the analysis of noncovalent bonded systems, NCI index is mostly used to obtain qualitative trends (indeed the choice of the computational method is very impactful in this case). A similar tool is named DORI, employing a different scalar field^[193].

A large number of groups, especially during the first years of the rediscovery of the HaB, have tried to define the “Nature” of σ -hole interactions by means of decomposition energies, often finding very different, if not incompatible, results. Nowadays, a “minimalistic” approach based on electrostatic charge, polarization and, if necessary, dispersion is the most commonly used approach^[194].

References.

- [1] S. Stepanow, M. Lingenfelder, A. Dmitriev, H. Spillmann, E. Delvigne, N. Lin, X. Deng, C. Cai, J. V. Barth, K. Kern, *Nat. Mater.* **2004**, *3*, 229–233.
- [2] G. Whitesides, J. Mathias, C. Seto, *Science (80-)*. **1991**, *254*, 1312–1319.
- [3] S. I. Stupp, L. C. Palmer, *Chem. Mater.* **2014**, *26*, 507–518.
- [4] E. Persch, O. Dumele, F. Diederich, *Angew. Chemie Int. Ed.* **2015**, *54*, 3290–3327.
- [5] C. B. Aakeröy, *Acta Crystallogr. Sect. B Struct. Sci.* **1997**, *53*, 569–586.
- [6] S. Varughese, *J. Mater. Chem. C* **2014**, *2*, 3499.
- [7] J. Vapaavuori, C. G. Bazuin, A. Priimagi, *J. Mater. Chem. C* **2018**, *6*, 2168–2188.
- [8] Z. Dong, Q. Luo, J. Liu, *Chem. Soc. Rev.* **2012**, *41*, 7890.
- [9] M. J. Webber, R. Langer, *Chem. Soc. Rev.* **2017**, *46*, 6600–6620.
- [10] M. Raynal, P. Ballester, A. Vidal-Ferran, P. W. N. M. van Leeuwen, *Chem. Soc. Rev.* **2014**, *43*, 1660–1733.
- [11] S. Scheiner, *Noncovalent Forces*, Springer International Publishing, Cham, **2015**.
- [12] E. Arunan, G. R. Desiraju, R. A. Klein, J. Sadlej, S. Scheiner, I. Alkorta, D. C. Clary, R. H. Crabtree, J. J. Dannenberg, P. Hobza, et al., *Pure Appl. Chem.* **2011**, *83*, 1637–1641.
- [13] C. G. Claessens, J. F. Stoddart, *J. Phys. Org. Chem.* **1997**, *10*, 254–272.
- [14] H. Schmidbaur, A. Schier, *Chem. Soc. Rev.* **2012**, *41*, 370–412.
- [15] S. Yamada, *Chem. Rev.* **2018**, *118*, 11353–11432.
- [16] A. Frontera, P. Gamez, M. Mascal, T. J. Mooibroek, J. Reedijk, *Angew. Chemie Int. Ed.* **2011**, *50*, 9564–9583.
- [17] P. Politzer, J. S. Murray, T. Clark, G. Resnati, *Phys. Chem. Chem. Phys.* **2017**, *19*, 32166–32178.
- [18] J. S. Murray, P. Lane, P. Politzer, *Int. J. Quantum Chem.* **2007**, *107*, 2286–2292.
- [19] J.-M. Lehn, *Resonance* **1996**, *1*, 39–53.
- [20] G. R. Desiraju, *J. Mol. Struct.* **2003**, *656*, 5–15.
- [21] G. R. Desiraju, *J. Chem. Sci.* **2010**, *122*, 667–675.
- [22] A. I. Kitaigorodsky, *Mater. Res. Bull.* **1974**, *9*, 199–200.
- [23] M. D. Allendorf, V. Stavila, *CrystEngComm* **2015**, *17*, 229–246.
- [24] P. Iqbal, J. A. Preece, P. M. Mendes, in *Supramol. Chem.*, John Wiley & Sons, Ltd, Chichester, UK, **2012**.
- [25] H. Goesmann, C. Feldmann, *Angew. Chemie Int. Ed.* **2010**, *49*, 1362–1395.
- [26] F. Cheng, J. Liang, Z. Tao, J. Chen, *Adv. Mater.* **2011**, *23*, 1695–1715.
- [27] H. Lv, W. Wang, F. Li, *Chem. - A Eur. J.* **2018**, *24*, 16588–16594.
- [28] D. Braga, F. Grepioni, *Coord. Chem. Rev.* **1999**, *183*, 19–41.
- [29] C. B. Aakeröy, J. Desper, B. Levin, J. Valdés-Martínez, *Inorganica Chim. Acta* **2006**, *359*, 1255–1262.
- [30] J.-M. Lehn, *Chem. Soc. Rev.* **2007**, *36*, 151–160.
- [31] J.-M. Lehn, *Eur. Rev.* **2009**, *17*, 263–280.
- [32] E. Weber, in *Mol. Incl. Mol. Recognit. — Clathrates I*, Springer-Verlag, Berlin/Heidelberg, **2005**, pp. 1–20.
- [33] E. M. M. Del Valle, *Process Biochem.* **2004**, *39*, 1033–1046.
- [34] J. Rebek Jr., *Chem. Commun.* **2000**, 637–643.
- [35] G. M. Dykes, *J. Chem. Technol. Biotechnol.* **2001**, *76*, 903–918.
- [36] M. Hird, *Chem. Soc. Rev.* **2007**, *36*, 2070.
- [37] V. Balzani, A. Credi, M. Venturi,

- Chem. Soc. Rev.* **2009**, 38, 1542.
- [38] O. Š. Miljanić, W. R. Dichtel, I. Aprahamian, R. D. Rohde, H. D. Agnew, J. R. Heath, J. F. Stoddart, *QSAR Comb. Sci.* **2007**, 26, 1165–1174.
- [39] R. P. Wool, *Soft Matter* **2008**, 4, 400–418.
- [40] F. Guthrie, *J. Chem. Soc.* **1863**, 16, 239–244.
- [41] M. Colin, *Ann. Chim.* **1814**, 91, 252–272.
- [42] R. S. Mulliken, *J. Am. Chem. Soc.* **1950**, 72, 600–608.
- [43] P. Politzer, K. Jayasuriya, *J. Mol. Struct. THEOCHEM* **1986**, 134, 381–388.
- [44] T. Brinck, J. S. Murray, P. Politzer, *Int. J. Quantum Chem.* **1993**, 48, 73–88.
- [45] G. Naray-Szabo, G. G. Ferenczy, *Chem. Rev.* **1995**, 95, 829–847.
- [46] R. F. Stewart, *J. Chem. Phys.* **1973**, 58, 4430–4438.
- [47] R. F. W. Bader, M. T. Carroll, J. R. Cheeseman, C. Chang, *J. Am. Chem. Soc.* **1987**, 109, 7968–7979.
- [48] M. Born, R. Oppenheimer, *Ann. Phys.* **1927**, 389, 457–484.
- [49] R. P. Feynman, *Phys. Rev.* **1939**, 56, 340–343.
- [50] E. Schrödinger, *Phys. Rev.* **1926**, 28, 1049–1070.
- [51] P. Metrangolo, G. Resnati, *Chem. - A Eur. J.* **2001**, 7, 2511–2519.
- [52] H. Weinstein, P. Politzer, S. Srebrenik, *Theor. Chim. Acta* **1975**, 38, 159–163.
- [53] P. Politzer, J. S. Murray, *Theor. Chem. Accounts Theory, Comput. Model. (Theoretica Chim. Acta)* **2002**, 108, 134–142.
- [54] T. Clark, M. Hennemann, J. S. Murray, P. Politzer, *J. Mol. Model.* **2007**, 13, 291–296.
- [55] T. Brinck, J. S. Murray, P. Politzer, *Int. J. Quantum Chem.* **1992**, 44, 57–64.
- [56] K. E. Riley, J. S. Murray, J. Fanfrlík, J. Řezáč, R. J. Solá, M. C. Concha, F. M. Ramos, P. Politzer, *J. Mol. Model.* **2011**, 17, 3309–3318.
- [57] M. Saccone, G. Cavallo, P. Metrangolo, A. Pace, I. Pibiri, T. Pilati, G. Resnati, G. Terraneo, *CrystEngComm* **2013**, 15, 3102.
- [58] J.-L. Syssa-Magalé, K. Boubekour, B. Schöllhorn, *J. Mol. Struct.* **2005**, 737, 103–107.
- [59] F. C. Pigge, V. R. Vangala, D. C. Swenson, *Chem. Commun.* **2006**, 2123–2125.
- [60] O. Hassel, K. O. Strømme, E. Hammarsten, C.-G. Hedén, B. Malmgren, H. Palmstierna, *Acta Chem. Scand.* **1959**, 13, 1781–1786.
- [61] O. Hassel, K. O. Strømme, H. Haraldsen, A. Grönvall, B. Zaar, E. Diczfalusy, *Acta Chem. Scand.* **1958**, 12, 1146–1146.
- [62] P. Politzer, J. S. Murray, T. Clark, *Phys. Chem. Chem. Phys.* **2010**, 12, 7748–7757.
- [63] R. Bianchi, A. Forni, T. Pilati, *Acta Crystallogr. Sect. B Struct. Sci.* **2004**, 60, 559–568.
- [64] P. Politzer, J. S. Murray, *ChemPhysChem* **2013**, 14, 278–294.
- [65] V. Amico, S. V. Meille, E. Corradi, M. T. Messina, G. Resnati, *J. Am. Chem. Soc.* **1998**, 120, 8261–8262.
- [66] R. Liantonio, P. Metrangolo, T. Pilati, G. Resnati, A. Stevenazzi, *Cryst. Growth Des.* **2003**, 3, 799–803.
- [67] P. Metrangolo, J. S. Murray, T. Pilati, P. Politzer, G. Resnati, G. Terraneo, *CrystEngComm* **2011**, 13, 6593–6596.
- [68] A. De Santis, A. Forni, R. Liantonio, P. Metrangolo, T. Pilati, G. Resnati, *Chem. - A Eur. J.* **2003**, 9, 3974–3983.
- [69] C. Präsang, A. C. Whitwood, D. W. Bruce, *Cryst. Growth Des.* **2009**, 9, 5319–5326.
- [70] P. Gagnaux, B. P. Susz, *Helv. Chim.*

- Acta* **1960**, 43, 948–956.
- [71] J. George, V. L. Deringer, R. Dronskowski, *J. Phys. Chem. A* **2014**, 118, 3193–3200.
- [72] J. Burdeniuc, M. Sanford, R. H. Crabtree, *J. Fluor. Chem.* **1998**, 91, 49–54.
- [73] N. Wang, J.-G. Wang, A.-J. Min, Y.-W. Fu, *Acta Crystallogr. Sect. E Struct. Reports Online* **2012**, 68, m164–m164.
- [74] A. Vargas Jentzsch, S. Matile, *J. Am. Chem. Soc.* **2013**, 135, 5302–5303.
- [75] A. V. Jentzsch, D. Emery, J. Mareda, S. K. Nayak, P. Metrangolo, G. Resnati, N. Sakai, S. Matile, *Nat. Commun.* **2012**, 3, 905.
- [76] A. Vargas Jentzsch, D. Emery, J. Mareda, P. Metrangolo, G. Resnati, S. Matile, *Angew. Chemie Int. Ed.* **2011**, 50, 11675–11678.
- [77] J.-L. Syssa-Magalé, K. Boubekour, P. Palvadeau, A. Meerschaut, B. Schöllhorn, *CrystEngComm* **2005**, 7, 302–308.
- [78] P. von R. Schleyer, R. West, *J. Am. Chem. Soc.* **1959**, 81, 3164–3165.
- [79] H. Torii, M. Yoshida, *J. Comput. Chem.* **2010**, 31, 107–116.
- [80] P. Politzer, K. E. Riley, F. A. Bulat, J. S. Murray, *Comput. Theor. Chem.* **2012**, 998, 2–8.
- [81] G. Cavallo, P. Metrangolo, R. Milani, T. Pilati, A. Priimagi, G. Resnati, G. Terraneo, *Chem. Rev.* **2016**, 116, 2478–2601.
- [82] G. R. Desiraju, P. S. Ho, L. Kloo, A. C. Legon, R. Marquardt, P. Metrangolo, P. Politzer, G. Resnati, K. Rissanen, *Pure Appl. Chem.* **2013**, 85, 1711–1713.
- [83] A. Farina, S. V. Meille, M. T. Messina, P. Metrangolo, G. Resnati, G. Vecchio, *Angew. Chemie Int. Ed.* **1999**, 38, 2433–2436.
- [84] P. Metrangolo, Y. Carcenac, M. Lahtinen, T. Pilati, K. Rissanen, A. Vij, G. Resnati, *Science (80-.)*. **2009**, 323, 1461–1464.
- [85] A. Brown, P. D. Beer, *Chem. Commun.* **2016**, 52, 8645–8658.
- [86] W. J. Cheong, S. H. Yang, F. Ali, *J. Sep. Sci.* **2013**, 36, 609–628.
- [87] A. Abate, M. Brischetto, G. Cavallo, M. Lahtinen, P. Metrangolo, T. Pilati, S. Radice, G. Resnati, K. Rissanen, G. Terraneo, *Chem. Commun.* **2010**, 46, 2724.
- [88] T. Takeuchi, Y. Minato, M. Takase, H. Shinmori, *Tetrahedron Lett.* **2005**, 46, 9025–9027.
- [89] D. Cinčić, T. Friščić, W. Jones, *Chem. - A Eur. J.* **2008**, 14, 747–753.
- [90] D. Cinčić, T. Friščić, W. Jones, *J. Am. Chem. Soc.* **2008**, 130, 7524–7525.
- [91] T. Friščić, *Chem. Soc. Rev.* **2012**, 41, 3493–3510.
- [92] C. Wilhelm, S. A. Boyd, S. Chawda, F. W. Fowler, N. S. Goroff, G. P. Halada, C. P. Grey, J. W. Lauher, L. Luo, C. D. Martin, et al., *J. Am. Chem. Soc.* **2008**, 130, 4415–4420.
- [93] L. Meazza, J. A. Foster, K. Fucke, P. Metrangolo, G. Resnati, J. W. Steed, *Nat. Chem.* **2013**, 5, 42–47.
- [94] H. L. Nguyen, P. N. Horton, M. B. Hursthouse, A. C. Legon, D. W. Bruce, *J. Am. Chem. Soc.* **2004**, 126, 16–17.
- [95] J. Xu, X. Liu, T. Lin, J. Huang, C. He, *Macromolecules* **2005**, 38, 3554–3557.
- [96] F. Kniep, S. H. Jungbauer, Q. Zhang, S. M. Walter, S. Schindler, I. Schnapperelle, E. Herdtweck, S. M. Huber, *Angew. Chemie - Int. Ed.* **2013**, 52, 7028–7032.
- [97] J. Vapaavuori, C. G. Bazuin, A. Priimagi, *J. Mater. Chem. C* **2018**, 6, 2168–2188.
- [98] D. Yan, A. Delori, G. O. Lloyd, T. Friščić, G. M. Day, W. Jones, J. Lu, M. Wei, D. G. Evans, X. Duan, *Angew. Chemie - Int. Ed.* **2011**, 50, 12483–12486.

- [99] O. Bolton, K. Lee, H. J. Kim, K. Y. Lin, J. Kim, *Nat. Chem.* **2011**, *3*, 205–210.
- [100] O. Bolton, D. Lee, J. Jung, J. Kim, *Chem. Mater.* **2014**, *26*, 6644–6649.
- [101] M. Fourmigué, P. Batail, *Chem. Rev.* **2004**, *104*, 5379–5418.
- [102] M. Fourmigué, *Struct. Bond.* **2008**, *126*, 181–207.
- [103] V. Andrea, H. P., *Curr. Top. Med. Chem.* **2007**, *7*, 1336–1348.
- [104] Á. M. Montaña, *ChemistrySelect* **2017**, *2*, 9094–9112.
- [105] N. Biot, D. Bonifazi, *Coord. Chem. Rev.* **2020**, *413*, 213243.
- [106] B. R. Beno, K.-S. Yeung, M. D. Bartberger, L. D. Pennington, N. A. Meanwell, *J. Med. Chem.* **2015**, *58*, 4383–4438.
- [107] J. A. Kapecki, J. E. Baldwin, *J. Am. Chem. Soc.* **1969**, *91*, 1120–1123.
- [108] R. E. Rosenfield, R. Parthasarathy, J. D. Dunitz, *J. Am. Chem. Soc.* **1977**, *99*, 4860–4862.
- [109] T. N. G. Row, R. Parthasarathy, *J. Am. Chem. Soc.* **1981**, *103*, 477–479.
- [110] M. Iwaoka, S. Takemoto, S. Tomoda, *J. Am. Chem. Soc.* **2002**, *124*, 10613–10620.
- [111] R. S. Drago, N. Wong, D. C. Ferris, *J. Am. Chem. Soc.* **1991**, *113*, 1970–1977.
- [112] M. Widhalm, C. Kratky, *Chem. Ber.* **1992**, *125*, 679–689.
- [113] F. Carré, C. Chuit, R. J. P. Corriu, P. Monforte, N. K. Nayyar, C. Reyé, *J. Organomet. Chem.* **1995**, *499*, 147–154.
- [114] F. Liu, L. Du, J. Gao, L. Wang, B. Song, C. Liu, *J. Comput. Chem.* **2015**, *36*, 441–448.
- [115] N. W. Mitzel, A. J. Blake, D. W. H. Rankin, *J. Am. Chem. Soc.* **1997**, *119*, 4143–4148.
- [116] U. Losehand, N. W. Mitzel, D. W. H. Rankin, *J. Chem. Soc. Dalton Trans.* **1999**, *23*, 4291–4297.
- [117] J. S. Murray, P. Lane, T. Clark, P. Politzer, *J. Mol. Model.* **2007**, *13*, 1033–1038.
- [118] J. S. Murray, P. Lane, P. Politzer, *Int. J. Quantum Chem.* **2008**, *108*, 2770–2781.
- [119] A. Bauzá, T. J. Mooibroek, A. Frontera, *ChemPhysChem* **2015**, *16*, 2496–2517.
- [120] W. Wang, B. Ji, Y. Zhang, *J. Phys. Chem. A* **2009**, *113*, 8132–8135.
- [121] A. Mohajeri, A. H. Pakiari, N. Bagheri, *Chem. Phys. Lett.* **2009**, *467*, 393–397.
- [122] P. Politzer, J. Murray, G. Janjić, S. Zarić, *Crystals* **2014**, *4*, 12–31.
- [123] P. Politzer, J. S. Murray, P. Lane, M. C. Concha, *Int. J. Quantum Chem.* **2009**, *109*, 3773–3780.
- [124] A. Bundhun, P. Ramasami, J. S. Murray, P. Politzer, *J. Mol. Model.* **2013**, *19*, 2739–2746.
- [125] O. V. Shishkin, I. V. Omelchenko, A. L. Kalyuzhny, B. V. Paponov, *Struct. Chem.* **2010**, *21*, 1005–1011.
- [126] S. P. Thomas, M. S. Pavan, T. N. Guru Row, *Chem. Commun.* **2014**, *50*, 49–51.
- [127] G. Cavallo, P. Metrangolo, T. Pilati, G. Resnati, G. Terraneo, *Cryst. Growth Des.* **2014**, *14*, 2697–2702.
- [128] P. Scilabra, G. Terraneo, G. Resnati, *Acc. Chem. Res.* **2019**, *52*, 1313–1324.
- [129] C. B. Aakeroy, D. L. Bryce, G. R. Desiraju, A. Frontera, A. C. Legon, F. Nicotra, K. Rissanen, S. Scheiner, G. Terraneo, P. Metrangolo, et al., *Pure Appl. Chem.* **2019**, *91*, 1889–1892.
- [130] R. B. Heiart, G. B. Carpenter, *Acta Crystallogr.* **1956**, *9*, 889–895.
- [131] P. Scilabra, G. Terraneo, G. Resnati, *J. Fluor. Chem.* **2017**, *203*, 62–74.
- [132] P. Scilabra, V. Kumar, M. Ursini, G. Resnati, *J. Mol. Model.* **2018**, *24*, 37.
- [133] A. Bauzá, A. Frontera, *Angew. Chemie Int. Ed.* **2015**, *54*, 7340–7343.
- [134] S. J. Grabowski, *ChemPhysChem*

- 2014**, *15*, 2985–2993.
- [135] G. Cavallo, J. S. Murray, P. Politzer, T. Pilati, M. Ursini, G. Resnati, *IUCrJ* **2017**, *4*, 411–419.
- [136] H. B. Biirgi, J. D. Dunitz, E. Shefter, *J. Am. Chem. Soc.* **1973**, *95*, 5065–5067.
- [137] S. J. Grabowski, *J. Comput. Chem.* **2018**, *39*, 472–480.
- [138] J. H. Stenlid, T. Brinck, *J. Am. Chem. Soc.* **2017**, *139*, 11012–11015.
- [139] A. C. Legon, N. R. Walker, *Phys. Chem. Chem. Phys.* **2018**, *20*, 19332–19338.
- [140] C. Trujillo, G. Sánchez-Sanz, J. Elguero, I. Alkorta, *Struct. Chem.* **2020**, *31*, 1909–1918.
- [141] A. Bauzá, M. De Las Nieves Pina, A. Frontera, *J. Phys. Chem. Lett.* **2020**, *11*, 8259–8263.
- [142] A. Frontera, A. Bauzá, *Chem. - A Eur. J.* **2018**, *24*, 7228–7234.
- [143] A. Daolio, A. Pizzi, G. Terraneo, M. Ursini, A. Frontera, G. Resnati, *Angew. Chemie - Int. Ed.* **2021**, *60*, 14385–14389.
- [144] E. Priola, G. Mahmoudi, J. Andreo, A. Frontera, *Chem. Commun.* **2021**, *57*, 7268–7271.
- [145] E. Priola, A. Giordana, P. P. Mazzeo, G. Mahmoudi, R. M. Gomila, F. I. Zubkov, K. M. Pokazeev, K. S. Valchuk, A. Bacchi, E. Zangrando, et al., *Dalt. Trans.* **2021**, DOI 10.1039/D1DT02632A.
- [146] A. Bauzá, I. Alkorta, J. Elguero, T. J. Mooibroek, A. Frontera, *Angew. Chemie - Int. Ed.* **2020**, *59*, 17482–17487.
- [147] R. M. Gomila, A. Bauzá, T. J. Mooibroek, A. Frontera, *CrystEngComm* **2021**, *23*, 3084–3093.
- [148] G. Mahmoudi, S. E. Lawrence, J. Cisterna, A. Cárdenas, I. Brito, A. Frontera, D. A. Safin, *New J. Chem.* **2020**, *44*, 21100–21107.
- [149] R. Llull, G. Montalbán, I. Vidal, R. M. Gomila, A. Bauzá, A. Frontera, *Phys. Chem. Chem. Phys.* **2021**, *23*, 16888–16896.
- [150] R. Wysokiński, W. Zierkiewicz, M. Michalczyk, S. Scheiner, *Phys. Chem. Chem. Phys.* **2021**, *23*, 13853–13861.
- [151] G. Li, J. H. Stenlid, M. S. G. Ahlquist, T. Brinck, *J. Phys. Chem. C* **2020**, *124*, 14696–14705.
- [152] A. Daolio, A. Pizzi, M. Calabrese, G. Terraneo, S. Bordignon, A. Frontera, G. Resnati, *Angew. Chemie* **2021**, *133*, 20891–20895.
- [153] A. Daolio, A. Pizzi, G. Terraneo, A. Frontera, G. Resnati, *ChemPhysChem* **2021**, 1–6.
- [154] G. Sánchez-Sanz, C. Trujillo, I. Alkorta, J. Elguero, *ChemPhysChem* **2019**, *20*, 1572–1580.
- [155] R. Paulini, K. Müller, F. Diederich, *Angew. Chemie - Int. Ed.* **2005**, *44*, 1788–1805.
- [156] J. S. Murray, P. Lane, P. Politzer, in *J. Mol. Model.*, **2009**, pp. 723–729.
- [157] U. Adhikari, S. Scheiner, *Chem. Phys. Lett.* **2012**, *532*, 31–35.
- [158] S. Moaven, J. Yu, M. Vega, D. K. Unruh, A. F. Cozzolino, *Chem. Commun.* **2018**, *54*, 8849–8852.
- [159] X. García-LLinás, A. Bauzá, S. K. Seth, A. Frontera, *J. Phys. Chem. A* **2017**, *121*, 5371–5376.
- [160] K. T. Mahmudov, M. N. Kopylovich, M. F. C. Guedes Da Silva, A. J. L. Pombeiro, *Dalt. Trans.* **2017**, *46*, 10121–10138.
- [161] J. Fu, S. Chen, K. Yang, S. Jung, J. Lv, L. Lan, H. Chen, D. Hu, Q. Yang, T. Duan, et al., *iScience* **2020**, *23*, 100965.
- [162] L. Vogel, P. Wonner, S. M. Huber, *Angew. Chemie - Int. Ed.* **2019**, *58*, 1880–1891.
- [163] L. J. Riwar, N. Trapp, K. Root, R. Zenobi, F. Diederich, *Angew. Chemie - Int. Ed.* **2018**, *57*, 17259–17264.
- [164] K. T. Mahmudov, M. N. Kopylovich, M. F. C. Guedes Da Silva, A. J. L.

- Pombeiro, *Dalt. Trans.* **2017**, *46*, 10121–10138.
- [165] L. M. Lee, M. Tsemperouli, A. I. Poblador-Bahamonde, S. Benz, N. Sakai, K. Sugihara, S. Matile, *J. Am. Chem. Soc.* **2019**, *6–10*.
- [166] S. Moaven, M. C. Andrews, T. J. Polaske, B. M. Karl, D. K. Unruh, E. Bosch, N. P. Bowling, A. F. Cozzolino, *Inorg. Chem.* **2019**, *58*, 16227–16235.
- [167] H. J. Trubenstein, S. Moaven, M. Vega, D. K. Unruh, A. F. Cozzolino, *New J. Chem.* **2019**, *43*, 14305–14312.
- [168] S. J. Grabowski, *Phys. Chem. Chem. Phys.* **2014**, *16*, 1824–1834.
- [169] O. Hassel, J. Hvoslef, E. H. Vihovde, N. A. Sørensen, *Acta Chem. Scand.* **1954**, *8*, 873–873.
- [170] Z. P. Shields, J. S. Murray, P. Politzer, *Int. J. Quantum Chem.* **2010**, *110*, 2823–2832.
- [171] A. Bondi, *J. Phys. Chem.* **1964**, *68*, 441–451.
- [172] W. B. Person, R. E. Humphrey, A. I. Popov, *J. Am. Chem. Soc.* **1959**, *81*, 273–277.
- [173] M. T. Messina, P. Metrangolo, W. Navarrini, S. Radice, G. Resnati, G. Zerbi, *J. Mol. Struct.* **2000**, *524*, 87–94.
- [174] A. I. Popov, J. C. Marshall, F. B. Stute, W. B. Person, *J. Am. Chem. Soc.* **1961**, *83*, 3586–3590.
- [175] Y. Yagi, *J. Phys. Chem.* **1967**, *71*, 2439–2444.
- [176] D. Hauchecorne, B. J. Van Der Veken, A. Moiana, W. A. Herrebout, *Chem. Phys.* **2010**, *374*, 30–36.
- [177] D. Hauchecorne, R. Szostak, W. A. Herrebout, B. J. Van Der Veken, *ChemPhysChem* **2009**, *10*, 2105–2115.
- [178] D. Hauchecorne, A. Moiana, B. J. Van Der Veken, W. A. Herrebout, *Phys. Chem. Chem. Phys.* **2011**, *13*, 10204–10213.
- [179] P. Klaboe, E. Kloster-Jensen, *Spectrochim. Acta Part A Mol. Spectrosc.* **1967**, *23*, 1981–1990.
- [180] Y. Geboes, F. De Vleeschouwer, F. De Proft, W. A. Herrebout, *Chem. - A Eur. J.* **2017**, *23*, 17384–17392.
- [181] D. Sethio, V. Oliveira, E. Kraka, *Molecules* **2018**, *23*, 2763.
- [182] V. Kumar, C. Leroy, D. L. Bryce, *CrystEngComm* **2018**, *20*, 6406–6411.
- [183] A. Daolio, P. Scilabra, M. E. Di Pietro, C. Resnati, K. Rissanen, G. Resnati, *New J. Chem.* **2020**, *44*, 20697–20703.
- [184] H. G. Löhr, A. Engel, H. P. Josel, F. Vögtle, W. Schuh, H. Puff, *J. Org. Chem.* **1984**, *49*, 1621–1627.
- [185] P. Scilabra, G. Terraneo, A. Daolio, A. Baggioli, A. Famulari, C. Leroy, D. L. Bryce, G. Resnati, *Cryst. Growth Des.* **2020**, *20*, 916–922.
- [186] B. Watson, O. Grounds, W. Borley, S. V. Rosokha, *Phys. Chem. Chem. Phys.* **2018**, *20*, 21999–22007.
- [187] A. C. Legon, *Angew. Chemie - Int. Ed.* **1999**, *38*, 2686–2714.
- [188] P. R. Joshi, N. Ramanathan, K. Sundararajan, K. Sankaran, *J. Phys. Chem. A* **2015**, *119*, 3440–3451.
- [189] P. Politzer, J. S. Murray, M. C. Concha, *J. Mol. Model.* **2008**, *14*, 659–665.
- [190] C. R. Wick, T. Clark, *J. Mol. Model.* **2018**, *24*, 1–9.
- [191] E. Pastorczak, C. Corminboeuf, *J. Chem. Phys.* **2017**, *146*, 120901.
- [192] J. Contreras-García, E. R. Johnson, S. Keinan, R. Chaudret, J.-P. Piquemal, D. N. Beratan, W. Yang, *J. Chem. Theory Comput.* **2011**, *7*, 625–632.
- [193] L. Vannay, B. Meyer, R. Petraglia, G. Sforazzini, M. Ceriotti, C. Corminboeuf, *J. Chem. Theory Comput.* **2018**, *14*, 2370–2379.
- [194] P. Politzer, J. S. Murray, *Crystals* **2017**, *7*, 212.

2. The Halogen Bond at Work

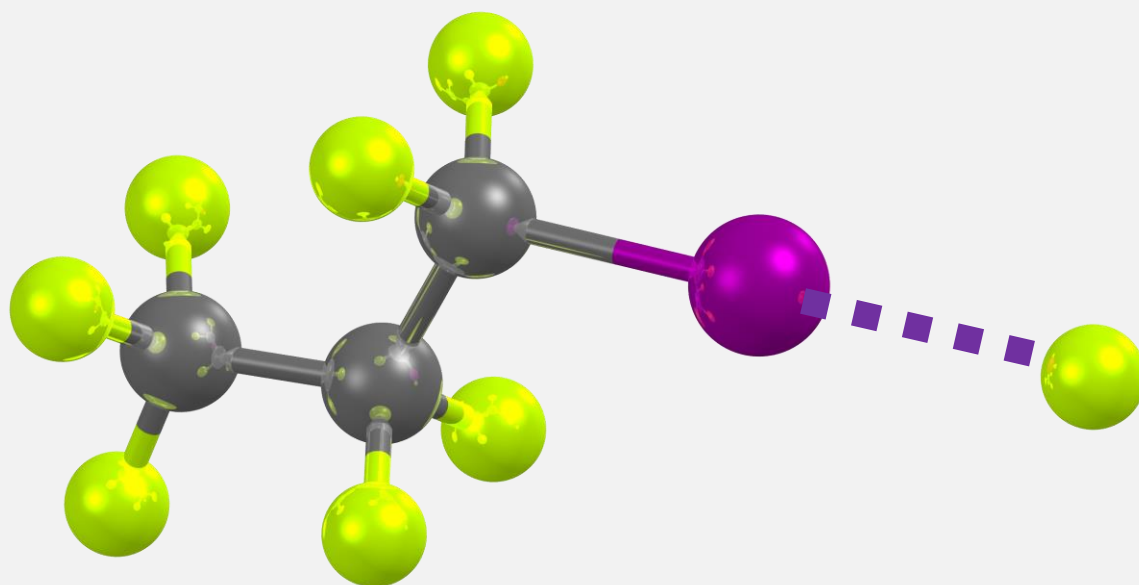


Figure 2. Intuitive representation of the geometrical features of a halogen bonded adduct displayed in 1-iodo heptafluoro propane-fluoride adduct (structure 1). Molecules not engaging in HaB were omitted for clarity. Rendered by POV-Ray with metallic textures (ball and stick visualization).

HaB is able to exert a dramatic impact on crystal structures by forming distinctive adducts and organizing them into unique supramolecular architectures^[1]. Numerous and specific strategies to build complex structures are well known and it is nowadays possible to find useful information regarding the best conditions to obtain a wide diversity of adducts^[2]. Many works are available where the competition (or cooperation) between HaB and other noncovalent interactions is examined and the relative strength of the different bonding is analysed^[3]. Nevertheless, it is still a challenge to obtain crystal structures where the fluoride anion acts as HaB acceptor. This is confirmed by a general scarcity of experimental works on the subject and of crystal structures where F^- is the donor of electron density. This chapter provides an example of a method to obtain crystal structures where a HaB is formed between iodoperfluoroalkanes and a fluoride anion. In the following pages two structures are presented, also showcasing the general features of the interaction under scrutiny.

2.1. Uncommon adducts between iodoperfluoroalkanes and a fluoride anion.

“The outcome of a battle depends on how one handles emptiness and fullness, weakness and strength.”

- *Gichin Funakoshi, the 14th principle of Shotokan Karate*

In the formation of halogen bonded adducts, many facets and phenomena must be taken into account. If in the crystallization medium are present interactions stronger than the HaB, the interaction of interest could not prevail in the formation of adducts. If one of the species involved in the formation of the desired adduct can engage in strong interactions with other moieties present in the medium, namely solvent molecules, the formation of the adduct can be impaired. It is because the molecules should first break their coordination sphere in order to aggregate. Aspects of that can be derived from the different growth kinetic of crystals of KCl, KBr and KI from water solutions^[4].

The disruption of the coordination sphere is considered a rate-determining step in the formation of halogen bonded adducts between highly polar or charged molecules. If that is the case, the formation of solvates can emerge and the HaB may not be experienced in many situations. In a related manner, decomposition products or impurities present in the solvent can hamper the formation of specific crystals^[5]. Another important factor is played by the geometry of the involved tectons that will be considered thoroughly in the next paragraph.

The design of both the electrophilic and the nucleophilic moieties play an important role in the formation of crystals. As already discussed in the previous chapter, highly polarizable species with strong electron attractor moieties bound to the backbone of the molecules are preferred in the formation of HaBs. Conversely, optimum electron density donors are small, highly nucleophilic moieties with minor to no steric hinderance That way the donation of electron density to the electron-poor halogen (while establishing the preferred geometrical conditions) is somewhat easier.

In principle, fluoride anions are supposed to have the geometrical characteristics necessary to act as strong donor of electron density. Calculated interaction strength, in fact, show that fluoride anions engage in the strongest HaB when acting as the HaB acceptor, while iodine is engaged in the weakest. Chloride and bromide, of course, afford intermediate HaB, as testified, among many other examples, by the computed energies for $FI \cdots X^-$ adducts (-75.0 and -41.9 kcal/mol when X is F and I, respectively)^[6,7]. However, the

fluoride anion has very high electronegativity and low polarizability, making it unsuitable for the establishment of σ -hole interactions. In addition, this small anion is known to engage in strong hydrogen bonds with most of the common solvents^[8]. F^- anions change substantially their properties, for example their Lewis basicity, in solution with respect to the gas phase. Interaction energies for HaB run parallel to those for the HB, the computed energies for a single HB $FH\cdots X^-$ adduct being -53.0 and -18.1 kcal/mol when X is F and I, respectively^[7,9].

Consistently with its very high hydration energy of 111 kcal/mol (for comparison, the hydration energy of iodide anion is 66 kcal/mol)^[10], fluoride anions, under common reaction conditions, exist mostly as solvated species. While the HaB formed with a suitable crystallization partner may be particularly favourable, the payoff is not always enough to allow for breaking the first coordination sphere of the halide and forming the HaB.

The past decades research explored possible ways to obtain a “naked” fluoride anion (i.e., an atomic species, indeed a more theoretical than real species^[11], which is not engaging in any strong hydrogen bond, or any other noncovalent interaction).

The “naked” fluoride should readily take part in fluorination reactions or in the formation of specific adducts while at the same time being significantly soluble in commonly used organic solvents. Some of the most promising results in this respect have focused on specific salts and adducts where the fluoride anion is engaging in very weak to null HBs. Tetraalkylammonium fluorides were pursued to overcome the low solubility of alkali metal fluorides in organic solvents. The first preparation of “anhydrous”^[12] tetramethylammonium fluorides proved particularly useful in establishing the features that tetraalkylammonium fluorides needed to have, i.e. big organic cations able to effectively delocalise their positive charge but without any β -hydrogens which might undergo Hoffman elimination.

Alternatively, adducts between HF and amines^[13] or pyridine^[14] were employed for various reactions. In these systems the nucleophilicity of the anion could be modulated by changing the HF:organic compound ratio. Over the years, much attention has been devoted in the synthesis of better performing compounds^[15-17], and their respective ability to produce the most “naked” fluoride anion has been tested both empirically^[18] and theoretically^[19]. Many different methods have been developed for the synthesis or organofluoro compounds, and the use of specific systems now outclasses older techniques (like phase-transfer catalysts^[20], ion-exchange resins^[21] and spray-dried KF ^[22]) that were the most common processes used to produce “naked” fluoride anions at the pioneering times of selective fluorination reactions. However, even these recently developed strategies are mostly employed in order to perform selective fluorination reactions and are not tailored to the formation of halogen bonded crystals, a field where the most used technique

nowadays is the still the cocrystallization of various synthons with ammonium fluoride salts.

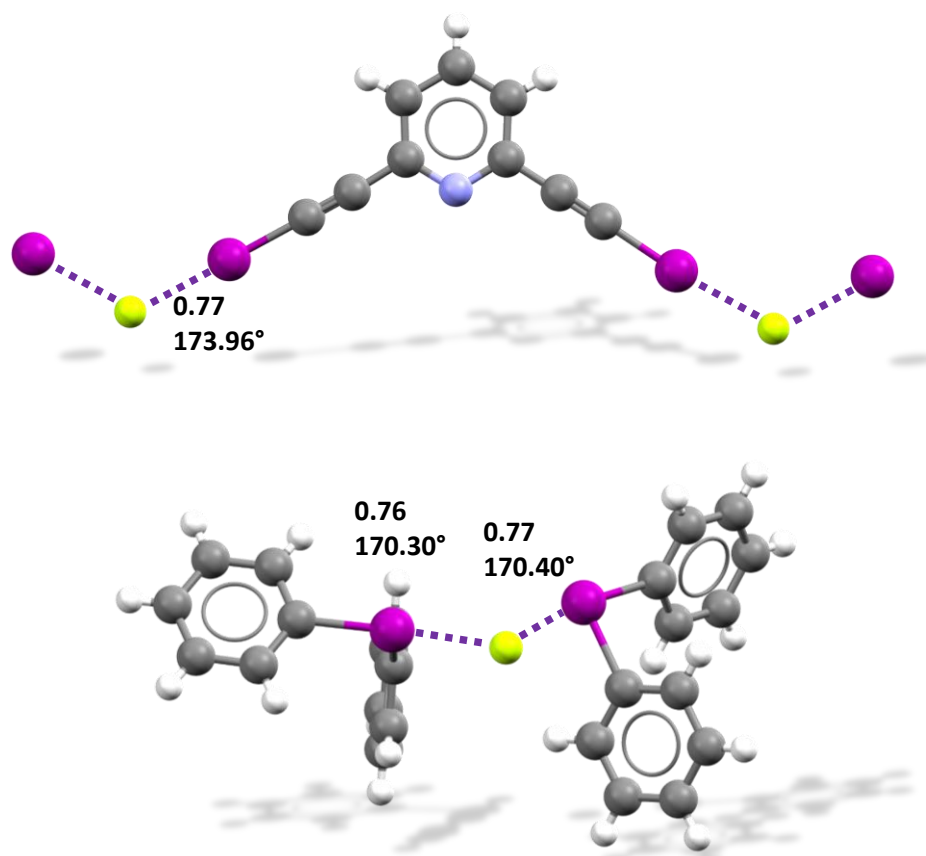


Figure 2.1.1. Above, ball and stick representation of the crystal structure of tetra-*n*-butylammonium bis(2,6-bis(iodoethynyl)pyridine) fluoride. Below, ball and stick representation of the crystal structure of diphenyliodonium fluoride. Molecules non involved in the HaB have been omitted for clarity.

Very few crystal structures displaying a HaB with a fluoride anion as the Lewis base are present in the Cambridge Crystallographic Database (CSD). This is particularly staggering if the recent high interest in σ -hole interactions is considered.

Furthermore, in structures present in the CSD, the fluoride anion is also engaged in strong and directional HBs that might play an important role in establishing the crystal packing. Two examples of these crystal structures are the tetra-*n*-butylammonium sesquikis(2,6-bis(iodoethynyl)pyridine) fluoride (Refcode EQUFAZ,^[23] Figure 2.1.1 top) and the diphenyliodonium fluoride acetonitrile solvate hemihydrate (Refcode UZOHAU,^[24] Figure 2.1.1 bottom). In these structures the fluoride anions engage both in HaB with iodine atoms and HB with hydrogen atoms of the cations. Consistent with computational studies^[25], the anions in both cases are present on the extension of I-C

covalent bonds and present normalized contacts of 0.77 and 0.76. These Nc are quite short and indicative of a very strong interaction, as expected for an HaB where the donor of electron density is a donor of electron density as strong as a fluoride anion.

Obtaining halogen bonded adducts with tunable strength is central for the development of the field, and consistently obtaining the strongest possible HaB, at least in the solid phase, may be of key importance in HaB applications. New techniques of general applicability are highly desirable in order to obtain crystal structures displaying HaBs where fluoride anions work as interaction acceptors.

We decided to assess the ability of fluoride anions to work as HaB acceptors by designing peculiar experimental conditions for the formation of naked fluoride anions. We tried to prevent the formations of HBs while favouring the formation of HaBs.

We report the formation of two crystal structures: 1-iodo-1,1,2,2,3,3,3-heptafluoro propane/18-crown-6/potassium fluoride (**1**) and 1,4-diiodo-1,1,2,2,3,3,4,4-octafluoro-butane/18-crown-6/potassium fluoride (**2**). Both structures display strong and linear HaBs between the iodine of the iodoperfluoroalkanes (the HaB donor) and naked fluoride anions (the HaB acceptor).

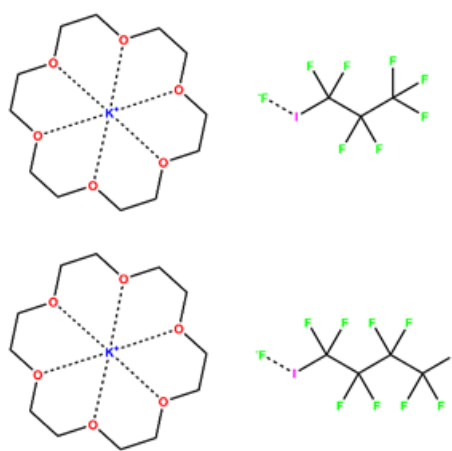


Figure 2.1.2. Structural schemes of 1-iodo-1,1,2,2,3,3,3-heptafluoro propane/18-crown-6/potassium fluoride adduct (**1**, top) and 1,4-diiodo-1,1,2,2,3,3,4,4-octafluoro-butane/18-crown-6/potassium fluoride adduct (**2**, bottom).

The crystals were obtained following this general procedure: a given quantity of 18-crown-6 (1,4,7,10,13,16-hexaoxacyclooctadecane) was heated until melting. Then, an equimolar amount of potassium fluoride was added and the mixture was stirred. A large excess of liquid iodoperfluoroalkane (1-iodo-1,1,2,2,3,3,3-heptafluoro propane for crystal **1** and 1,4-diiodo-1,1,2,2,3,3,4,4-octafluoro-butane for crystal **2**) was rapidly added to the

reaction until a homogeneous solution was obtained. The resulting liquids were cooled down slowly to 0 °C and small crystals suitable for X-Ray analysis were collected on the bottom of the reaction vial.

These systems and experimental conditions were designed to prevent two of the stronger interactions the fluoride anion can engage in. The ion pairing between potassium cation and fluoride anion is largely prevented by the presence of 18-crown-6 which coordinates the potassium and promotes the formation of a highly nucleophilic fluoride anion. The use of the liquid iodoperfluoroalkanes as solvents aimed at preventing the strong HBs typically formed by the fluoride anion with most common solvents. The formation of a “naked” fluoride anion ready to establish HaBs with the iodide is expected. Importantly, the obtained structures **1** and **2** match those previously reported adopting other potassium salts as KCl or KI^[26].

The crystal structures will be described in terms of their noncovalent interactions and corresponding normalised contact (Nc). In the structure **1** (space group R3m), the most notable interaction is the close contact between the iodine atom of 1-iodo-1,1,2,2,3,3,3-heptafluoro propane and the fluoride anion from KF. This HaB is remarkably short (2.543 Å, Nc = 0.76) and quite close to linearity (the C–I...F angle is 178.02°).

A single fluoride anion is surrounded by three iodine atoms from as many 1-iodo-1,1,2,2,3,3,3-heptafluoro propanes, the I...F...I angles are 106.45°. Another interaction involving the fluoride anion is the coordination with one potassium atom (the three K...F...I angles are 112.34°). The coordination of the potassium, as designed, is established mostly with the six oxygens of 18-crown-6.

This supramolecular array made by the potassium·18-crown-6 adduct and three 1-iodo-1,1,2,2,3,3,3-heptafluoro propane units then assembles in a complex two-dimensional architecture. Every 18-crown-6 molecule is surrounded, on the ring plane, by 6 1-iodo-1,1,2,2,3,3,3-heptafluoro propane units (Figure 2.1.3). From a supramolecular standpoint the crystal is then made of interacting layers where units of potassium·18-crown-6 alternates with F·(1-iodo-1,1,2,2,3,3,3-heptafluoro propane)₃. (Figure 2.1.3)

It is noteworthy that there are no HBs as neither the fluoride anion from KF nor the neutral fluorine atoms from the 1-iodo-1,1,2,2,3,3,3-heptafluoro propanes form any short contact with 18-crown-6 hydrogen atoms. Lastly, it is interesting to observe that the cocrystal present several C–F...F–C close contacts which might be either attractive or repulsive. The stabilizing effect of the quite short C–I...F HaBs is nevertheless remarkable enough to overcome the unfavourable effect of these latter interactions, if any.

The crystal structure of **2** (space group $C2/c$) presents similar close contacts, but also some important differences. In this structure the potassium cation is coordinated to the 18-crown-6 but also to two units of 1,4-diiodo-1,1,2,2,3,3,4,4-octafluoro-butanes

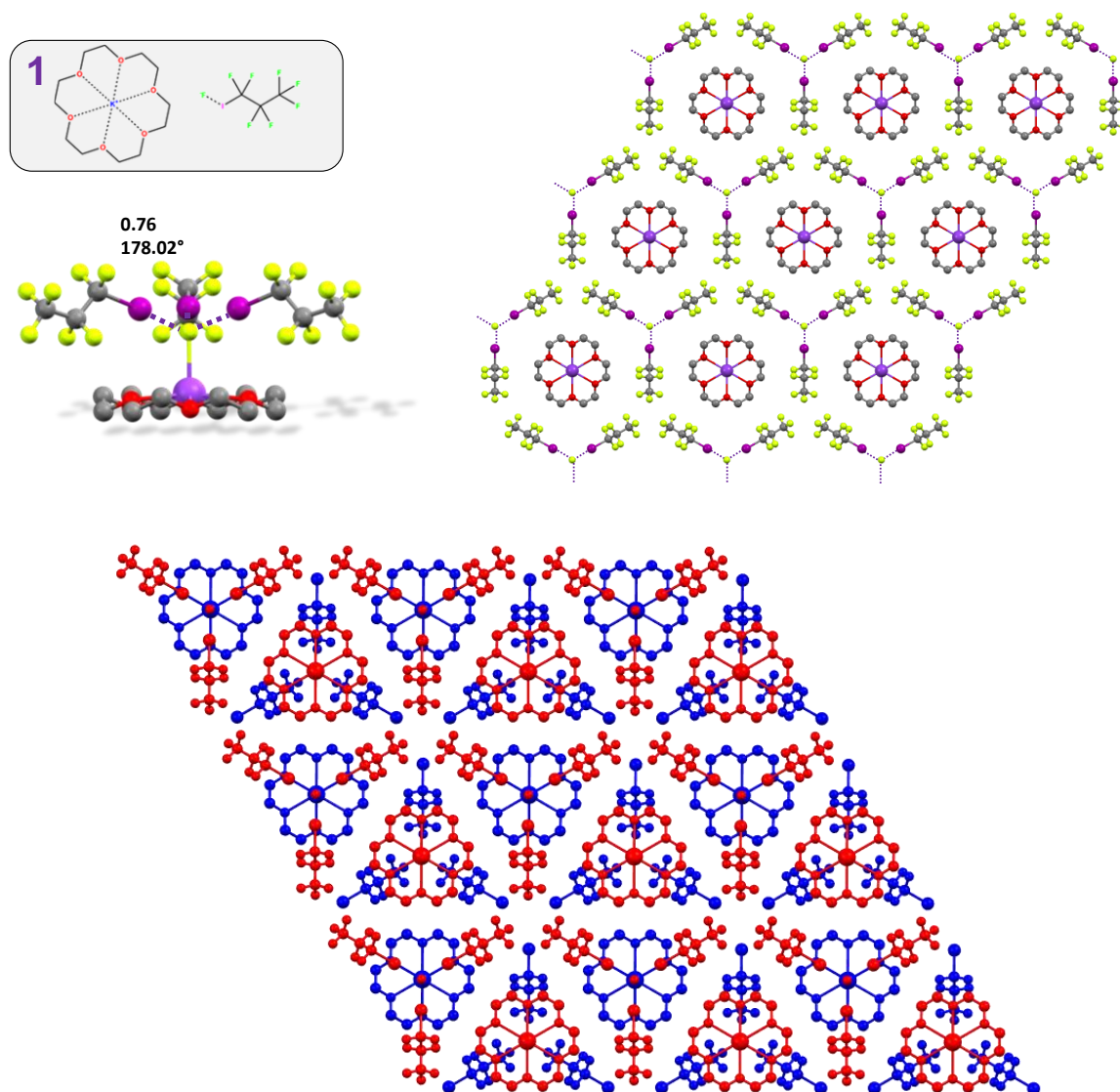


Figure 2.1.3. Ball and stick representation of the supramolecular structural unit (upper left), a layer (upper right) of alternating units of potassium·18-crown-6 and $F \cdot (1\text{-iodo-}1,1,2,2,3,3,3\text{-heptafluoro propane})_3$ and a colour coded self-assembly of two layers (blue bottom layer, red upper layer) in crystal **1**. Scheme of the compounds is boxed near the structures. HaBs are purple dotted lines. N_c of $I \cdots F^-$ separation and $C-I \cdots F^-$ angles are reported near the contacts. Hydrogen atoms have been omitted for clarity. Colour code: *gray* carbon; *lime* fluorine; *red* oxygen; *purple* iodine; *violet* potassium.

through four different K \cdots F close contacts, two from each side of the 18-crown-6 ring. The potassium atom is coordinated to ten different atoms, six oxygen atoms and four fluorine atoms of two different fluorobutyl chains. The stacking of 1,4-diiodo-1,1,2,2,3,3,4,4-octafluoro-butane and potassium \cdot 18-crown-6 adducts produces pillars extending along the *a* and *c* axes of the crystal. The fluoride anions are located between the pillars and it is possible to see some strong HaBs that seem to be largely responsible for holding together the pillars. There are two different 1,4-diiodo-1,1,2,2,3,3,4,4-octafluoro-butananes that engage in interactions with the fluorides, two are the already mentioned units that compose the pillars. This contact is remarkably close and linear, the distance being 2.552 Å ($N_c = 0.76$) and the C–I \cdots F angle being 178.22°. The remaining two units of 1,4-

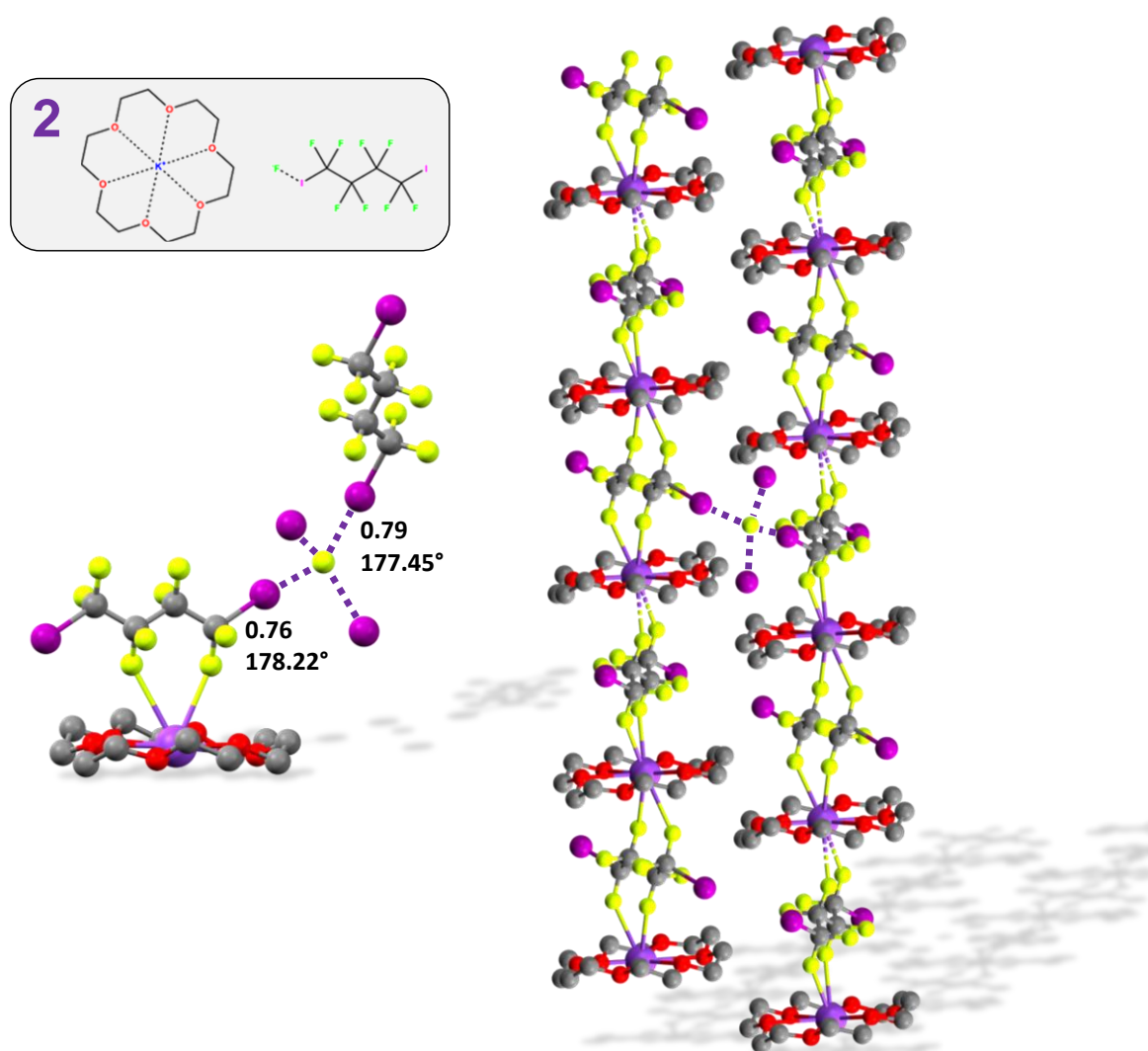


Figure 2.1.4. Ball and stick representation of the crystal structure of **2**, details of the HaB motif (left) and pillars assembling (right). Hydrogen atoms and 1,4-diiodo-1,1,2,2,3,3,4,4-octafluoro-butane units parallel to the pillars (right) have been omitted for clarity. Scheme of the compounds is boxed near the structures. HaBs are purple dotted lines. N_c of I \cdots F separation and C–I \cdots F angles are reported near the contacts. Colour code: gray carbon; lime fluorine; red oxygen; purple iodine; violet potassium.

diiodo-1,1,2,2,3,3,4,4-octafluoro-butanes are located roughly parallel to the pillars and engage in close contacts with the fluoride anions, each one establishing a close contact with two different fluorides.

These contacts are slightly longer (2.646 Å, $N_c = 0.79$) and less linear ($C-I\cdots F$ angle = 177.45°) than those previously discussed. HaBs are the shortest interactions in the structure and are likely playing a major role in determining the crystalline architecture. In both the structures obtained, the length and strength of the two HaBs can be at least partly attributed to the -1 charge of the fluoride anion.

The analysis of crystal structure **1** with Hirschfeld Surface analysis gives some additional information regarding the structure and the interactions. This analysis is seen as a complementary tool to the traditional “angles and length between atoms” approach. The Hirschfeld surfaces encompass most of the electron density of a molecule and can be useful to observe more subtle and weak effects in the solid state. The possibility of compute properties as the electrostatic potential over the surface can also bring some insights about the electron density distribution, being considered a rudimentary form of computational analysis.

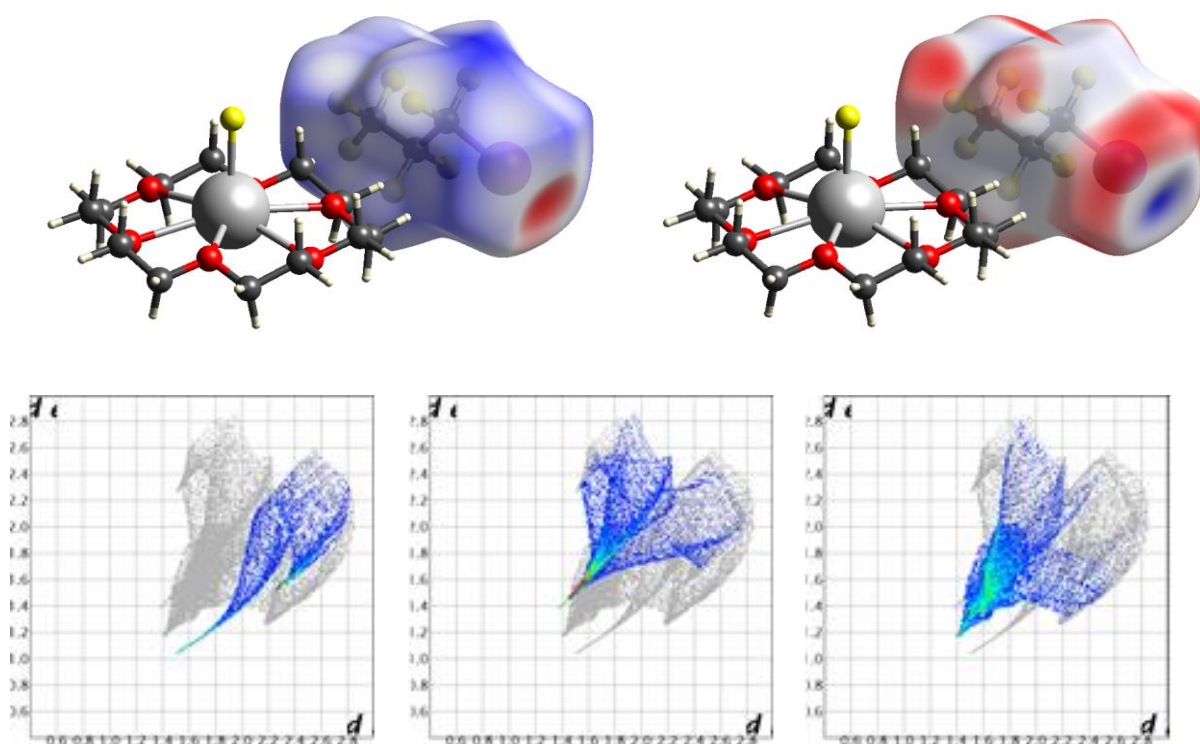


Figure 2.1.5. Above, Hirschfeld Surface of 1-iodo-1,1,2,2,3,3,3-heptafluoro propane in crystal **1**. Left, d_{norm} (red, short; blue, long), right, electrostatic potential (red, negative, blue, positive, white neutral). Below, Fingerprint plot (d_{internal} vs d_{external}) of the Hirschfeld surface. Left, I...F contribution, center F...F contribution, right F...H contribution.

For this work, both d_{norm} and the electrostatic potential have been considered. On the surface of 1-iodo-1,1,2,2,3,3,3-heptafluoro propane it is possible to see a small area located on the back end of the C–I bond. The d_{norm} parameter is much smaller than the rest of the surface, pointing out to a specific close contact between the iodide and the nucleophilic fluoride anion. This region corresponds to the positive region of the electrostatic potential plot, consistent with the definition of a HaB. The fingerprint plot of this surface reveals it as the closest contact on the surface. The electrostatic potential also identifies the negative region associated with the electronegative fluorides. The rest of the d_{norm} surface is represented by a large blue area, indicative of weak or absent interactions. It accounts for larger distances where the fluorine atoms and the negative belt of the iodine are located near the hydrogen atoms of the 18-crown-6. This portion of the surface could be associated with an interaction between the hydrogens of the cryptand and the fluorine atoms of the iodoperfluoroalkane.

Considering the fingerprint plot, it is possible to see that, even if F...H contributions account for a larger surface area, F...F contribution presents lower d_{norm} values. This comparison is considered particularly noteworthy, as an additional confirmation of the inability of the hydrogens of the 18-crown-6 cryptand to engage in HB with close nucleophilic species.

The surface of 18-crown-6 confirms the points discussed above, lacking any relevant interaction, except for the already discussed K...O coordination.

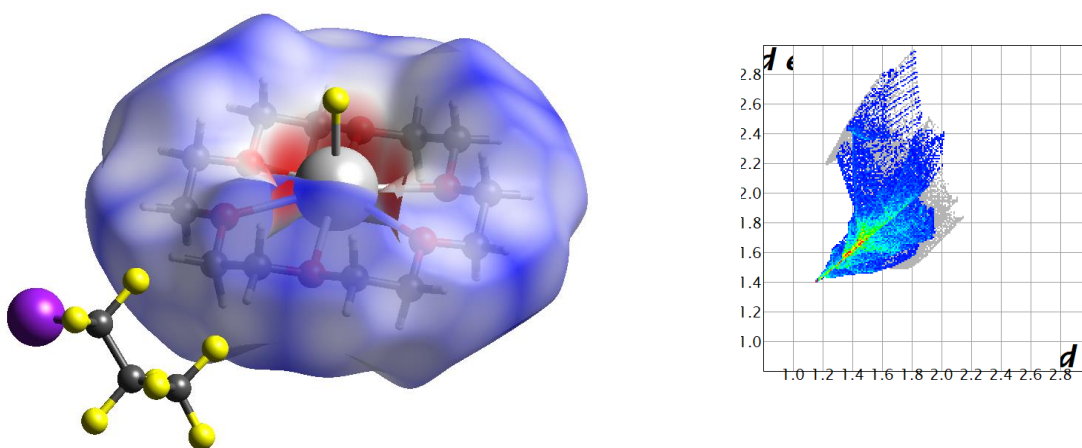


Figure 2.1.6. Hirschfeld Surface of 18-crown-6 as in crystal **1**. Left, d_{norm} , right Fingerprint plot of H...F contribution.

Both the crystal structure and the Hirschfeld surface analyses confirm that the more relevant interaction in this crystal is the I...F HaB and that this close contact likely plays a major role in determining the crystal packing. The analysis also reveals that, in the reported structures, there are no HBs between the hydrogen atoms of 18-crown-6 and the “naked” fluoride anion.

Importantly, specific reaction’s conditions have been identified allowing for the formation of cocrystals where non water molecule is hydrogen bonded to the fluoride anion also when potassium fluoride is handled in the air. The extensive use of this or similar crystallization conditions could in principle lead to a wide array of halogen bonded systems where “naked” fluoride anions are the donor of electron density. These systems may afford more detailed indications about the HaBs involving this halide anion.

Additional Data.

The experimental section contains CSD surveys, computational details and crystallographic data of the structures reported in this chapter.

References.

- [1] G. Cavallo, P. Metrangolo, R. Milani, T. Pilati, A. Priimagi, G. Resnati, G. Terraneo, *Chem. Rev.* **2016**, *116*, 2478–2601.
- [2] P. Metrangolo, G. Resnati, T. Pilati, S. Biella, in *Halogen Bond.*, Springer Berlin Heidelberg, Berlin, Heidelberg, **2008**, pp. 105–136.
- [3] C. C. Robertson, J. S. Wright, E. J. Carrington, R. N. Perutz, C. A. Hunter, L. Brammer, *Chem. Sci.* **2017**, *8*, 5392–5398.
- [4] G. Bliznakov, E. Kirkova, R. Nikolayeva, *Krist. und Tech.* **1971**, *6*, 33–38.
- [5] In unpublished results different attempts of obtaining an halogen bonded adduct between iodoperfluoroalkanes and a fluoride anion resulted in the formation of an HaB adduct with iodide anion formed after the decomposition of the iodoperfluoroalkane
- [6] M. S. Taylor, *Coord. Chem. Rev.* **2020**, *413*, 213270.
- [7] L. P. Wolters, P. Schyman, M. J. Pavan, W. L. Jorgensen, F. M. Bickelhaupt, S. Kozuch, *Wiley Interdiscip. Rev. Comput. Mol. Sci.* **2014**, *4*, 523–540.
- [8] J. W. Larson, T. B. McMahon, *J. Am. Chem. Soc.* **1983**, *105*, 2944–2950.
- [9] L. P. Wolters, F. M. Bickelhaupt, *ChemistryOpen* **2012**, *1*, 96–105.
- [10] Y. Marcus, *Biophys. Chem.* **1994**, *51*, 111–127.
- [11] K. Seppelt, *Angew. Chemie Int. Ed. English* **1992**, *31*, 292–293.
- [12] K. O. Christe, W. W. Wilson, R. D. Wilson, R. Ban, J. an Feng, *J. Am. Chem. Soc.* **1990**, *112*, 7619–7625.
- [13] M. K. Whittlesey, R. N. Perutz, B. Greener, M. H. Moore, *Chem. Commun.* **1997**, *2*, 187–188.
- [14] G. A. Olah, J. T. Welch, Y. D. Vankar, M. Nojima, I. Kerekes, J. A. Olah, *J. Org. Chem.* **1979**, *44*, 3872–3881.
- [15] R. Schwesinger, R. Link, G. Thiele, H. Rotter, D. Honert, H. -H Limbach, F. Männle, *Angew. Chemie Int. Ed. English* **1991**, *30*, 1372–1375.
- [16] B. K. Bennett, R. G. Harrison, T. G. Richmond, *J. Am. Chem. Soc.* **1994**, *116*, 11165–11166.
- [17] A. Kornath, F. Neumann, H. Oberhammer, *Inorg. Chem.* **2003**, *42*, 2894–2901.
- [18] R. Z. Gnann, R. I. Wagner, K. O. Christe, R. Bau, G. A. Olah, W. W. Wilson, *J. Am. Chem. Soc.* **1997**, *119*, 112–115.
- [19] K. O. Christe, H. D. B. Jenkins, *J. Am. Chem. Soc.* **2003**, *125*, 9457–9461.
- [20] F. Montanari, D. Landini, A. Maia, S. Quici, P. L. Anelli, *Am. Chem. Soc. Div. Pet. Chem. Prepr.* **1985**, *30*, 387–393.
- [21] C. L. Liotta, H. P. Harris, *J. Am. Chem. Soc.* **1974**, *96*, 2250–2252.
- [22] N. Ishikawa, T. Kitazume, T. Yamazaki, Y. Mochida, T. Tatsuno, *Chem. Lett.* **1981**, *10*, 761–764.
- [23] D. E. Barry, C. S. Hawes, S. Blasco, T. Gunnlaugsson, *Cryst. Growth Des.* **2016**, *16*, 5194–5205.

- [24] CSD Private Communication, CCDC Deposition Number 776799.
- [25] M. Mascal, I. Yakovlev, E. B. Nikitin, J. C. Fettinger, *Angew. Chemie - Int. Ed.* **2007**, *46*, 8782–8784.
- [26] A. V. Jentsch, D. Emery, J. Mareda, S. K. Nayak, P. Metrangolo, G. Resnati, N. Sakai, S. Matile, *Nat. Commun.* **2012**, *3*, 905.

3. The Chalcogen Bond at Work.

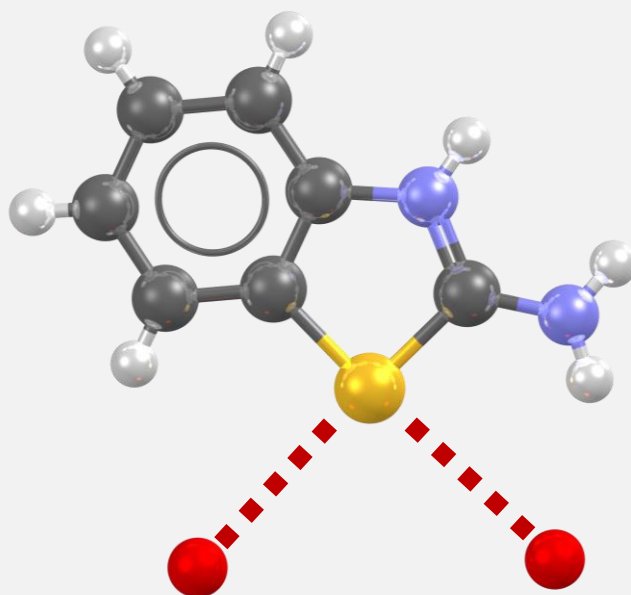


Figure 3. Intuitive representation of the geometrical features of a chalcogen bonded adduct displayed in 2-Amino-1,3-benzothiazol-3-ium dihydrogen-phosphate adduct (refcode DUSKAE). Molecules not engaging in ChB were omitted for clarity. Rendered by POV-Ray with metallic textures (ball and stick visualization).

A chalcogen bond (ChB) is defined as a net attractive force where an atom of group 16 of the periodic table acts as an electrophile. Chalcogen atoms are ubiquitous in drugs and bioactive compounds and many of these molecules form this interaction *in vivo* and/or *in vitro*. Many biochemical mechanisms have been proven to be influenced by this interaction. As an example, we mention the pivotal role of thiamine (vitamin B₁) in the conversion of glucose into energy in most living systems^[1]. Five-membered heterocyclic systems, e.g. thiazoles, are present in many drugs and metabolites thereof^[2]. They have attracted great attention in relation to ChB as they possess the optimal geometric conditions to engage in one or more of these interactions. In recent years a particular interaction motif composed by a nucleophile establishing a ChB *in tandem* with a HB in benzothiazole-like molecules has been explored and even proposed as a new supramolecular synthon^[3]. This interaction motif has proven apt to explain the biological activity of some drugs, e.g., ebselen, a compound endowed with anti-inflammatory, anti-oxidant and cytoprotective activity^[4]. The work of this chapter follows this mindset and expands on it by analysing two distinct classes of molecules endowed with applicatively useful profile, i.e., benzisothiazolinones and chalcogen containing cyanines.

3.1. Benzisothiazolinones as ChB Donors and their Structure-Functions Relationship.

My plan was all based on a very simple miscalculation

- Magnus Carlsen

Noncovalent interactions hold a central role in biochemistry^[5]. They are the basis of the lock-and-key processes of enzymes and are known to play a role in drug activity and selectivity^[6]. Nowadays, new potential drugs are being investigated not only on the basis of their chemical structure but also on the basis of their interactional landscape, e.g., via their Hirschfeld Surfaces^[7].

Ebselen is a prime example of how the chemical structure of the compound influences the noncovalent interactions *in vivo*. It in turn translates into a specific reactivity and pharmacological action. Specifically, the anti-inflammatory, antibacterial and cytoprotective actions of ebselen are all related to its molecular mechanism of action^[8].

Ebselen is known to irreversibly bind to the active site of many enzymes through its selenium atom, forming a strong selenylsulfide bridge^[9]. The formation of this S–Se bond occurs through the cleavage of the Se–N bond of the drug by the action of a cystine or a methionine^[10]. The drug has an extremely low cytotoxicity^[11] (LD₅₀ in rats > 4.600 mg/kg) and is used as a GPx mimic, its safety in humans being already evaluated^[12]. Moreover, ebselen is active against many RNA pathogens like HCV^[13], HIV^[14], and Sars-Cov-2.

Recent computational calculations and experimental evidences^[4,15] brought to the discovery that ebselen likely first binds to the substrate by simultaneously establishing a ChB and a HB with the target enzyme (Figure 3.1.1.). This binding causes a lengthening and subsequent breaking of the Se–N bond.

The ability of the benzoselenazole moiety to act as ChB donors is already established, and a large set of drugs structurally related to ebselen features a mechanism of action similar to that sketched below.

Ebsulfur is the sulfurated analogue of ebselen. It is expected to show a tendency to display ChBs in a similar, yet reduced, manner with respect to ebselen^[16].

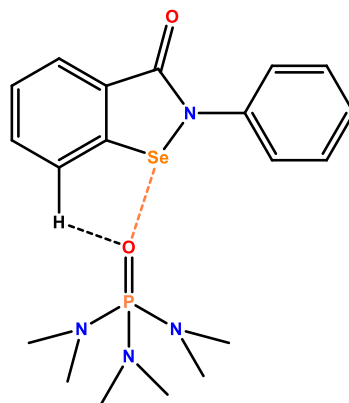


Figure 3.1.1. Proposed interaction mechanism of ebselen and hexamethylphosphoramide, a model system for nucleophilic sites in the target enzyme.

As a confirmation of this expectation, it has to be noted that the structures present in the CSD containing ebselen all show close and linear C–Se···nucleophile contacts consistent with the definition of ChB, while this is not always the case for ebsulfur and its analogues^[17].

That said, medical literature provides convincing evidence that the ebsulfur mechanism of action is quite similar to that of ebselen. Ebsulfur in low concentrations can act as a weak peroxidase mimic to remove reactive oxygen species (ROS), but also irreversibly bind and oxidise the active sites of different enzymes^[18]. Perhaps counterintuitively, in high concentration the irreversible binding of ebsulfur to ROS scavengers leads to an intracellular increase of the ROS which ultimately lead to microbial death^[19].

When the phenyl ring is substituted with less sterically bulky groups, the cytotoxic activity of the drug is enhanced even more. Benzisothiazolinones are possibly the most widely used biocides added to industrial products^[20], able to display enzymatic inhibition and, in turn, antimicrobial activity over a wide range of organisms^[21–23].

The most commonly used member of this family, 1,2-benzisothiazol-3(2H)-one (BIT in the following) is routinely used in food packaging^[24] and it is commonly added to many industrial products like laundry^[25] and dish detergents^[26], adhesives^[27], lubricants and even sunscreens. Being a cyclic sulfenamide, it is analogous in its biochemical effects to other related commercial products like Captan or Folpet (whose X-Ray structures show strong ChBs^[28]).

It has to be noted that the 1,1-dioxide relative, saccharin^[29], is a synthetic sweetener that poses little to no threat to humans^[30]. In the same fashion, sulfonamides are widely used fungicides and pesticides that, while possessing a mechanism of action

that involves the cleavage of the S–N bond, are relatively safe for human consumption due to lack of the dihydropteroate synthetase enzyme^[31], the latter having a key role in bacterial replication.

All those information depict an extraordinarily rational picture where the strength and presence of ChBs (possibly aided by the HBs) are a prerequisite for triggering the reactions of interest. To test this hypothesis and gain some additional understanding on the behaviour of some of these compounds, a number of benzisothiazolinone derivatives have been synthesized (in collaboration with Prof. Viani's Group), characterized and crystallized. The interactional landscape has been evaluated and, in some cases, compared to the biocidal activity of the compound. A survey on the CSD has been performed in order to confirm the trends highlighted by the study of the structures also on a statistical basis. This work may help in better establishing the ability of this class of compounds to work as ChB donors and it may provide better instruments to forecast the biochemical activity of these biocides and improve the design of new ones, as well as providing convincing evidences that this supramolecular synthon can be considered an additional tool in supramolecular chemistry.

The synthesis and characterization of benzisothiazolinones adduct has been reported elsewhere^[32]. Most of them formed small and poorly diffracting crystals, hence a synchrotron radiation source was employed to obtain high quality diffraction data. To better assess the correlation between the structure of the compounds and their most reliable mechanism of action, the X-ray crystal structure of six BIT derivatives (Figure 3.1.2) has been obtained. BIT derivatives might show the presence of the same supramolecular synthon highlighted previously for ebselen and various ebsulfur derivatives. The invariable presence of corresponding interactions would confirm the electrophilic nature of the sulfur atom when conveniently activated by the presence of strong electron withdrawing substituents and its potential role in the mechanism of action of these biocides. The derivatives considered hereinafter bear different functional pendant groups at nitrogen (Figure 3.1.2) and possess a wide range of polarities and electron-withdrawing ability, from the allyl to the carboxymethyl group. Their effects on the strength and geometry of the interaction will be discussed.

Consistent with our assumptions, all crystals obtained display short ChBs. In all of the structures considered the electron donor is an oxygen atom, quite often it is the carbonyl oxygen of the isothiazolinone ring. In all structures one interaction occurs on the extension of the N–S covalent bond, and in some structures a second ChB is formed on the extension of the C–S bond. The higher electron withdrawing ability of the nitrogen atom with respect to the carbon atom (possibly enhanced by the partial positive character of the nitrogen atom in the resonance structure of the amide) may be responsible for this preference.

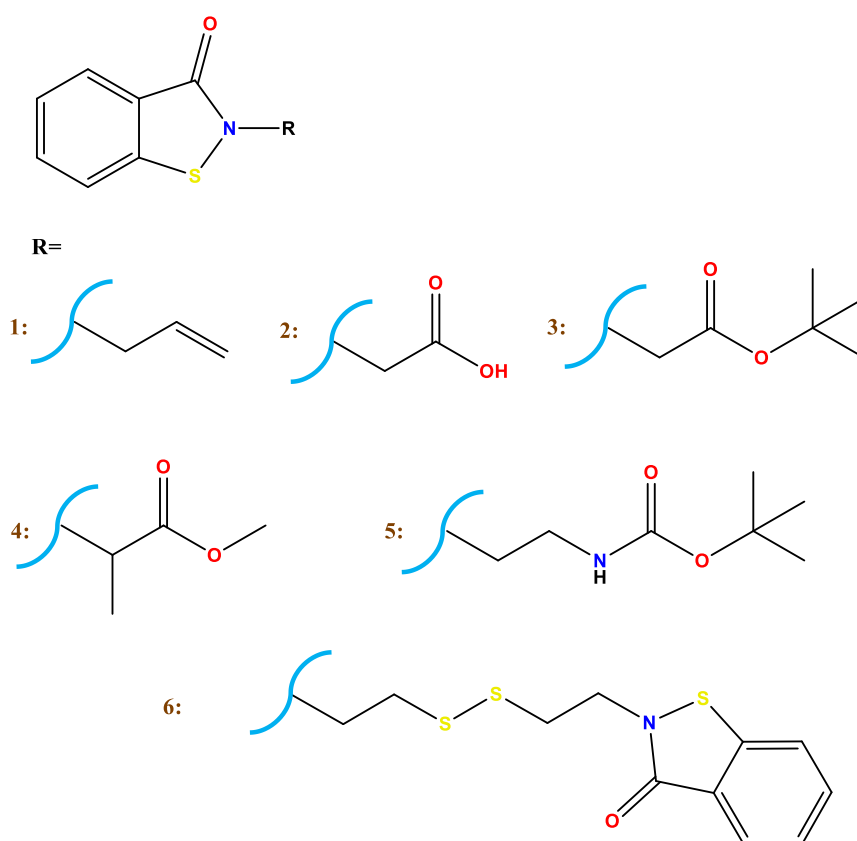


Figure 3.1.2. Structural schemes of the BIT derivatives considered in this paragraph. The different pendant at nitrogen are listed at the bottom of the figure.

The formation of the ChB on the extension of the N–S bond is probably favoured by the concomitant formation of an HB involving the hydrogen atom in *peri*-position. Surprisingly, since the effects of cooperative (or competitive) interactions usually leads to less linear close contacts, the HB in this case helps in establishing very linear N–S⋯O angles, given the optimal geometry of the system.

The X-ray single crystal structure of compound **1** (Figure 3.1.3) crystallizes in the space group $P2_1/c$, with the asymmetric unit containing only one molecule. It is possible to see a fairly short (2.720 Å, corresponding to an Nc of 0.82) and linear (N–S⋯O angle 174.76°) ChB established between the carbonyl group of the ring and the sulfur atom. The carbonyl oxygen atom in this interaction is also pinned down to its position by an HB with the hydrogen atom in *peri* position on the aromatic ring (Figure 3.1.3, left). The crystal packing is further stabilised along the *b* axis of the crystal by C–H⋯ π contacts between the methylene unit and three aromatic carbons of another molecular entity. Since every single molecular entity engages in two different ChB, one as the acceptor and one as the donor of electron density, the molecules arrange in an infinite and chalcogen bonded

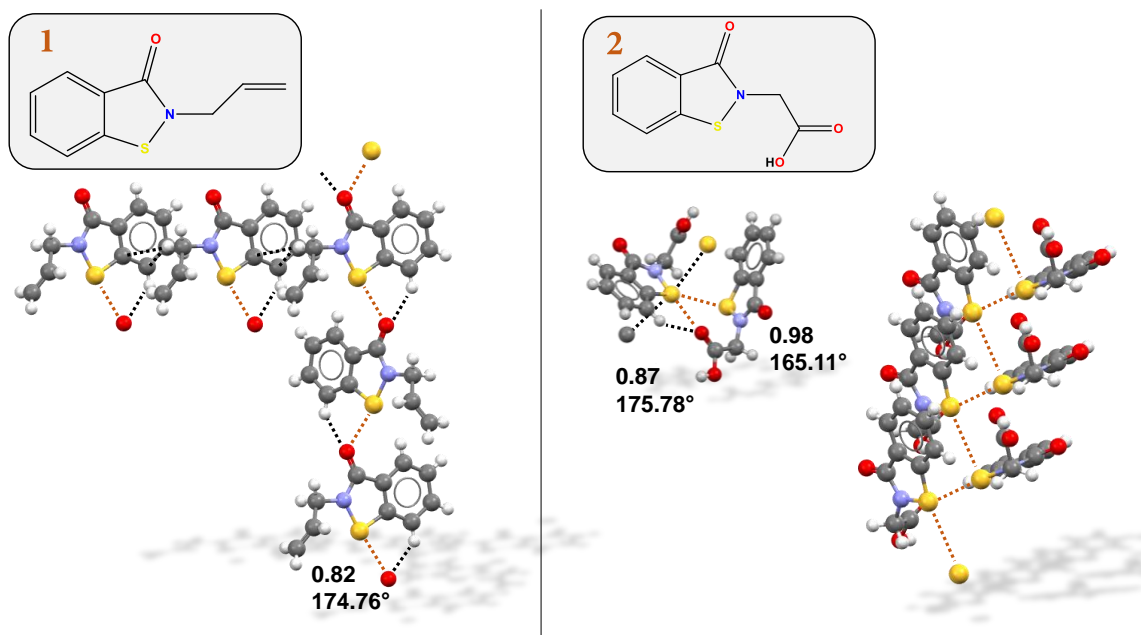


Figure 3.1.3. Crystal packing of structures **1** (left, infinite ChB chain and C–H \cdots π contacts) and **2** (right, tetratopic sulfur contacts and infinite ChB chain). Scheme of the compounds is boxed near the structures. ChBs denoted as ochre dotted lines. HBs and other interactions are black dotted lines. Nc of S \cdots Nu separation and N/C–S \cdots Nu angles are reported near the contact. Colour code: *gray* carbon; *whitish* hydrogen; *light blue* nitrogen; *red* oxygen; *yellow* sulfur.

chain along the *c* axis of the crystal. It is noteworthy that this compound displays a very effective antibacterial activity (the second most active compound between a library of twenty-eight derivatives) and one of the strongest ChB observed in this work. While other factors must be taken into account when evaluating the biological action of this class of compounds, most notably their lipophilicity, this parallel is interesting.

The crystal structure of **2** crystallizes instead in the $P 2_12_12_1$ space group, once again containing only one molecule in its asymmetric unit (Figure 3.1.3, right).

In this structure, the sulfur atom acts as a tetratopic supramolecular site. It is possible to observe two ChBs located along the extension of the two covalent bonds of the atom. One oxygen of the carboxylic group is located along the extension of the N–S bond. Consistent with the trends highlighted previously, this ChB is both stronger (S \cdots O distance 2.876 Å, Nc 0.87) and more linear (N–S \cdots O angle 175.78°) than the second ChB.

The nucleophile is also held in position by a HB, whose length is approximately 2.587 Å. The sulfur atom of the benzisothiazolinone unit already engaged in the above-described ChB forms a fairly long and poorly linear C–S \cdots C contact (S \cdots S distance 3.516 Å, Nc, 0.98, C–S \cdots S angle 165.11°). The chalcogen bonded sulfur atom also engages in two additional interactions after an orthogonal geometry. One interaction is an S \cdots S contact like that described above (but in this latter case the sulfur acts as the nucleophile) and the

other one is a S...C contact involving an aromatic carbon. This complex interaction pattern results in a parallel, infinite stacks of molecular units, forming infinite chains in a seesaw conformation that grow orthogonal to the stacks already described.

The *tert*-butyl derivative **3** (Figure 3.1.4, left) crystallizes in the Pbc_a space group, this time with two distinct units in the asymmetric unit. The first unit self-assembles in an infinite chain driven by a very short and linear ChB (2.610 Å, Nc 0.79) with the most linear angle presented in this section, 176.58°. Once again, an HB with the hydrogen in *peri* position on the benzofused ring is also present. The units are piled approximately orthogonal to the *b* axis of the crystal, forming repetitive voids that are filled with the second molecular entity present in the asymmetric unit, possibly stabilising their position thanks to the proximity of the aromatic units. These new set of molecules still engage in HB-aided ChB but present a completely distinct set of geometrical features. The interaction involves here the carbonyl oxygen of the carbalkoxy group in the pendant at nitrogen. This interaction is longer and less linear than that described above (S...O distance 3.20 Å, Nc 0.96, N-S...O angle 163.0°). The oxygen engaging in the ChB is still aided by an HB involving the -NCH₂-hydrogen atoms.

The three crystal structures described in the following display somewhat less linear ChBs. The crystal structure of the methyl-2-propanoate derivative **4** (Figure 3.1.4, right), for example, crystallizes in the group space P2₁/n, where two distinct molecules are present in the asymmetric unit.

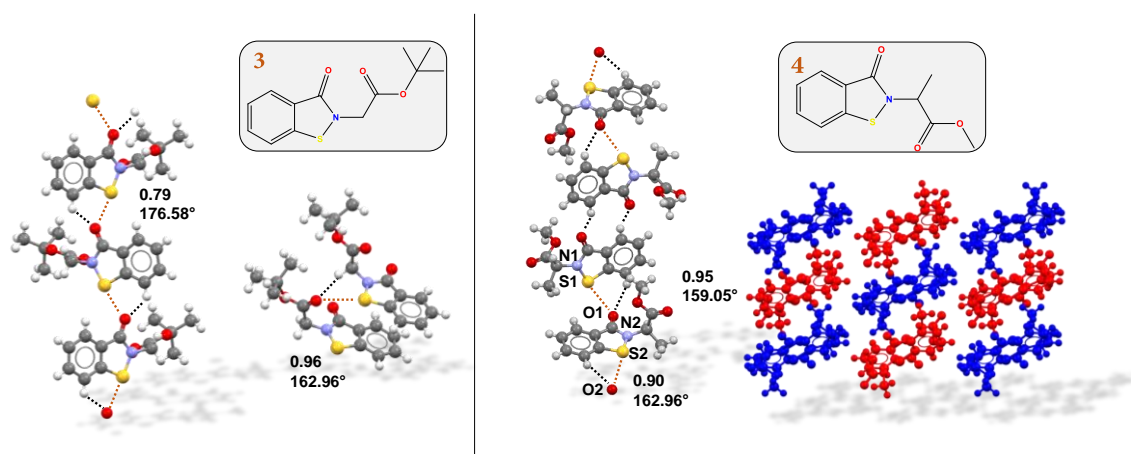


Figure 3.1.4. Infinite chains formed by **3** (left, infinite ChB chain and detail of the second ChB) and **4** (right, example of an infinite chain and spatial distribution of the two molecular units in the cell, coloured). Scheme of the compounds is boxed near the structures. ChBs denoted as other dotted lines. HBs and other interactions are black dotted lines. Nc of S...Nu separation and N/C-S...Nu angles are reported near the contact. Colour code: *gray* carbon; *whitish* hydrogen; *light blue* nitrogen; *red* oxygen; *yellow* sulfur.

The two set of molecules engage in different ChBs, forming a complex infinite seesaw chain also involving HBs.

The infinite chains are very close to each other thanks to a series of S $\cdots\pi$ and C $\cdots\pi$ interactions that further stabilize the crystal, aided by a number of HBs involving the carbonyl oxygen. The high number of competitive interactions in this case make the ChBs less linear and longer (e.g., S1 \cdots O1 distance 3.136 Å, Nc 0.95, N1–S1 \cdots O1 angle 159.05°; S2 \cdots O2 distance 3.002 Å, Nc 0.90, N2–S2 \cdots O2 angle 162.96 °). The HB with the *peri* hydrogen is retained in both molecules of the unit cell.

The interaction landscape of compound **5** (2-*tert*-butyl ethylcarbamate derivative, Figure 3.1.5 left) features a large number of short contacts consistent with the higher complexity of the substituent. The single molecular entity in the asymmetric unit crystallizes in the group space P2₁/n and self-assembles once again in infinite chains formed by ChBs involving a carbonyl oxygen and the sulfur atom of two different molecules. The C–S \cdots O interaction is longer and less linear than in structurally simpler benzisothiazolinones (distance 2.874 Å, Nc 0.86, angle 167.53°) and the HB involving the *peri* hydrogen is once again retained for this molecule. Different from the other described derivatives, however, this particular chain is formed involving the carbonyl in the nitrogen pendant. Every unit engages in two different HB-aided ChBs, one as a donor and one as the acceptor, roughly on the same side of the molecule and a complex and 3D architecture is produced. Along the *b* axis, in addition, infinite layers of parallel-oriented molecular units are formed, firmly held together by H \cdots S and H \cdots O HBs, where the partners are a methylene hydrogen and the sulfur or a carbonyl oxygen, respectively.

The last compound, **6** (Figure 3.1.5, right), presents a peculiar crystalline architecture that differs significantly from those already described above. This crystal structure actually resembles that of compound **1** (Figure 3.1.3 left) as it allows for the formation of antiparallel infinite chains driven by the formation of HB-aided ChBs. The presence of a second benzisothiazolinone covalently bound through a disulfide bridge allows **6** to engage in two identical interactions between the two sulfur atoms and the carbonyl oxygens of other units. Given the structural complexity of the system, this interaction is neither particularly strong (2.884 Å, Nc 0.87) nor linear (160.09°). Each molecule (crystallising in the group space C2/c) is therefore engaging in four different HB-aided ChBs, two as the donor and two as the acceptor. The sulfur of the disulfide bridge do not engage in any interaction, further confirming the importance of the electron withdrawing effect of the N–C(O) group in determining the ChB donor potential of BIT systems.

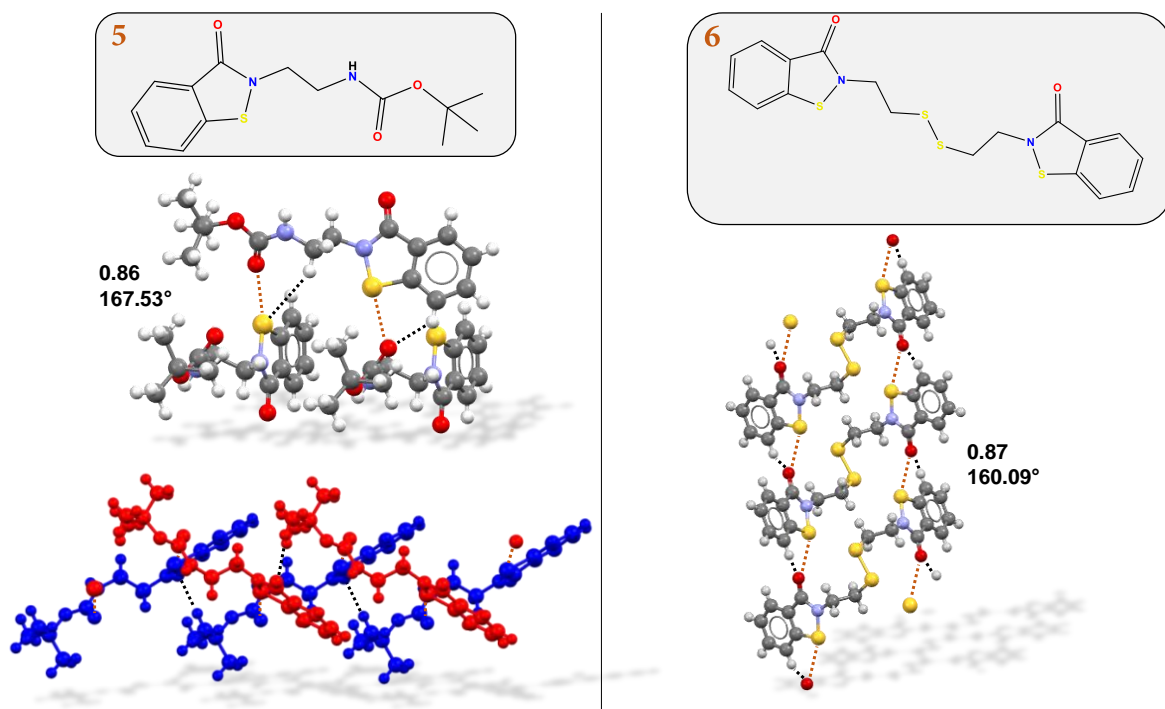


Figure 3.1.5. X-Ray crystal structures of compounds **5** (left, detail of ChB and infinite ChB chain, coloured) and **6** (right, infinite ChB chain). Scheme of the compounds is boxed near the structures. ChBs denoted as other dotted lines. HBs and other interactions are black dotted lines. Nc of S...Nu separation and N/C-S...Nu angles are reported near the contact. Colour code: *gray* carbon; *whitish* hydrogen; *light blue* nitrogen; *red* oxygen; *yellow* sulfur.

The ability of this class of compounds to engage in the interaction of interest has also been assessed through a statistical analysis performed of the CSD. As of 2021, 1166 structures (hits) are present in the database where a sulfur atom is covalently bound to a nitrogen. A subset of 423 structures, (36%) present a short contact between the sulfur and a nucleophilic atom (Nu), even if this is not enough to consider the interaction a ChB, since linearity - the second important feature of this interaction - is not taken into account. A smaller group of structures meet the criteria of N-S...Nu and/or C-S...Nu angles higher than 160°. Specifically, 118 structures fulfil this angular requirement on the extension of the N-S bond, 109 on the extension of the C-S bond, 36 on both extensions.

By contrast, survey on tetrahydrothiophene ring (Query 2 of Figure 3.1.6.) still brings out a comparable (1152) number of hits, but the percentage of structures engaging in the interaction decreases to about a half (192 hits, 16%). The percentage of linear contacts along the two C-S covalent bonds seem to be roughly the same and the number of structures involved in both contacts is 40, more than 50% of both the hits of the single queries. This highlights the fact that the actual number of structures engaging in the two C-S...Nu linear contacts largely overlap between the two subsets.

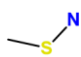

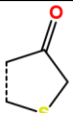
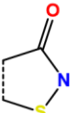
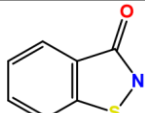
Query	Fragment	Hits	Contacts involving S	N-S...Nu angle > 160°	C-S...Nu angle > 160°
1		1166	(423) 36%	(154) 36%	(145) 34%
2		1152	(192) 16%	(62) 32%	(78) 40%
3		155	(20) 13%	(5) 25%	(11) 55%
4		84	(41) 48%	(28) 68%	(5) 12%
5		44	(26) 59%	(21) 81%	(2) 7%

Figure 3.1.6. Statistics of the CSD survey regarding the occurrence of ChBs in various chemical moieties. The considered nucleophilic species are N, P, O, S, Se, F, Cl, Br, I. Percentages in red are weighted on the third column (hits). Percentages in blue are weighted on the fourth column (contacts involving S).

These two queries suggest that the tetrahydrothiophene ring by himself has a reduced ability to form ChBs with respect to the isothiazolinone system and the statistics related to the 3-oxo subset (query 3) support this conclusion. In particular, this query indicates that the less common presence of ChBs in thiophene systems is more likely a consequence of the absence of electron withdrawing residues bound to sulfur than of the absence of a nucleophilic site in the systems. An in-depth look at the specific hits engaging in ChBs of Query 2 seem to holistically confirm this hypothesis (the list is given in the experimental section).

The introduction of the nitrogen atom in position 2 of the ring produces major differences in the statistics. The sulfur atom engages in interaction with a nucleophile in 41, namely near a half, of the 84 structures containing the isothiazolinone moiety present in the CSD (Query 4). In 28 of them (about 70%) the N-S...Nu angle is > 160°. 44 structures in the CSD contain the benzisothiazolinones ring systems (query 5), 26 of them (59%) present an interaction with a nucleophile and in 81% of them the interaction occurs along the extension of the N-S bond. 18 of the 21 structures engaging in a ChB are also engaged in a HB with the hydrogen in *peri*- position on the ring, and in the remaining

three the nucleophile maintain the correct angular features of the interaction but is located at a distance just slightly higher than the sum of van der Waals radii.

In conclusion, in the present section it was possible to display the inherent ability of benzisothiazolinones to act as donors of ChBs, the carbonyl moiety present on the isothiazolinone ring frequently acting as the acceptor site. This conclusion was also corroborated by a statistical analysis of the CSD. The non-minor ChB donor ability of the sulfur atom and the ChB acceptor ability of the isothiazolinone carbonyl group are confirmed and also the important role of the benzofused ring to act as a source of ancillary HB useful to act synergistically with the ChB is highlighted. This interaction is known to play a role in the self-assembly of other related classes of azoles (e.g., thiadiazoles and thiazolium salts) and in the mechanism of action of related sulfur and selenium containing drugs (e.g. ebselen). The HB-aided ChB may represent the first step of a specific biological activity leading to the inhibition of specific enzymes crucial for bacteria replication. It is interesting, in this regard, that the only compound to display strong enzymatic inhibition between the library of compounds presented is the N-allyl substituted derivative **1**, the only compound bearing a lipophilic substituent at nitrogen, similar to ebsulfur or ebselen.

Additional Data.

The experimental section contains synthesis and characterization of all the compounds, crystallographic details and the full list of entries in the CSD surveys.

3.2. Chalcogen Bond Drives the Packing of Cyanine Crystals.

Similar to other non-covalent interactions, a tailored design of the target compounds (*i.e.* the foresight of the different forces that may play a role in the formation of the crystalline architecture) is of prime importance in the pursuing of crystal structures that are able to display strong ChBs.

ChBs seem to arise with particular ease in structures bearing benzothiazolium and benzoselenazolium moieties^[3,33]. Both steric and electronic reasons may be responsible for this behaviour. Similar to the benisothiazolinones discussed above, the inclusion of the chalcogen atom in a ring allows for exposing to the nucleophile approach an atom surface larger than when most acyclic compounds are used. Most important, the nitrogen alkylation provides a strong electron attractive group which distorts the electron density distribution in the ring and boosts the chalcogen atom electrophilicity. Interestingly, the thiazole and selenazole moieties are ubiquitous in drugs^[34] and there is evidence suggesting the role of ChB in their mechanism of action^[35] and many compounds endowed with useful applications, spanning from drugs to dyes, contain a benzothiazolium or benzoselenazolium moieties.

From the supramolecular point of view, chalcogenazolium compounds can be considered as analogues of halonium salts^[36,37]. The geometric and electronic features of the interactions involving the two types of arrays present some similarities which translates into similar HaB and ChB patterns, namely into similar topology of σ -hole interactions. In compounds like diphenyliodonium or diphenylbromonium cations a recurring short contact between the halogen atom and a nucleophile (most often the counteranion) can be seen (Figure 3.2.1).

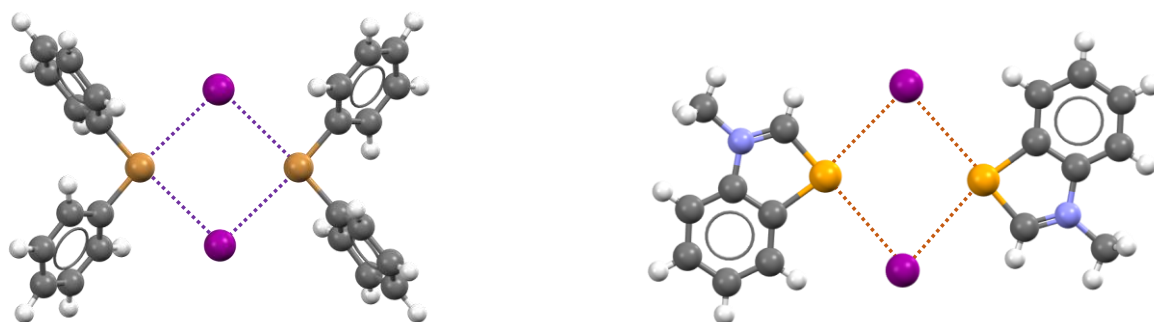


Figure 3.2.1. Schematic representation of the similar interaction motives present in diphenylbromonium (refcode DOHYII) iodide and 1-methyl benzoselenazolium iodide . HaBs are purple dotted lines, ChBs are orange dotted lines.

As to halonium salts, although the entire surface of the halogen is positive, it is most positive along the extension of the C–halogen covalent bonds. Computational investigations, carried out in collaboration with P. Politzer, demonstrated the anisotropic electron distribution around the chalcogen atom in chalcogenazolium cations.

Two σ -holes are present on the extension of the C–chalcogen covalent bonds. These σ -holes were more pronounced for selenium than for sulphur, consistent with the general tendency for heavier and more polarizable elements to show more positive and more extended σ -holes. Once again in supramolecular analogy with halonium salts, the possibility for chalcogenazolium compounds to form two ChB opens the possibility of organizing crystalline architectures with 1D, 2D and 3D patterns.

CSD surveys prove the marked tendency of chalcogenazolium derivatives to routinely engage in ChB with nucleophiles. A large number of molecules bearing this moiety engage in interactions with nucleophiles and the linearity of said interactions is preserved for a vast majority of them^[38].

A class of compounds of particular interest bearing such moieties are cyanines^[39,40]. Designed more than a century ago as photosensitizers, these derivatives found applications in many fields of industrial and medical relevance^[41] as dyes and fluorescent contrast agents for cancer detection, respectively^[42,43].

A sulphur atom is frequently present in cyanines to improve their water solubility. Cyanine salts wherein a benzothiazolium or benzoselenazolium moiety is linked to another heterocyclic or carbocyclic moiety through a methine chain are extensively employed in different fields. A better understanding of the ChBs involving benzochalcogenazolium moieties might contribute to a better understanding of the processes these compounds are employed for and might provide a new rational tool in their design.

In this section we analyse four cyanine cations, differing from each other in the number of their methine groups and in the nature of their chalcogen atom. Three of them contain two benzothiazolium moieties and one possesses one benzothiazole and one benzoselenazole system. The cations were paired with different counterions, specifically iodide, bromide, perrhenate and nitrate.

These anions invariably engaged in ChB with the cation. The ability of ChB to allow for the formation of small adducts and infinite 3D architectures is displayed. The different strength of sulfur and selenium based ChBs were analysed in particular for compound **8** (See Figure 3.2.2),

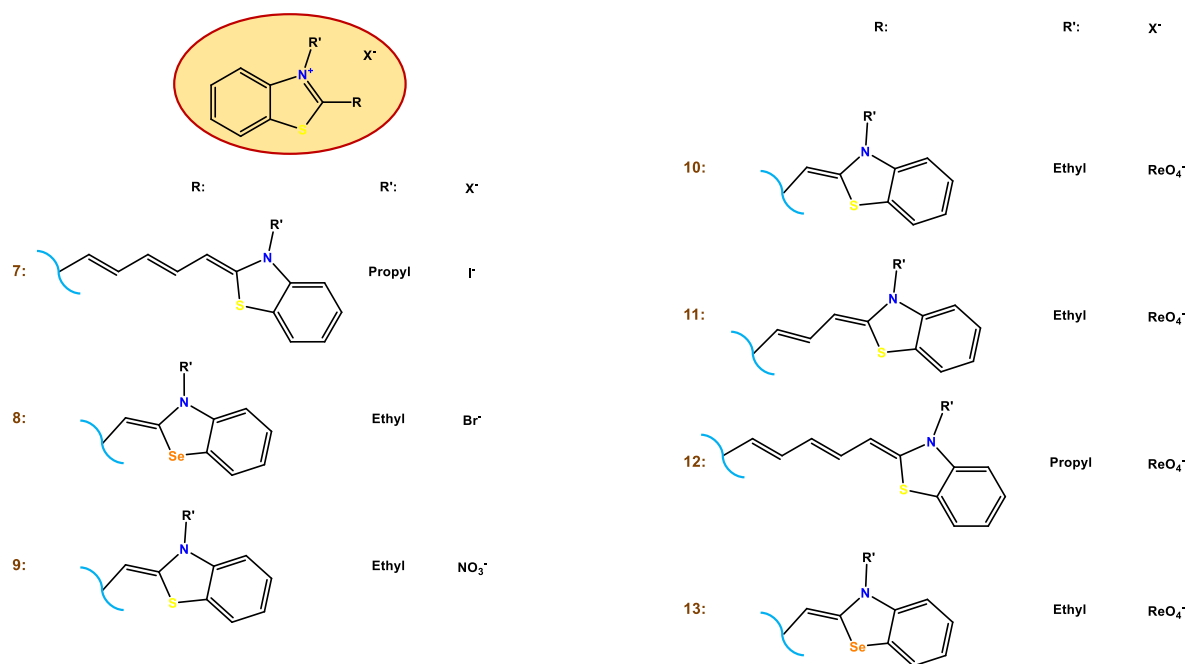


Figure 3.2.2. Structural schemes of the cyanine dyes considered in this paragraph. The different pendant are listed at the bottom of the figure.

While the pairing of sulfur based cyanines with nucleophiles of different strength provides information about the competition between ChB and π - π interaction in driving the crystalline architecture. This is a particularly interesting aspect considering that π - π stacking was for a long time considered one of the primary aggregation features responsible for the properties of said compounds.

Computational studies. To better evaluate the presence of areas of depleted electron density on the surface of the compounds analysed herein, *in silico* studies on the electrostatic potential of model compounds were carried out. In particular, in collaboration with P. Politzer's group, the electrostatic potential on 0.001 au cationic surfaces of some benzothiazolium and benzoselenazolium molecules were computed. Geometry optimizations were carried out using Gaussian 09, with the hybrid meta density functional M06-2X and the 6-311G(d) basis set. The WFA-SAS code was used to compute the electrostatic potential on 0.001 au cationic surfaces.

A graphical representation of the model structures is reported in Figure 3.2.3. The most positive values of the electrostatic potential, reported as $V_{s, \max}$ are almost invariably located along the extension of the C–Ch covalent bonds. While the MEP is positive on the entire surface of the examined systems, as expected for a cation, the benzofused ring possesses a poorly positive area.

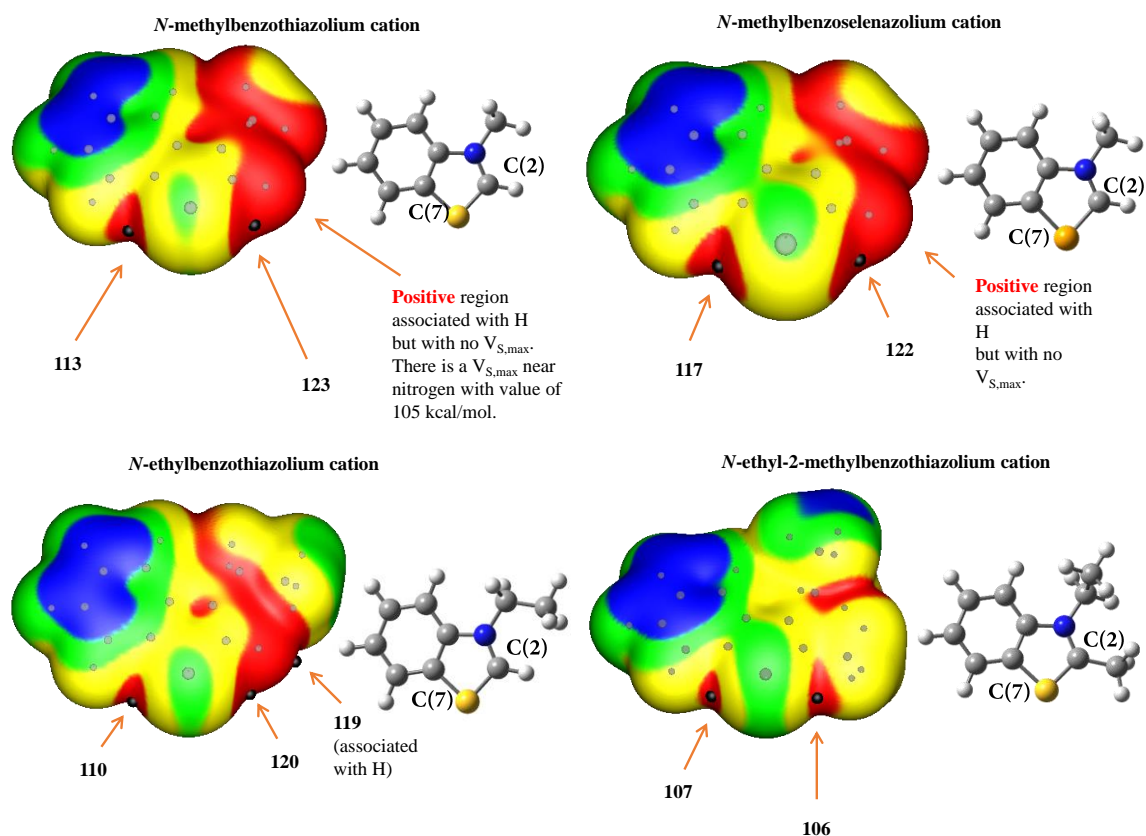


Figure 3.2.3. Molecular electrostatic potential calculated over the 0.001 au surface of different benzothiazolium and benzoselenazolium cations. Color ranges for all plots are, in kcal/mol: red, greater than 100; yellow, between 100 and 85; green, between 85 and 75; blue, less positive than 75. The most positive values of $V_{s(r)}$, the $V_{s, \text{max}}$, near the sulfur and selenium atoms are shown as black hemispheres and their values are given, in kcal/mol.

In *N*-methylbenzothiazolium cation, for example, the least positive values can be found on this portion of the surface and span approximately from 85 to 75 kcal/mol. In contrast, on the thiazolium moiety two areas with MEP values higher than 100 kcal/mol are present, at the center of them two distinct $V_{s, \text{max}}$ can be found. The first one has a value of 113 kcal/mol and is located approximately on the extension of the C(2)–S bond (the C(2)–S \cdots V $_{s, \text{max}}$ angle is about 163°). The second positive area in this particular structure is not located precisely along the extension of a covalent C–S bond, but instead is spread over a larger region of the surface, likely resulting from the contributions of the C–S bond and the acidity of the hydrogen in position 2. This maximum is 123 kcal/mol and establishes a C(7)–S \cdots V $_{s, \text{max}}$ angle of 151°. The deviation from linearity in these structures are not at all unexpected, as the lone-pairs on the chalcogen atom affect the overall distribution of the electron density in the thiazolium ring and displaces the position of the σ -holes. The electrostatic potential at the surface of *N*-ethylbenzothiazolium cation is similar to the *N*-methyl analogue described above. In particular, the two $V_{s, \text{max}}$ of both structures are analogues (display values close to 110 and 120 kcal/mol, respectively) and

lay on the approximate extension of the covalent C–S bonds. In the *N*-ethylbenzothiazolium cation the C–S \cdots V_{s, max} angles are 165 and 152°. In addition, for *N*-ethylbenzothiazolium it is possible to find a third V_{s, max} to be associated with the acidic hydrogen in position 2. This maximum has a value of 119 kcal/mol, incidentally providing a useful comparison between the effect on the MEP of σ -holes and fairly acidic site. In *N*-ethyl 3-methylbenzothiazolium, the last thiazolium structure considered in this part, the two V_{s, max} are still clearly visible and are less positive, measuring 107 and 106 kcal/mol. These two regions present much more linear C–S \cdots V_{s, max} angles in respect to the two previously reported compounds. The surface of this third compound presents, in addition to the benzofused ring, a second less positive area around the *N*-ethyl region.

Computational analyses were carried out also for a benzoselenazolium model compound, allowing for a useful comparison with the benzothiazolium systems. The *N*-methylbenzoselenazolium cation presents features quite similar to those discussed above for the *N*-methylbenzothiazolium cation, the only notable difference is the V_{s, max} values. The potential at the most positive sites located on the extension of the covalent bonds are 117 and 122 kcal/mol; as expected, they are a bit more positive than those present in the sulfurated analogue. Summarizing, it can be stated that the calculations nicely complements the experimental observation of the X-ray structures presented hereinafter. In benzothiazolium and benzoselenazolium moieties there are two maxima located on the extension of the C–Ch covalent bonds and their position is influenced by all the closeby groups. When there is an hydrogen in 2-position, the region opposite to the C(2)–S covalent bond is more positive than when there is a methyl.

Crystallographic studies. The crystal structures of the cyanine iodide **7** and the cyanine bromide **8** both display ChBs between the halide anions and the chalcogen atom. The 3,3'-diethyl-pentamethine-dithia-cyanine **7** crystallizes in the P₂1 space group. This cyanine is significantly longer in one of its three dimensions than in the two others. Its molecules pack parallel in a seesaw conformation, just tilted enough to make room for the propyl chains bound to the nitrogens (Figure 3.2.4, right). No contact between the aromatic portions of the two heteroaromatic moieties is observed, suggesting that this packing arises more from the geometric characteristics mentioned above rather than from π - π stacking.

As revealed by MEP studies (Figure 3.2.3), cyanines have two most positive regions, namely the molecular portions around the nitrogen and chalcogen atoms. Iodide anions of **7** establish close contacts with both of these portions, specifically they form a C–H \cdots I HB with one of the hydrogen atoms of the methylene bound to nitrogen and a C–S \cdots I ChB opposite to C2 of the thiazolium ring. The HB is not particularly linear and most likely results from a poorly specific attraction of electrostatic origin with the

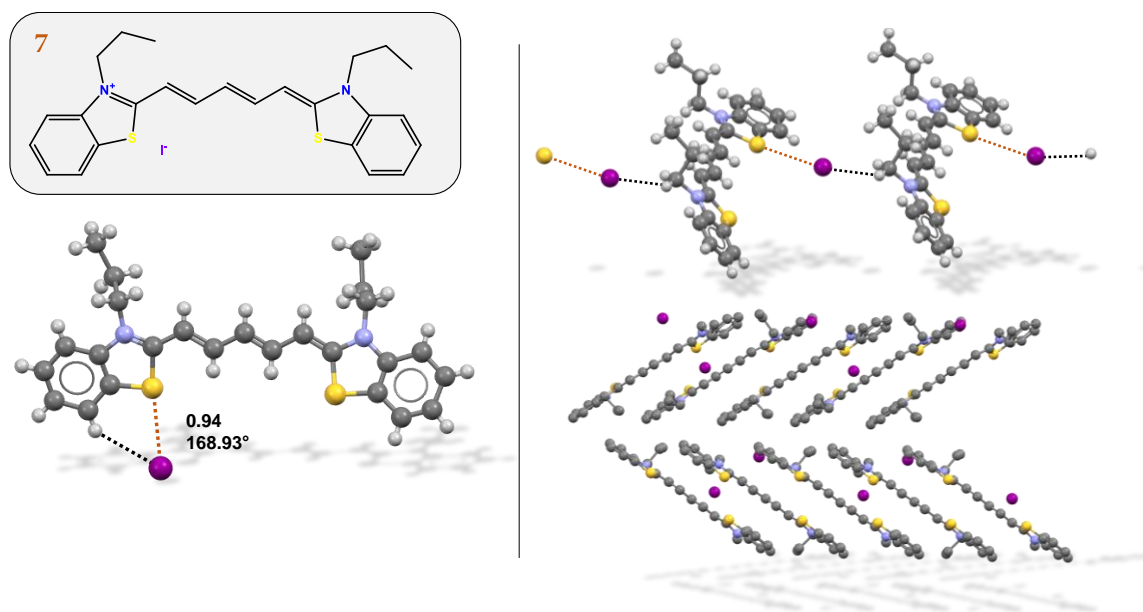


Figure 3.2.4. Asymmetric unit of structure **7** (left) and its packing (right, hydrogen atoms omitted for clarity). Scheme of the compound is boxed near the structure. ChBs denoted as other dotted lines. HBs are black dotted lines. Nc of S...Nu separation and C-S...Nu angles are reported near the contact. Color code: whitish, hydrogen; grey, carbon; yellow, sulfur; purple, iodine; light blue, nitrogen.

quaternary nitrogen. The ChB is closer to linearity than the HB (the C-S...I angle is 168.93°).

The 3,3'-diethyl-monomethine-thia-selena-cyanine **8** crystallizes in the P-1 space group and cations engage in π - π stacking with each other, forming dimers approximately along the *a* axis of the crystal. In such dimers, two cyanines are stacked antiparallel to each other and the nitrogen of one molecule roughly faces the chalcogen of another molecule and *vice versa*. The crystal packing of cyanine **8** shows the presence of a C-H...Br HB with one of the hydrogen atoms of the methylene bound to nitrogen and a C-S/Se...Br ChB opposite to C2 of the chalcogenazolium ring (Figure 3.2.5). These interactions are the analogues of the C-H...I HB and C-S...I ChB observed in **7**.

The molecular structure of cyanine **8** is quite different from that of **7** as the bridge between the two heteroaromatic moieties is a single methylene rather than a pentamethylene chain and the two heteroaromatics are a benzothiazole and a benzoselenazole ring rather than two benzothiazole rings. The observed strict similarity in the interactional landscapes around chalcogen atoms of the two cyanines indicates the relevance of the described HBs and ChBs in controlling the respective crystal packings.

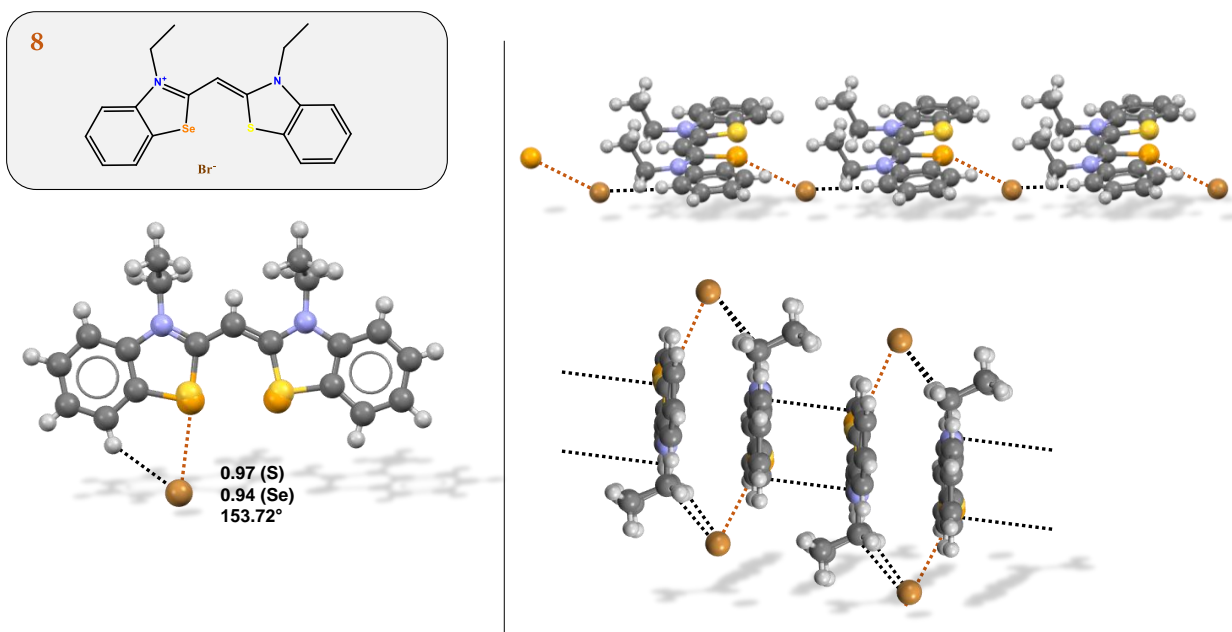


Figure 3.2.5. Asymmetric unit of structure **8** (left) and its packing (right, hydrogen atoms omitted for clarity). Scheme of the compound is boxed near the structure. ChBs denoted as orange dotted lines. HBs and other noncovalent interactions are black dotted lines. Nc of S...Nu separation and C-S...Nu angles are reported near the contact. Color code: *whitish*, hydrogen; *grey*, carbon; *yellow*, sulfur; *purple*, iodine; *light blue*, nitrogen.

The pseudo-symmetry of the dye **8**, related to the steric and electronic similarity between the benzothiazole and benzoselenazole moieties, causes a positional disorder in the crystal packing. Any chalcogen atom site is occupied by both sulfur and selenium so that they both are involved in ChB formation. The occupancy of the chalcogen bonded site is 66% by selenium and 34% by sulfur, consistent with the general tendency of a more polarizable element of a given group of the periodic table to act as more effective σ -hole donor than a less polarizable element of the same group. The Nc value of the C-Ch...Br ChB is 0.97 when the chalcogen atom is sulphur and 0.94 when it is selenium, once again consistent with the general features of σ -hole bondings.

Nitrate anions are not usually regarded as effective electron density donors in σ -hole interactions. In our hands, many attempts to obtain cyanine dyes crystals using nitrate anions afforded samples which were not useful for single crystal X-ray analyses and the 3,3'-diethyl-monomethine-dithia-cyanine was the only cation which formed useful crystals (compound **9**).

Compound **9** crystallizes in the P-1 space group wherein cyanine units stack in pillars along the *a* axis.

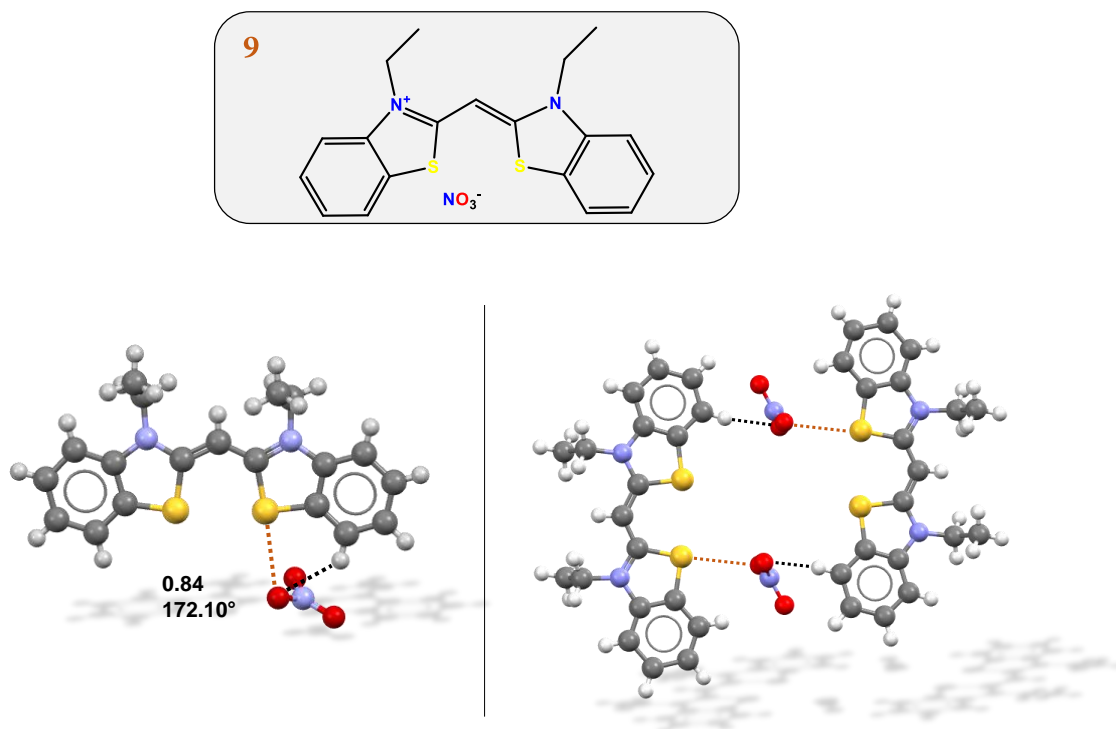


Figure 3.2.6. Asymmetric unit of structure **9** (left) and its tetrameric packing (right). Scheme of the compound is boxed near the structure. ChBs denoted as ocher dotted lines. HBs are black dotted lines. Nc of S...Nu separation and C-S...Nu angles are reported near the contact. Color code: *whitish* hydrogen; *grey* carbon; *yellow* sulfur; *purple* iodine; *red* oxygen; *light blue* nitrogen.

Cyanine separations in these pillars indicate that their formation is not supported by π - π stacking interactions. Different pillars are connected by nitrate anions via HBs and ChBs where the anion is the interaction acceptor (nucleophilic site) and the cyanine the interaction donor (electrophilic site). Cyanine units engage in C7-H...O HBs and fairly short and directional C2-S...O ChBs (Figure 3.2.6) (the S...O separation is 2.983 Å, namely Nc is 0.84, and the C-S...O angles is 172.10°). The unexpectedly short separation may be a consequence of the synergistic cooperation of the HB and the ChB.

Consistent with the high nucleophilic nature of the perrhenate anion, we were able to obtain a number of structures where this unit is working as the electron donor species. In the perrhenate dye **10** the cation is the 3,3'-diethyl-monomethine-dithia-cyanine, namely the same as in nitrate dye **9**. In the packing of the dye **10**, which crystallizes in the P-1 space group, cyanine units pile antiparallel each other (Figure 3.2.7, right) and form cationic columns similar to those found in 3,3'-diethyl-monomethine-thia-selena-cyanine dye **8** (Figure 3.2.5, right).

Perrhenate anions are located near the sulphur atoms of one of the two benzothiazole moieties of cyanines.

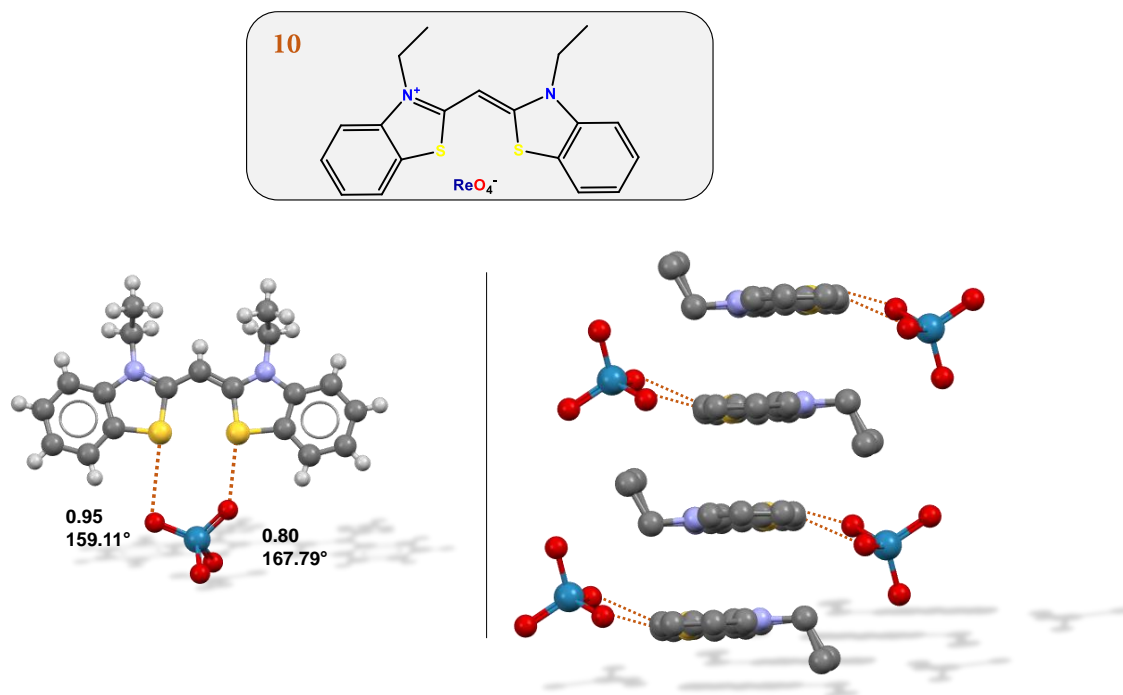


Figure 3.2.7. Asymmetric unit of structure **10** (left) and its packing (right, hydrogens omitted for clarity). Scheme of the compound is boxed near the structure. ChBs denoted as orange dotted lines. HBs are black dotted lines. Nc of S...Nu separation and C-S...Nu angles are reported near the contact. Color code: *whitish* hydrogen; *grey* carbon; *yellow* sulfur; *purple* iodine; *red* oxygen; *light blue* nitrogen; *navy* rhenium.

In fact, well defined cation-anion couples are assembled via short and linear C-S...O ChBs (the S...O separation is 2.844 Å, namely Nc is 0.80, and the C-S...O angles is 167.79°). In these couples the cation-anion pairing is probably assisted also by a second ChB between the cyanine sulphur atom and a perrhenate oxygen not involved in the ChB described above. The separation in this second ChB is a little bit longer (the S...O distance is 3.372 Å, namely Nc is 0.95) and the C-S...O angle is less linear than in the ChB described above (the C-S...O angles is 159.11°). These features may suggest that in the crystal the cyanine positive charge is not equally located on the two benzothiazole rings but is preferentially located on the benzothiazole forming the shorter and more directional ChB. Interestingly, in perrhenate dye **10** no C7-H...O HB is present, consistent with the perrhenate anion being drifted away from C7-H by the second ChB.

Cyanine **11** is the trimethyne analogue of cyanine **10**. Despite its overall crystal structure is different from that of other dyes highlighted above, here too perrhenate oxygen atoms function as bidentate donors of electron density and form C-S...O ChBs and a C7-H...O HBs (Figure 3.2.8).

This confirms that the triangular supramolecular synthon where the thiazoles chalcogen atom and the benzene hydrogen atom act as electrophiles and the anion as the

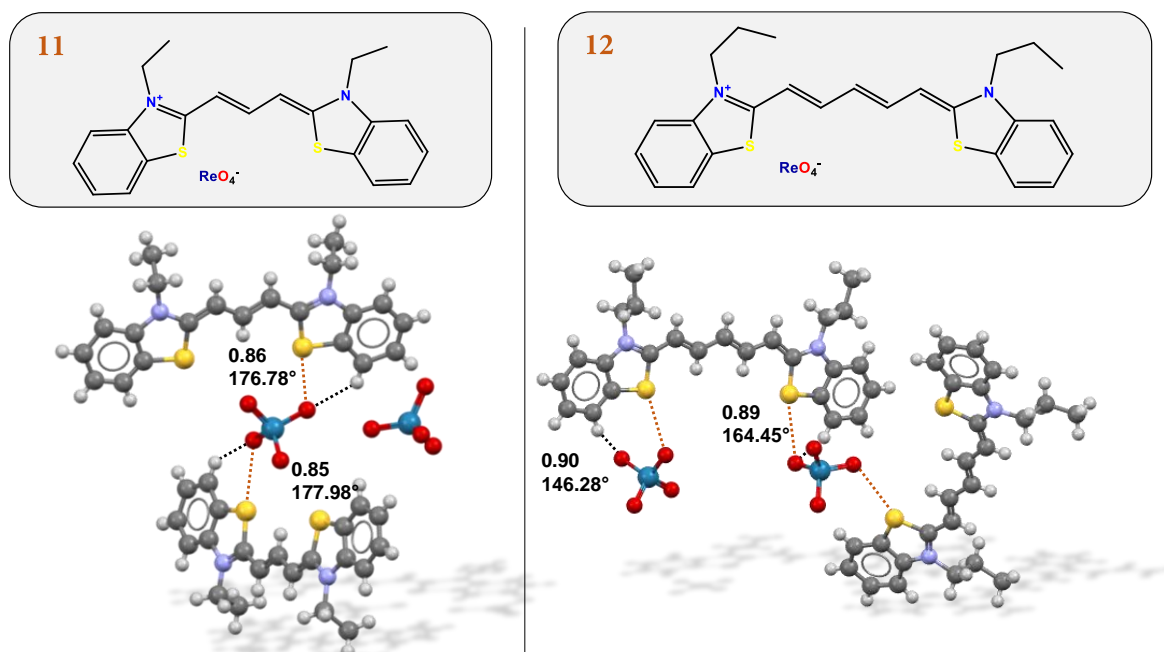


Figure 3.2.8. packing of cyanine **11** (left) and **12** (right). Scheme of the compounds is boxed near the structures. ChBs denoted as other dotted lines. HBs are black dotted lines. Nc of S...Nu separation and C-S...Nu angles are reported near the contact. Color code: *whitish* hydrogen; *grey* carbon; *yellow* sulfur; *purple* iodine; *red* oxygen; *light blue* nitrogen; *navy* rhenium.

nucleophiles is robust enough to be present independently of other features of the interactional landscape of the crystal.

The crystal structure of cyanine **11** adopts the $P2_1/c$ space group and in the unit cell two different cyanine cations and perrhenate anions are present. One of the two perrhenate anions bridges two cyanine cations via two different triangular supramolecular synthons described above. The ChBs of the resulting trimers are quite short (3.037 and 3.069 Å, corresponding to a Nc of 0.85 and 0.86) and remarkably linear (177.98°, 176.78°, respectively). These trimers are nearly planar packed together thanks both to HBs and π - π stacking which create layers extending along the b axis. Interestingly the second ReO_4^- anion of the unit cell which does not give rise to the trimers is not engaged in any other relevant interaction and presents some disorder related to its mobility.

Cyanine **12** is the pentamethyne analogue of cyanine **11** and crystallizes in the $P2_1/c$ space group. Cyanine units do not pack in π - π stacking and the interactions mainly responsible for the adopted crystal packing are the HBs formed by the perrhenate anions and the ChBs involving the benzothiazolium sulfur atom (Figure 3.2.8).

Perrhenate anions and cyanine units interact with each other via two C-S...O interactions wherein the S...O separation is below the sum of O and S van der Waals

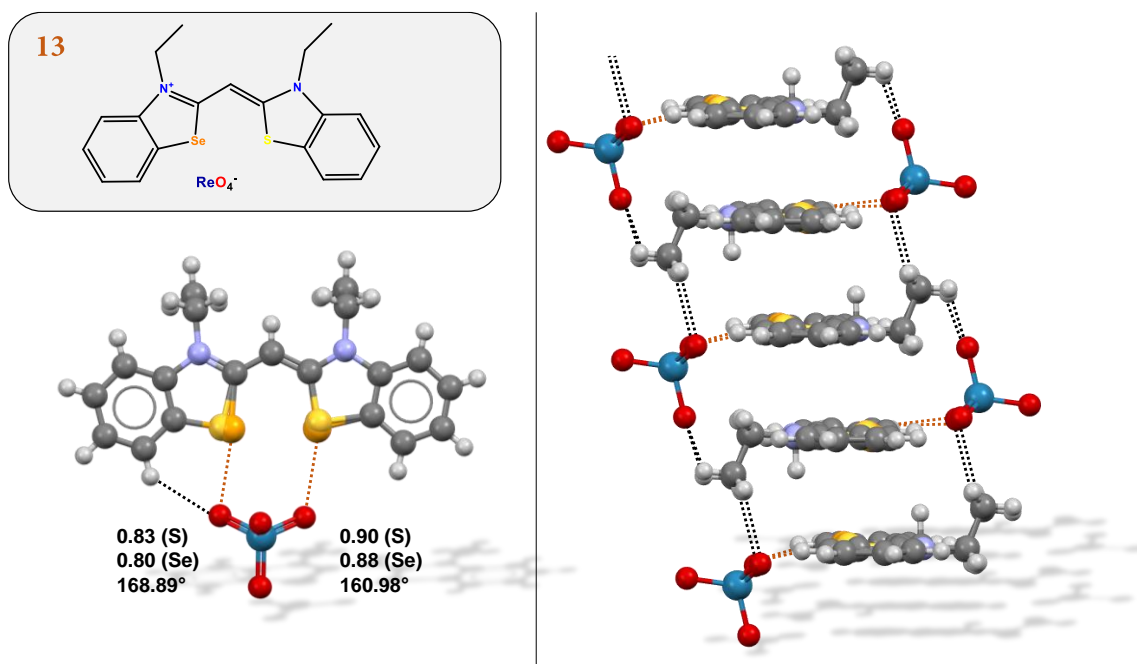


Figure 3.2.9. Asymmetric unit (left) and packing (right) of structures **13**. Scheme of the compounds is boxed near the structures. ChBs denoted as ochre dotted lines. HBs are black dotted lines. Nc of S...Nu separation and C-S...Nu angles are reported near the contact. Color code: *whitish*, hydrogen; *grey* carbon; *yellow* sulfur; *purple* iodine; *red* oxygen; *light blue* nitrogen; *navy* rhenium; *ochre* selenium.

radii, the C-S separations being 3.215 and 3.220 Å, namely corresponding to Nc values of 0.90 and 0.89.

Any perrhenate anion is bound to two different cyanines and supramolecular infinite chains are formed wherein the cationic and anionic modules alternate. The perrhenate and cyanine units connected by the C-S...O interactions are further bound each other via a C7-H...O HBs. For the perrhenate anion forming the shorter and longer S...O contact, the oxygen atom forming the C7-H...O HBs is the same oxygen giving the S...O contact or another oxygen, respectively. The C-S...O angle for the shorter S...O interaction is not far from linearity (this C-S...O angle is 164.45°) and the interaction can no doubt be rationalized as a ChB. Differently, the same angle for the longer S...O interaction shows a major deviation from linearity (this C-S...O angle is 146.28°), but we nevertheless propose to consider the interaction a bona fide ChB

Lastly, compound **13** is the perrhenate analogue of compound **8**, namely it is a 3,3'-diethyl-monomethine-thia-selena cyanine. It crystallizes in the P2₁/n space group. As can be seen from Figure 3.2.9, the compound displays a positional disorder similar to that of structure **8** so that the two chalcogen atoms sites are occupied by both sulfur and selenium, the site occupancy being 50/50. Interestingly, in compound **13** the perrhenate anion engages in interaction with both sites occupied by S/Se of a cyanine units and the two C-S/Se...O ChBs form a well-defined dimeric ion pair. These C-S/Se...O ChBs are

remarkably short (they measure 2.957 and 322.7 Å, spanning the Nc range of 0.80-0.90) and fairly linear (C–S/Se...O angles vary in the range 160.98° - 168.89°). Similar to other structures, the most linear ChB is aided by a C7–H...O HB. Another similarity with cyanine bromide **8**, is that the cyanine units in **13** pack in pillars approximately along the *a* axis of the crystal held together by HBs established with the perrhenate anion.

In conclusion, one or two C–S/Se...O ChBs are invariably present in the crystals structures of the small library bearing benzothiazole and one benzoselenazole ring of cyanine dyes. The ChBs are observed in mono-, tri- and pentamethyne dyes and when the counterion is an iodide, bromide, nitrate or perrhenate anion. The tendency of the sulphur and the selenium atoms of these dyes to work as effective electrophilic sites is forcefully proven. Despite being ChBs between anions and cations, the length of the interactions are not invariably shorter than those observed in section 5.1 (a relevant exception is structure **9**). A possible reason for this behaviour might be the presence of the ancillary HBs. In several structures, a C7–H...anion HB is also observed. This further pinning of the anion close to the elongation of the C2–S/Se covalent bond likely promotes the ChB formation. Finally, π - π interactions between the heteroaromatic ring systems are present only in some of the examined structures. It suggests that while these interactions belong to the interactional landscape of these dyes, they do not belong to the subset of the interactions typically driving the formation of the adopted crystal packing.

Additional Data.

The experimental section contains synthesis, characterization of all the compounds and crystallographic details of all the structures discussed herein.

References.

- [1] N. -H Hu, S. -L Zhang, *Acta Crystallogr. Sect. C* **1993**, 49, 1178–1180.
- [2] P. Yadav, V. Patel, A. Ballabh, *J. Solid State Chem.* **2018**, 263, 231–238.
- [3] S. P. Thomas, V. Kumar, K. Alhameedi, T. N. Guru Row, *Chem. – A Eur. J.* **2019**, 25, 3591–3597.
- [4] A. Daolio, P. Scilabra, M. E. Di Pietro, C. Resnati, K. Rissanen, G. Resnati, *New J. Chem.* **2020**, 44, 20697–20703.
- [5] K. E. Riley, P. Hobza, *Wiley Interdiscip. Rev. Comput. Mol. Sci.* **2011**, 1, 3–17.
- [6] R. W. Newberry, R. T. Raines, *Acc. Chem. Res.* **2017**, 50, 1838–1846.
- [7] P. R. Spackman, L.-J. Yu, C. J. Morton, M. W. Parker, C. S. Bond, M. A. Spackman, D. Jayatilaka, S. P. Thomas, *Angew. Chemie Int. Ed.* **2019**, 58, 16780–16784.
- [8] N. Singh, A. C. Halliday, J. M. Thomas, O. V. Kuznetsova, R. Baldwin, E. C. Y. Woon, P. K. Aley, I. Antoniadou, T. Sharp, S. R. Vasudevan, et al., *Nat. Commun.* **2013**, 4, 1332.
- [9] G. K. Azad, R. S. Tomar, *Mol. Biol. Rep.* **2014**, 41, 4865–4879.
- [10] T. Sakurai, M. Kanayama, T. Shibata, K. Itoh, A. Kobayashi, M. Yamamoto, K. Uchida, *Chem. Res. Toxicol.* **2006**, 19, 1196–1204.
- [11] J. W. Renson, M., Etschenberg, E., 2-PHENYL-1,2-BENZISOSELENAZOL 3(2H)-ONE CONTAINING PHARMACEUTICAL PREPARATIONS AND PROCESS FOR THE TREATMENT OF RHEUMATIC DESEASES, **1982**.
- [12] J. Kil, E. Lobarinas, C. Spankovich, S. K. Griffiths, P. J. Antonelli, E. D. Lynch, C. G. Le Prell, *Lancet* **2017**, 390, 969–979.
- [13] S. Mukherjee, W. S. Weiner, C. E. Schroeder, D. S. Simpson, A. M. Hanson, N. L. Sweeney, R. K. Marvin, J. Ndjomou, R. Kolli, D. Isailovic, et al., *ACS Chem. Biol.* **2014**, 9, 2393–2403.
- [14] S. Thenin-Houssier, I. M. S. de Vera, L. Pedro-Rosa, A. Brady, A. Richard, B. Konnick, S. Opp, C. Buffone, J. Fuhrmann, S. Kota, et al., *Antimicrob. Agents Chemother.* **2016**, 60, 2195–2208.
- [15] S. P. Thomas, K. Satheeshkumar, G. Mugesh, T. N. Guru Row, *Chem. - A Eur. J.* **2015**, 21, 6793–6800.
- [16] A. C. Joice, M. T. Harris, E. W. Kahney, H. C. Dodson, A. G. Maselli, D. C. Whitehead, J. C. Morris, *Int. J. Parasitol. Drugs Drug Resist.* **2013**, 3, 154–160.
- [17] Y. Han, Q. Luo, X. Hao, X. Li, F. Wang, W. Hu, K. Wu, S. Lü, P. J. Sadler, *Dalt. Trans.* **2011**, 40, 11519.
- [18] J. Su, J. Liu, C. Chen, Y. Zhang, K. Yang, *Bioorg. Chem.* **2019**, 84, 192–201.
- [19] J. Lu, S. K. Vodnala, A.-L. Gustavsson, T. N. Gustafsson, B. Sjöberg, H. A. Johansson, S. Kumar, A. Tjernberg, L. Engman, M. E. Rottenberg, et al., *J. Biol. Chem.* **2013**,

- 288, 27456–27468.
- [20] H. X. Ngo, S. K. Shrestha, S. Garneau-Tsodikova, *ChemMedChem* **2016**, *11*, 1507–1516.
- [21] Y. Bravo, P. Teriete, R.-P. Dhanya, R. Dahl, P. S. Lee, T. Kiffer-Moreira, S. R. Ganji, E. Sergienko, L. H. Smith, C. Farquharson, et al., *Bioorg. Med. Chem. Lett.* **2014**, *24*, 4308–4311.
- [22] T. N. Gustafsson, H. Osman, J. Werngren, S. Hoffner, L. Engman, A. Holmgren, *Biochim. Biophys. Acta - Gen. Subj.* **2016**, *1860*, 1265–1271.
- [23] P. J. Collier, P. Austin, P. Gilbert, *Int. J. Pharm.* **1990**, *66*, 201–206.
- [24] P. Appendini, J. H. Hotchkiss, *Innov. Food Sci. Emerg. Technol.* **2002**, *3*, 113–126.
- [25] J.-T. Kwon, M. Lee, G.-B. Seo, H.-M. Kim, I. Shim, D.-H. Lee, T. Kim, J. K. Seo, P. Kim, K. Choi, *Nat. Prod. Commun.* **2013**, *8*, 1934578X1300800.
- [26] O. Aerts, A. Goossens, J. Lambert, J.-P. Lepoittevin, *Eur. J. Dermatology* **2017**, *27*, 115–122.
- [27] M. Ayadi, P. Martin, *Contact Dermatitis* **1999**, *40*, 115–116.
- [28] A. B. Carle, J. A. Krause Bauer, R. M. Wilson, *Acta Crystallogr. Sect. C Cryst. Struct. Commun.* **2000**, *56*, 97–98.
- [29] M. D’Ascenzio, S. Carradori, C. De Monte, D. Secci, M. Ceruso, C. T. Supuran, *Bioorg. Med. Chem.* **2014**, *22*, 1821–1831.
- [30] D. L. Arnold, D. Krewski, I. C. Munro, *Toxicology* **1983**, *27*, 179–256.
- [31] A. Tacic, V. Nikolic, L. Nikolic, I. Savic, *Adv. Technol.* **2017**, *6*, 58–71.
- [32] F. Viani, B. Rossi, W. Panzeri, L. Merlini, A. M. Martorana, A. Polissi, Y. M. Galante, *Tetrahedron* **2017**, *73*, 1745–1761.
- [33] K. F. Konidaris, T. Pilati, G. Terraneo, P. Politzer, J. S. Murray, P. Scilabra, G. Resnati, *New J. Chem.* **2018**, *42*, 10463–10466.
- [34] M. T. Chhabria, S. Patel, P. Modi, P. S. Brahmikshatriya, *Curr. Top. Med. Chem.* **2016**, *16*, 2841–2862.
- [35] A. Mikherdov, A. Novikov, M. Kinzhalov, A. Zolotarev, *Crystals* **2018**, *8*, 112.
- [36] G. Cavallo, J. S. Murray, P. Politzer, T. Pilati, M. Ursini, G. Resnati, *IUCrJ* **2017**, *4*, 411–419.
- [37] L. Catalano, G. Cavallo, P. Metrangolo, G. Resnati, G. Terraneo, *Top. Curr. Chem.* **2016**, *373*, 289–310.
- [38] Y. Liu, P. A. Bonvallet, S. A. Vignon, S. I. Khan, J. F. Stoddart, *Angew. Chemie - Int. Ed.* **2005**, *44*, 3050–3055.
- [39] E. E. Rastede, M. Tanha, D. Yaron, S. C. Watkins, A. S. Waggoner, B. A. Armitage, *Photochem. Photobiol. Sci.* **2015**, *14*, 1703–1712.
- [40] J. Wang, P. Zhao, X. Li, H. Fu, X. Yang, G. Wang, Y. Yang, H. Wei, Z. Zhou, W. Liao, *ACS Appl. Bio Mater.* **2020**, *3*, 1580–1588.
- [41] H. A. Shindy, *Dye. Pigment.* **2017**, *145*, 505–513.
- [42] X. Yang, C. Shi, R. Tong, W. Qian, H. E. Zhau, R. Wang, G. Zhu, J. Cheng, V. W. Yang, T. Cheng, et al., *Clin. Cancer Res.* **2010**, *16*, 2833–2844.
- [43] K. K. Maiti, A. Samanta, M. Vendrell, K. S. Soh, M. Olivo, Y. T. Chang, *Chem. Commun.* **2011**, *47*, 3514–

3516.

4. The Tetrel Bond at Work.

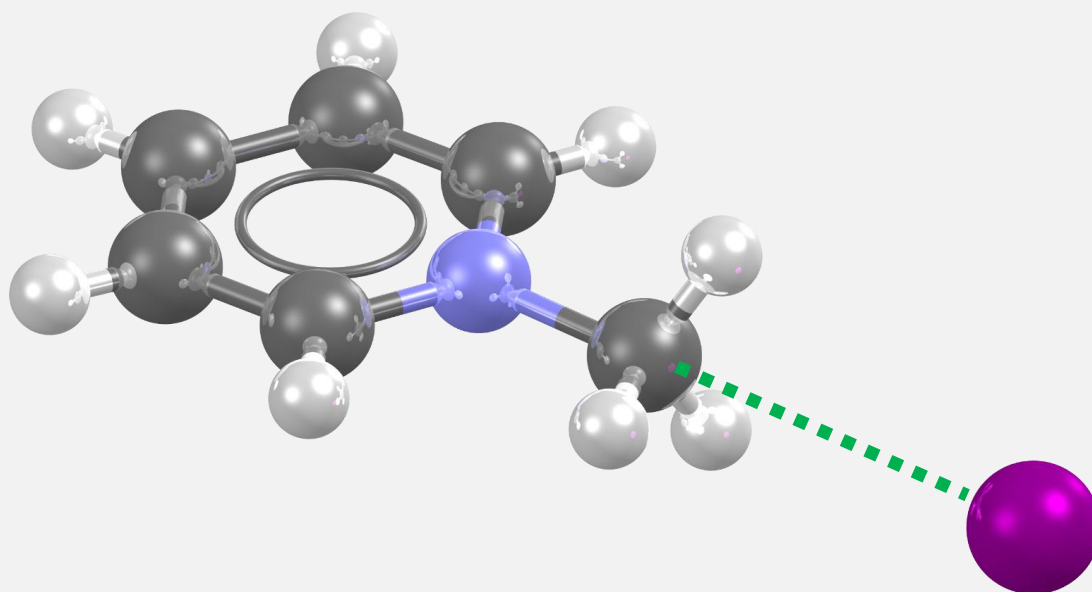


Figure 4. Intuitive representation of the geometrical features of a tetrel bond displayed in an adduct between *N*-methyl pyridinium cation and an iodine atom (REFCODE PAQLEB). Molecules not engaging in TtB were omitted for clarity. Rendered by POV-Ray with metallic textures in ball and stick visualization.

Atoms of the second period generally display weak σ -holes, if any, on the elongation of the covalent bonds they are involved in^[1]. This is a consequence of their high electronegativity and low polarizability. For this reason, it is commonly accepted that carbon atoms display small and poorly positive σ -holes. However, due to the ubiquity of carbon in chemistry and biology the study of any possible interaction involving this element is of paramount relevance and impact.

The carbon TtB contributes to the explanation of the functioning of many phenomena, e.g. S_N2 reactions^[2] or hydrophobic attraction^[3].

In general, σ -holes of a given element are stronger if the element is covalently bound to electron attractive moieties like fluoride and cyano groups. For this reason ammonium and pyridinium residues, with their high electron withdrawal ability, are at the centre of this study^[4].

In this chapter we report the investigation of sp^3 carbon atoms directly bound to different positive charged moieties. Methyl ($-CH_3$) and methylene ($-CH_2-$) groups involved in TtBs are discussed and computationally characterized.

4.1. The *N*-methylammonium moiety: a tetrel bond donor site.

Few things are harder to put up with than the annoyance of a good example.

- Mark Twain, *Pudd'nhead Wilson*

N,N,N,N',N',N'-hexamethylhexane-1,6-diaminium (hexamethonium in the following, Figure 4.1.1) is a dication bearing two trimethylammonium heads. It is commonly used in crystal engineering, organic chemistry and biochemistry. It can act as an acetylcholine mimic^[5] and its ability to block nicotinic receptors is known^[6]. In the same fashion, it was studied as an agent for the cholinergic control of neocortical output neurons^[7,8]. Lastly, it is commonly used to build microporous compounds^[9] or encapsulating agents^[10]. It can form complex crystalline architectures held together by a tight array of interactions between the two positive heads and electron rich atoms or moieties (usually, but not always, their counter ions)^[11].

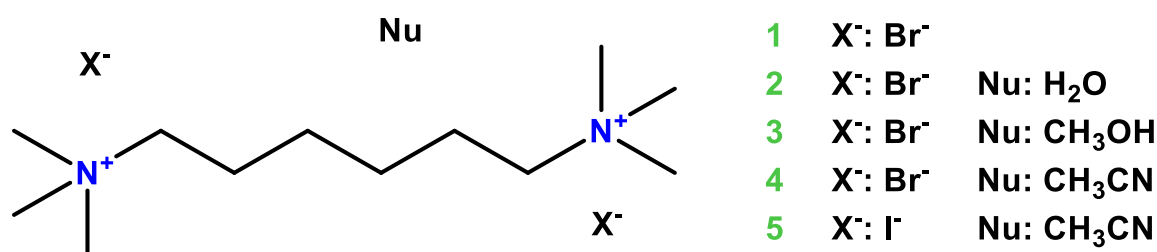


Figure 4.1.1. Scheme of the hexamethonium salts (*left*) and list of the compounds and crystal structures presented in this paragraph (*right*).

In the adducts formed between the hexamethonium cation and different electron-rich partners available on the CSD^[12] there is a remarkable tendency for nucleophiles to locate along the extension of the N⁺-CH₃ covalent bonds of the dication. 42% of the hexamethonium structures available on the database display one or more close contacts between an electron rich atom (Nu=N, P, O, S, Se, F, Cl, Br, I) and the carbon of one of the CH₃ groups where the N⁺-C...Nu angle is comprised between 160° and 180°. This number can become as high as 57% when considering a C...Nu distance 20 pm higher than the sum of their respective Bondi van der Waals radii. Surveys carried out on similar compounds like octamethonium and decamethonium (*N,N,N,N',N',N'*-octamethylhexane-1,8-

diaminium and N,N,N,N',N',N' -decamethylhexane-1,10-diaminium, respectively) reveal analogous tendencies. Such inspections are not enough to allow for a rigorous statistical comparison, but the crystal habits of the compounds remain anomalous. In fact, the general tendency to engage in short contacts along the extension of covalent bonds is often taken as a good indicator of the presence of σ -hole interactions. A purely electrostatic cation-anion attraction does not account for such a preferential localization of the noncovalent bonding^[13].

A TtB involving an sp^3 carbon can be seen as an initial step of an S_N2 reaction^[2]. The tetrel bonded adduct can be considered as a preliminary stage towards the pseudo-hypervalent state adopted by carbon in the S_N2 transition state where the carbon atom assumes a bipyramidal trigonal geometry with the nucleophile and residue generating the σ -hole at carbon occupying the apical positions (Figure 4.1.2)^{[14-16][17]}.

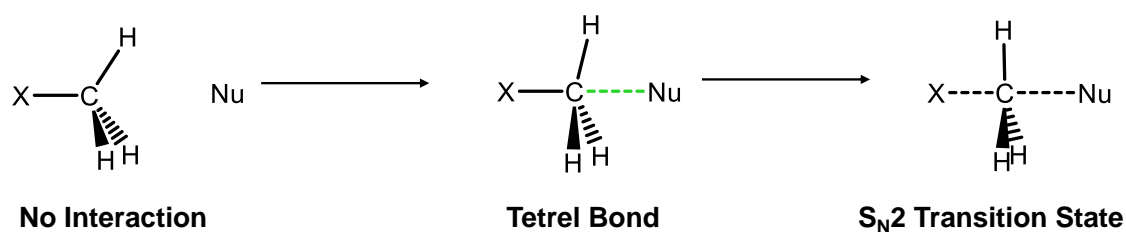


Figure 4.1.2. Schematic representation of a tetrel bonded atom as a preliminary stage towards the transition state in an S_N2 reaction at a methyl center.

TtB interactions involving sp^3 carbon atoms as the electrophilic site are inherently weak and difficult to study through spectroscopic techniques. In addition, the localization of the nucleophile on the extension of one of the covalent bonds formed by the carbon is not *per se* a definitive indication of the TtB presence as it does not rule out the possibility for the geometry to be determined by hydrogen bonds (HBs) involving the methyl hydrogen atoms. This possibility was discussed even in the very first paper introducing evidence of the formation of carbon-based TtB adducts in the solid state^[18]. The same issue has been tackled recently in a paper by Frontera et al., wherein a large body of computational evidence allowed for proposing strict geometric rules to distinguish between TtBs and HBs^[19].

A computational approach based on crystallographic features will be presented in this section as a complement of previous works on the subject. In collaboration with Prof. Genoni's group, the crystal structures obtained in this work were refined both with the Independent Atom Model (IAM) and the Hirschfeld Atom Refinement (HAR)^[20-23]. The latter is an emerging tool in quantum crystallography^[24,25] and allows routinely obtainable

single crystal X-ray diffraction data to be used for locating the position of hydrogen atoms with accuracy similar to approaches based on neutron scattering^[26].

In this paragraph, we present five single crystal X-ray structures where hexamethonium salts seem to engage in TtB with different electron-rich partners, both anions and neutral molecules (Figure 4.1.1). The crystals were obtained by slow evaporation of hexamethonium bromide or iodide solutions from different solvents, mostly resulting in the formation of solvate adducts.

The crystal structures were refined through AIM and HAR and the differences between the two refinements results are highlighted, focusing on the localization of the hydrogen atoms. This process helps in determining the nature of the interaction between the nucleophiles and $-\text{CH}_3$ carbons. To assess the experimental evidence and confirm the initial assumptions, quantum topological analysis is then carried out. Namely, Bader's analysis (QTAIM) and Noncovalent Interaction Index (NCI) were performed to part the two different interactions^[27-30]. In line with previous studies^[31], we found that the directionality of the $\text{N}^+-\text{C}\cdots\text{Nu}$ angle may serve as a better descriptor of this interaction in respect of the normalised contact (Nc).

The structural formulas and a Mercury representation of the hexamethonium systems **1-5** are reported in Figure 4.1.3 along with the TtBs between the nucleophiles and the trimethylammonium heads.

N,N,N,N',N',N'-hexamethylhexane-1,6-diaminium dibromide (**1**) crystallizes in the space group $P2_1/c$ and the unit cell contains one bromide anion. The hexamethonium adopts an all trans conformation. Br^- anions are engaged in HBs with different hexamethonium units and form two $\text{N}-\text{C}\cdots\text{Br}$ contacts with the $-\text{CH}_3$ groups of two different hexamethonium groups. The structural features of both motifs are consistent with the rationalization of these $\text{C}\cdots\text{Br}$ contacts as TtBs. The first contact (involving the bromide indicated as Br1 in Figure 4.1.3) is not particularly close, in fact the $\text{C}\cdots\text{Br}$ distance is slightly longer than the sum of C van der Waals radius and Br^- Pauling anionic radius (3.701 Å, corresponding to an Nc of 1.01); however, the $\text{N}-\text{C}\cdots\text{Br1}$ angle is very close to 180° (177.91°). The second contact (involving the bromide indicated as Br2 in Figure 4.1.3) engages in a shorter interaction (the $\text{C}\cdots\text{Br}$ distance is 3.593 Å, corresponding to an Nc of 0.98) characterized by a greater deviation from linearity (the $\text{N}-\text{C}\cdots\text{Br2}$ angle is 166.63°).

N,N,N,N',N',N'-hexamethylhexane-1,6-diaminium dibromide water solvate (**2**) also crystallizes in space group $P2_1/c$. In this structure a possible TtB between the bromide (Br3 in Figure 4.1.3) and a CH_3 carbon atom of one of the trimethylammonium heads is the closest contact, so this interaction will be the focus of the discussion. This contact is quite close to linearity (the $\text{N}-\text{C}\cdots\text{Br}$ angle is 175.70°) and the $\text{C}\cdots\text{Br}$ distance is 3.492 Å, corresponding to an Nc of 0.96. The asymmetric unit of this structure comprises only half

of the hexamethonium, so that the other half molecule engages in an identical interaction represented in Figure 4.1.3.

N,N,N,N',N',N'-hexamethylhexane-1,6-diaminium dibromide methanol solvate (**3**) crystallizes instead in the $P2_1/n$ space group. In this structure as well, interactions consistent with the definition of a TtB are the closest contacts and will be the focus of this discussion. Both of the bromide anions in the asymmetric unit and the oxygen atom of the solvate methanol seem to engage in interactions with three different methyl carbon atoms. The shorter and most linear contact of the three is the one held with a bromide (Br4 in Figure 4.1.3). The distance between the involved atoms is 3.534 Å, corresponding to an Nc of 0.97, and the N–C⋯Br4 angle is 173.18°. The contact with the oxygen of the solvate methanol is slightly longer. The C⋯O distance is 3.215 Å (the Nc is 0.99), and the N–C⋯O angle is 168.87°. The second anion (Br5 in Figure 4.1.3) is also located in a position consistent with the presence of a TtB, lying at a distance of 3.659 Å from the closest CH₃ carbon atom, corresponding to an Nc of 1.00, and establishing a N–C⋯O angle of 164.82°.

N,N,N,N',N',N'-hexamethylhexane-1,6-diaminium dibromide acetonitrile solvate (**4**) crystallizes in the space group $P2_1/c$. As for structure **3**, possible TtBs are held between CH₃ carbon atoms and nucleophiles, both charged and neutral. This structure features the most directional short contact presented in this section, where the nitrogen atom of a solvate acetonitrile molecule (N1 in Figure 4.1.3) approaches a –CH₃ carbon atom. The Nc is very small, 0.94, and the N–C⋯N1 angle is 179.87°. A bromide anion (Br6 in Figure 4.1.3) also establishes a close contact with another CH₃ carbon atom, although the N–C⋯Br6 angle is not particularly linear (166.51°) and the C⋯Br6 distance is longer than the first contact (3.596 Å, Nc 0.98).

N,N,N,N',N',N'-hexamethylhexane-1,6-diaminium diiodide acetonitrile solvate (**5**), while crystallising in the space group $P2_1/n$, bears many resemblances to structure **4**. As of the precedent structure, in **5** an acetonitrile solvate molecule (N2 in Figure 4.1.3) is engaging in a close contact with the closest methyl's carbon atom. In this contact the separation is even shorter than the one discussed previously, the distance being 3.016 Å, corresponding to an Nc of 0.93. This is the shortest interaction presented in this paragraph but not the most linear, the N–C⋯N2 angle being 173.95°. Interestingly, the shorter and more linear interactions under scrutiny are held with neutral molecules acting as donors of electron density instead of the anions. Additionally, this structure displays two different close contacts between iodide anions and a CH₃ carbon atom. The two present similar geometrical features (Table 4.1.1). The Nc is 0.99 for both of them and the N–C⋯I angles are roughly 3° apart from each other (169.33° for N–C⋯I1 and 167.60° for N–C⋯I2, Figure 4.1.3).

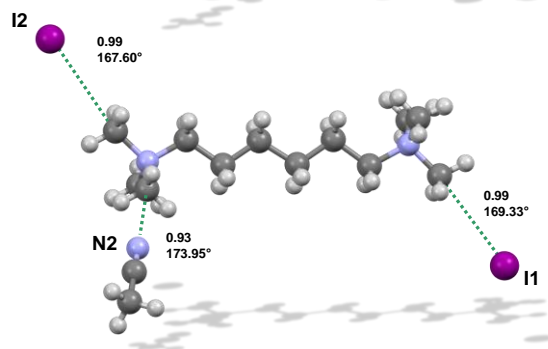
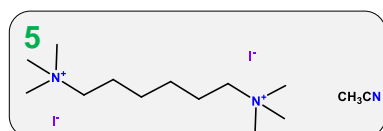
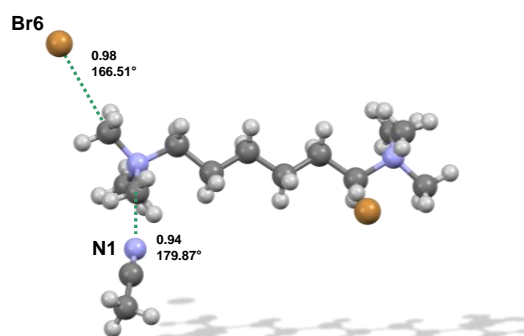
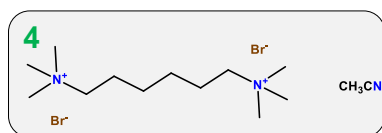
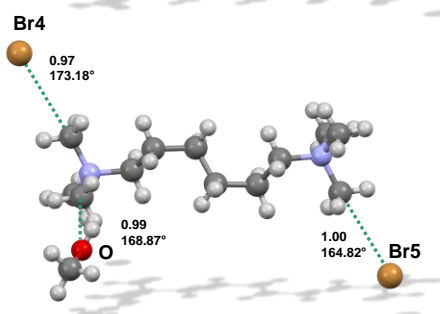
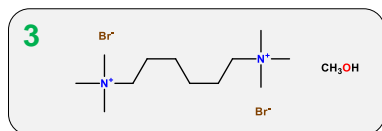
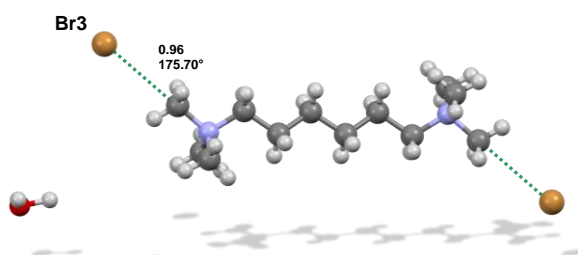
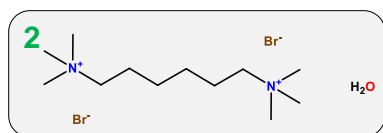
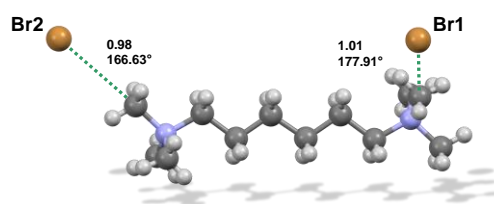
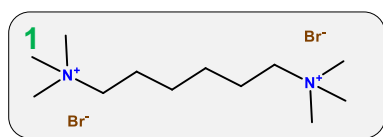


Figure 4.1.3. Structural formulas (left) and Mercury representation of hexamethonium salts **1-5** (IAM refinement) presented in this section. Interactions between CH₃ groups and approaching nucleophiles denoted as green dotted lines. Nc of C...Nu separation and N-C...Nu angles are reported near the contact. Anions and nucleophiles are numbered for the sake of clarity. Colour code: *gray* carbon; *whitish* hydrogen; *light blue* nitrogen; *red* oxygen; *ocher* bromine; *purple* iodine.

To sum up, all the structures reported in this work display many close contacts with anions and neutral electron rich molecules consistent with the typical geometric features of a carbon-based TtB. A complete list of the geometrical features of the interaction is reported in Table 4.1.1. The Ncs and angles can slightly differ. On the basis of crystallographic analysis alone it is not trivial to unequivocally determine if the interactions should be considered HBs or TtBs. It can be arguably stated that these two interaction modes should present fairly different geometrical features. For this reason, a careful consideration of the hydrogen atoms position thanks to HAR analysis is imperative to have reliable indications on the nature of these interactions.

Structure	Nu	C...Nu separation (Å)	Nc	N-C...Nu angle (degrees)
1	Br1	3.701	1.01	177.91
	Br2	3.593	0.98	166.63
2	Br3	3.492	0.96	175.70
3	Br4	3.534	0.97	173.18
	Br5	3.659	1.00	164.82
	O	3.215	0.99	168.87
4	N1	3.065	0.94	179.87
	Br6	3.596	0.98	166.51
5	N2	3.016	0.93	173.95
	I1	3.818	0.99	167.60
	I2	3.816	0.99	169.33

Table 4.1.1. List of the close contacts considered in this section between a nucleophile and the closest CH₃ carbon atom. Structures obtained with IAM refinement

When the quality of the experimental X-Ray structures was sufficiently high, Hirschfeld Atom Refinement (HAR) was carried out. The final goal of this analysis is to correctly determine the position of the hydrogen atoms with an accuracy and precision close to the one of neutron scattering. This analysis was performed on structures **1**, **2** and **5**, resulting on crystal structures **1'**, **2'** and **5'**.

As expected, HAR refined structures present geometrical features slightly different from those resulting from IAM. The first structure, **1'**, displays two possible TtB interactions equivalent to those found for **1** (bromide anions are Br1' and Br2', they correspond to Br1 and Br2 in structure **1** of Figure 4.1.3, respectively). The angles between the CH₃ carbon atoms and the two bromide anions are slightly closer to 180° in **1'**, as well

as in all the other HAR refined structures. More significantly, the hydrogen atoms position with respect to the carbon atom and the nucleophiles can now be detailedly evaluated.

In hexamethonium dibromide **1'** the C–H bonds are longer and the same occurs in all structures refined with HAR. This is not unexpected, and it is a common behaviour encountered in HAR structures as well as those collected with neutron scattering. The geometrical features of the hydrogen atoms in CH₃ groups engaging in short contacts with Br1' and Br2' are qualitatively different, as they likely account for two different types of interaction. The hydrogen atoms of the methyl engaging in a short contact with Br1' will be considered first. The three H...Br1' distances are 3.496 Å (H_a), 3.547 Å (H_b) and 3.557 Å (H_c). The N⁺–C–H angles are lower than the value obtained with IAM (109.44°) for all three hydrogens. It indicates a minor flattening of the CH₃ group, a typical fingerprint of TtB formation, and the geometry is closer to the transition state of a S_N2 reaction. All the C–H...Br1' angles in this CH₃ group roughly span from 89 to 93° (Table 4.1.2). All the geometrical features are consistent with the ideal TtB arrangement discussed above. The three hydrogen atoms are roughly equally distanced from the incoming nucleophile and the flattening of the –CH₃ group is reminiscent of the pseudo-hypervalent transition state of an S_N2 reaction.

The interaction of Br2' with the hydrogens of the –CH₃ group is then considered. The relative distances between Br2' and the hydrogen atoms are significantly different from each other: 3.198 Å (H_d) being closer than 3.460 Å (H_e) and 3.626 Å (H_f). The H...Br2' distances span a range of 0.43 Å while the three H...Br1' distances differ only by 0.061 Å (Table 4.1.2). The N⁺–C–H angles are not significantly different from those reported in the respective IAM structure, but it is worth pointing out that the N⁺–C–H_d angle is slightly wider than the other two. The angle C–H_d...Br2' is much wider (102.58°) than C–H_e...Br2' and C–H_f...Br2' (88.50° and 80.03°, respectively, Table 4.1.2). The C–H...Br2' angles span a range of 22.55° while the range of C–H...Br1' angles measure much less (3.22°). The geometrical features are more consistent with the definition of an HB between H_d and Br2' rather than a TtB involving the methyl carbon.

A close contact between a bromide owning to another asymmetric unit (Br7' in the following and in Figure 4.1.4) and a hydrogen atom located on a third –CH₃ group is also discussed to compare the two interactions analysed above with an HB.

The distance between the carbon and Br7' is 3.728 Å and the N⁺–C...Br7' angle is 129.55°. The geometrical features are strongly consistent with an HB between one of the hydrogen atoms of the methyl (H_g) and the bromide anion. There is a qualitative difference between the geometrical features of this interaction and those reported for Br1'. The C–H_g...Br7' angle is much wider than C–H...Br1' and C–H...Br2' angles and somewhat closer to C–H...Br2'.

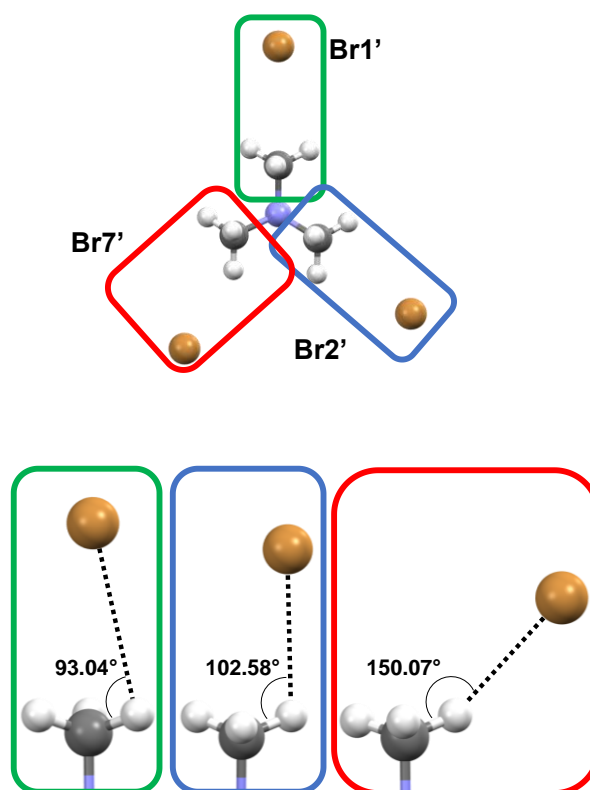


Figure 4.1.4. (*above*) three interacting motifs in the HAR refined crystal structure **1'**. The three CH₃ of a trimethylammonium head are boxed together with the nearest bromide anion. Scheming of the Br⁻ reported near the atoms. (*below*) Magnification of the three boxes. The wider C–H...Br angle is a dotted black line. The angle is reported near the line.

Other parameters of the Br^{7'}-methyl contacts are consistent with the presence of an HB (Table 4.1.2). In conclusion, thanks to the HAR analysis, it is possible to state that C...Br^{1'} interaction is a *bona fide* TtB, while C...Br^{2'} is the result of an HB interaction between the anion and hydrogen H_d.

In hexamethonium dibromide hydrate **2'**, the C...Br^{3'} separation is 3.493 Å (Br^{3'} correspond to Br₃ in structure **2**, Figure 4.1.3) and the N⁺–C...Br^{3'} angle is 175.56°. The improved refinement of the hydrogen position reveals geometrical features very akin to those of the interaction of Br^{1'} and the methyl carbon in structure **1'**. The distances between the nucleophile and the hydrogen atoms are fairly similar: 3.253 Å (H_j), 3.368 Å (H_k) and 3.384 Å (H_i). The three H...Br^{3'} length differ from each other less than 0.131 Å, about 30% of the H...Br^{2'} length differences in structure **1'**. The three C–H...Br^{3'} angles measure 93.89°, 94.00° and 86.80°, namely they differ from each other 7.09° at most. The interaction taking place between the bromide anion and the CH₃ can thus be interpreted as a TtB.

Structure	Nu	Hydrogen	Nu...H distance (Å)	N ⁺ -C-H angle (degrees)	Nu...H-C angle (degrees)
1'	Br1'	H _a	3.496	107.58	93.04
		H _b	3.547	107.82	90.36
		H _c	3.557	107.30	89.82
	Br2'	H _d	3.198	108.10	102.58
		H _e	3.460	106.20	88.50
		H _f	3.626	107.62	20.03
	Br7'	H _g	2.782	109.81	150.07
		H _h	3.919	106.23	71.90
		H _i	4.174	106.09	57.51
2'	Br3'	H _j	3.253	108.75	93.89
		H _k	3.268	110.09	94.00
		H _l	3.384	109.10	86.80
5'	N2'	H _m	2.758	108.70	92.98
		H _n	2.873	109.08	87.08
		H _o	2.983	107.11	82.35
	I1'	H _p	3.298	109.84	105.21
		H _q	3.651	107.30	89.82
		H _r	3.888	106.43	78.54
	I2'	H _s	3.459	106.77	98.02
		H _t	3.733	103.32	86.92
		H _u	3.826	106.12	81.06

Table 4.1.2. Geometrical features of the hydrogen atoms in the HAR structures discussed in this section. Only hydrogen atoms bound to carbon atoms engaging in a close contact with a nucleophile (or mentioned in the text) are reported and numbered.

Finally, hexamethonium didiodide acetonitrile solvate **5'** presents different interactions worth a more insightful consideration. All the geometrical features of the interaction between the acetonitrile nitrogen atom (N2', correspondent to acetonitrile N2 in structure **5**, Figure 4.1.3) and the carbon of the hexamethonium methyl seem consistent with a TtB. The CH₃ is slightly flattened, the N⁺-C-H angles all being smaller than 109.44°. C-H...N2' angles differences are always smaller than 10.63°. The two interactions with iodide atoms I1' and I2' (corresponding to I1 and I2 in structure **5**, Figure 4.1.3), are less straightforward to analyse. The short contact between I1' and the -CH₃ group displays geometrical features consistent with the presence of a HB, where the hydrogen H_p establishes a C-H_p...I1' angle of 105.21° (Table 4.1.2). Conversely, the interaction involving I2' presents intermediate geometrical features between those analysed above. Namely, the N⁺-C-H angles are the narrowest presented in this work, with the highest flattening of the CH₃, but the C-H...I2' angles, while if always smaller than 100°, vary from each other, their differences being as large as 16.96°. The crystallographic data are not enough to

unequivocally interpret the interaction as a TtB or an HB, and quantum topological analysis was needed to acknowledge the short contact as a TtB.

QTAIM and NCI analyses were performed employing the B3LYP/DGDZVP basis set, the analysis focused only on the HAR structures, to exploit the more reliable position of the hydrogens. The nature of the contacts was initially investigated with the aid of non-covalent interaction (NCI) analysis. The obtained reduced gradient isosurface resulting from the calculation are reported in Figure 4.1.5. Concerning crystal structure **1'**, while Br1' establishes a clear interaction with the closest CH₃ carbon, Br2' is involved in a noncovalent interaction with the closest hydrogen atom, nicely supporting the geometrical considerations of the previous sections. An additional confirmation is given by structure **2'**, where the reduced density gradient isosurface reveals the presence of a direct C...Br3' TtB interaction. Lastly, for structure **5'**, again in agreement with the previous sections, the isosurfaces indicate the presence of different interactions. It is trivial to recognize the interaction between the N2' nitrogen of the acetonitrile solvate molecule as a TtB. In the contacts between the iodides and hexamethonium cations, the higher dimension of the anions may complicate the reading of the isosurfaces and an easy discrimination of the bonding pattern is not possible. Since the nature of this interaction was yet to be clarified, QTAIM analysis was performed, and result are summarized below.

QTAIM analysis locates paths of electron density, usually regarded as a strong clue of the presence of an interaction, between the atom couples found through NCI. The topological properties of the calculated electron density paths are reported in Table 4.1.3. It can be observed that, in crystal **1'**, for bromide Br1' only a bond critical point between the bromide and the methyl carbon atom can be found.

For Br2' the interaction is, as predicted by the crystallographic analysis, held between the anion and hydrogen atom H_d. Pertaining to crystal **2'**, the C...Br3' contact is characterized by a bond path between the two atoms, confirming the nature of the interaction as a TtB.

For structure **5'**, QTAIM reveals the presence of three bond critical points, one between a CH₃ carbon and the N2' nitrogen atom of the acetonitrile solvate molecule, and

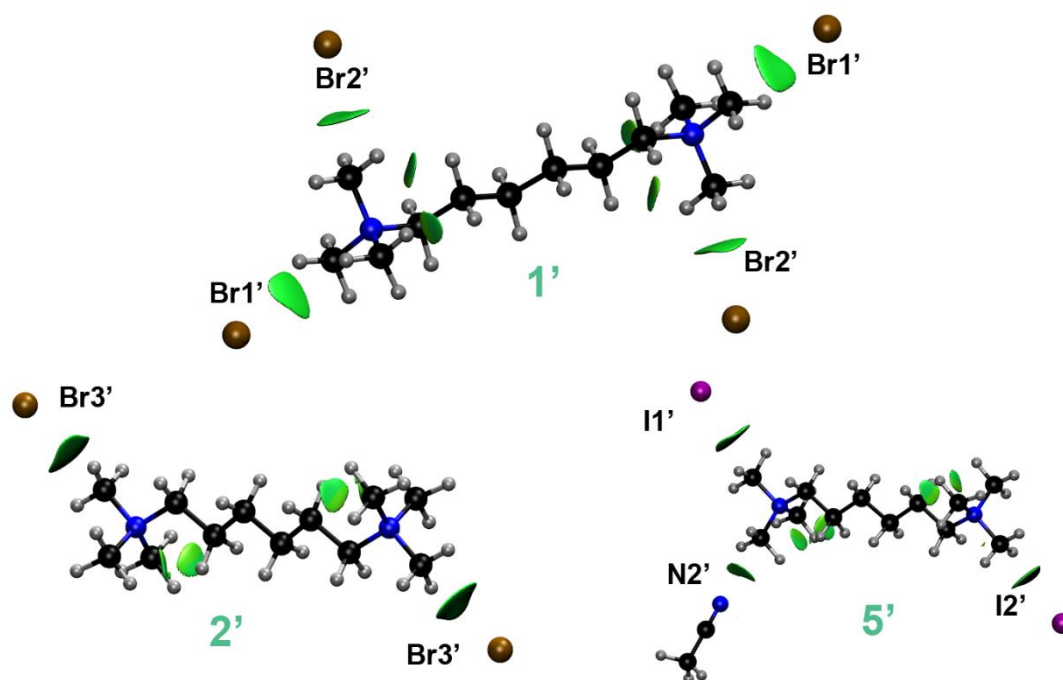


Figure 4.1.5. Reduced density gradient isosurfaces ($s=0.5$ a.u.) obtained from the NCI analyses performed on the HAR structures of (a) crystal **1'**, crystal **2'** and crystal **5'**. The NCI analyses are based on electron densities resulting from DFT calculations at B3LYP/DGDZVP level.

one between a H_p hydrogen atom and the iodide anion $I1'$, consistent with the structural analysis carried out. QTAIM also confirms that the interaction between $I2'$ and the closest CH_3 carbon is held solely with the carbon atom and not the hydrogen atoms. The interaction is thus interpreted as a TtB.

The values of electron density at the bond critical points (ρ_{bcp}) are quite small (Table 4.1.3). The V_{bcp} value for interactions $C\cdots Br3'$ and $C\cdots I2'$ in crystals **2'** and **5'**, respectively, are similar in value, and greater than the value obtained for $Br1'\cdots C$ in crystal **1'**. In other words, this computational approach suggests that the $C\cdots Br3'$ and $C\cdots I2'$ TtBs in crystals **2'** and **5'** are stronger than the $Br1'\cdots C$ TtB in crystal **1'**.

Table 4.1.3 can be further analysed. Observing that all the ρ_{bcp} are relatively small and all the Laplacian values ($\nabla^2\rho_{bcp}$) are positive, the considered TtBs can be categorized as closed shell interactions. The ratio between the absolute value of the potential energy density (V_{bcp}) at the bcp with the kinetic energy density (G_{bcp}) is always lower than 1, hence the interactions, following the classification made by Espinosa^[32], are pure closed shell and the bond degree (BD) parameter can be used as an additional strength-index for the interaction (the two values are inversely proportional, the lower the BD, the stronger the interaction). The BD values nicely correlate with the ρ_{bcp} data already evaluated and further demonstrate that the contacts in **2'** and **5'** are stronger than those in crystal **1'**.

Structure	Atoms	ρ_{bcp} ($\text{e}\text{\AA}^{-3}$)	$\nabla^2\rho_{\text{bcp}}$ ($\text{e}\text{\AA}^{-5}$)	G_{bcp} (kJ mol^{-1} bohr^{-3})	V_{bcp} (kJ mol^{-1} bohr^{-3})	$ V_{\text{bcp}} /G_{\text{bcp}}$	BD	DI
1'	C... Br1'	0.005	0.015	0.0031	-0.0023	0.76	0.14	0.04
	H _d '... Br2'	0.007	0.021	0.0043	-0.0032	0.75	0.15	0.03
2'	C... Br3'	0.008	0.023	0.0049	-0.0040	0.81	0.12	0.08
5'	H _p '... I1'	0.007	0.018	0.0036	-0.0028	0.77	0.12	0.05
	C... I2'	0.007	0.016	0.0034	-0.0026	0.78	0.11	0.07
	C... N2'	0.008	0.035	0.0069	-0.0051	0.74	0.21	0.04

Table 4.1.3. Bond critical points and associated topological properties corresponding to tetrel and hydrogen bonds for the B3LYP/DGDZVP electron densities computed on the crystal structures resulting from Hirshfeld atom refinement.

The BD parameter for the C...I2' is slightly lower than C...Br3' in **2'**. It follows that C...I2' in structure **5'** may be stronger than C...Br3' in **2'**. The trends highlighted in this section is confirmed by a third topological descriptor, the delocalization index (DI). It is a measure of the electrons shared between the two interacting partners. The DI values for C...Br3' in **2'** and C...I2' in **5'** are roughly double than the same parameter for C...Br1' in **1'**. Lastly, BD and DI clearly indicate that the C...N2' contact in structure **5'**, even if the ρ_{bcp} is comparable to the others, is less strong than those that involve the other nucleophiles.

The topological analysis confirmed that most interactions observed in the HAR structures were in fact TtBs. This highlights a possible general method to distinguish between HB and TtB thanks to crystallographic analysis. The IAM structures (Table 4.1.4.) provide similar information to those considered in the previous analysis, albeit less reliably. Due to a lower degree of accuracy of IAM data, all the N⁺-C-H angle are too similar to allow for a significant comparison. The distances between the hydrogen atoms and the nucleophiles are also generally longer, as a result of the different refinement methods.

However, the C-H...Nu angle range seem consistent with a carbon-based TtB for C...N1', the difference between the angles spanning just a little more than 1°. The remaining short contacts present C-H...Nu angles wider and more akin to an HB between the nucleophiles and one of the hydrogen atoms of the corresponding CH₃ group (Table 4.1.4. for a detailed list).

Structure	Nu	Hydrogen	Nu...H distance (Å)	N ⁺ -C-H angle (degrees)	Nu...H-C angle (degrees)
3	O	H _v	2.899	109.45	100.15
		H _w	2.988	109.47	94.01
		H _x	3.213	109.45	81.45
	Br4	H _y	3.249	109.47	99.04
		H _z	3.325	109.41	94.36
		H _{aa}	3.445	109.50	79.29
	Br5	H _{ab}	2.323	109.50	102.59
		H _{ac}	3.362	109.44	100.11
		H _{ad}	3.713	109.52	79.29
4	N1	H _{ae}	2.888	109.49	90.95
		H _{af}	2.889	109.50	90.89
		H _{ag}	2.892	109.47	90.71
	Br6	H _{ah}	3.202	109.49	105.93
		H _{ai}	3.411	109.44	92.88
		H _{aj}	3.598	109.44	82.08

Table 4.1.4. Geometric features of the hydrogen atoms in IAM structures **3** and **4** discussed in this section. Only hydrogen atoms bound to carbon atoms engaging in a close contact with a nucleophile (or mentioned in the text) are reported and numbered.

In summary, in the present section, we were able to analyse under various aspects the geometric and topological features typical of σ -hole interactions involving carbon atoms. We obtained different solvated structures of the same salt; therefore, it was possible to observe small variations between structures. This is crucial in the analysis of weak, elusive interactions like carbon-based TtB. The obtained structures display close contacts consistent with the definition of carbon based TtB, both with negatively charged species (halide anions) and neutral nucleophiles (acetonitrile solvent molecule). In order to better characterize the interactions taking place in the crystals, a series of computational tools were employed. First of all, HAR was performed on selected structures in order to obtain more reliable positions of the hydrogen atoms. The analysis of the bond critical points, besides confirming our initial assessment, was used to estimate the strength of the interactions. We were able to analyse the distinctive geometric and topological features of TtBs, distinguishing them from HBs by means of HAR, both with charged and neutral molecules. The experimental and computational data suggest that a higher linearity of the interaction serves as a better indicator the TtB presence than the normalised contact. The TtBs are invariably the contacts that display N⁺-C...Nu angles closer to 180° and not necessarily the shortest. As an example, -CH₃...Br1' in **1'** has even a N_c > 1. A tentative analysis on two structures refined with the standard IAM bring results similar to the ones described above. This highlights a possible generality of this approach that will be extended to the following sections.

Additional Data.

The experimental section contains crystallographic and computational details as well as CSD surveys.

4.2. Bis(pyridinium)methylene Salts as $-C(sp^3)H_2-$ -Tetrel Bond Donors.

In the pursuing of moieties able to display carbon TtBs, we focused our attention on the obtainment of crystal structures able to display short contacts between a nucleophile and a $-C(sp^3)H_2-$ moiety. A good candidate has been found in 1,1'-methylenebis(pyridinium) salts (bis-pyridyl methylene, Figure 4.2.1). The organic cation presents many useful perks that can allow for a TtB to occur. First, this molecule bears some resemblance to hexamethonium dication, as both display carbon atoms directly bound to a positive nitrogen. Second, the presence of two formally charged atoms directly bound to the $-C(sp^3)H_2-$ may make the methylene carbon atom a stronger electrophilic site than the methyl carbon atoms in hexamethonium dication. Third, the cation is fairly rigid, with a suitable area for approaching nucleophiles. Its niche application in building flexible and structure-directing coordination polymers^[33], MOFs^[34] and catenanes^[35] also draw attention to the noncovalent interaction profile of this compound.

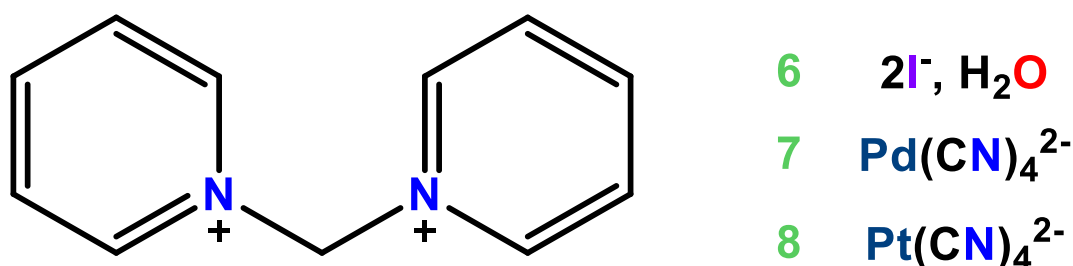


Figure 4.2.1. Scheme of the bis-pyridyl methylene salts obtained and presented in this work.

Differently from the methonium cations, the geometry of the selected system allows for a straightforward distinction of TtB from the HB involving the $-CH_2-$ atom. The competition between the two possible modes of interaction (TtB or HB) must still be taken into account when designing the interacting modules. On the CSD in fact, many of the structures including bis-pyridyl methylene cation display both TtB and HB involving the methylene group. Structures wherein HBs occur between the cation and nucleophilic species seem to be more numerous. Between the structures displaying a TtB, however, a preference for inorganic nitriles is noticeable. Among the 76 structures present on the CSD containing this organic cation, 49 present a short contact between the $-CH_2-$ carbon atom and a nucleophilic atom (Nucleophile=Nu=N, P, O, S, Se, F, Cl, Br, I; $N^+-C\cdots Nu > 160^\circ$). A relevant portion of them (8) are the nitrogen atom of a cyano group.

The compounds described in this section have been synthesized and characterized via single crystal X-Ray diffraction, the structures invariably revealed the presence of short and linear close contacts between the organic cation and the anion. A computational study, demonstrating the electrophilic role of carbon thanks to the calculation of the electrostatic potential of the dication mapped over the 0.001 a.u. electron density isosurface, has been performed.

The obtainment of the salts started from the synthesis of the halides. The synthesis (Figure 4.2.2) was carried out by using a slight modification of a reported procedure^[36]. A solution of pyridine (20 mL) was added to an equimolar amount of CH_2X_2 (X= Cl, I). The resulting solution was stirred at 40 °C for 48 hours.

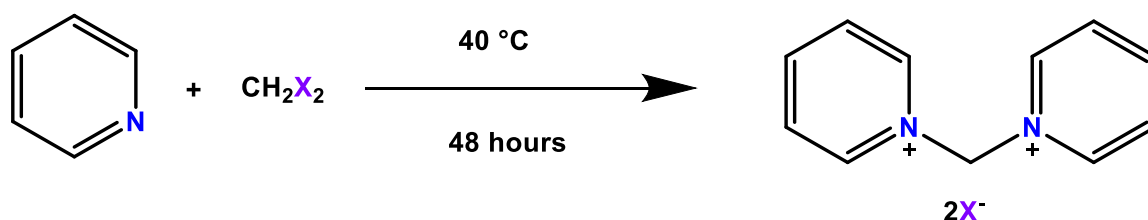


Figure 4.2.2. Schematic representation of the synthesis of bis-pyridyl methylene halides (X = Cl, I).

The diiodide hydrate **6** crystallizes in the space group Fdd2 and is isomorphous to the already published hydrate chloride^[37] and bromide^[38] salts. The iodide anions are located remarkably close to the electrophilic $-\text{CH}_2-$ carbon and form two identical $\text{C}\cdots\text{I}$ close contacts giving rise to a well-defined and neutral trimeric unit in the crystal (Figure 4.2.3.). The $\text{C}\cdots\text{I}$ separation is 3.639 Å (the corresponding Nc is 0.94) and the $\text{N}^+-\text{C}\cdots\text{I}$ angle is 168.51°.

These geometrical features are consistent with the presence of a strong charge assisted TtB between the interacting partners. The $\text{C}\cdots\text{I}$ distance is much shorter in diiodide **6** than in monoiodide **5** (Figure 4.1.3), demonstrating that the electrophilicity of the $-\text{CH}_2-$ carbon (bound to two positively charged nitrogen atoms) is higher than that of the $-\text{CH}_3$ carbon (bound to one positively charged nitrogen). The isostructural chloride analogous presents a slightly longer (the Nc value is 0.95) but more linear (the $\text{N}^+-\text{C}\cdots\text{Cl}$ angle is 173.29°) TtB. This is likely the consequence of the reduced dimension of the chloride anion in respect to the iodide. Importantly, there is no $\text{H}\cdots\text{I}$ short contact between the iodide anions and the $-\text{CH}_2-$ hydrogen atoms of the tetrel bonded bis-pyridyl methylene dication. Instead, each iodide anion of a tetrel bonded trimeric unit

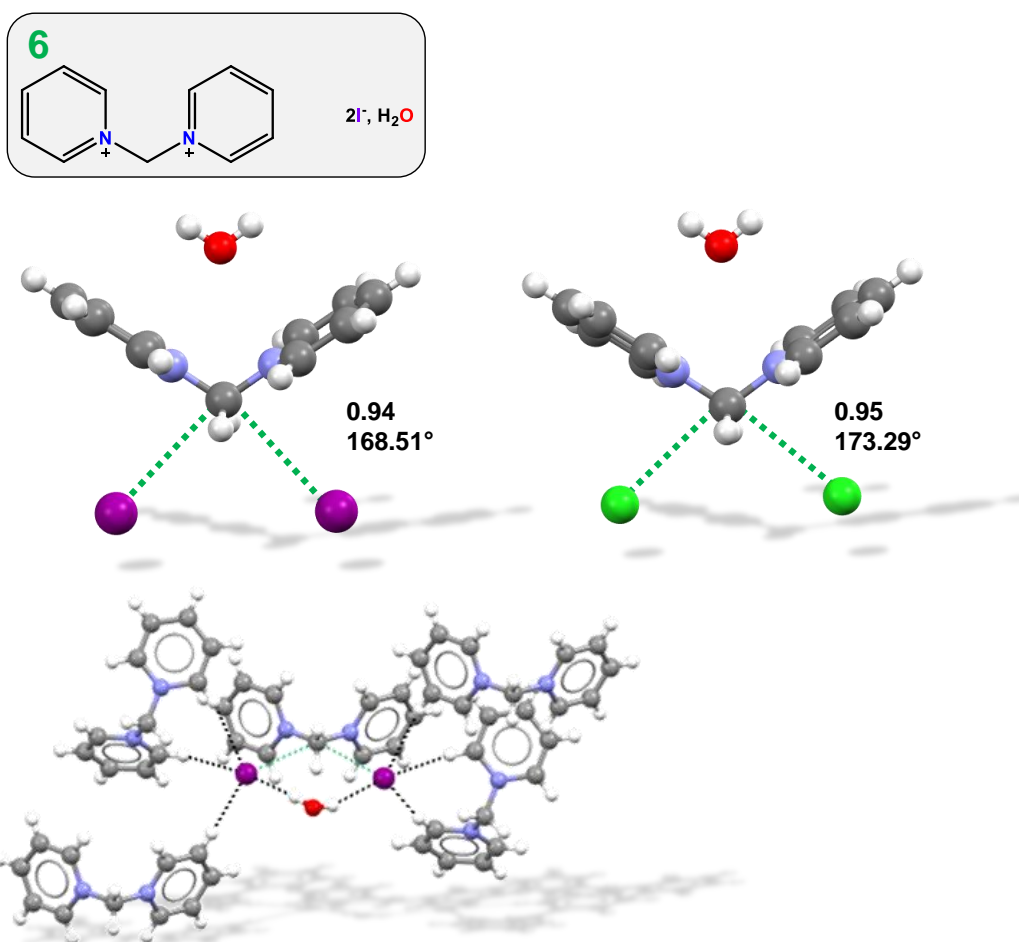


Figure 4.2.3. Structural formula of bis-pyridyl methylene diiodide dehydrate **6** (*top*). Ball and stick representation of the trimeric and tetrel bonded structural unit in **6** (*mid left*) and its isostructural unit formed by the chloride analogue (refcode NUQXED, *mid right*). Ball and stick representation of a trimeric and tetrel bonded structural unit and the bis-pyridyl methylene and water molecules hydrogen bonded to the two iodide anions (*bottom*). TtBs between CH₂ groups and approaching nucleophiles are denoted as green dotted lines. HBs are black dotted lines. Nc of C...Nu separation and N⁺-C...Nu angles are reported near the contact. Colour code: gray carbon; whitish hydrogen; light blue nitrogen; red oxygen; green chlorine; purple iodine.

forms four H...I HBs with the *ortho* and *meta* hydrogens of pyridyl groups belonging to two different bis-pyridyl methylene dications and a water molecule (Figure 4.2.3, bottom).

The tetracyanopalladate salt **7** crystallizes in the space group P2₁/c. In the unit cell of the crystal there are two crystallographically independent tetracyanopalladate anions and one bis-pyridyl methylene cation. The bis-pyridyl methylene cation functions as bidentate TtB donor and forms two different N⁺-C...N contacts with two nitrogen atoms of two different tetracyanopalladate anions (Figure 4.2.4). The shorter TtB measures 3.168 Å (Nc

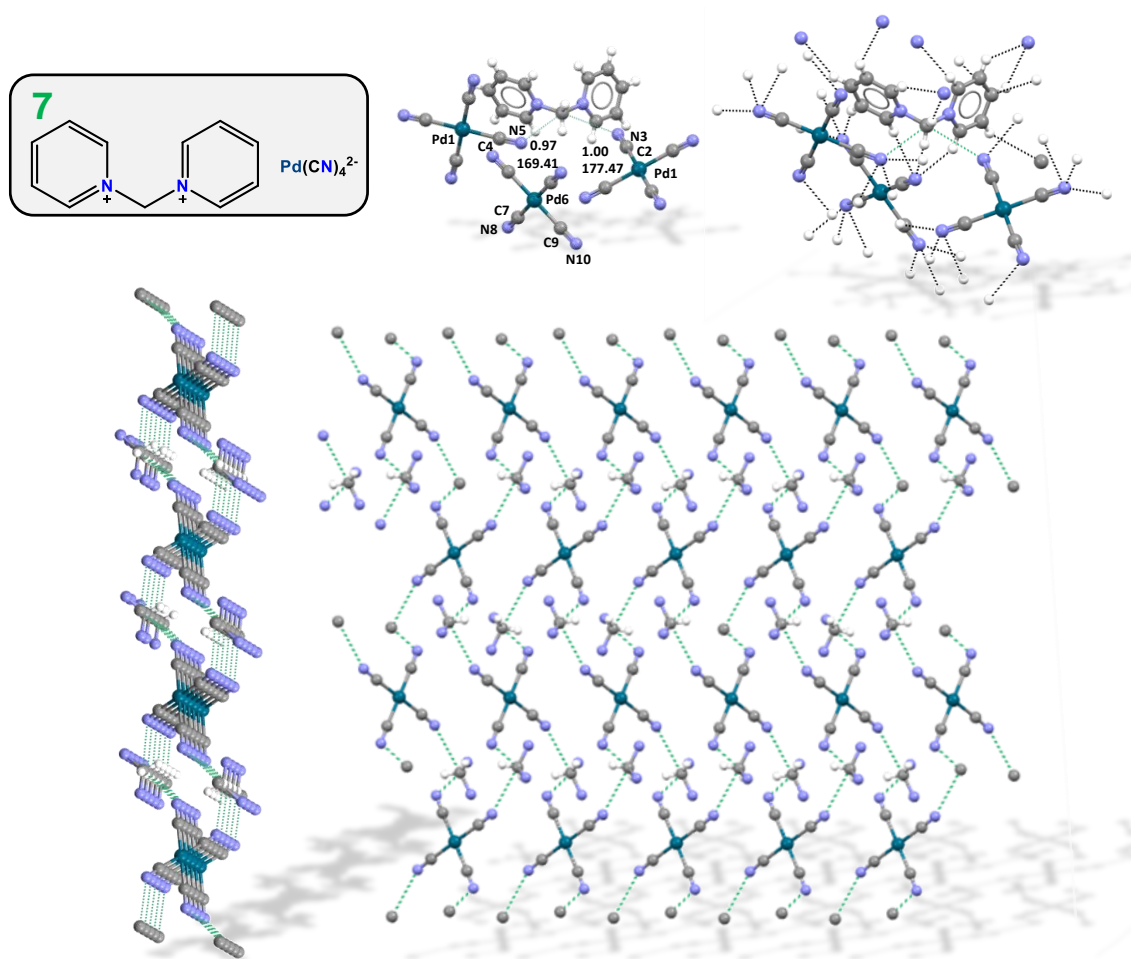


Figure 4.2.4. Structural formula of bis-pyridyl methylene tetracyanopalladate(II) **7** (*top left*). Ball and stick representation of the trimeric and tetrel bonded structural unit in **7**; also the tetracyanopalladate anion present in the unit cell of the depicted bis-pyridyl methylene and forming no TtB is displayed (*top mid*). Network of HBs formed by the trimeric and tetrel bonded structural unit of **7** displayed in *top mid* (*top right*). Partial view of the (4,4) network formed by the $N^+-C\cdots N$ TtBs approximately along the *b* axis (*bottom left*) and along the *a* axis (*bottom right*); for sake of simplicity, the two pyridinium groups are represented by their nitrogen atoms only (namely the CH groups have been deleted). The TtBs between CH_2 groups and approaching nitrogen atoms are green dotted lines. HBs are black dotted lines. N_c of $C\cdots Nu$ separation (Å) and $N^+-C\cdots Nu$ angles (°) are reported near the contact. Colour code: *gray* carbon; *whitish* hydrogen; *light blue* nitrogen; *bluish* palladium.

= 0.97) and establishes an $N^+-C\cdots N$ angle of 169.41°. The longer one (3.268 Å, N_c 1.00) is much more linear, with an $N^+-C\cdots N$ angle of 177.47°.

One of the tetracyanopalladate anions forms no $N^+-C\cdots N$ short contacts and the other acts as tetradentate TtB acceptor. From a topological point of view a two-dimensional network is formed (Figure 4.2.4), specifically a (4,4) net where the tetracyanopalladate anions sits at the nodes and the bis-pyridyl methylene cations act as spacers between two anions. Finally, the cyano groups of both crystallographically independent

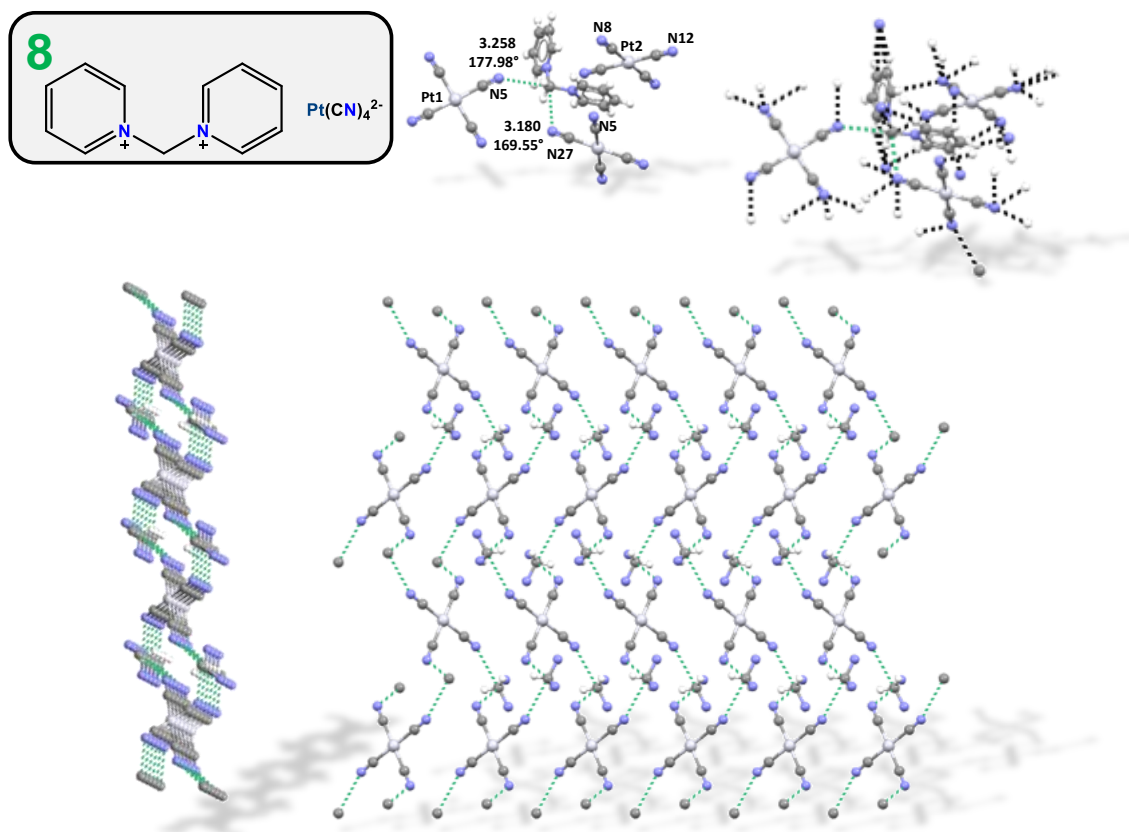


Figure 4.2.5. Structural formula of bis-pyridyl methylene tetracyanoplatinate(II) **8** (*top left*). Ball and stick representation of the trimeric and tetrel bonded structural unit in **8**; also the tetracyanoplatinate anion present in the unit cell of the depicted bis-pyridyl methylene and forming no TtB with the $-\text{CH}_2-$ unit is displayed (*top mid*). Network of HBs formed by the trimeric and tetrel bonded structural unit of **8** displayed in *top mid* (*top right*). Partial view of the (4,4) network formed by the $\text{N}^+-\text{C}\cdots\text{N}$ TtBs approximately along the b axis (*bottom left*) and along the a axis (*bottom right*); for sake of simplicity, the two pyridinium groups are represented by their nitrogen atoms only (namely the CH groups have been deleted). The TtBs between CH_2 groups and approaching nitrogen atoms are green dotted lines. HBs are black dotted lines. N_c of $\text{C}\cdots\text{N}$ separation (Å) and $\text{N}^+-\text{C}\cdots\text{N}$ angles ($^\circ$) are reported near the contact. Colour code: *gray* carbon; *whitish* hydrogen; *light blue* nitrogen; *pearl* palladium.

tetracyanopalladate units gives rise to a dense network of HBs, but unequivocally the $-\text{CH}_2-$ group forms the $\text{H}\cdots\text{N}$ HBs with tetracyanopalladate units different from those forming the $\text{C}\cdots\text{N}$ TtBs.

Crystal structure **8** (tetracyanoplatinate salt, Figure 4.2.5) crystallizes in the space group $\text{P2}_1/\text{n}$, retaining remarkable similarities with **7**. Here too the $-\text{CH}_2-$ moiety functions as bidentate TtB donor and forms two different $\text{N}^+-\text{C}\cdots\text{N}$ contacts with two nitrogen atoms of two different tetracyanoplatinate anions. The shorter contact measures 3.177 Å ($N_c=0.98$) and establishes an $\text{N}^+-\text{C}\cdots\text{N}$ angle of 169.55° , the longer one (3.256 Å, $N_c=1.00$)

is much more linear, with an $N^+-C\cdots N$ angle of 177.98° . Two tetracyanoplatinate anions are present in the unit cell, one of them forms no TtBs involving the $-CH_2-$ moiety while the other forms four TtBs. The $-CH_2-$ group forms the $H\cdots N$ HBs with tetracyanoplatinate units different from those forming the $C\cdots N$ TtBs.

The molecular electrostatic potential (MEP) of the dipyriddy methylene cation was computed by using the M06-2x/6-311(d)G level of theory. The potential was calculated over the 0.001 a.u. electron density isosurface for the symmetric conformation adopted by the cation in the diiodide **6** (Figure 4.2.6). The whole molecular surface is positive, as expected for a cation, but the region of the $-CH_2-$ moiety is the most positive part. Two local maxima where the potential is most positive ($V_{s,max} = 818.42$ kJ/mol) are found approximately on the extension of the N^+-C covalent bonds (the $N^+-C\cdots\sigma$ -hole angle is 170.710°) and this computed geometric feature nicely correlates with the experimental $N^+-C\cdots$ nucleophile angles in the crystal structures.

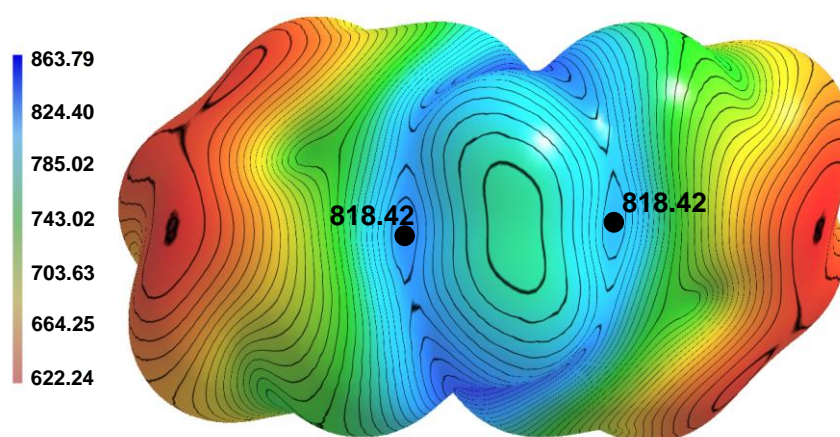


Figure 4.2.6. Molecular electrostatic potential calculated over the 0.001 au surface of dipyriddy methylene dication. The values of the $V_{s,max}$ are given in kJ/mol. Electron densities resulting from DFT calculations at M06-2x/6-311(d)G level.

These calculations unambiguously support the rationalization of the $C(sp^3)\cdots$ nucleophile close contacts observed in **6-8** as TtBs.

The results herein presented complement the analysis carried out for hexamethonium salts discussed in the previous section, as well as our precedent work on barbituric acid derivatives^[39]. Specifically, they prove that the tendency of the N^+-CH_3 and $N^+-CH_2-N^+$ -moieties to work as TtB donor sites is strong enough to affect and possibly direct the crystal packing adopted by solid materials. Interestingly, the latter moiety has a marked tendency to act as bidentate TtB donor site.

Additional Data.

The experimental section contains synthetic, crystallographic and computational details as well as CSD surveys.

4.3. Tetrel Bonds in Choline and Betaine derivatives.

Choline and its derivatives are a family of compounds where a $-\text{CH}_2\text{CH}_2-$ bears a quaternary ammonium cation at one end and an oxygenated and electron rich group at the opposite end. Most cholines exist both as salts with different anions or in zwitterionic form when the oxygenated group can be negatively charged. Choline hydroxide is generally known as choline base^[40], while other compounds, given their importance in many organisms, are usually referred to with common names. Between them, the most important are acetylcholine (2-acetoxy-*N,N,N*-trimethylethanaminium)^[41,42], phosphatidylcholine (2-phosphonoxy-*N,N,N*-trimethylethanaminium)^[43] and betaine (*N,N,N*-trimethylglycine)^[44], all retaining important functions in many different organisms, including humans. A complete list of the quaternary ammonium salts considered in this study and their common name is given in Figure 4.3.1.

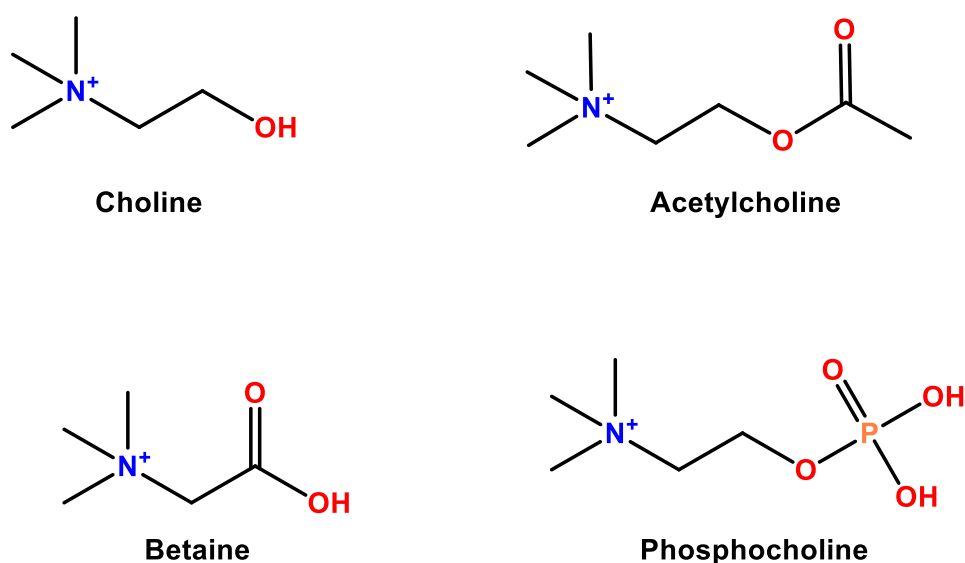


Figure 4.3.1. Structural formulas and common names of some compounds of the choline family.

Choline serves many functions in the human body^[40]. Its most important function is to be a key component in the biosynthesis of many other bioactive compounds. It can be converted into different phospholipids like phosphatidylcholine (an important metabolic product, accounting for roughly 95% of the choline present in the human body) or sphingomyelins (cell membranes constituents). Alternatively, choline can serve as the precursor of the important neurotransmitter acetylcholine or of the osmoregulator betaine^[45].

These compounds are related to each other in vivo thanks to choline metabolism (Figure 4.3.2). Transformations in this metabolic map occur via many different routes which will not be discussed thoroughly, but a few information regarding the relations between the compounds suggest a possible role of the noncovalent interactions most relevant to the respective biological pathway. Different routes involve the loss or acquisition of methyl groups on the nitrogen, e.g., when *S*-adenosyl methionine acts as the methyl source. This methyl exchange seems particularly interesting as TtB and ChB may possibly be involved in the initial stages of the reactions, as confirmed by computational analyses on the subject^[46,47].

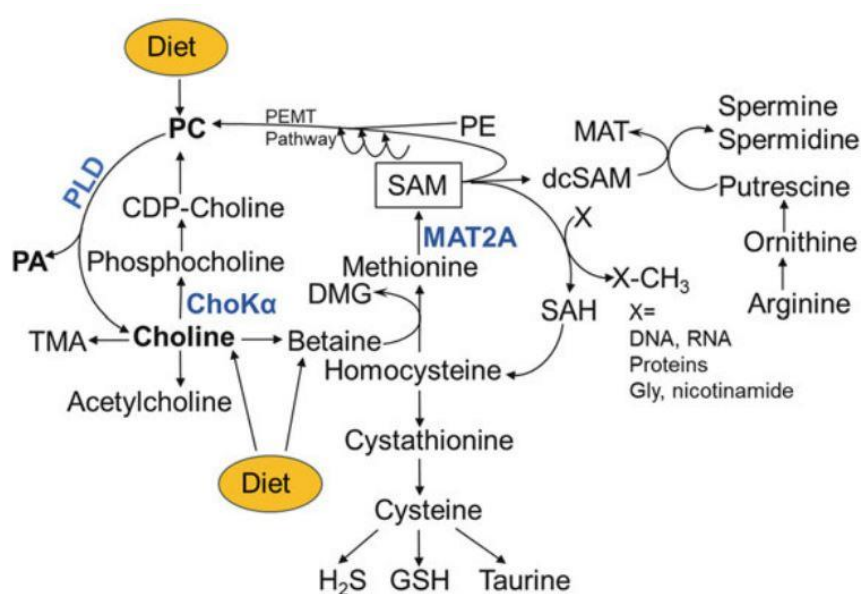


Figure 4.3.2. General and partial scheme of choline metabolism. Reprinted from Handbook of Experimental Pharmacology, 2019. Phospholipase D and Choline Metabolism. (Chapter 320).

There is a significant body of work regarding the synthesis, transport, storage and excretion of choline and related compounds,^[48] in addition to the studies of the enzymes mediating these processes^[49]. However, only a small part of these researches are devoted to exploring the interaction between enzymes and their choline-based substrates. The most relevant studies available, as of 2021, revolve around the two main families of receptors for acetylcholine: nicotinic and muscarinic receptors^[50]. The first family was studied thoroughly in the past years, concluding that cation... π is likely the main force governing the interaction between the positive trimethylammonium head of acetylcholine and the tyrosine residues of said receptors^[51]. Considering the latter, there is one example of muscarinic receptor binding tiotropium (an antagonist of acetylcholine) where the

interaction is interpreted as a strong TtB between an aspartate residue of the active site and the N^+-CH_3 methyl group of the tiotropium^[15,52].

Even if the study of the specific interaction motives of this family of compounds with biological receptors is scarce, the Cambridge Structural Database (CSD) provides good examples of carbon atoms of choline derivatives engaging in close contacts with nucleophiles along their N^+-C covalent bonds^[53–57]. Although a more rigorous search and assessment of the modes of interaction has to be performed, we felt that those evidence were enough to deserve further study.

We decided to focus our attention on the obtainment of various choline and choline-related salts able to engage in the interactions of interest. Salts of small, strongly nucleophilic anions served as a model to study the interaction motif.

The chemical and structural diversity of adducts proposed in this section ultimately confirm the robustness of the N^+-CH_3 synthon, which is able to emerge as a reliable TtB donor over the wide variety of the structures and experimental conditions adopted and the resulting interactional landscapes.

On slow isothermal evaporation of an isopropanol solution of betaine zwitterion (*N,N,N*-trimethylglycine) and of perchloric acid, the betaine perchlorate was isolated as its monohydrate form **9** (Figure 4.3.2). The compound shows in the solid a short and quite

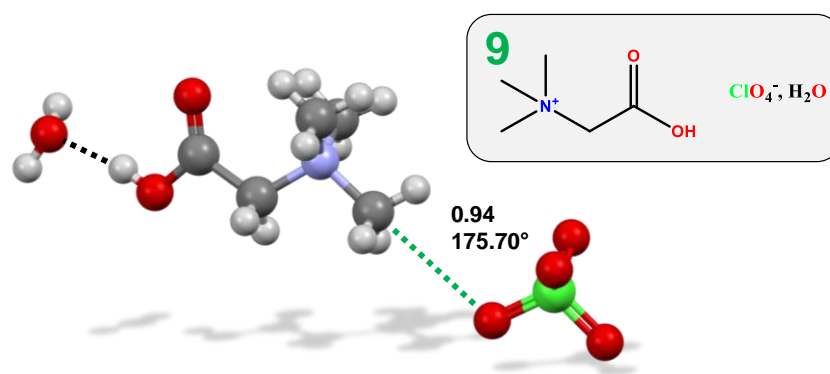


Figure 4.3.2. Structural formula of betaine perchlorate hydrate **9** and partial ball and stick representation of the packing evidencing the $\text{N}^+-\text{C}\cdots\text{O}$ TtB (green dotted line). N_c of $\text{C}\cdots\text{O}$ separation and $\text{N}^+-\text{C}\cdots\text{O}$ angle are reported near the contact. Hydrogen bond is a black dotted line. Colour code: *gray* carbon; *whitish* hydrogen; *light blue* nitrogen; *red* oxygen; *green* chlorine.

linear $\text{N}^+-\text{C}\cdots\text{O}$ contact between a betaine methyl residue and a perchlorate oxygen (the N_c value of the $\text{C}\cdots\text{O}$ separation is 0.94, the $\text{N}^+-\text{C}\cdots\text{O}$ angle is 175.50°). The rationalization of this contact as a TtB is supported by the $\text{C}-\text{H}\cdots\text{O}$ angles which are all close to 90° and are

quite similar to each other (Table 4.3.1). This system thus provides a reliable example of the general ability^[58,59] of this class of compounds to engage their N⁺-CH₃ residue(s) in C(sp³)...nucleophile σ -hole interactions. Importantly, it can be expected that the overall crystal packing of **9** is mainly determined by the strong electrostatic cation-anion attraction and by the net of HBs involving the perchlorate anion, the water molecule and the carboxylic residue. The presence of the N⁺-C...O TtB in the crystal suggests that the N⁺-CH₃ moiety is a TtB donor moiety robust enough to show out despite the severe constraints resulting from interactions as strong as the cation-anion and HB attractions mentioned above. Indeed, it effectively cooperate with them in determining the adopted crystal packing.

Acetylcholine perrhenate salt **10** crystallizes in the P-1 space group. Acetylcholine units function as monodentate donors of C(sp³) TtBs via one of their ammonium methyl residues and as monodentate acceptors via the oxygen of the carbonyl functionality. The normalized contact of the resulting C...O separation is 3.047 Å (corresponding to an Nc value of 0.95) and the N⁺-C...O angle is 172.46°. These σ -hole bonds form infinite chains of acetylcholine units, suggesting that the TtB has a non-minor role in driving the formation of this crystal packing (Figure 4.3.3). The three C-H...O angles fall in the range between 86 and 99° (Table 4.3.1), namely, once again, the position of the hydrogen atoms is consistent with the definition of a TtB.

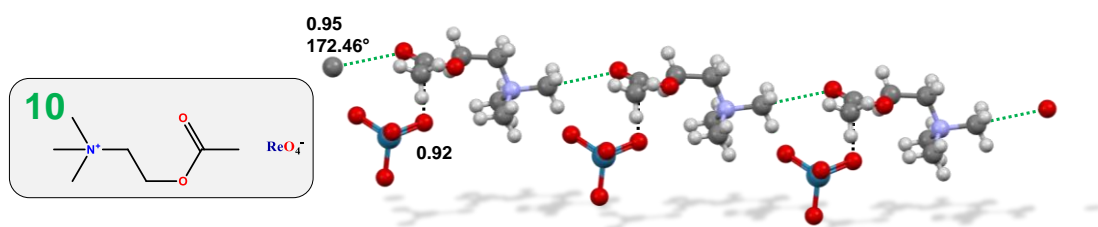


Figure 4.3.3. Structural formula of acetylcholine perrhenate **10** and partial ball and stick representation of one supramolecular infinite chain assembled via σ -hole TtBs (light green dotted lines) between the carbonyl oxygen (TtB acceptor site) and the (sp³) carbon of one ammonium methyl groups (TtB donor site). Perrhenate anions are appended to this chain via π -hole TtBs (dark green dotted lines) between one perchlorate oxygen (TtB acceptor site) and the carbonyl carbon /TtB donor site). Nc values of C...O separations and N⁺-C...O angle are reported near the contacts. Colour code: *gray* carbon; *whitish* hydrogen; *light blue* nitrogen; *red* oxygen; *navy blue* rhenium.

The perrhenate anions are appended to the chains assembled by these σ -hole bonds via π -hole bonds, specifically TtBs wherein the donor site is the (sp²) carbon atom of the carboxylic group of the cation and the acceptor site is one of the oxygen atoms of the

perrhenate anion. The separation of the two interacting atoms in this π -hole bond is 3.167 Å, corresponding to an Nc of 0.92.

Phosphocholine perrhenate sodium salt (phosphoryl choline perrhenate sodium salt) was obtained as its heptahydrate **11** from commercially available phosphocholine chloride sodium salt through an anion metathesis reaction by using silver perrhenate. Interestingly, 22 structures in the CSD contain the phosphocholine moiety. Two of the phosphory oxygen atoms are covalently bonded to a carbon or a second phosphoryl residue in 21 of them and compound **11** is the second case wherein the phosphory unit of phosphocholine is in the dianionic form (the only other system containing the $-\text{PO}_3^{2-}$ moiety is phosphocholine chloride calcium salt, Refcode PHSCHL). The compound **11** crystallizes in the P-1 space group. Sodium cations form a cluster with water molecules pinned in their coordination sphere and giving rise to a network of HBs which heavily affect the overall crystal packing. Also, perrhenate anions are pinned in the coordination sphere of sodium cations, but despite the overall structural constrains, they form two short, directional and quite similar $\text{N}^+-\text{C}\cdots\text{O}-\text{Re}$ TtBs ($\text{C}\cdots\text{O}$ separations are 3.147 and 3.188 Å, corresponding to an Nc value of 0.91 and 0.92 respectively, and $\text{N}^+-\text{C}\cdots\text{O}$ angles are 173.66° and 179.30° , respectively) (Figure 4.3.4). Here too, the position of the hydrogen atoms of the tetrel bonded methyl groups supports the rationalization of these $\text{C}\cdots\text{O}$ interactions as TtBs rather than HBs (Table 4.3.1).

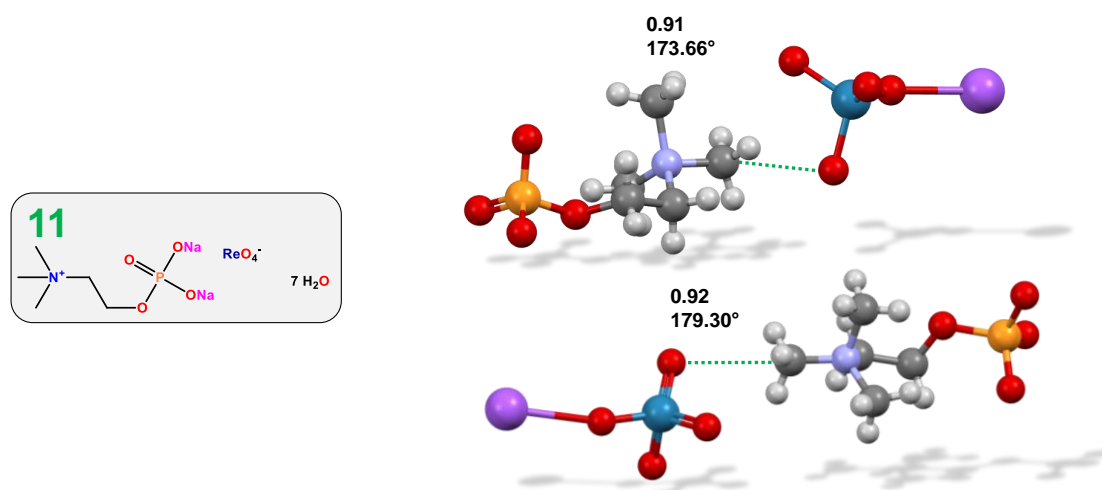


Figure 4.3.4. Structural formula of phosphocholine perrhenate sodium salt heptahydrate **11** and partial ball and stick representation of the two tetrel bonded dimeric systems. Water molecules and half sodium cations present in the unit cell are not depicted for sake of clarity. TtBs are green dotted lines, Nc values of $\text{C}\cdots\text{O}$ separations and $\text{N}^+-\text{C}\cdots\text{O}$ angles are reported near the contacts. Colour code: *gray* carbon; *whitish* hydrogen; *light blue* nitrogen; *red* oxygen; *navy blue* rhenium; *ocher* phosphorous; *magenta* sodium.

When choline chloride is treated with HAuCl_4 in isopropanol, the corresponding tetrachloridoaurate(III) salt **12** is obtained and betaine zwitterion similarly affords betaine tetrachloridoaurate(III) salt **13**. Single crystal X-ray analyses of these two systems reveals that unit cells are remarkably big and contain several crystallographic independent cation and anion units. The unit cell volume of choline salt **12** is 3614 \AA^3 and of betaine salt is **13** 4952 \AA^3 , the respective Z values being 12 and 15 (Figure 4.3.5). The interactional landscape is quite complex, comprising $\text{O-H}\cdots\text{O}$, $\text{O-H}\cdots\text{Cl}$, $\text{C-H}\cdots\text{Cl}$, and even $\text{Au}\cdots\text{O}$ short contacts.

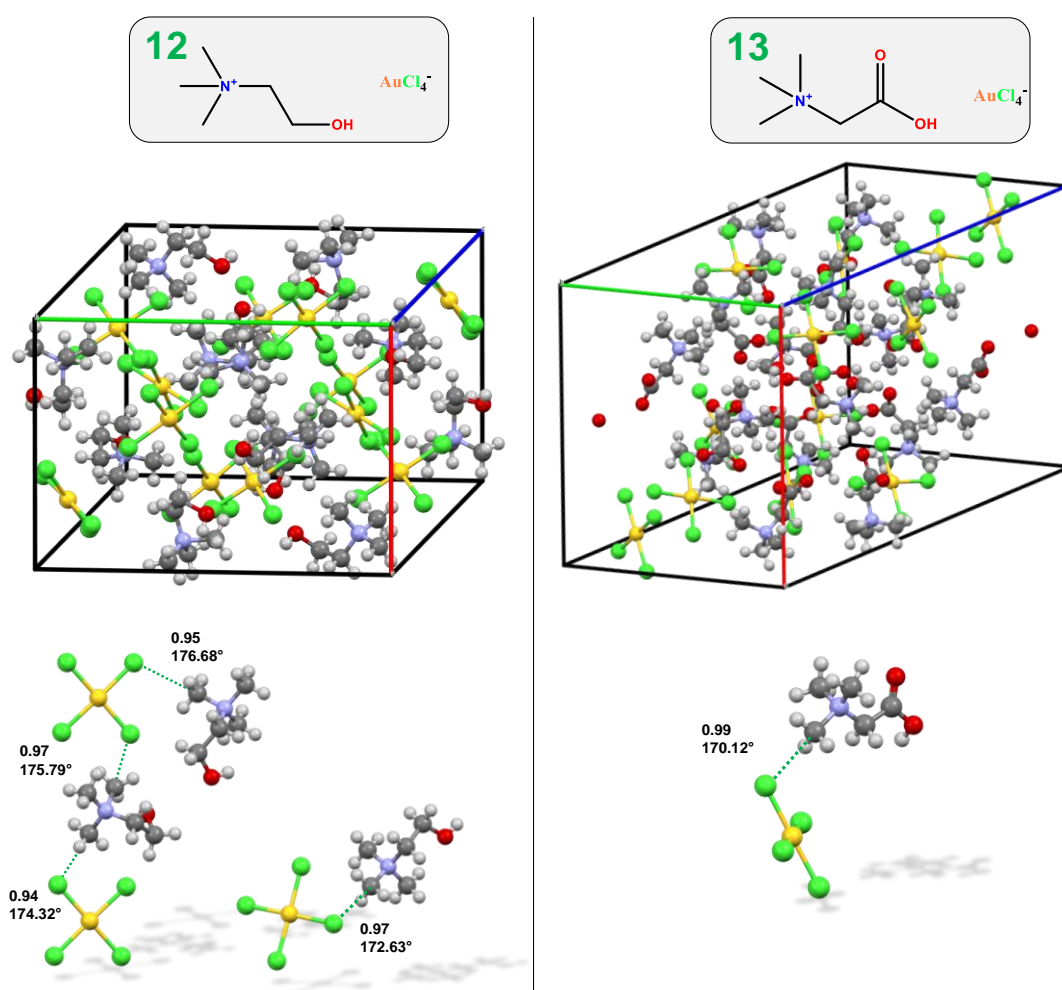


Figure 4.3.5. (above) Unit cell contents of the tetrachloridoaurate(III) salts of choline **12** (left) and betaine **13** (right). Structural formulas are also reported. (below) Ball and stick representation of the four (left) and one (right) tetrel bonded adducts fulfilling the adopted geometric requirements in the tetrachloridoaurate(III) salts of choline **12** and betaine **13**, respectively. TtBs are denoted as green dotted lines. Nc values of $\text{C}\cdots\text{Cl}$ separation and $\text{N}^+-\text{C}\cdots\text{Cl}$ angles are reported near the contact. Colour code: gray carbon; whitish hydrogen; light blue nitrogen; red oxygen; green chlorine; golden gold.

Several $N^+-C\cdots Cl$ which might be rationalized as TtB are present in both structure. In order to avoid possible misinterpretations in this rationalization, we adopted quite rigid and demanding geometric prerequisites, namely $N^+-C\cdots Cl$ angle $> 170^\circ$ and $C\cdots Cl$ separation below 3.51 Å (sum of van der Waals radius of carbon (1.70 Å) and Pauling anionic radius of chloride (1.81 Å)). Four and one of the $N^+-C\cdots Cl$ close contacts present in **12** and **13** passed this selection, respectively. They are depicted in Figure 4.3.5 and the geometric features are reported in Table 4.3.1.

In all ammonium systems described above, the $C(sp^3)$ atom involved in the TtB is of a $-CH_3$ group. It was also possible to find derivatives where the tetrel bonded $C(sp^3)$ atom belongs also to a $-CH_2-$ moiety. The structural formulas of the two systems showing this behaviour are reported in Figure 4.3.7.

Structure	Nucleophile	$N^+-C\cdots Nu$ (degrees)	$C\cdots Nu$ separation (Å) (Nc)	$C-H\cdots Nu$ angles (degrees)
9	O	175.70	3.269 (0.94)	87.95
				92.87
				95.29
10	O	172.46	3.047 (0.95)	86.21
				87.56
				98.41
11	O	173.66	3.171 (0.92)	86.36
				90.55
	O	179.30	3.148 (0.91)	97.39
				90.98
12	Cl	172.63	3.405 (0.97)	91.38
				91.66
	Cl	176.68	3.353 (0.95)	85.96
				95.00
Cl	174.32	3.317 (0.94)	98.35	
			91.15	
Cl	175.79	3.417 (0.97)	91.16	
			96.19	
13	Cl	170.12	3.501 (0.99)	88.42
				91.33
				98.21
				89.31
				93.56
				96.62
				84.14
				95.82
				100.59

Table 4.3.1. List of the short contacts between CH_3 carbons and nucleophiles reported in this paragraph.

Succinylcholine chloride (suxamethonium chloride, Figure 4.3.7) is a mimic of acetylcholine and its cation shares some similarities in structure and properties with the

methonium salts **1-5** described in the first paragraph of this chapter. It is an ultra-short acting, depolarising, neuromuscular blocking agent used in human anaesthesia. It is a skeletal muscle relaxant and facilitates tracheal intubation and mechanical ventilation surgical procedures. Crystals of succinylcholine perrhenate **14** show the presence of two identical and symmetry related O–C⋯O–Re contacts which involve the –CH₂O choline moieties and the perrhenate anions (Figure 4.3.8, left). The interactions occur approximately on the extension of the O–C covalent bond of choline molecules, namely they possibly involve the most positive σ -hole at this carbon. While these TtBs are not particularly linear (the O–C⋯O angle is 162.42°), the C⋯O separation is remarkably short (3.093 Å, corresponding to an Nc value of 0.89). Succinylmonocholine, namely the partial hydrolyses product of succinyl choline, is a metabolic product of succinyl choline. Crystals of succinylmonocholine nitrate **15** show the presence of a O–C⋯O–N TtB (Figure 4.3.8, right) very similar to the O–C⋯O–Re TtBs observed in succinylcholine perrhenate **14**.

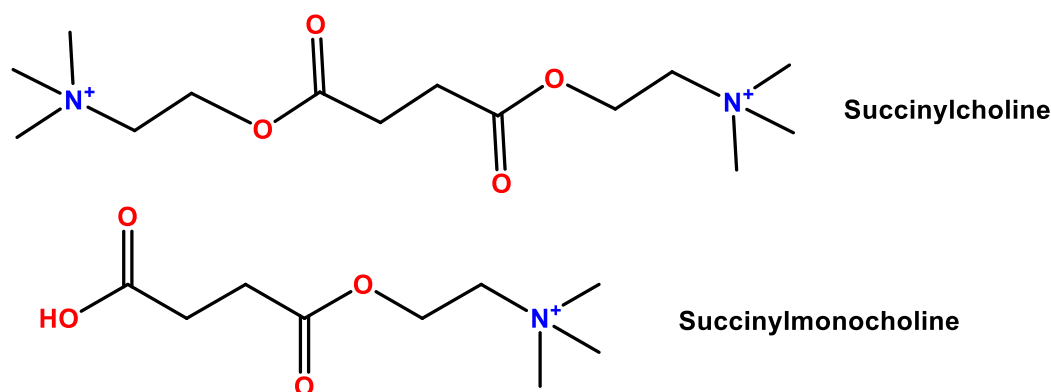


Figure 4.3.7. Structural formulas and common names of the two systems showing the presence of O–C⋯O TtBs involving –CH₂– groups as donor sites.

Specifically, the O–C⋯O TtB in **14** is slightly longer and more directional than in **15** (the C⋯O separation is 3.189 Å, corresponding to an Nc value of 0.92, and the O–C⋯O angle is 168.12°). The finding of short O–C⋯O contacts in crystals where the TtB donor is either succinylcholine or succinylmonocholine cation and the TtB acceptor is either the ReO₄[–] or the NO₃[–] (i.e., in the salts **14** and **15**), suggests that the formation of the O–C⋯O interaction is more a result of the inherent interactional profile of the (CH₃)₃N⁺CH₂CH₂–O–C(=O) moiety rather than of a crystal packing effect.

The structures discussed in this section confirm the propensity of derivatives of choline and betaine to engage in TtBs, both through their methyl and methylene carbon atoms. Previous sections served as working examples of the structural motifs enabling for the

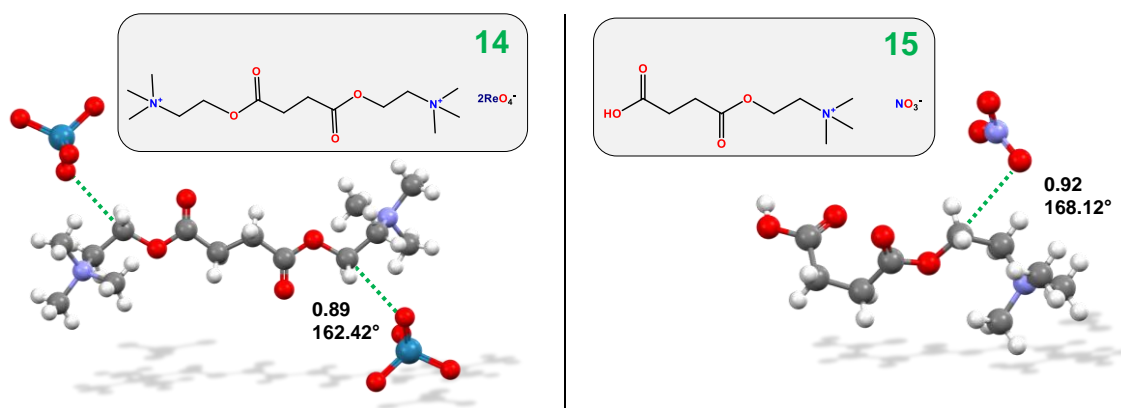


Figure 4.3.8. Structural formulas and ball and stick representation of the tetrel bonded adducts in succinylcholine perrhenate **14** (left) and succinylmonocholine nitrate **15** (right). TtBs are denoted as green dotted lines. Nc values of C...O separations and N⁺-C...O angles are reported near the contact. Colour code: gray carbon; whitish hydrogen; light blue nitrogen; red oxygen; navy blue rhenium.

formation of robust short contacts at C(sp³) carbon atoms (sections 4.1 and 4.2) and of the geometrical features enabling for the dependable rationalization of these short contacts as TtBs (section 4.1). This section demonstrates how the TtBs discussed in previous sections can be a distinctive feature of important bioactive compounds. Specifically, it is shown how a wide diversity of choline derivatives (spanning acetylcholine, phosphocholine, succinylcholine, and succinylmonocholine) all function as TtB donors, and they form contacts which can be so short that the respective Nc value are as small as 0.90 when both -CH₃ and -CH₂- groups are serving as donor sites. A wide diversity of anions can act as TtB acceptor sites (i.e., ClO₄⁻, ReO₄⁻, AuCl₄⁻ and NO₃⁻). This variety in the involved modules forcefully suggest that observed TtBs are not a result of crystal packing effects, but of the inherent interactional profile of the cations. It is thus likely that they may survive in solution and contribute to the interactional profile determining the recognition processes of these compound in living systems.

Additional Data.

The experimental section contains synthetic procedures, characterization, and crystallographic details of the reported structures.

References.

- [1] A. Daolio, P. Scilabra, G. Terraneo, G. Resnati, *Coord. Chem. Rev.* **2020**, *413*, 213265.
- [2] S. J. Grabowski, *Phys. Chem. Chem. Phys.* **2014**, *16*, 1824–1834.
- [3] D. Mani, E. Arunan, *Phys. Chem. Chem. Phys.* **2013**, *15*, 14377–14383.
- [4] M. H. Nantz, L. Li, J. Zhu, K. L. Aho-Sharon, D. Lim, K. L. Erickson, *Biochim. Biophys. Acta - Lipids Lipid Metab.* **1998**, *1394*, 219–223.
- [5] R. M. Eglén, A. D. Michel, C. M. Cornett, E. A. Kunysz, R. L. Whiting, *Br. J. Pharmacol.* **1989**, *98*, 499–506.
- [6] D. Malin, *Pharmacol. Biochem. Behav.* **1997**, *58*, 695–699.
- [7] T. Sugino, J. Yamaura, M. Yamagishi, Y. Kurose, M. Kojima, K. Kangawa, Y. Hasegawa, Y. Terashima, *Biochem. Biophys. Res. Commun.* **2003**, *304*, 308–312.
- [8] S. R. Williams, L. N. Fletcher, *Neuron* **2019**, *101*, 486-499.e4.
- [9] X. Liu, U. Ravon, A. Tuel, *Microporous Mesoporous Mater.* **2012**, *156*, 257–261.
- [10] J. Martí-Rujas, L. Meazza, G. K. Lim, G. Terraneo, T. Pilati, K. D. M. Harris, P. Metrangolo, G. Resnati, *Angew. Chemie Int. Ed.* **2013**, *52*, 13444–13448.
- [11] J. X. Lin, A. Daolio, P. Scilabra, G. Terraneo, H. Li, G. Resnati, R. Cao, *Chem. - A Eur. J.* **2020**, *26*, 11701–11704.
- [12] C. R. Groom, I. J. Bruno, M. P. Lightfoot, S. C. Ward, *Acta Crystallogr. Sect. B Struct. Sci. Cryst. Eng. Mater.* **2016**, *72*, 171–179.
- [13] E. Bartashevich, Y. Matveychuk, V. Tsirelson, *Molecules* **2019**, *24*, 1083.
- [14] A. Karim, N. Schulz, H. Andersson, B. Nekoueshahraki, A.-C. C. Carlsson, D. Sarabi, A. Valkonen, K. Rissanen, J. Gräfenstein, S. Keller, M. Erdélyi, *J. Am. Chem. Soc.* **2018**, *140*, 17571–17579.
- [15] K. Akiba, Y. Moriyama, M. Mizozoe, H. Inohara, T. Nishii, Y. Yamamoto, M. Minoura, D. Hashizume, F. Iwasaki, N. Takagi, K. Ishimura, S. Nagase, *J. Am. Chem. Soc.* **2005**, *127*, 5893–5901.
- [16] K. Y. Akiba, M. Yamashita, Y. Yamamoto, S. Nagase, *J. Am. Chem. Soc.* **1999**, *121*, 10644–10645.
- [17] A. Daolio, P. Scilabra, G. Terraneo, G. Resnati, *Coord. Chem. Rev.* **2020**, *413*, 213265.
- [18] S. P. Thomas, M. S. Pavan, T. N. Guru Row, *Chem. Commun.* **2014**, *50*, 49–51.
- [19] A. Bauzá, A. Frontera, *Crystals* **2016**, *6*, 26.
- [20] S. C. Capelli, H.-B. Bürgi, B. Dittrich, S. Grabowsky, D. Jayatilaka, *IUCrJ* **2014**, *1*, 361–379.
- [21] M. Fugel, D. Jayatilaka, E. Hupf, J. Overgaard, V. R. Hathwar, P. Macchi, M. J. Turner, J. A. K. Howard, O. V. Dolomanov, H. Puschmann, B. B. Iversen, H.-B. Bürgi, S. Grabowsky, *IUCrJ* **2018**, *5*, 32–44.
- [22] E. K. Wieduwilt, G. Macetti, L. A. Malaspina, D. Jayatilaka, S. Grabowsky, A. Genoni, *J. Mol. Struct.* **2020**, *1209*, 127934.
- [23] L. A. Malaspina, E. K. Wieduwilt, J. Bergmann, F. Kleemiss, B. Meyer, M. F. Ruiz-López, R. Pal, E. Hupf, J. Beckmann, R. O. Piltz, A. J. Edwards, S. Grabowsky, A. Genoni, *J. Phys. Chem. Lett.* **2019**, *10*, 6973–6982.
- [24] S. Grabowsky, A. Genoni, H.-B. Bürgi, *Chem. Sci.* **2017**, *8*, 4159–4176.
- [25] A. Genoni, L. Bučinský, N. Claiser, J. Contreras-García, B. Dittrich, P. M. Dominiak, E. Espinosa, C. Gatti, P. Giannozzi, J.-M. Gillet, D. Jayatilaka,

- P. Macchi, A. Ø. Madsen, L. Massa, C. F. Matta, K. M. Merz, P. N. H. Nakashima, H. Ott, U. Ryde, K. Schwarz, M. Sierka, S. Grabowsky, *Chem. - A Eur. J.* **2018**, *24*, 10881–10905.
- [26] M. Woińska, S. Grabowsky, P. M. Dominiak, K. Woźniak, D. Jayatilaka, *Sci. Adv.* **2016**, *2*, e1600192.
- [27] R. F. W. Bader, *Chem. Rev.* **1991**, *91*, 893–928.
- [28] E. R. Johnson, S. Keinan, P. Mori-Sánchez, J. Contreras-García, A. J. Cohen, W. Yang, *J. Am. Chem. Soc.* **2010**, *132*, 6498–6506.
- [29] D. Arias-Olivares, E. K. Wieduwilt, J. Contreras-García, A. Genoni, *J. Chem. Theory Comput.* **2019**, *15*, 6456–6470.
- [30] F. Peccati, *J. Chem. Inf. Model.* **2020**, *60*, 6–10.
- [31] P. Politzer, J. S. Murray, *Struct. Chem.* **2021**, *32*, 623–629.
- [32] E. Espinosa, I. Alkorta, J. Elguero, E. Molins, *J. Chem. Phys.* **2002**, *117*, 5529–5542.
- [33] Y. Han, Z. Zhang, Y. Liu, Y. Niu, D. Ding, B. Wu, H. Hou, Y. Fan, *Cryst. Growth Des.* **2011**, *11*, 3448–3455.
- [34] Y.-Y. Niu, B.-L. Wu, X.-L. Guo, Y.-L. Song, X.-C. Liu, H.-Y. Zhang, H.-W. Hou, C.-Y. Niu, S.-W. Ng, *Cryst. Growth Des.* **2008**, *8*, 2393–2401.
- [35] A. Garci, Y. Beldjoudi, M. S. Kodaimati, J. E. Hornick, M. T. Nguyen, M. M. Cetin, C. L. Stern, I. Roy, E. A. Weiss, J. F. Stoddart, *J. Am. Chem. Soc.* **2020**, *142*, 7956–7967.
- [36] A. B. Rudine, M. G. Walter, C. C. Wamser, *J. Org. Chem.* **2010**, *75*, 4292–4295.
- [37] W.-Z. Fu, W.-J. Wang, Y.-Y. Niu, S. W. Ng, *Acta Crystallogr. Sect. E Struct. Reports Online* **2010**, *66*, o1211–o1211.
- [38] Z.-F. Zhang, *Zeitschrift für Krist. - New Cryst. Struct.* **2011**, *226*, 553–554.
- [39] V. Kumar, P. Scilabra, P. Politzer, G. Terraneo, A. Daolio, F. Fernandez-Palacio, J. S. Murray, G. Resnati, *Cryst. Growth Des.* **2021**, *21*, 642–652.
- [40] S. H. Zeisel, *Annu. Rev. Nutr.* **1981**, *1*, 95–121.
- [41] R. C. Hogg, M. Raggenbass, D. Bertrand, *Rev. Physiol. Biochem. Pharmacol.* **2003**, *147*, 1–46.
- [42] K. Frydenvang, B. Jensen, *Acta Crystallogr. Sect. B Struct. Sci.* **1996**, *52*, 184–193.
- [43] O. Geiger, C. Sohlenkamp, I. M. Lo, *Prog. Lipid Res.* **2003**, *42*, 115–162.
- [44] C. R. Day, S. A. Kempson, *Biochim. Biophys. Acta - Gen. Subj.* **2016**, *1860*, 1098–1106.
- [45] M. Lever, S. Slow, *Clin. Biochem.* **2010**, *43*, 732–744.
- [46] R. C. Trievel, S. Scheiner, *Molecules* **2018**, *23*, 1–17.
- [47] R. J. Fick, G. M. Kroner, B. Nepal, R. Magnani, S. Horowitz, R. L. Houtz, S. Scheiner, R. C. Trievel, *ACS Chem. Biol.* **2016**, *11*, 748–754.
- [48] J. C. Lin, N. Gant, *Magn. Reson. Spectrosc. Tools Neurosci. Res. Emerg. Clin. Appl.* **2013**, 104–110.
- [49] W. D., H. L.B., *J. Neurochem.* **1994**, *62*, 1653–1663.
- [50] A. C. Kruse, B. K. Kobilka, D. Gautam, P. M. Sexton, A. Christopoulos, J. Wess, *Nat. Rev. Drug Discov.* **2014**, *13*, 549–560.
- [51] J. D. Schmitt, C. G. V. Sharples, W. S. Caldwell, *J. Med. Chem.* **1999**, *42*, 3066–3074.
- [52] P. P. Bhojane, M. R. Duff, K. Bafna, G. P. Rimmer, P. K. Agarwal, E. E. Howell, *Biochemistry* **2016**, *55*, 6282–6294.
- [53] J. Baran, M. Drozd, T. Głowiak, M. Śledź, H. Ratajczak, *J. Mol. Struct.* **1995**, *372*, 131–144.
- [54] B. Jensen, R. Tegman, B. Lindberg, S. Svensson, J. Koskikallio, S. Kachi, *Acta Chem. Scand.* **1971**, *25*, 3388–3396.
- [55] B. Jensen, R. Stølevik, E. Kvamme, R. Ohlson, A. Shimizu, *Acta Chem. Scand.* **1970**, *24*, 2517–2524.
- [56] M. A. Beckett, S. J. Coles, M. E. Light, L. Fischer, B. M. Stiefvater-Thomas, K. S. Varma, *Polyhedron* **2006**, *25*, 1011–1016.
- [57] E. Haussühl, J. Schreuer, *Zeitschrift für Krist.* **2001**, *216*, 616–622.
- [58] K. Frydenvang, B. Jensen, *Acta Crystallogr. Sect. B Struct. Sci.* **1996**, *52*, 184–193.

[59] R. Pažout, J. Maixner, M. Dušek, B. Kratochvíl,
Acta Crystallogr. Sect. C Cryst. Struct. Commun.

2011, 67, o391–o393.

5. Beyond the p Block.

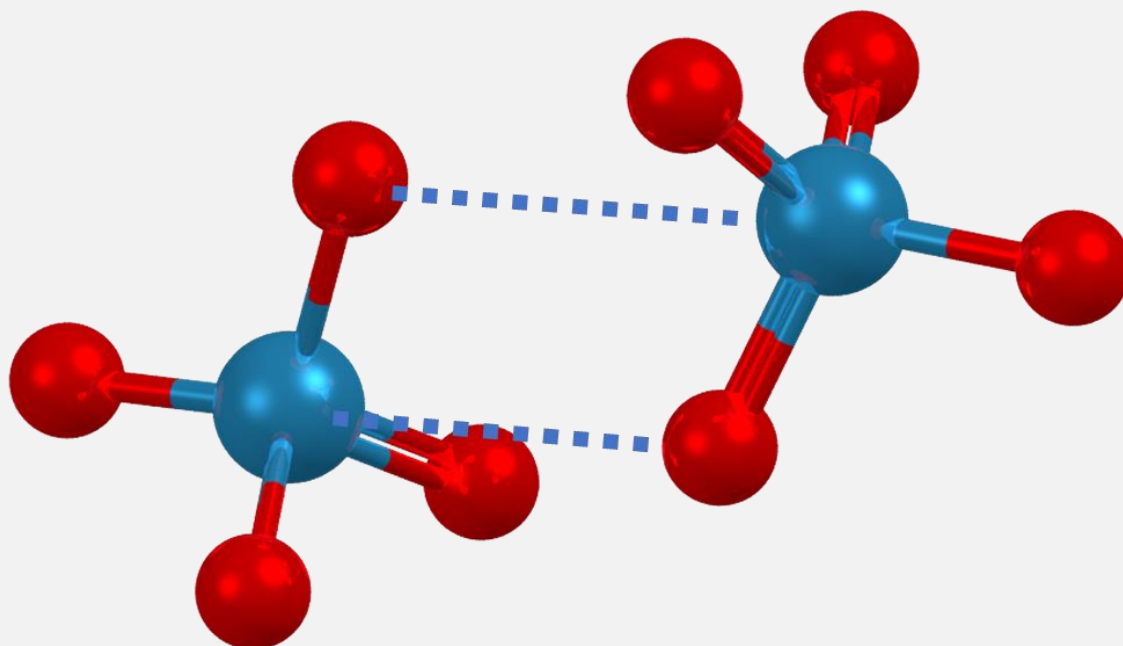


Figure 5. Representation of the geometrical features of a matere bond displayed in an adduct between two units of perrhenate anions. The two bonds are navy dotted lines. Molecules not engaging in the interaction were omitted for clarity. Rendered by POV-Ray with metallic textures (ball and stick visualization).

More than a century has passed since the introduction of the concept of metallic complex by Alfred Werner in 1906. Metallic complexes are stable compounds wherein a metallic species (coordination centre) is bonded to neutral molecules or ions (ligands). Werner's work brought to important advancements for the entire field of chemistry. The subsequent studies of G. N. Lewis are a relevant example^[1]. He proposed that a covalent bond should require a sharing of an electron pair^[2]. But in some systems both bonding electrons come from a single atom; in these cases, the bond should be considered a coordinative one (a Lewis acid and Lewis base forming a Lewis pair). This classification, in the words of the author, was not “clear-cut” and a more rigorous distinction between the two situations came from quantum mechanics in the form of HOMO-LUMO theory. Recent studies on the anisotropic distribution of electron density in the form of σ - and π -holes rationalization built up on these seminal works. They provide strong confirmations of past theories based upon physically observable quantities, circumventing the need of attributing shared (and undistinguishable) electrons to specific atoms.

As of 2021, this rationalization already invested elements of group 12^[3] (spodium bond), group 11^[4] (coinage or regium bond), group 8^[5] (osme bond), and group 7^[6] (matere bond). Coinage and Osme bond are the main subject of this chapter.

5.1. Tetrachloridoaurate anions as an Effective Anion...Anion Coinage Bond Donor.

“- Dear God, Mr. Boulez, are we going to carry out another revolution?

- Mais oui, sans pitié. “

- conversation between Luciano Berio and Pierre Boulez as reported by Alex Ross,
The Rest is Noise.

The σ -hole rationalization invested most of the p block of the periodic table. Indeed, nearly all block elements have been analysed in their propensity to establish σ -hole interactions^[7] and in the geometrical and energetical features of the resulting adducts^[8]. This approach proved to be solid enough to be extended to several metallic elements of the d block^[9], specifically to the respective adducts where the electrophilic behaviour of the metal could be unequivocally identified, namely to adducts where no back-donation was occurring from the ligand to the metal or to adducts where the assembly was not driven by metallophilic interactions. Many elements of the d block of the periodic table display close contacts consistent with the definition of σ -hole or π -hole interactions and frequently this behaviour was overlooked in previous years. Interactions where the electrophilic end is an element of group 12^[3] (spodium bond, SpB) and 11^[10] (regium or coinage bond, RgB or CiB) are now more and more common in the literature. Some papers also report computational findings of regions of positive potential consistent with the presence of σ -holes and π -holes on other atoms of the d block, e.g., molybdenum^[11]. Data strongly suggest that σ -hole interactions could be a common

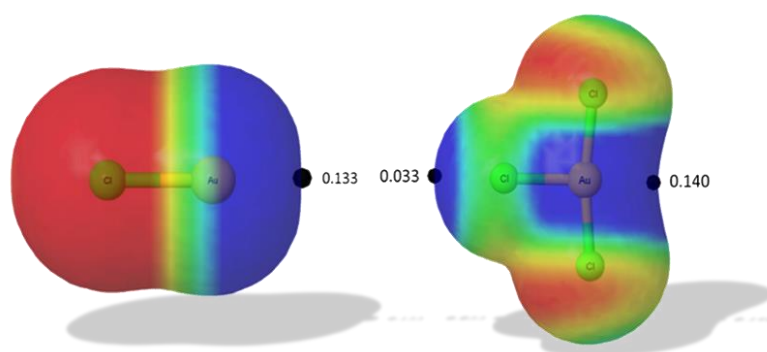


Figure 5.1.1. Molecular electrostatic potential (blue positive, red negative, yellow and green intermediate) calculated over the 0.001 au electron density isosurfaces of Au(I)Cl (left) and Au(III)Cl₃ (right). $V_{s, \max}$ are black hemispheres. Values of MEP at the $V_{s, \max}$ (au) are reported near the structures. Reprinted and slightly modified from *Struct. Chem.* **2020**, *31*, 1909-1918.

phenomenon encompassing all p block elements and many elements of the d block of the periodic table. These interactions may partially expand, and overlap with, the concept of Lewis acids and bases^[12].

Indeed, a positive σ -hole is present on the metal and opposite to the halogen in CiX and CiX_3 derivatives of group 11 elements ($\text{Ci}=\text{Cu, Ag, Au}$; $\text{X}=\text{F, Cl, Br, I}$) (Figure 5.1.1)^[13]. The understanding of these complexes as σ -hole adducts was helpful in recognizing the electronic basis of observed geometries^[14,15]. The presence of the hole opposite to the Cu/Ag/Au-halogen bond allowed for an intuitive rationalization of the linear geometry of the adducts formed by these metal halides with anions and lone-pair possessing atoms.^[16,17] An analogous rationalization has been suggested for the geometries of some adducts given by group 12 elements^[18].

This mindset is targeted toward the understanding of many self-assembly and aggregation phenomena that result in the formation of inorganic and metallorganic crystal structures. The peculiar behaviour of many transition metal compounds are frequently collected without a complete rationalization of their stereoelectronic basis or analysed by using the molecular orbital approach^[19-21]. A nontrivial example is the anion...anion^[22,23] contact often encountered in the structures of tetrahalidoaurate(III) salts. The square planar tetrachloridoaurate(III) anion AuCl_4^- has useful applications in the purification of gold metal and in organic catalysis^[24,25]. In the solid state, AuCl_4^- readily forms adducts where the gold atom forms short contacts at one or both faces of its planar structure with other molecular entities, either anions or neutral molecules containing lone pair possessing atoms. When the approaching molecular entity is another AuCl_4^- anion, supramolecular "corner-to-plane" infinite chains are formed^[26,27] (Figure 5.1.2), analogous architectures being formed also by analogous tetrahalido, or tetrapseudohalido, anions. To the best of our knowledge, the only attempt to explain these interactions was from L.E. Pope^[28], who tentatively described them as charge-transfer phenomena between the entering atom and gold. D. B. Leznoff in his papers on tetracyanidoaurate(III) salts pointed out that further studies should be required^[29] to fill the knowledge lack on the attractive interaction between nucleophiles and anionic gold(III) derivatives.

Short $\text{Cl}_4\text{Au}\cdots\text{Cl-AuCl}_3$ interactions seem to occur quite commonly in crystal structures. A large portion of the CSD structures containing the AuCl_4^- anions display it. 180 of the 354 CSD structures containing the AuCl_4^- anions show at least one such contact shorter than the sum of the van der Waals radii of gold and chlorine and for 103 of them (corresponding to 29% of the hits) the $\text{Cl-Au}\cdots\text{Nu}$ angles are comprised between 80 and 100°. Similar behaviour can be observed for related tetrabromidoaurate and tetracyanidoaurate compounds. While these sets are too small to allow for a rigorous statistical evaluation, they may be considered a strong indication that these anion...anion

short contacts are a non-exceptional phenomenon. A CSD analyses revealed that while chlorine atoms are the nucleophiles most commonly engage in short contacts formation with the gold(III) atom, ^[29] structures where the interaction is held between the gold atom and other atoms can be found. The oxygen atom of nitro compounds^[30], *N*-oxides^[31] and ethers^[32] can also act as the electron rich site approaching the gold atom at one of the faces of the tetrachloridoaurate plane. After this mindset, the gold atom can be understood as the electrophilic end of the interaction.

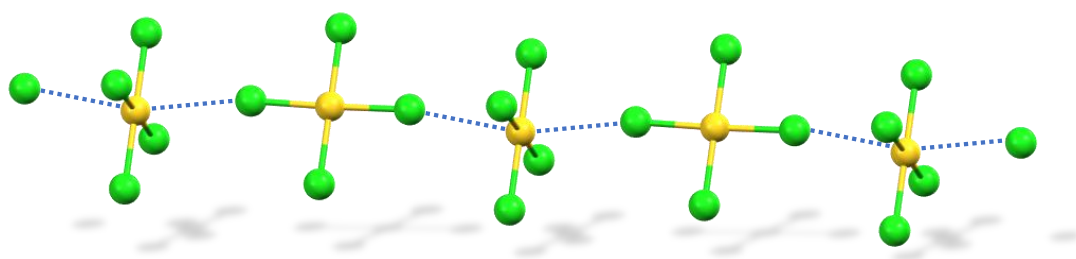


Figure 5.1.2. Ball and stick representation of the supramolecular infinite “corner-to-face” chain formed by AuCl_4^- anions (refcode BIHXIC). Molecular entities not engaged with the interaction have been omitted for clarity. CiB are navy dotted lines. Colour code: *green* chlorine; *golden* gold.

Gold is a soft atomic species, i.e., has a low electronegativity and is highly polarizable. It can thus be expected that in the tetrachloridoaurate(III) anion the Au–Cl covalent bonds are highly polarized and the negative charge is mostly shifted on the highly electronegative and poorly polarizable chlorine atoms. The electrophilic character of the gold atom might be increased further by noncovalent interactions between chlorine atoms and the cationic counterpart of the salt. For instance, if chlorine atoms are engaged in short $\text{H}\cdots\text{Cl}$ hydrogen bonds or other noncovalent interactions wherein they function as the nucleophilic end, the electron density on the whole ion can be reduced. This might decrease the electron density on gold to the point that areas with positive electrostatic potential might exist on its surface, consistent with the definition of π -hole. This possibility has already been studied on other harder and smaller anions than tetrachloridoaurate(III), as for example NO_3^- ^[33]. The two phenomena described above (polarizability and ancillary interactions) when pronounced enough, might be sufficient to enable for an attractive interaction where the gold atom acts as the electrophile.

To test our assumptions, we obtained the single crystal X-ray structure of the tetrachloridoaurate(III) of 3-(dimethylsulfonio)methylpropionate (propiothetin, **1**) and acetylcholine (**2**). Both crystals show the presence of a close contact between the gold atom of one AuCl_4^- anions and the chlorine atom of a nearby AuCl_4^- anions. The

interaction is occurring on one face of the AuCl_4^- unit and on the other face an oxygen of the cation is getting close to the gold after a direction orthogonal the anion plane.

In addition to the analysis of the crystal structures, a large set of theoretical calculations were employed in order to reveal the energetic and electronic features of this interaction. The structural formulas of the two salts is reported in Figure 5.1.3.



Figure 5.1.3. Structural formulas of 3-(dimethylsulfony)methylpropionate tetrachloridoaurate(III) (propiothetin, **1**, left) and acetylcholine tetrachloridoaurate(III) (**2**, right).

Compound **1** crystallizes in the $P2_12_12_1$ space group, an uncommon example of an achiral molecule crystallizing in a chiral space group. The AuCl_4^- unit can adopt, as customary, a square planar conformation, and two different nucleophilic atoms get close to gold orthogonal the two faces of the anion. On one side, a short contact with a chlorine atom of another anion is established. The $\text{Au}\cdots\text{Cl}$ distance is 3.312 Å, corresponding to an Nc of 0.80 (Batsanov value^[35,36] is used for the van der Waals radius). Overall, the $\text{Cl}-\text{Au}\cdots\text{Cl}$ angles fall in the range 80-100°. This contact, at least for a purely crystallographic point of view, should fall in the category of π -hole CiB bonding. The second contact is held between the gold atom and an ester oxygen of the propiothetin. The $\text{Au}\cdots\text{Cl}$ distance is 3.134 Å, which correspond to an Nc of 0.85. All the $\text{Cl}-\text{Au}\cdots\text{O}$ angles are comprised between the range 85-95°. This contact too should be interpreted as a π -hole CiB. It is possible to notice that every anion is at the same time engaging in two identical CiBs, one as the donor and one as the acceptor, so a supramolecular and coinage bonded infinite chain is formed bearing the propiothetin cations appended to gold via the $\text{Au}\cdots\text{O}$ CiB (Figure 5.1.4). There are other noteworthy contacts involving the tetrachloridoaurate anion. Different HBs between the cation hydrogen atoms and the chlorine atoms in AuCl_4^- are present. In addition, a chlorine atom of the AuCl_4^- anion and the positive sulfur atom of the propiothetin cation lie at a distance just slightly greater than the sum of their respective van der Waals radii (the separation corresponds to an Nc value of 1.01) and establishes a $\text{C}-\text{S}\cdots\text{Cl}$ angle of 172.15°, so that the interaction can be considered as a charge assisted ChB. This last interaction, together with the HBs mentioned above, likely decreases the electron density of the AuCl_4^- anions, namely they may make less negative, possibly positive, the electrostatic potential in some regions of gold surface anions and thus promote its electrophilic character.

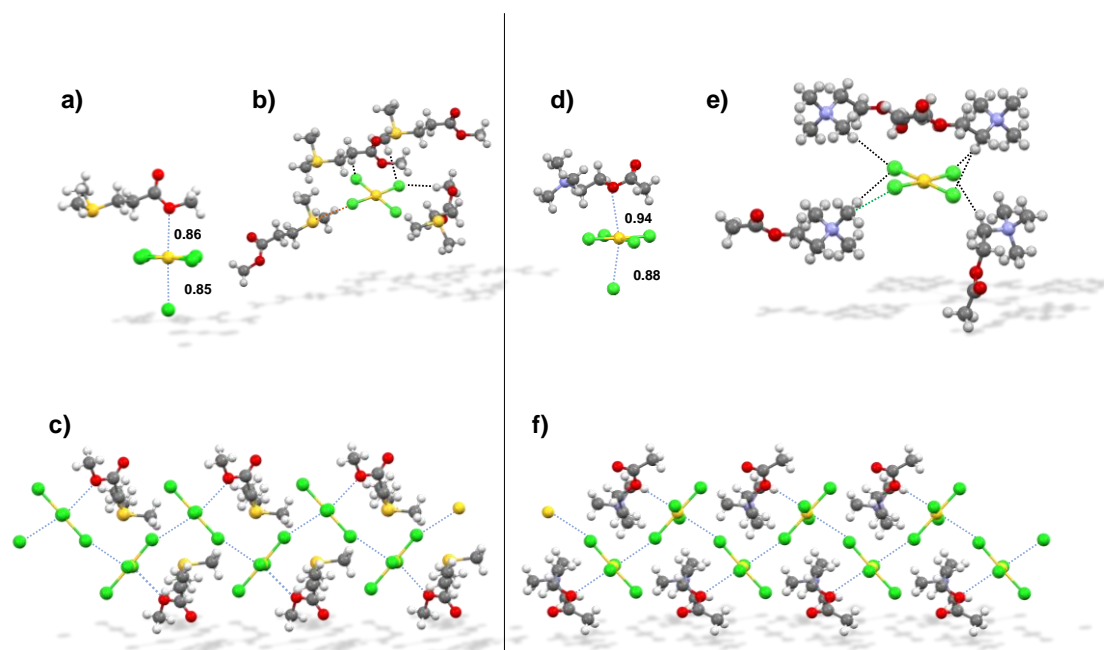


Figure 5.1.4. Ball and stick representation of: the coinage bonded assembly formed by the gold atom of a AuCl_4^- unit functioning as electrophilic site in propiothetin tetrachloridoaurate(III) **1** (a) and acetylcholine tetrachloridoaurate(III) **2** (d); the hydrogen and chalcogen bonded assembly formed by one AuCl_4^- unit in propiothetin tetrachloridoaurate(III) **1** (b) and acetylcholine tetrachloridoaurate(III) **2** (e); the coinage bonded supramolecular “corner-to-face” chains formed by AuCl_4^- units in propiothetin tetrachloridoaurate(III) **1** (c) and acetylcholine tetrachloridoaurate(III) **2** (f), the cations appended to the chain via $\text{Au}\cdots\text{O}$ CiB are also reported. CiBs, HBs and ChB are navy, black and orange dotted lines, respectively. Nc values of $\text{Au}\cdots\text{Cl}/\text{O}$ separation are reported near the contact. Colour code: gray carbon; whitish hydrogen; light blue nitrogen; red oxygen; yellow sulfur; golden gold; green chlorine.

The crystal structure **2** crystallizes in the more common $P2_1/c$ space group and features many similarities with **1** (Figure 5.1.4). As in **1**, it is possible to notice different contacts involving the gold(III) atom, e.g., the $\text{Au}\cdots\text{Cl}$ and $\text{Au}\cdots\text{O}$ short contacts which are 3.434 and 3.446 Å long, corresponding to Nc values of 0.88 and 0.94, respectively. Both these contacts display $\text{Cl}-\text{Au}\cdots\text{Cl}/\text{O}$ angles close to 90° . These geometrical features are consistent with the rationalization of the close contacts as π -hole CiB. In this structure in particular the acetylcholine is also slightly tilted over the plane of tetrachloridoaurate(III), so that the lone pair of the oxygen is directly oriented over the metal atom. This feature is absent in structure **1**. $\text{Cl}\cdots\text{H}$ HBs between the cation and the anion are present in **2** and they are even more numerous than in **1**.

The energetic features of the adducts analysed in this work were calculated at the PBE0-D3/def2-TZVP level of theory using the crystallographic coordinates.

The first step of the computational study was the analysis of the molecular electrostatic potential (MEP) surfaces of the AuCl_4^- anion and of the entire salt. In detail, data for **1**

and **2** are reported in Figure 5.1.5, top. When considering the AuCl_4^- unit alone, the entire surface is negative due to the global charge, as expected for an anion. The global minimum is found at the bisectors of the Cl–Au–Cl angles. Various areas of less negative electrostatic potential are also present. The areas of most positive (less negative) potential are located on the four extension of the Au–Cl bonds (-79.6 kcal/mol, σ -holes at chlorine) and at the outer regions of gold above and below the atom (-78.3 kcal/mol, π -holes at gold). The MEP surface of the salts (Figure 5.1.5, mid left and bottom left) are still entirely negative on the whole AuCl_4^- surface, but the electrostatic potential is drastically less negative. In particular, the negative charge seems to diminish more on the π -hole (-25.1 and -20.1 kcal/mol for **1** and **2**, respectively) than the σ -holes (-30.5 and -27.0 kcal/mol for **1** and **2**, respectively, respectively).

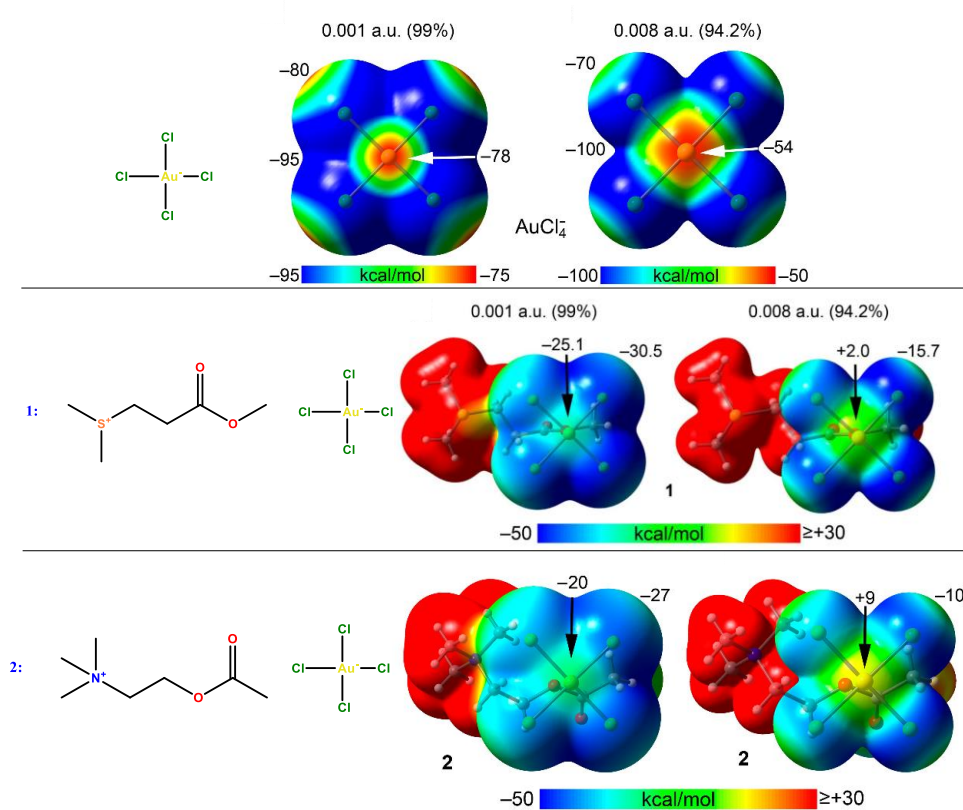


Figure 5.1.5. Molecular electrostatic potential (MEP) surfaces of AuCl_4^- unit (top), compound **1** (mid), and compound **2** (bottom) using 0.001 a.u. (left) and 0.008 a.u. (right) isovalues at the PBE0-D3/def2-TZVP level of theory. Structural scheme of the system analysed reported near the structure. The values at some points of the surface are given in kcal·mol⁻¹.

The MEP surfaces discussed above are built, as customary, on the Bader's 0.001 au surface^[35] which embraces about 99% of the total electron density. This surface far exceeds

the contact surface of atoms interacting in the crystalline solids and it thus seemed appropriate to consider inner surfaces to have a more realistic insight of the electronic situations in the crystals. When higher isovalues of electron density are considered, the molecular electrostatic potential progressively becomes more positive as the volume decreases (Table 5.1.1). Importantly, the π -hole maxima around gold becomes rapidly less negative/more positive than the chlorine atoms. The 0.008 isovalue contains 94.2% of the total electron density of the molecule, and the contacts observed are found at a distance up to 20% lower than the sum of their respective van der Waals radii. At the 0.008 au isosurface the π -holes on gold atom are +2 kcal/mol for salt **1** and +9.1 kcal/mol for salt **2**. This means that, at the distance encountered in the crystal, the nucleophilic atoms (O and Cl) perceive a positive potential around the gold atom.

cmpnd ^[a]	isovalue (% e in the surface)			
	0.001 (99.0)	0.002 (98.2)	0.004 (96.7)	0.008 (94.2)
AuCl ₄ ⁻ ; σ (Cl)	-79.6	-79.6	-77.8	-70.2
AuCl ₄ ⁻ ; π (Au)	-78.3	-74.6	-67.8	-54.8
1 ; σ (Cl)	-30.5	-29.7	-26.3	-15.7
1 ; π (Au)	-25.1	-20.5	-12.6	+2.0
2 ; σ (Cl)	-27.0	-24.8	-19.4	-10.0
2 ; π (Au)	-20.1	-14.4	-6.0	+9.1

Table 5.1.1. MEP values (in kcal mol⁻¹) of AuCl₄⁻, **1** and **2** at the σ -hole on chlorine and π -hole on gold using different isovalues (a.u.) for the electron density.

The formation of a Au...Cl CiB between two AuCl₄⁻ anions may be disfavoured by the repulsion between the negative regions of the nucleophilic chlorine atom of the incoming AuCl₄⁻ unit and the negative regions of chlorine atoms covalently bonded to the gold atom acting as π -hole donor. But consistent with the observation by Politzer and Murray^[36] that polarizability is at the core of σ -hole adducts formation, it may be expected that a redistribution of the electron density occurs on Au...Cl CiB formation. Indeed, it is known that molecules, to get close to the global energy minimum of a molecular adduct, are generally well-willing to “pay a price” and to adopt conformational and/or electronic states different from the most stable ones. Typical examples can be found in adducts assembled via σ -hole interactions wherein the σ -hole donor distorts its ground state geometry to display more positive and/or more extended σ -holes^[37,38].

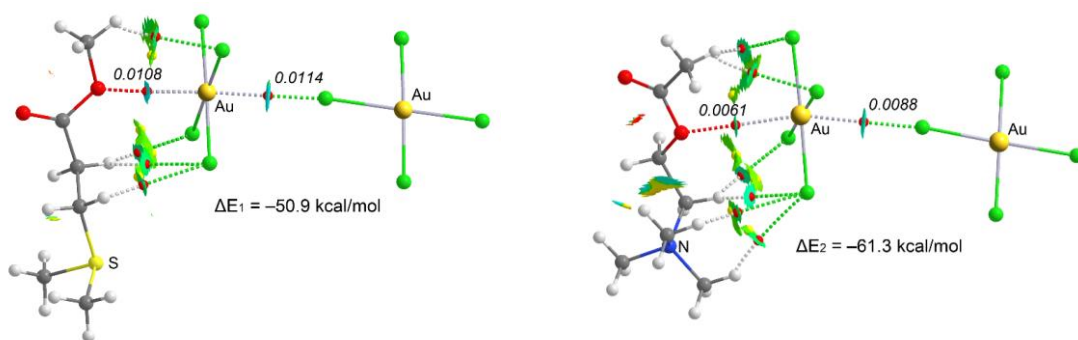


Figure 5.1.6. QTAIM distribution of intermolecular bond and ring critical points (red and yellow spheres, respectively) and bond paths for the coinage bonded assemblies in compound **1** (left) and **2** (right). The density at the bond CPs that characterize the CiBs are given in italics (a.u.) The superimposed NCIplot isosurface (RDG isovalue = 0.4 a.u.) is shown. The cut-off $\rho = 0.04$ a.u. has been used. Color range -0.02 a.u. $\leq (\text{sign}\lambda^2)\rho \leq 0.02$. Level of theory: PBE0-D3/def2-TZVP.

The contacts formed by the gold atom has been then characterized by QTAIM and NCI analysis in their ternary assemblies (two anions and one cation). Data retrieved from the analysis are reported in Figure 5.1.6, including the formation energies. First of all, QTAIM confirms the presence of Au...Cl/Cl contacts. Both of them are characterized by a bond critical point (bcp) and bond paths that connects the involved atoms. The analysis also confirms the presence of several C–H...Cl ancillary hydrogen bonds allowing the CiB to occur. The same features are confirmed by the NCI plot analysis, with the presence of green or bluish (hence attractive) surfaces roughly in the same position of the bcps. The values of electron density at the bcps are reported in the Figure and are consistent with the experimental findings. The Au...Cl and Au...O bond paths are stronger for structure **1** than structure **2**, as shown by the shorter Ncs found in the first case. Surprisingly, the formation energy of the trimeric assembly for **2** is larger than for **1**, likely as a consequence of the higher number of hydrogen bonds in this structure, which further stabilize the overall packing.

Orbital contribution of this interaction has also been studied by means of natural bond orbitals (NBO) second order perturbation analysis. Remarkably, the study reveals important orbital contributions in both the structures, in the form of electron donations from the nucleophile to the empty $6p_z$ orbital of the gold(III) atom. The stabilisation energies (Figure 5.1.7) reveal that this orbital contribution is stronger for Cl than for O in both adducts, in agreement with previous results. This analysis finally reveals unequivocally the nature of the interaction as a π -hole CiB where the gold atom is the electrophilic site, while chlorine and oxygen atoms are the donors of electron density.

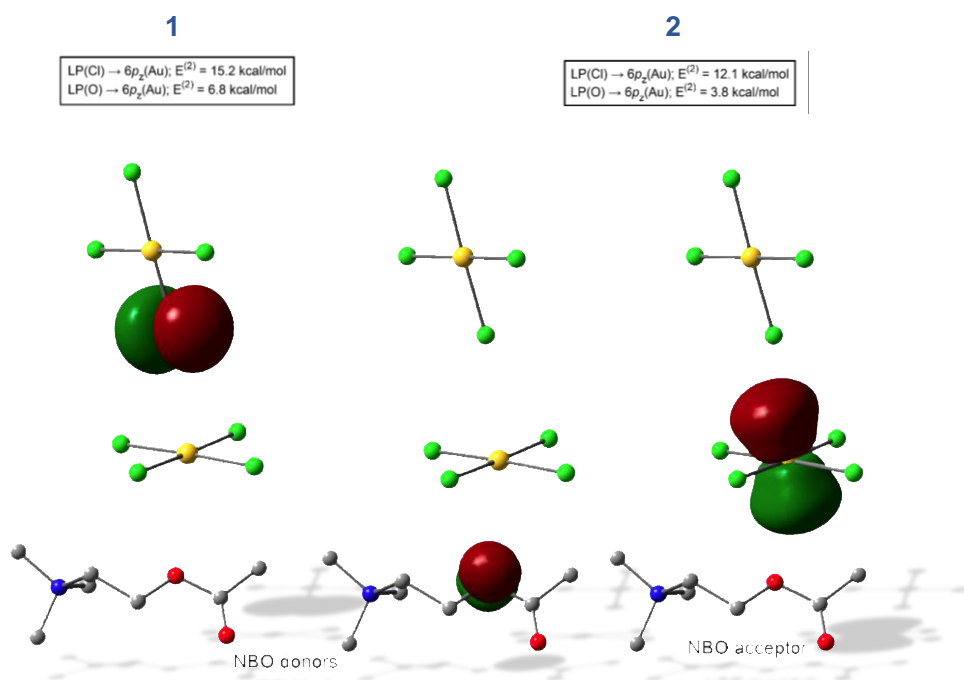


Figure 5.1.7. Localized NBOs of compound **2** involved in the donor-acceptor interactions. The donor orbitals are p-type atomic orbitals (LPs) localized at the Cl and O atoms above and below the π -hole. The acceptor NBO is an Au p-atomic orbital perpendicular to the AuCl_4^- plane. The localized NBOs of compound **1** involved in the donor-acceptor interactions are the same.

In this section a strong example of how the σ -hole rationalization of the phenomena occurring in the solid state can shed new light on known and interesting adducts has been presented. The $\text{Cl}_4\text{Au}^- \cdots \text{Cl}-\text{AuCl}_3^-$ interactions had already been observed but they had never been rationalized in terms of polarization and dispersion (π -hole interactions).

Additional Data.

The experimental section contains CSD surveys, synthetic, crystallographic and computational details.

5.2. Group 8 elements as electrophilic sites: The formation of osme bonded adducts.

Osmium tetroxide (OsO_4) is a neutral metallic compound where the central osmium metal atom is in the +8 oxidation state, the highest stable oxidation state for osmium and one of highest oxidation states ever reported. Osmium tetroxide is known to form adducts with nitrogen and oxygen bearing ligands. The formation of these adducts promotes the osmium catalyzed dihydroxylation of olefins (Figure 5.2.1). The reactivity of OsO_4 toward carbon-carbon double bonds and the stability of the resulting osmate ester are dependent on the nature of the N-donor ligand. The observed “ligand-acceleration” arises from the formation of $\text{O}_4\text{Os}\cdots\text{N}$ -donor adducts, which add more rapidly to the alkene. If the amine is chiral, then the dihydroxylation proceeds with enantioselectivity^[39-42]. The formation of the $\text{O}_4\text{Os}\cdots\text{N}$ adducts in solution is usually accompanied by a strong color change, ascribed to contact charge-transfers by early studies of Wallis and Kochi.^[43] The same studies also reported strong similarities between these adducts and those now categorized as halogen bonded systems^{[44][45,46]}. The color change phenomena are in accordance with the occurrence of σ -hole adducts also if it is taken into account that, as first reported by Chen and Martínez^[47] and later confirmed by Politzer,^[48] “charge transfer is an extreme manifestation of polarization”.

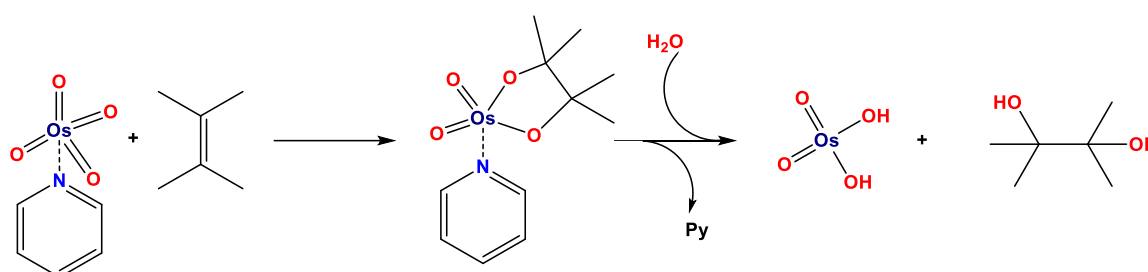


Figure 5.2.1. Oxidative addition of $\text{Py}\cdots\text{OsO}_4$ adduct to a carbon-carbon double bond. The process is slower in the absence of the ligand.

In Cambridge Structural Database (CSD) entries containing OsO_4 , the osmium atom is almost invariably in close proximity with a nucleophilic moiety (typically, but not always, a pyridine derivative)^{[49,50][39,51]}. $\text{Os}\cdots\text{N}$ short contacts are approximately on the extension of one of $\text{O}=\text{Os}$ covalent bonds of OsO_4 , namely the geometrical features of these adducts are in strong accordance with the presence of σ -hole interactions. $\text{O}=\text{Os}\cdots\text{Nu}$ angles are often close to 180° and $\text{Os}\cdots\text{Nu}$ distances are always very short (the Ncs are invariably <0.75). In structures where the nucleophile is a nitrogen atom, the Nc is usually 0.67 to 0.68, regardless of the functional group associated with the nitrogen. Interestingly, the approaching of the nucleophile to the metal center determines a slight

distortion of the OsO₄ tetrahedral geometry and this feature has been shown to correlate with interaction strength. Tetramethylammonium fluorotetraoxoosmium(VIII) (REFCODE XAKBUG^[52]), the structure associated with the lower Nc (0.59) has three O=Os=O angles spanning from 115° to 119°, very close to the trigonal bipyramidal arrangement of the transition state of an S_N2 reaction at carbon. Remarkably, this is one of the few structures on the database where a halide interacts with the osmium atom (the other is Tetraphenylphosphonium chlorotetraoxoosmium(VIII) dichloromethane solvate, REFCODE COTTEK^[53], where the nucleophile is a chloride anion). A last structure worth mentioning is (*N*-Methylmorpholine *N*-oxide)tetraoxoosmium(viii) (REFCODE NOLTIR^[54]) which is the only reported example of an oxygen atom (of an *N*-oxide) interacting with the osmium atom. In this case the Nc is a little lower compared to pyridine derivative adducts (0.64, See the experimental section for more details).

Ruthenium tetroxide (RuO₄) seems to behave similar to OsO₄, but the higher reactivity of RuO₄ toward nucleophiles has prevented the extensive characterization of its adducts and no such system is reported in the CSD.

Moving from this state of the art, we decided to further investigate the formation of OsO₄ adducts in order to have a deeper insight in the nature of the metal-ligand bonding. We synthesized some new adducts between OsO₄ and different neutral donors of electron density, specifically pyridine and pyridine *N*-oxide derivatives.

We characterized these systems through a variety of techniques in solution (IR and ¹³C/¹⁵N NMR) and in the solid (SSXRD, IR and ¹³C/¹⁵N NMR). Importantly, solid-state NMR analyses (SSNMR) indicated that the pyridine and *N*-oxide derivatives act as the electron donor species (nucleophiles) in the cocrystals. We also mapped the interactional landscape in the different systems through a variety of computational approaches which also proved the electrophilic and nucleophilic role of osmium and nitrogen/oxygen atoms in the adducts.

The overall aim was to prove that σ -holes with positive electrostatic potential can be present at the surface of group 8 elements in some of their derivatives and that these holes are involved in the formation of attractive interactions with lone pair possessing atoms. The obtained results consistently confirmed these working hypotheses and the similarities of the interactions under study with other σ -hole bondings. In order to acknowledge these similarities, these attractive interactions might be named referring to the electrophilic site and hereinafter the term osme bond (OmB, Om= Fe, Ru, Os, (Hs)) will be used to designate them. Osme is the transliteration of ὀσμῆ, the old Greek word for smell, which was used by S. Tennant to name the element osmium in relation to the smoky odor of OsO₄.

Adducts **3-8** (Table 5.2.1) were obtained on isothermal evaporation of a CH₂Cl₂ solution of the respective starting modules. The solvent was removed under a gentle stream of anhydrous nitrogen gas. In some cases (adducts **3-5**) crystals suitable for single

crystal X-ray analyses were obtained and this characterization technique afforded detailed information on the composition and structural aspects of the systems. In some other cases (adducts 6-8) microcrystalline/amorphous materials were formed. For these systems the composition was determined via ^1H NMR analyses in the presence of an internal standard (1,2,4,5 tetrafluorobenzene) and the OsB presence in the solid was established via IR and ^{15}N NMR (see onwards and Experimental section).

The crystal structure of 3 adopts the orthorhombic space group $P4_2/mbc$. A trimeric adduct is present in the system as nitrogen atoms of 4,4'-dipyridyl afford a single short contact with the osmium atoms of two different OsO_4 units (Figure 5.2.2, top), The $\text{Os}\cdots\text{N}$ distance is 2.394 Å (accounting for a normalized contact $(\text{Nc})^{[55,56]}$ of 0.67) and the $\text{O}=\text{Os}\cdots\text{N}$ angle is 179.69° (namely the interaction is on the elongation of one of the $\text{O}=\text{Os}$ bonds).

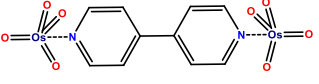
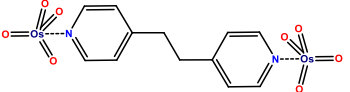
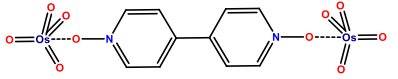
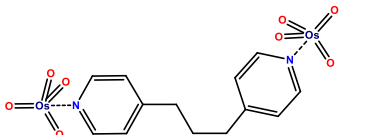
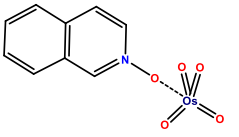
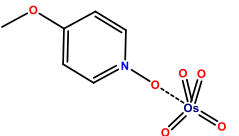
Lewis base	Predicted Structure	Compound
4,4'-dipyridyl		3
bis(4-pyridyl) ethane		4
4,4'-dipyridyl N-oxide		5
bis(4-pyridyl) propane		6
Isoquinoline N-oxide		7
4-methoxy pyridine N-oxide		8

Table 5.2.1. List of the obtained adducts between OsO_4 and nitrogen or oxygen donors of electron density.

As already noted for similar structures^[51], the osmium-nitrogen separation is longer than what expected for a $\text{Os}-\text{N}$ covalent bond (the distance is longer than the sum of the covalent radii in the solid state^[57]). In this adduct, the tetrahedral conformation of pure

OsO₄ is distorted, the O=Os=O angles spanning the range 101°-113°. Analogous changes of the geometry at the σ -hole donor on interaction formation have already been observed^{[58],[59]}, notably when a tetrahedral group 14 element is involved in tetrel bond formation^[60]. Apart from some HBs between the hydrogens of the dipyridyl unit and the OsO₄ oxygen atoms, there are no other notable short contacts.

On interaction with OsO₄, 1,2-bis(4-pyridyl)ethane behaves similar to 4,4'-dipyridylethane and affords the trimeric adduct **4** wherein the two nitrogen atoms form two short and linear contacts with two OsO₄ units (Figure 5.2.2, mid). The separation between the two atoms is 2.380 Å (again corresponding to an Nc of 0.67) and the O=Os...N angle is 179.30°. The osmium tetroxide is in a distorted tetrahedral conformation similar to that adopted in **3**. The Ncs of the interactions are well consistent with the structure present in the CSD and their O=Os...N angles are the most linear (**3**) and one of the most linear (**4**) example ever reported.

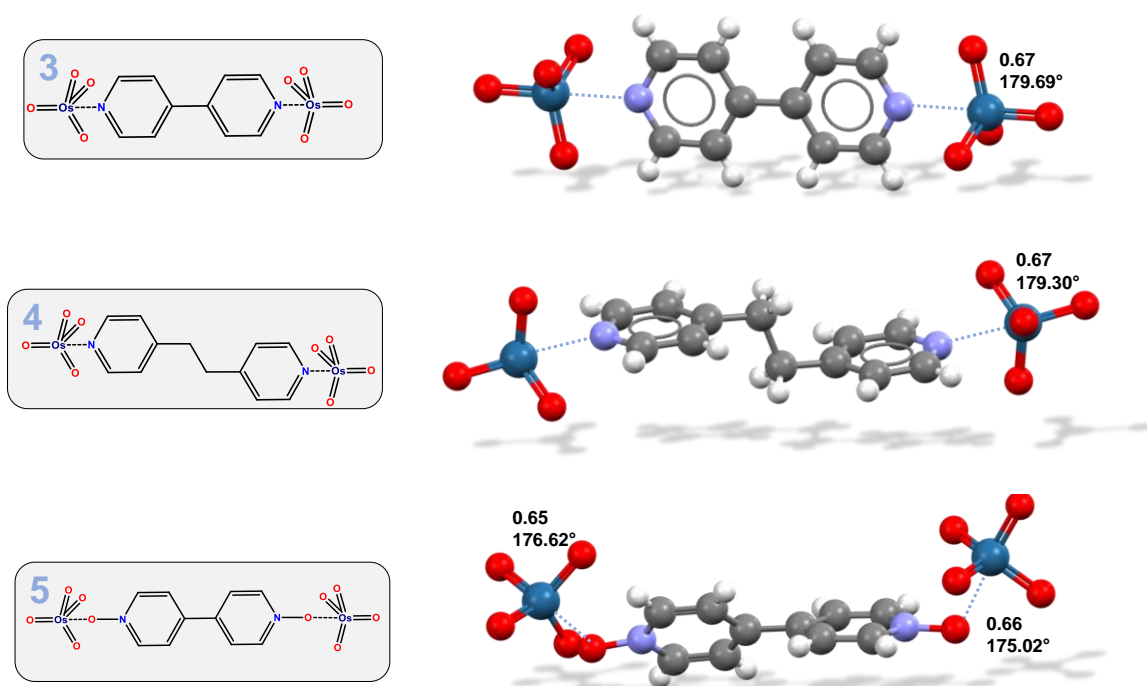


Figure 5.2.2. Ball and stick representation of the trimeric assemblies of adducts **3-5**. Structural schemes are boxed near the structures. OmB are navy dotted lines. Os...N/O separations Nc and O=Os...N/O angles are reported near the contacts. Colour code: *gray* carbon; *whitish* hydrogen, *light blue* nitrogen, *red* oxygen, *navy* rhenium.

The adduct **5** between osmium tetroxide and 4,4'-dipyridyl *N,N'*-dioxide crystallizes in the P2₁/n space group. Here too a trimeric assembly is formed (Figure 5.2.2, bottom) and the asymmetric unit comprises the entire molecular adduct of one 4,4'-dipyridyl dioxide and two OsO₄ molecules, so that the two Os...O interactions are slightly different. In detail, one Os...O contact is a little bit shorter and more linear (2.305 Å, corresponding

to an Nc of 0.65, O=Os...O angle of 176.62°) and the other is slightly longer and less linear (2.362 Å, corresponding to an Nc of 0.66, O=Os...O angle of 175.02°). Once again, the Ncs and O=Os...N angles are in accordance with similar structures to be found in CSD.

The adducts formation determines well-visible effects in FTIR and ¹⁵N/¹³C NMR spectra in the solid state. Pure OsO₄ shows a strong vibration at 960 cm⁻¹ in the gas phase and at 954 cm⁻¹ in CCl₄ solution.^[61] This vibration was shifted at 900-910 cm⁻¹ for adducts **3-8** in the solid and at higher frequency in the liquid (e.g., 955 and 922 cm⁻¹ for the adduct **3** in CCl₄ solution). This difference between solid and solution spectra indicates that a partial dissociation of the adduct occurs in solution^[49] and is consistent with measured dissociation constants of similar osmium adducts.^[62] The nearly instantaneous cleavage of the Os...O bonding on cocrystal dissolution indicates that electrostatic factors rather than covalent bonds formation play a major role in the cocrystal assembly.

In addition, signal intensities of pure starting modules underwent notable changes on OmB formation. For instance, the ν_{C-H} of the pyridyl moieties around 3000 cm⁻¹ underwent a major weakening, similar to other cases wherein the nitrogen atoms were acting as donors of electron density.^[63] Importantly, the results mirror previous reports of halogen bonded adducts involving the same nucleophiles, confirming a decrease of electron density at C-H groups in the cocrystals consistent with the σ-hole nature of the osme bond.

SSNMR spectra of compounds **3-6** showed interesting differences with respect to the dipyridyl components. Changes in the ¹³C spectra were minor. Major shifts were instead recorded for the ¹⁵N nucleus. Adducts **3** displays a strong upfield shift of 31.7 ppm signal with respect to pure dipyridyl, while adduct **4** shows an even stronger one of 41.7 ppm.

OmB acceptor	Pure OmB acceptor	OsO ₄ adduct	DITFB adduct
4,4'-dipyridyl	313.7	282.0	285.0
<i>bis</i> (4-pyridyl) ethane	313.0	271.3	271.4
4,4'-dipyridyl N-oxide	283.8	280.9	282.5
<i>bis</i> (4-pyridyl) propane	313.0	272.1	-

Table 5.2.2. ¹⁵N NMR chemical shifts (solid state spectra, ppm) of some of the cocrystals components considered in this work (electron donors, OmB acceptors, first column) when in pure form (second column), in the respective adduct with osmium tetroxide (third column) or with 1,4-diiidotetrafluorobenzene (DITFB).

The chemical shift change of **6** is very similar to that of **4**, while that for adduct **5** (3.3 ppm) is smaller compared to those of **3** and **4** consistent with oxygen atom acting as the donor of electron density (Table 5.2.2). The results are comparable with those obtained with a halogen bonded adducts of the same nucleophiles with 1,4 diiodotetrafluorobenzene (DITFB).^[63]

Of note, in competitive cocrystal formations, it has been demonstrated that the formation of the adducts between 4,4'-dipyridyl *N,N'*-dioxide and SbF₃ (a pnictogen bonded adduct) prevails over the self-assembly of the dioxide with diiodotetrafluorobenzene, which in turn prevails over the formation of the hydrated adduct^[64]. The ¹⁵N SSNMR of the three adducts assembled via pnictogen bond, halogen bond and hydrogen bond are progressively red shifted. This suggest that the ¹⁵N SSNMR chemical shift of 4,4'-dipyridyl *N,N'*-dioxide in its adducts can relate to the tendency of forming that specific adduct. Indeed, in **5** the interaction is seemingly strong enough to prevail over the formation of the hydrogen bonded adduct of 4,4'-dipyridyl *N,N'*-dioxide oxide with water. Similar parallel between ¹⁵N SSNMR chemical shifts and osme vs. hydrogen bonded adducts formation was shown by isoquinoline *N*-oxide (affording cocrystal **7**) and 4-methoxypyridine *N*-oxide (affording cocrystal **8**).

The molecular electrostatic potential (MEP) surfaces of the OmO₄ species (Om=Os, Ru, Fe) have been computed in order to verify the existence of σ -holes in OmO₄ and assess its role in affecting recognition processes involving the compounds. FeO₄ is not known, nevertheless it has been included for comparison purposes, allowing to examine how the intensity of the σ -hole changes in derivatives of the group 8 elements.

Figure 5.2.3. shows the MEP surfaces of the three tetraoxides of group 8 elements. Four symmetrically equivalent σ -holes are observed, located opposite to the Om=O bonds. The strength of the σ -holes increases going from Fe to Os, being significantly more intense for Ru and Os (+31.4 and +36.4 kcal/mol, respectively) than for Fe (+18.0 kcal/mol). Additionally, the MEP minimum values in the three compounds are located on the oxygens and are quite small, thus confirming the overall electrophilic nature of these molecules in the formation of relevant adducts.

In order to analyse the ability of OmO₄ compounds to establish OmBs with nitrogen bases, the six adducts of acetonitrile and pyridine, two typical Lewis bases, with OsO₄, RuO₄, and FeO₄ have been fully optimized at the PBE0-D3/def2-TZVP level of theory. Additionally, the quantum theory of "atoms-in-molecules" (QTAIM) combined with the noncovalent interaction plot (NCIPlot) index analyses have been carried out in the three experimental structures as they are very convenient computational tools to reveal interactions and to identify specific interacting areas and moieties. The results are gathered in Table 5.2.3 and Figure 5.2.4. All the optimized adducts reveal strong NCIs between Om and N. These interactions are characterized in the six compounds by the

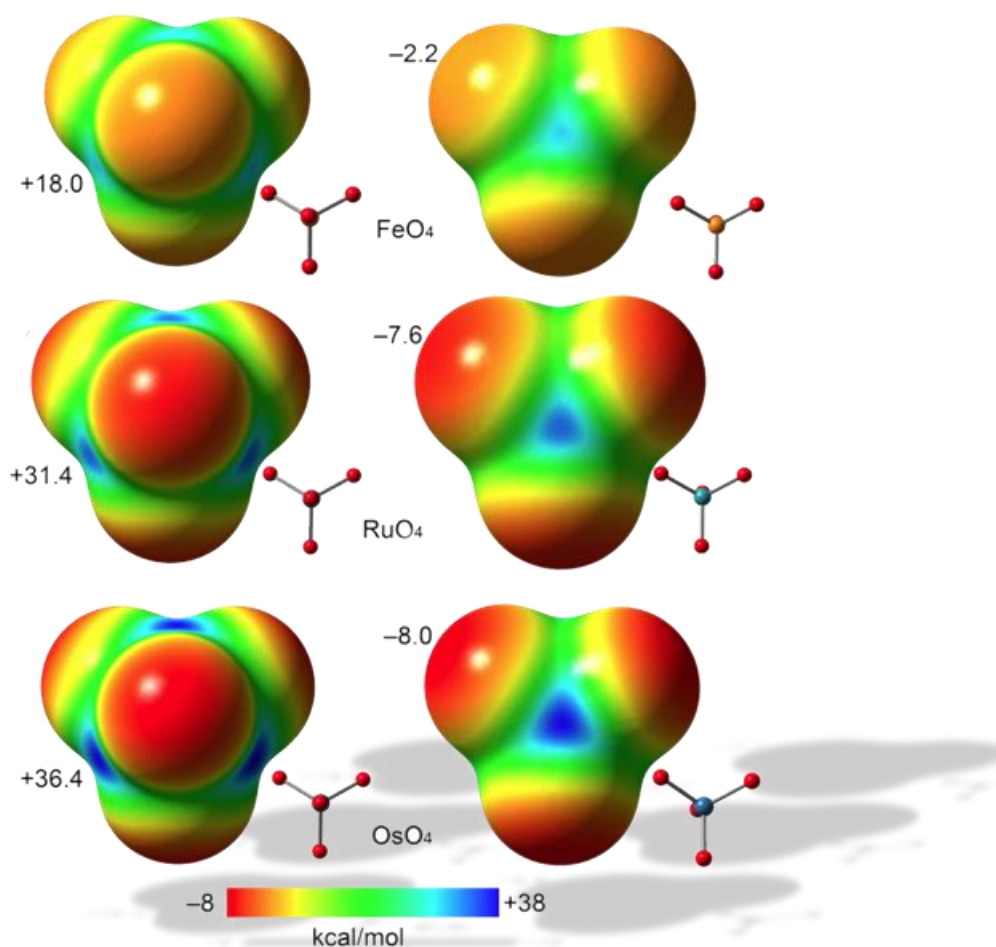


Figure 5.2.3. MEP surfaces of FeO_4 (a), RuO_4 (b) and OsO_4 (c) at the PBE0-D3/def2-TZVP level of theory. Isosurface 0.001 a.u. The MEP maximum and minimum energies are indicated in $\text{kcal}\cdot\text{mol}^{-1}$. The same energy scale is used in the three derivatives.

corresponding bond critical points (CPs) and bond paths connecting the N atom to the Om atom in QTAIM. The NCIPLOT index analysis is able to reveal isosurfaces of different colors located between the Om atoms and the Lewis bases: green for both FeO_4 adducts (namely weaker interactions), light blue for $\text{O}_4\text{Ru}\cdots\text{NCCH}_3$ and $\text{O}_4\text{Os}\cdots\text{NCCH}_3$ adducts, and finally dark blue for $\text{O}_4\text{Ru}\cdots\text{NC}_5\text{H}_5$ and $\text{O}_4\text{Os}\cdots\text{NC}_5\text{H}_5$ (namely stronger interactions). They are also in line with the calculated interaction energies ranging from -2.2 to -11.4 kcal/mol . The interaction energies are in good agreement with the MEP values at the σ -holes and with the relative basicity of acetonitrile and pyridine. In respective adducts with

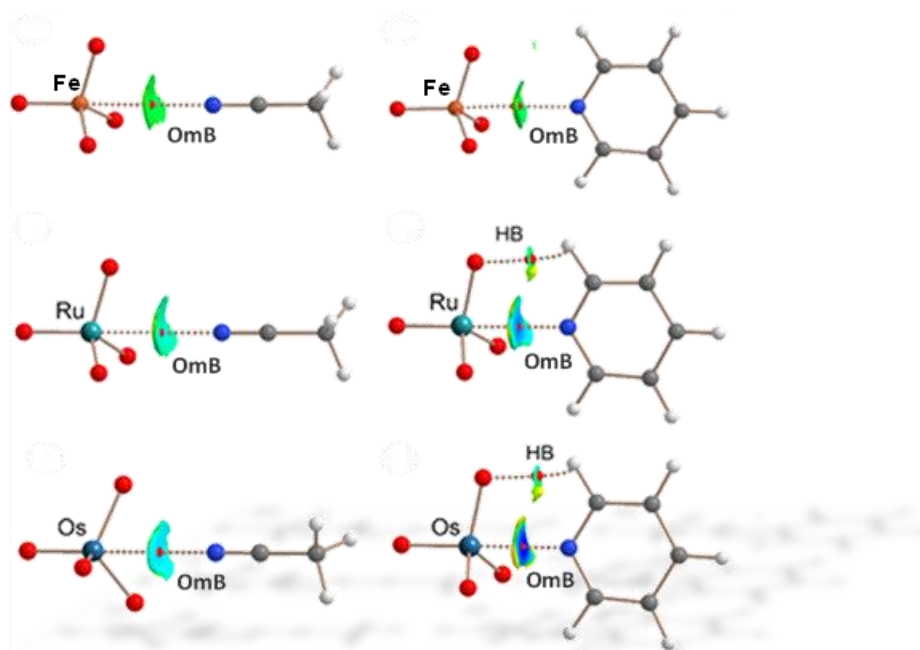


Figure 5.2.4. PBE0-D3/def2-TZVP optimized geometries of six OmB complexes. QTAIM analysis: bond CPs in red and ring CPs in yellow. NCIPLOT: $|R_{GB}|$ isosurface 0.4 a.u.; Color range 0.04 a.u. (red) $\leq (\text{sign}\lambda^2)\rho \leq -0.04$ a.u. (blue). Only the intermolecular interactions are shown.

Complex	ΔE	Distance	ρ_r	LP(N) $\rightarrow\sigma^*(\text{Om}-\text{O})$
$\text{O}_4\text{Fe}\cdots\text{NCCH}_3$	-2.2	3.407	0.0058	0.24
$\text{O}_4\text{Fe}\cdots\text{NC}_5\text{H}_5$	-3.7	3.279	0.0083	0.67
$\text{O}_4\text{Ru}\cdots\text{NCCH}_3$	-3.6	3.251	0.0082	0.81
$\text{O}_4\text{Ru}\cdots\text{NC}_5\text{H}_5$	-7.6	2.705	0.0279	2.29
$\text{O}_4\text{Os}\cdots\text{NCCH}_3$	-4.2	3.142	0.0109	1.89
$\text{O}_4\text{Os}\cdots\text{NC}_5\text{H}_5$	-11.4	2.513	0.0468	5.63

Table 5.2.3. Interaction energies (ΔE , kcal/mol), equilibrium distances measured from the N to the Om atoms (d , Å) and electron charge densities (ρ_r , a.u.) at the bond CPs connecting the N to the Om atoms for the OmO_4 adducts (Om = Fe, Ru, Os) with acetonitrile and pyridine (Py). The stabilization energies from the second order perturbation analysis $E(2)$ corresponding to the LP(N) $\rightarrow\sigma^*(\text{Om}-\text{O})$ orbital donor-acceptor interactions are also indicated.

both RuO₄ and OsO₄, pyridine hydrogen atoms engage in C–H...O interactions, characterized by a bond CP, bond path and green NCIplot isosurface. These adducts exhibit quite short Om...N distances, especially in the OsO₄ one. The NCIplot index shows that the outer part of the isosurface is yellow, to be attributed to some N...O repulsion between the negative O atoms and the N atom of the pyridine. While being quite short, the theoretical distance computed in the gas phase (~2.5 pm) is in reasonable agreement with the experimental distances observed in the cocrystals (~2.4 pm).

In Table 5.2.3 the results from the natural bond orbital analysis applied to the adducts in the gas phase are summarized. In all complexes, modest to moderate orbital donor-acceptor contributions were found, ranging from 0.24 to 5.63 kcal/mol. This contribution is attributed as an electron donation from the lone pair of nitrogen to the antibonding σ^* orbitals of Om=O bond. Since the orbital contribution is very sensitive to the equilibrium distance in the weakest complex O₄Fe...NCCH₃ (with the longest equilibrium distance) the contribution is around 10% of the interaction energy. In sharp contrast, for the strongest adduct (O₄Os...NC₅H₅) the orbital contribution is approximately 50% of the interaction energy.

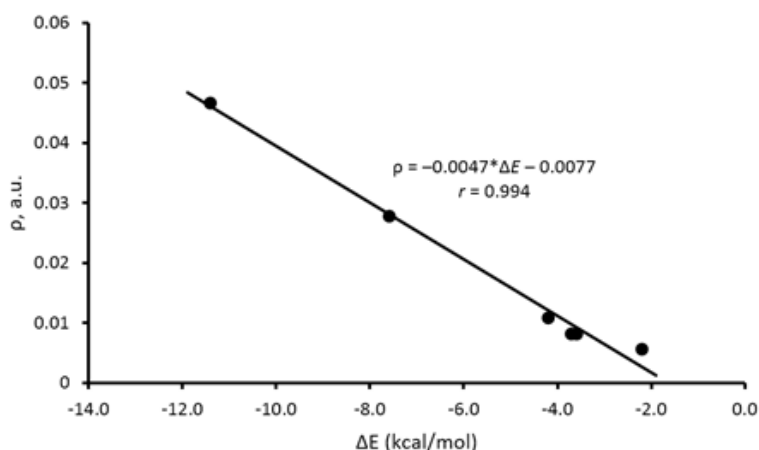


Figure 5.2.5. Regression plot of the interaction energy versus the electron charge density at the bond CP that characterize the OmB in the adducts shown in Figure 5.2.4.

The strong correlation ($r = 0.994$) between the interaction energies and the values of the charge density at the bond CPs (Figure 5.2.5) is noteworthy and it suggests that the value of ρ can be used as an energy predictor for OmBs.

A combined QTAIM/NCIplot analysis has been performed for the cocrystal **3-8** in order to have information on the interactions as they stand in the solid state. The results for the OsO₄ adducts are summarized in Figure 5.2.6. In all systems the existence of the interaction is confirmed by the corresponding bond CP and bond path connecting the N/O atom to the Os atom. The analysis identifies also the weak C–H...O HBs, found in

the crystal, characterized by the corresponding bond CPs and bond paths. The Os...N/O interaction is strong (dark-blue isosurface) in all adducts and once again the existence of N/O...O repulsion characterized by the yellow (weak repulsive) parts of the surfaces is found. Short Os...N experimental distances can be explained by the fact that the electrostatic potential at the O atoms are smaller in module than those at the σ -holes, thus the O...N repulsion is weaker than the Os...N attraction.

Finally, the interaction energies of the contacts have been estimated using the equation shown in Figure 5.2.5, getting very similar results (-14.5 to -14.9 kcal/mol). These values agree well with the crystallographic short Os...N/O distances and the dark blue color of the NCIplot isosurfaces.

We have here demonstrated that the interactions taking place in the formation of OsO₄ adducts can be considered a σ -hole interactions. This breakthrough finally bridges together σ -hole interaction and charge-transfer complexes revealing a continuum of the periodic properties of group 8 elements in the formation of this adducts. More analyses on this kind of adducts are expected in the near future.

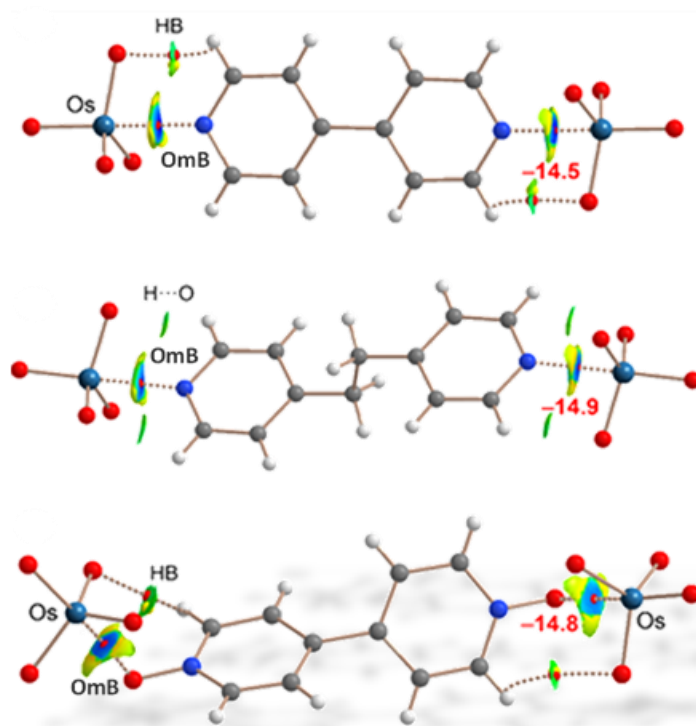


Figure 5.2.6. Combined QTAIM/NCIplot analysis of adducts **3** (top), **4** (middle) and **5** (bottom). Bond CPs in red and ring CPs in yellow. NCIPlot: $|RGB|$ isosurface 0.4 a.u.; Color range 0.04 a.u. (red) $\leq (\text{sign}\lambda^2)\rho \leq -0.04$ a.u. (blue). Only the intermolecular interactions are shown. In red, the OmB energies estimated using the ρ values.

Additional Data.

The experimental section contains CSD surveys, computational, synthetic and crystallographic details.

References.

- [1] G. N. Lewis, *J. Am. Chem. Soc.* **1916**, *38*, 762–785.
- [2] G. N. Lewis, *Valence and the Structure of Atoms and Molecules*, Chemical Catalog Company, Incorporated, **1923**.
- [3] A. Bauzá, I. Alkorta, J. Elguero, T. J. Mooibroek, A. Frontera, *Angew. Chemie Int. Ed.* **2020**, *59*, 17482–17487.
- [4] A. C. Legon, N. R. Walker, *Phys. Chem. Chem. Phys.* **2018**, *20*, 19332–19338.
- [5] A. Daolio, A. Pizzi, M. Calabrese, G. Terraneo, S. Bordignon, A. Frontera, G. Resnati, *Angew. Chemie* **2021**, *133*, 20891–20895.
- [6] A. Daolio, A. Pizzi, G. Terraneo, A. Frontera, G. Resnati, *ChemPhysChem* **2021**, 1–6.
- [7] W. Dong, Q. Li, S. Scheiner, *Molecules* **2018**, *23*, 1–17.
- [8] L. Brammer, *Faraday Discuss.* **2017**, *203*, 485–507.
- [9] J. Joy, E. D. Jemmis, *J. Chem. Sci.* **2019**, *131*, 1–8.
- [10] F. Zhou, Y. Liu, Z. Wang, Q. Yang, B. Zheng, *Comput. Theor. Chem.* **2020**, *1179*, 112800.
- [11] V. Angarov, S. Kozuch, *New J. Chem.* **2018**, *42*, 1413–1422.
- [12] I. Alkorta, J. Elguero, A. Frontera, *Crystals* **2020**, *10*, 180.
- [13] A. C. Legon, N. R. Walker, *Phys. Chem. Chem. Phys.* **2018**, *20*, 19332–19338.
- [14] G. Resnati, P. Metrangolo, *Coord. Chem. Rev.* **2020**, *420*, 213409.
- [15] G. Cavallo, P. Metrangolo, T. Pilati, G. Resnati, G. Terraneo, *Cryst. Growth Des.* **2014**, *14*, 2697–2702.
- [16] C. F. Albert, P. C. Healy, J. D. Kildea, C. L. Raston, B. W. Skelton, A. H. White, *Inorg. Chem.* **1989**, *28*, 1300–1306.
- [17] P. G. Jones, B. Ahrens, *New J. Chem.* **1998**, *22*, 1041–1042.
- [18] A. Bauzá, I. Alkorta, J. Elguero, T. J. Mooibroek, A. Frontera, *Angew. Chemie Int. Ed.* **2020**, *59*, 17482–17487.
- [19] J. Halldin Stenlid, A. J. Johansson, T. Brinck, *Phys. Chem. Chem. Phys.* **2018**, *20*, 2676–2692.
- [20] J. H. Stenlid, T. Brinck, *J. Am. Chem. Soc.* **2017**, *139*, 11012–11015.
- [21] G. Li, J. H. Stenlid, M. S. G. Ahlquist, T. Brinck, *J. Phys. Chem. C* **2020**, *124*, 14696–14705.
- [22] R. Wysokiński, W. Zierkiewicz, M. Michalczyk, S. Scheiner, *ChemPhysChem* **2020**, *21*, 1119–1125.
- [23] Y. V Nelyubina, M. Y. Antipin, K. A. Lyssenko, *Russ. Chem. Rev.* **2010**, *79*, 167–187.
- [24] V. Terrasson, S. Marque, M. Georgy, J.-M. Campagne, D. Prim, *Adv. Synth. Catal.* **2006**, *348*, 2063–2067.
- [25] C. Trujillo, G. Sánchez-Sanz, J. Elguero, I. Alkorta, *Struct. Chem.* **2020**, *31*, 1909–1918.
- [26] M. Hasan, I. V. Kozhevnikov, M. R. H. Siddiqui, A. Steiner, N. Winterton, *Inorg. Chem.* **1999**, *38*, 5637–5641.
- [27] D. Paliwoda, M. Szafranski, M. Hanfland, A. Katrusiak, *J. Mater. Chem. C* **2018**, *6*, 7689–7699.
- [28] L. E. Pope, J. C. A. Boeyens, *Structural*, **1975**, 47–58.
- [29] E. V. Makotchenko, I. A. Baidina, L. A. Sheludyakova, *Russ. J. Inorg. Chem.* **2011**, *56*, 713–720.
- [30] M. Calleja, S. A. Mason, P. D. Prince, J. W. Steed, C. Wilkinson, *New J. Chem.* **2001**, *25*, 1475–1478.
- [31] T. Asaji, F. Tajima, M. Hashimoto, *Polyhedron* **2002**, *21*, 2207–2213.

- [32] T. K. Hagos, S. D. Nogai, L. Dobrzańska, S. Cronje, H. G. Raubenheimer, *Acta Crystallogr. Sect. E Struct. Reports Online* **2009**, *65*, m255–m256.
- [33] A. Bauzá, A. Frontera, T. J. Mooibroek, *Nat. Commun.* **2017**, *8*, 1–6.
- [34] S. S. Batsanov, *Inorg. Mater.* **2001**, *37*, 871–885.
- [35] R. F. W. Bader, *Chem. Rev.* **1991**, *91*, 893–928.
- [36] J. Murray, P. Politzer, *ChemPhysChem* **2021**, DOI 10.1002/cphc.202100202.
- [37] A. Grabarz, M. Michalczyk, W. Zierkiewicz, S. Scheiner, *ChemPhysChem* **2020**, *21*, 1934–1944.
- [38] R. Wysokiński, M. Michalczyk, W. Zierkiewicz, S. Scheiner, *Phys. Chem. Chem. Phys.* **2021**, *23*, 4818–4828.
- [39] D. W. Patrick, L. K. Truesdale, S. A. Biller, K. B. Sharpless, *J. Org. Chem.* **1978**, *43*, 2628–2638.
- [40] M. Schroeder, *Chem. Rev.* **1980**, *80*, 187–213.
- [41] B. S. McGilligan, J. Arnold, G. Wilkinson, B. Hussain-Bates, M. B. Hursthouse, *J. Chem. Soc., Dalton Trans.* **1990**, 2465–2475.
- [42] K. Muñiz, *New J. Chem.* **2005**, *29*, 1371.
- [43] J. M. Wallis, J. K. Kochi, *J. Am. Chem. Soc.* **1988**, *110*, 8207–8223.
- [44] J. M. Wallis, J. K. Kochi, *J. Org. Chem.* **1988**, *53*, 1679–1686.
- [45] E. Munusamy, R. Sedlak, P. Hobza, *ChemPhysChem* **2011**, *12*, 3253–3261.
- [46] I. S. Youn, D. Y. Kim, W. J. Cho, J. M. L. Madrdejos, H. M. Lee, M. Kołaski, J. Lee, C. Baig, S. K. Shin, M. Filatov, et al., *J. Phys. Chem. A* **2016**, *120*, 9305–9314.
- [47] J. Chen, T. J. Martínez, *Chem. Phys. Lett.* **2007**, *438*, 315–320.
- [48] P. Politzer, K. E. Riley, F. A. Bulat, J. S. Murray, *Comput. Theor. Chem.* **2012**, *998*, 2–8.
- [49] W. P. Griffith, R. Rossetti, *J. Chem. Soc. Dalton Trans.* **1972**, *22*, 1449–1453.
- [50] W. P. Griffith, *Partial Coordination in Amine Adducts of Osmium Tetraoxide: X-Ray Molecular Structure of Quinuclidinetetraoxo-Osmium(VIII)*, **1978**.
- [51] D. W. Nelson, A. Gypser, P. T. Ho, H. C. Kolb, T. Kondo, H.-L. Kwong, D. V. McGrath, A. E. Rubin, P.-O. Norrby, K. P. Gable, et al., *J. Am. Chem. Soc.* **1997**, *119*, 1840–1858.
- [52] M. Gerken, D. A. Dixon, G. J. Schrobilgen, *Inorg. Chem.* **2000**, *39*, 4244–4255.
- [53] R. Weber, K. Dehnicke, U. Muller, D. Fenske, *Zeitschrift für Anorg. und Allg. Chemie Anorg. und Allg. Chemie* **1984**, *516*, 214–222.
- [54] A. J. Bailey, M. G. Bhowon, W. P. Griffith, A. G. F. Shoair, A. J. P. White, D. J. Williams, *J. Chem. Soc. Dalton Trans.* **1997**, *516*, 3245–3250.
- [55] The “Normalized Contact” N_c for an Interaction Involving Atoms i and j Is the Ratio $D_{ij}/(R_{vdW,i} + R_{vdW,j})$ Where D_{ij} Is the Experimental Distance between i and j and $R_{vdW,i}$ and $R_{vdW,j}$ Are the van Der Waals Radii of i and j , **n.d.**
- [56] S. S. Batsanov, *Inorg. Mater.* **2001**, *37*, 1031–1046.
- [57] P. F. Lang, B. C. Smith, *Glob. J. Sci. Front. Res. B Chem.* **2016**, *16*, 55–60.
- [58] R. Wysokiński, M. Michalczyk, W. Zierkiewicz, S. Scheiner, *Phys. Chem. Chem. Phys.* **2021**, *23*, 4818–4828.
- [59] J. Fanfrlík, W. Zierkiewicz, P. Švec, Z. Růžičková, J. Řezáč, M. Michalczyk, A. Růžička, D. Michalska, P. Hobza, *J. Mol. Model.* **2017**, *23*, 328.
- [60] A. Grabarz, M. Michalczyk, W. Zierkiewicz, S. Scheiner, *ChemPhysChem* **2020**, *21*, 1934–1944.
- [61] R. E. Dodd, *Trans. Faraday Soc.* **1959**, *55*, 1480.
- [62] F. N. Hosseini, *Polyhedron* **2010**, *29*, 349–353.
- [63] M. Saccone, G. Cavallo, P. Metrangolo, A. Pace, I. Pibiri, T. Pilati, G. Resnati, G. Terraneo, *CrystEngComm* **2013**, *15*, 3102.
- [64] P. Scilabra, G. Terraneo, A. Daolio, A. Baggioli, A. Famulari, C. Leroy, D. L. Bryce, G. Resnati, *Cryst. Growth Des.* **2020**, *20*, 916–922.

6. Experimental Section.

The research described in this thesis is the result of the collaborative effort of students in G. Resnati group, staff, and occasional external collaborators. The contribution of the following coworkers are described:

GR – Giuseppe Resnati, full Professor at Politecnico di Milano.

GT – Giancarlo Terraneo, full Professor at Politecnico di Milano.

PP – Peter Politzer, full professor at University of New Orleans.

JM – Jane Murray, full professor at University of New Orleans.

AF – Antonio Frontera, full Professor at Universidad de las Islas Baleares.

AG – Alessandro Genoni, full Professor at University of Lorraine.

FV – Fiorenza Viani, Researcher of CNR (Consiglio Nazionale delle Ricerche).

TP – Tullio Pilati, former Researcher of Politecnico di Milano and CNR.

ND – Nicola Demitri, researcher at Elettra Synchrotron, Trieste.

SN - Susantha Nayak, former PhD student at Politecnico di Milano.

SB – Simone Bordignon, postdoctoral fellow at University of Torino.

EW – Erna Wieduwilt, postdoctoral fellow at University of Lorraine.

AP – Andrea Pizzi, postdoctoral fellow at Politecnico di Milano (RTDa).

AD – Andrea Daolio, PhD student at Politecnico di Milano author of this thesis.

MC – Miriam Calabrese, PhD student at Politecnico di Milano.

MU – Maurizio Ursini, laboratory technician at Politecnico di Milano.

CG – Christian Grassi, undergraduate student at Politecnico di Milano.

6.1. The Halogen Bond at Work.

Contributions:

6.1.1. Uncommon adducts between iodoperfluoroalkanes and a fluoride anion.

SN and GR designed the experiments.

GT and TP oversaw the crystallography refinement and characterization.

AD, SN and GR interpreted the results.

AD performed CSD surveys and Hirschfeld surface analysis.

6.1.1. Uncommon adducts between iodoperfluoroalkanes and a fluoride anion.

Materials.

KF, 1,4,7,10,13,16-Hexaoxacyclooctadecane, 1-iodo-1,1,2,2,3,3,3-heptafluoro propane and 1,4-diiodo-1,1,2,2,3,3,4,4-octafluoro-butane were purchased from Sigma Aldrich or TCI and used without further purification.

Methods.

The single crystal data of **1** and **2** were collected at Bruker SMART APEX II CCD area detector diffractometer at room temperature. Data collection, unit cell refinement and data reduction were performed using Bruker SAINT. The structure was solved by direct methods using SHELXT and refined by full-matrix least-squares on F^2 with anisotropic displacement parameters for the non-H atoms using SHELXL-2016/6. Absorption correction was performed based on multi-scan procedure using SADABS. Structure analysis was aided by use of the program PLATON. The hydrogen atoms were calculated in ideal positions with isotropic displacement parameters set to $1.2 \times U_{eq}$ of the bonded atom.

Representation and analysis of Hirshfeld Surface and their fingerprints has been obtained with the program CrystalExplorer¹, the electronic potential plotted over the Hirshfeld surface was calculated with the Tonto program², with HF methods and STO-3G basis set, as implemented in CrystalExplorer 17.5.

¹ CrystalExplorer 3.1; University of Western Australia: Albany, AU, 2012.

² Jayatilaka, D.; Grimwood, D. J. Tonto: A Fortran Based Object-Oriented System for Quantum Chemistry and Crystallography. In Computational Science ICCS 2003. ICCS 2003. Lecture Notes in Computational Science, Melbourne, AU; St. Petersburg, RU, June 2-4, 2003; Sloot, P. M. A.; Abramson, D.; Bogdanov, A. V.; Gorbachev, Y. E.; Dongarra, J. J.; Zomaya, A. Y., Eds.; Springer: Berlin, Heidelberg, DE, 2003; pp 142–151

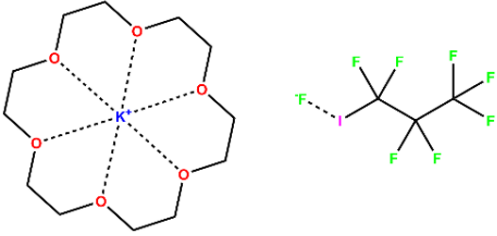
CSD Surveys.

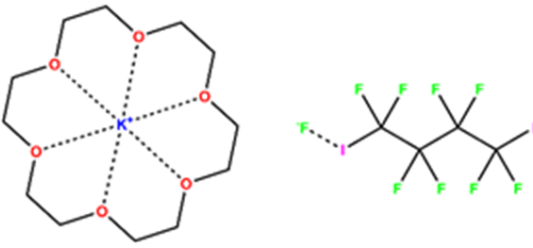
CSD Structures displaying σ -hole interactions where a fluoride anion is acting as the HaB acceptor.

Table 6.1.1. report all the structures and relative REFCODEs in the CSD where a fluoride anion is taking part in a σ -hole interaction as the interaction acceptor. The table reports also the nature of the interaction (HaB, ChB etc...) and if the fluoride anion is also engaging in hydrogen bonds.

Table 6.1.1. Detailed entries for CSD structures where a fluoride anion is engaging in σ -hole interactions. Cage-like anion trapping structures involve several factors other than the noncovalent interactions taking place in the solid state and therefore were not taken into consideration for his survey. Atoms considered as the interaction donor: Cl, Br, I, S, Se, P, As, Sb, Si, Ge. First-row elements have not been considered due to the low polarizability. No geometrical feature other than the presence a close contact has been taken into consideration in spite of the different geometrical features of the interactions,

REFCODE	Interaction Nature	Presence of hydrogen bonds
ASEWOM	HaB	Yes
EQUFAZ	HaB	Yes
GOXTUI	HaB	Yes
UZOHOU	HaB	Yes
UZOHEY	HaB	Yes
ZOMNUK	HaB	Yes
BIBRUB	ChB	Yes
MEFSUM	ChB	Yes
OTIRAM	ChB	Yes
OTIREQ	ChB	Yes
OTIRIU	ChB	Yes
OTISAN	ChB	Yes
OTISER	ChB	Yes
QWLAD	ChB	Yes

1	Formula: $C_{21}H_{24}F_{22}I_3KO_6$ Formula Weight: 1210.20 Name: 1-iodo-1,1,2,2,3,3,3-heptafluoro propane-18-crown-6-potassium fluoride	<input type="checkbox"/> Slow evaporation <input type="checkbox"/> Vapor diffusion <input type="checkbox"/> Solvent layer <input checked="" type="checkbox"/> Other Solvent(s)/Other agents:																		
		<input type="checkbox"/> Twinned Temperature: 100 K <table border="0" style="width: 100%;"> <tr> <td>a: 16.1882</td> <td>α: 90</td> <td>R₁:</td> <td>0.0333</td> </tr> <tr> <td>b: 16.1882</td> <td>β: 90</td> <td>System:</td> <td>Trigonal</td> </tr> <tr> <td>c: 12.4062</td> <td>γ: 120</td> <td>Space Group:</td> <td>R3m</td> </tr> <tr> <td>Vol: 2815.6</td> <td></td> <td></td> <td></td> </tr> </table>	a: 16.1882	α : 90	R ₁ :	0.0333	b: 16.1882	β : 90	System:	Trigonal	c: 12.4062	γ : 120	Space Group:	R3m	Vol: 2815.6					
a: 16.1882	α : 90	R ₁ :	0.0333																	
b: 16.1882	β : 90	System:	Trigonal																	
c: 12.4062	γ : 120	Space Group:	R3m																	
Vol: 2815.6																				
<u>Synthesis:</u> An amount of 18-crown-6 was heated up until melt, then an equimolar amount of potassium fluoride was added to the cryptand. To the stirred mixture was then added an excess of 1-iodo-1,1,2,2,3,3,3-heptafluoro propane enough to completely dissolve the mixture of 18-crown-6 and KF. The liquid were then let cool down. Small crystals suitable for X-Ray analysis were formed on the bottom of the flask.																				
<u>Characterization:</u>		<table border="1" style="width: 100%; border-collapse: collapse;"> <tr> <td style="text-align: center;">Z</td> <td style="text-align: center;">3</td> </tr> <tr> <td style="text-align: center;">$\rho_{\text{calc}} / \text{g/cm}^3$</td> <td style="text-align: center;">2.141</td> </tr> <tr> <td style="text-align: center;">μ / mm^{-1}</td> <td style="text-align: center;">2.752</td> </tr> <tr> <td style="text-align: center;">F(000)</td> <td style="text-align: center;">1722.0</td> </tr> <tr> <td style="text-align: center;">Radiation</td> <td style="text-align: center;">MoKα ($\lambda = 0.71073$)</td> </tr> <tr> <td style="text-align: center;">Reflections Collected</td> <td style="text-align: center;">16079</td> </tr> <tr> <td style="text-align: center;">Goodness-of-fit on F²</td> <td style="text-align: center;">0.976</td> </tr> <tr> <td style="text-align: center;">Final R indexes [I > 2σ (I)]</td> <td style="text-align: center;">R₁ = 0.0333, wR₂ = 0.0593</td> </tr> <tr> <td style="text-align: center;">Final R indexes (all data)</td> <td style="text-align: center;">R₁ = 0.0378, wR₂ = 0.0607</td> </tr> </table>	Z	3	$\rho_{\text{calc}} / \text{g/cm}^3$	2.141	μ / mm^{-1}	2.752	F(000)	1722.0	Radiation	MoK α ($\lambda = 0.71073$)	Reflections Collected	16079	Goodness-of-fit on F²	0.976	Final R indexes [I > 2σ (I)]	R ₁ = 0.0333, wR ₂ = 0.0593	Final R indexes (all data)	R ₁ = 0.0378, wR ₂ = 0.0607
Z	3																			
$\rho_{\text{calc}} / \text{g/cm}^3$	2.141																			
μ / mm^{-1}	2.752																			
F(000)	1722.0																			
Radiation	MoK α ($\lambda = 0.71073$)																			
Reflections Collected	16079																			
Goodness-of-fit on F²	0.976																			
Final R indexes [I > 2σ (I)]	R ₁ = 0.0333, wR ₂ = 0.0593																			
Final R indexes (all data)	R ₁ = 0.0378, wR ₂ = 0.0607																			

2	Formula: $C_{20}H_{24}F_{17}I_4KO_6$ Formula Weight: 1230.09 Name: 1,4-diiodo-1,1,2,2,3,3,4,4-octafluoro-butane-18-crown-6-potassium fluoride	<input type="checkbox"/> Slow evaporation <input type="checkbox"/> Vapor diffusion <input type="checkbox"/> Solvent layer <input checked="" type="checkbox"/> Other																		
		Solvent(s)/Other agents:	<input type="checkbox"/> Twinned Temperature: 100 K																	
<p><u>Synthesis:</u></p> <p>An amount of 18-crown-6 was heated up until melt, then an equimolar amount of potassium fluoride was added to the cryptand. To the stirred mixture was then added an excess of 1,4-diiodo-1,1,2,2,3,3,4,4-octafluoro-butane, enough to completely dissolve the mixture of 18-crown-6 and KF. The liquid were then let cool down. Small crystals suitable for X-Ray analysis were formed on the bottom of the flask.</p>		<table border="1" style="width: 100%; border-collapse: collapse;"> <tr> <td>a: 9.922</td> <td>α: 90</td> <td>R_1:</td> <td>0.0363</td> </tr> <tr> <td>b: 26.983</td> <td>β: 90.29</td> <td>System:</td> <td>Monoclinic</td> </tr> <tr> <td>c: 13.673</td> <td>γ: 90</td> <td>Space Group:</td> <td>C2/c</td> </tr> <tr> <td>Vol: 3660.8</td> <td></td> <td></td> <td></td> </tr> </table>	a: 9.922	α : 90	R_1 :	0.0363	b: 26.983	β : 90.29	System:	Monoclinic	c: 13.673	γ : 90	Space Group:	C2/c	Vol: 3660.8					
a: 9.922	α : 90	R_1 :	0.0363																	
b: 26.983	β : 90.29	System:	Monoclinic																	
c: 13.673	γ : 90	Space Group:	C2/c																	
Vol: 3660.8																				
<p><u>Characterization:</u></p>		<table border="1" style="width: 100%; border-collapse: collapse;"> <tr> <td style="text-align: center;">Z</td> <td style="text-align: center;">4</td> </tr> <tr> <td style="text-align: center;">$\rho_{calc} / g/cm^3$</td> <td style="text-align: center;">2.232</td> </tr> <tr> <td style="text-align: center;">μ/mm^{-1}</td> <td style="text-align: center;">3.637</td> </tr> <tr> <td style="text-align: center;">F(000)</td> <td style="text-align: center;">2304.0</td> </tr> <tr> <td style="text-align: center;">Radiation</td> <td style="text-align: center;">MoKα ($\lambda = 0.71073$)</td> </tr> <tr> <td style="text-align: center;">Reflections Collected</td> <td style="text-align: center;">36602</td> </tr> <tr> <td style="text-align: center;">Goodness-of-fit on F²</td> <td style="text-align: center;">1.024</td> </tr> <tr> <td style="text-align: center;">Final R indexes [I > 2σ (I)]</td> <td style="text-align: center;">$R_1 = 0.0363, wR_2 = 0.0719$</td> </tr> <tr> <td style="text-align: center;">Final R indexes (all data)</td> <td style="text-align: center;">$R_1 = 0.0605, wR_2 = 0.0806$</td> </tr> </table>	Z	4	$\rho_{calc} / g/cm^3$	2.232	μ/mm^{-1}	3.637	F(000)	2304.0	Radiation	MoK α ($\lambda = 0.71073$)	Reflections Collected	36602	Goodness-of-fit on F²	1.024	Final R indexes [I > 2σ (I)]	$R_1 = 0.0363, wR_2 = 0.0719$	Final R indexes (all data)	$R_1 = 0.0605, wR_2 = 0.0806$
Z	4																			
$\rho_{calc} / g/cm^3$	2.232																			
μ/mm^{-1}	3.637																			
F(000)	2304.0																			
Radiation	MoK α ($\lambda = 0.71073$)																			
Reflections Collected	36602																			
Goodness-of-fit on F²	1.024																			
Final R indexes [I > 2σ (I)]	$R_1 = 0.0363, wR_2 = 0.0719$																			
Final R indexes (all data)	$R_1 = 0.0605, wR_2 = 0.0806$																			
<input type="checkbox"/> IR <input type="checkbox"/> ¹ H-NMR <input type="checkbox"/> Other <input type="checkbox"/> UV <input type="checkbox"/> ¹³ C-NMR 																				

6.2. The Chalcogen Bond at Work.

Contributions:

6.2.1 Benzisothiazolinones as Chalcogen Bond Donors and their Structure-Functions Relationship.

FV synthesized the compounds.

FV, AD and AP crystallized or recrystallized the compounds.

ND performed the synchrotron experiments and structure refinement.

AD, AP and GR interpreted the results and performed CSD surveys.

6.2.2. Chalcogen Bond Drives the Packing of Cyanine Crystals.

PP and JM performed the calculations.

AD and GR designed the experiments and interpreted the results.

AD performed the synthesis, characterization of the compounds, crystallizations, and structure refinement.

GT oversaw the crystallography refinement and characterization.

ND performed occasional synchrotron experiments and structure refinement on **10, 11, 12**.

6.2.1 Benzisothiazolinones as Chalcogen Bond Donors and their Structure-Functions Relationship.

Synthesis and characterization of the compounds is described elsewhere³. They are all reported at the end of the paragraph.

Methods.

Data collections for compounds **1-6** were performed at the X-ray diffraction beamline (XRD1) of the Elettra Synchrotron, Trieste (Italy)⁴. The crystals were dipped in NHV oil (Jena Bioscience, Jena, Germany) and mounted on the goniometer head with kapton loops (MiTeGen, Ithaca, USA). Complete datasets were collected at 100 K (nitrogen stream supplied through an Oxford Cryostream 700 - Oxford Cryosystems Ltd., Oxford, United Kingdom) through the rotating crystal method. The diffraction data were indexed and integrated using XDS.⁵ The structures were solved by the dual space algorithm implemented in the SHELXT code⁶. Fourier analysis and refinement were performed by the full-matrix least-squares methods based on F^2 implemented in SHELXL (Version 2018/3)⁷. The Coot program was used for modeling.⁸ Anisotropic thermal motion refinement have been used for all atoms. Geometric restrains (SAME) have been applied on disordered fragments of d. Hydrogen atoms were included at calculated positions with isotropic Ufactors = $1.2 \times U_{eq}$ or Ufactors = $1.5 \times U_{eq}$ for methyl and hydroxyl groups (U_{eq} being the equivalent isotropic thermal factor of the bonded non hydrogen atom). All the samples showed compact crystal packing without solvent inclusions.

Data collection for compound a was performed on a Bruker Kappa Apex II diffractometer at 100 K by using a fine-focus sealed Mo-K α tube, $\lambda = 0.71073 \text{ \AA}$. Data collection and reduction was performed by using the program SAINT,⁹ and absorption correction, based on multiscan procedure, was achieved by using the program SADABS.¹⁰ Structures were solved with SHELXS¹¹ software and refined on all independent reflections by full-matrix least-squares based on F^2 by using the SHELXL program. Anisotropic thermal motion

³ F. Viani, B. Rossi, W. Panzeri, L. Merlini, A. M. Martorana, A. Polissi, Y. M. Galante, *Tetrahedron* 2017, 73, 1745-1761.

⁴ A. Lausi, M. Polentarutti, S. Onesti, J. R. Plaisier, E. Busetto, G. Bais, L. Barba, A. Cassetta, G. Campi, D. Lamba, A. Pifferi, S. C. Mande, D. D. Sarma, S. M. Sharma, G. Paolucci, *Eur. Phys. J. Plus* 2015, 130, 1-8.

⁵ W. Kabsch, *Acta Cryst. Section D* 2010, 66(2), 125-132

⁶ G. M. Sheldrick, *Acta Cryst. Section A* 2015, 71, 3-8.

⁷ G. M. Sheldrick, *Acta Cryst. Section C* 2015, 71, 3-8.

⁸ P. Emsley, B. Lohkamp, W. G. Scott, K. Cowtan, *Acta Cryst. Section D* 2010, 66(4), 486-501

⁹ Bruker (2012). SAINT. Bruker AXS Inc., Madison, Wisconsin, USA.

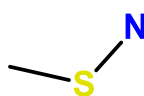
¹⁰ Bruker (2001). SADABS. Bruker AXS Inc., Madison, Wisconsin, USA.

¹¹ G. M. Sheldrick, *Acta Cryst. Section A* 2008, 64, 112-122

refinement has been used for all the atoms. Hydrogen atoms were placed in calculated positions and refined by using a riding model. 3D figures were prepared with CCDC Mercury¹² software.

CSD Surveys.

Table 6.2.1. Hits on the CSD containing the following structure:



In bold, structures showing a close contact on the chalcogen atom. In red, structures where the Nu...S-N angle is $> 160^\circ$, in green where the Nu...S-C angle is $> 160^\circ$. In yellow when the structure display both a contact with an Nu...S-N and Nu...S-C angle $> 160^\circ$.

JEKCIO01	DOCFIK	IQOLAC	MIETDZ20	QICWII	VEFBIS
JUDZEQ	DOMMEX	ISTZCN	MIJQUR	QILLUV	VEFBOY
LORGEH	DOQBAO	ISTZCN10	MIJVUZ	QIQWAQ	VETXIE
LORGIL	DOVCIA	ITIKIH	MIJWAE	QIQWEU	VEZCAE
LORGOR	DPTSIM	ITUZAY	MIJWEI	QOBFOC	VEZCEI
LOWHOX	DTOLSN	ITUZAY01	MIXQAL	QOBFUI	VEZCIM
LOWHOX01	DUCQEY	ITUZAY02	MIXQEP	QOBVIN	VIBLUQ
QOSZUW	DUDKIW	IXEXEQ	MIXQIT	QODCUH	VIHXIW
QOWNAU	DUDPAT	IXEXEQ01	MODIAZ	QODCUH01	VILMIM
SUKTOK	DUHSUU	IXEXIU	MOHBAN	QOGMOP	VIQDUU
SUKTUQ	DUJGEU	IYEVAK	MOKJAZ	QOGMUV	VIQFAC
SUKVAY	DUJGIY	IYEZIV	MOKJED	QOHJEC	VIRGIM
UGUNES	DUNTEL	IZESEN	MOKVIR	QOPHOU	VIRGOS
XOPWUX	DUPPOU	IZESEN01	MOQCAX	QOPHUA	VIRGOS01
ABAZUY	DUQNIO	IZESOX	MOSNCO	QOPJAI	VIRGUY
ABIPEG	DURKOR	IZIYIB	MOTZEA	QOPJEM	VIXRID
ABTITZ	DUWFIK	JAQCOU	MOTZIE	QOPJIQ	VOFTIV
ACIHEA	DUWMOY	JAQCUA	MOTZOK	QOPJOW	VOFTOB
ACMTHZ	DUZDUY	JAQMUM	MOTZUQ	QUCHEC	VONVAY
AEBZTZ	EABZIT	JARSAW	MOVBAA	QUFRAM	VONVEC
AFIPIR	ECITZP	JAVGAO	MOZTAW	QULLIS	VONVIG
AHEFEY	ECOBUU02	JAXMOL	MPDTZF	QURSON	VOPMOF
AHOLOZ	ECOBUU03	JAYWIQ	MPITDZ01	QURSUT	VUFWOI
AJAPEG	EDICUP	JEKBWU	MPITDZ10	QURTAA	VUFWUO

¹² C. F. Macrae, I. J. Bruno, J. A. Chisholm, P. R. Edgington, P. McCabe, E. Pidcock, L. Rodriguez-Monge, R. Taylor, J. van de Streek, P. A. Wood., *J. Appl. Cryst.* **2008**, *41*, 466-470.

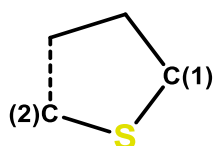
AJAPIK	EDIDAW	JEKCEH	MTCBML	QURTEE	VUJRUO
AKOCAE	EDIDEA	JEKCIO	MTDZDT	QURTH	VUYBEY
AMOCEL	EDIDIE	JEKCOS	MTMORT	QURTH01	WADLES
AMTHTZ	EHULAW	JELVUU	MTSITZ	QURVOQ	WADLIW
ANUBUI	EIMPTZ	JELWAB	MTXITZ	QUXCIX	WAFYIL
ANUWEM	EITDZL	JEZNIL	MUQKAK	RAGXEE	WAGKOG
APENTN01	EJNOA	JIFKOB	MUQKAK01	RAGXII	WAGKOG01
APENTN02	EKIBUV	JIGCIL	MUSPAS	RAJGER	WAGKUM
APENTN20	EKIPEU	JIMVAC	MUSPEW	RECLAN	WAGKUM01
APMOPF	ELAVEU	JISZUH	MUSYIJ	RECLAN01	WALCOC
AQEBII	EMOBAK	JITBAQ	MUVCAJ	REDHAK	WALCOC01
AQEBUU	EMOBE0	JIZXEW	MUVQID	REGQEZ	WARPEK
ASAXUP	EPHTRZ	JIZXEW01	MUVQUP	REHSIJ	WARPIO
ASIDIP	EQACAB	JIZXEW02	MUWKAS	REMQEI	WAXCUV
ASIZAE	EQACEF	JIZYID	MUWQIE	REMQIM	WECXAF
AXASIB	EQACOP	JOFMEY	MUWQOK	REQXOC	WECXEJ
AXASOH	EQETOL	JOFNUP	MUZYOV	REQXUI	WEDGUJ
AXOWOZ	EQETUR	JOFNUP01	NACJAF	REQYAP	WEDHAQ
AXOWOZ01	EQEVAZ	JOFNUP02	NADXUL	REQYET	WEDHEU
AXOWUF	EQEVED	JOLNIK	NAGSAP	REQYIX	WEDHIY
AXOXAM	EQEVII	JOLVOV	NAJBAB	RESJIK	WEDHOE
AYEXOS	EQEVON	JONFUN	NAJBEF	RESJOQ	WEDHUK
AYOREM	EQEVUT	JONSAG	NAJBEF01	REVVUK	WEDXUY
AYORIQ	EQEWAA	JONXOZ	NBXTPH	RIDGOB	WEFBIS
AZAXEF	ERUQAJ	JONXOZ01	NEBSMS	RIDGUH	WEKCEU
BABFIW	EWACUB	JOQMEK	NEWYET	RIDHAO	WEMTEN
BABFOC	EXIJUR	JOQMIO	NEWYET01	RIVHAF	WEMVIT
BABFUI	EYOXEW	JORLOR	NEWYIX	RIXCUW	WEVWAW
BABGAP	FAMWAR	JORLOS	NEZNEL	RIZDEJ	WIDKAX
BAGDES	FAPGAH	JORLOS01	NEZNIP	ROCJUP	WIFNUX
BAPLUZ	FAPGEL	JOZKIS	NIGJAR	ROFJAX	WIPBOO
BAPNOW	FAPGOV	JUGDUK	NIGJAR01	ROHMEG	WIPBUU
BAPNUC	FAQCEH	JUGVUC	NILQAD	ROKDIG	WIPBUU01
BARDUT	FAWREA	JUKSAL	NIMKIE	RONYOI	WIPJOW
BATJUC	FECZAO	JUKSEP	NIMKOK	ROPKUC	WIPXIE
BAVVOM	FEDMOR	JUTZAB	NINREI	ROYZUC	WIPXOK
BAXBAD	FEXROR	JUTZEF	NIXGAC	RUFMAG01	WOFFED
BAXPAU	FEXRUX	KABFAV	NOFKOJ	RUFMAG02	WOFFIH
BECHIB	FEYSEJ	KABFEZ	NOJJUU	RULWAW	WOLZIG
BECHOH	FEYSIN	KACGAY	NOJJUU01	SAGRAU	WOLZOM
BEHGAX	FEZFEW	KACGIG	NOJKED	SAGREY	WOWCAM
BEHGEB	FINLAQ	KALJAL	NOKVAK	SAGRIC	WUSBIW
BELZUP	FIVRAD	KAMGUA	NONDOK	SAKLEV	WUSBOC
BEMDOM	FOBQET	KAMYAY	NONDOK01	SAWBAT	WUXCIB
BERBAE	FOGHOY	KAMYEC	NOPCEC	SAWBEX	XADPUO
BEYFAO	FOGHUE	KAMYIG	NOPPIT	SAXPOW	XADQAV

BEZPOM	FOGJAM	KAPWOO	NOPPOZ	SAXPOW01	XAHLOJ
BEZPOM01	FOTWOA	KASVOQ	NOPPUF	SAXPOW02	XALLIF
BEZQAZ	FOVBEX	KEBKEH	NOPQAM	SAXPOW03	XALLIF01
BEZQAZ01	FUBJOB	KEBKIL	NOPQEQ	SAXPOW04	XASXOG
BEZQAZ02	FUBPAT	KECWUL	NOPQOA	SAXPOW05	XATFAA
BEZQAZ03	FUBQAU	KECWUL01	NOYTUQ	SAXPOW06	XAZKEQ
BIBBIX	FUCFIS	KECXAS	NOYVAY	SAXPOW07	XEGBEQ
BICJEC	FUHLID	KEFROD	NOYVEC	SAYXAS	XEGJUO
BIMTDZ10	FUSZID	KEGKOY	NOZCEK	SEBQUO	XEZPEZ
BIPTAZ	GALLEN	KEHFAF	NUGPAI	SEBRAV	XEZYAD
BIPXEG	GAWMEX	KEHZIG	NUNHIN	SEHGUI	XEZYEH
BIXNAX	GAWPAW	KELZAD	NUSJUI	SEJMOJ	XEZYIL
BIXNAX10	GAXMAT	KETWIR	NUXBOX	SEMJAV	XIFRIO
BIXNEB	GEDTUF	KEWSOW	NUXBUD	SENROT	XILCAW
BMQZTZ	GEDVER	KEZLAD	NZBITH	SEQDIB	XILMEK
BOCYEY	GEHFAB	KEZLOQ	OAZFAS	SEQDOH	XINGUW
BOCYIC	GEHFEF	KICSUN	OBARIU	SEQMAF	XIPZUU
BOHWUR	GEHZEB	KIKNEZ	OBITUO	SESYEV	XIPZUU01
BOPTUV	GEJGOR	KIKNID	OBIVAW	SIXCIL	XIVNEX
BOTMED	GERNUM	KIKNOJ	OBIVEA	SIXCOR	XIVNIB
BOTMIH	GEVWOT	KILLAU	OBIVIE	SIYBEJ	XIVNOH
BOTMON	GIBQEO	KILLEY	OBIVOK	SIYBIN	XIVNUN
BOTSTZ	GIFYAX	KINLEY	OBORAA	SIYBOT	XIVPAV
BOVDEY	GILVIH	KINLIC	OBOYIQ	SIYBUZ	XIVPEZ
BOWMEF	GITQOR	KIPYAJ	OBOYIQ01	SOBPAD	XIVPID
BOXSIS	GITREI	KIQVEL	OBOYOW	SODQIL	XIVPOJ
BPTSTZ	GITWEO	KIQVIP	OBOYOW01	SOKZUO	XIVROJ
BRBTAZ	GIVDIB	KIQVOV	OBUZAO	SOLBAX	XIXKAR
BTZACN	GIYFOJ	KIQVUB	OCAGIL	SOLBEB	XIXKEV
BUMDOC	GIYYUJ	KOGXOU	OCAVUL	SOLBIF	XIXKIZ
BUSHIG	GIYZAQ	KOGYAH	OCEZIF	SOLKAG	XOGVOF
BZITHO	GONSIN	KOGYEL	ODILAP	SOYMOI	XOGVOF01
BZITHO01	GUHDUI	KOKSEI	ODILET	SOYXUZ	XOPPAV
BZSTMP	GUHLIE	KOLCUJ	OGENEV	SOYXUZ10	XOQHER
BZTZMK	GULCIZ	KONQOV	OGEXIJ	SUNRAU	XOTJAR
CACNIF	GULCOF	KOPPIQ	OGEXIJ01	SUSYEM	XOTJEV
CAGGOJ	GULCUL	KOQKIK	OGUCUO	SUXMII	XURWOW
CAGHAW	GUVHOV	KOQKIK01	OGUDID	SUXMOO	XUVXIW
CATJEN	GUXHEM	KOVYID	OHALAM	TABTIB	YADPIC
CATJIR	HADVOX	KOWRUL	OJIQIJ	TADJAL	YALKEE
CATJOX	HAFQOW	KUBDOC	OJUKEK	TADJEP	YALSIQ
CAXBEI	HAFQUC	KUBXAG	OLAPIA	TADNUH	YAPWIW
CAXDUA	HAHHON	KUCLID	OLAPOG	TAHGEP	YAPWIW01
CAXFAI	HAJYAT	KUKZEW	OMAKAQ01	TAJVUV	YAPWOC
CBITAZ	HAKCEC	KUKZIA	OMELIC	TAJWAC	YAPWOC01
CBTHAZ10	HALJIP	KUSDEI	OMELIC01	TAPWUF	YEHQAD

CEBYUD	HANDUW	KUTYOO	OPABAJ	TAPZOZ	YEMLOR
CECQAD	HASCUZ	KUXSUS	OPIROV	TARXOB	YEQZOM
CECQEH	HAVSEC	LADVAN	OPIRUB	TAVSOA	YINC UW
CEGDUO	HAXXUZ	LADVAN01	OPISAI	TAVSUG	YINC UW01
CEHHII	HBMTHZ	LAJCUW	OPISEM	TAZZAX	YITCUC
CETNEU	HEGSIY	LAJDAD	OQOZEB	TCHZET	YITDAJ
CEXNAV	HELCEG	LAKHAG	OQOZIF	TECFAK	YIYHAS
CEXNOJ	HEMWUR	LAKHEK	OQOZOL	TECHOB	YIYWUB
CIKCIJ	HEMXAY	LAKHIO	OQUBIN	TECJAN	YODFIJ
CIKCOP	HEMXEC	LAKHOU	OQUBOT	TECLIX	YOPWEG
CIMLOB	HEMXIG	LAKHUA	OQUBUZ	TECVAZ	YOPWEG01
CIMLUH	HEMYON	LAKJAI	OTACHN	TEDPUO	YOPWEG02
CIRCOV	HEMYUT	LAXFUM	OTIPUD	TEHDAL	YORBEM
CIRZUA	HIJDOT	LAXZAM	OTIQAK	TEHXAG	YORBOW
CISBAJ	HIJDUZ	LAYJEA	OTIQEO	TELHAT	YUCYOL
CIYFEV	HIJKES	LAYKAA	OVAGOJ	TENHEZ	YUFCEH
CMBTDZ	HIKWED	LEBPOY	OWAFIC	TEQSOX	YUTCOH
CMSIAS	HIMRIH	LEBPUE	OWAFOI	TEQXET	YUTCUN
CMTHAZ	HIMRON	LEMJUJ	OWEDEA	TEQXIX	YUWVUJ
COBKOV	HIMSAA	LENQUQ	OWEDIE	TESTEQ	ZAFNOM
COBKUB	HIPTIJ	LEPNAV	OXTZOL	TESTIU	ZAJMUS
CODNUH	HISZAM	LEVZER	OYEMOW	TEYZUS	ZAJMUS01
COHKOZ	HIVWUF	LEVZIV	OYENOX	TEZZOP	ZAKFAS
COLGIW	HIZXIZ	LEWHIH	OYENUD	TFMTAB	ZAKMEG
COLJUL	HIZXOF	LEWHON	OYUJAU	THDZWA	ZAKMIK
COSLOL	HIZYEW	LEWJAB	OYUJEY	THZOLA	ZAKMOQ
COSYOA	HIZYIA	LIDBIK	OZEROC	TIBXAF	ZAMTIQ
COSYUG	HMITZC	LIDCOR	PABGEE	TIGXAJ	ZAPLEJ
COVPEK	HMSPTZ	LIMYOV	PADNAK	TIMFUQ	ZAQKEK
COWLEH	HOBZON	LIPLUR	PADNEO	TIMFUQ01	ZAQLAE
COYSOA	HOJJUO	LIQCEW	PAFNAL	TIMGAX	ZARBOJ
COYSOA01	HOKREF	LIQCIA	PAFVEY	TIMGAX01	ZARBUP
COYSOA02	HONLIF	LIQCOG	PAHSID	TIRNEN	ZARCAW
CPATHP	HOQABS	LIQCUM	PANSAB	TIRNIR	ZARCEA
CTAZCD10	HOQABS01	LIQDAT	PANSEF	TIVXUS	ZARDED
CUBGIQ	HOQBEU	LIQDEX	PAQGUM	TIVXUS01	ZAYREW
CURBUM	HUFZIT	LIQGAW	PAQGUM01	TIXTAX	ZAZYIK
CURCAT	HUFZOZ	LIQJED	PAYWER	TIXTAX01	ZEJSEP
CURCEX	HUGWUB	LIQJIH	PAZFED	TIXTAX02	ZEJSUC
CUVHEG	HUKGAV	LISTAJ	PEKXEJ	TOBVEN	ZELXOD
CUVLIO	HUTXEZ	LISTAL	PEMBEO	TOBVIR	ZELXUJ
CYSECO	HUTXID	LOCSAA	PEQJAW	TODVAL	ZESJOZ
DACSEF	IBAQUX	LOCSII	PESGUS	TOFQIR	ZIBVIP
DAHROT	IBARAE	LOCSOO	PESPUZ	TOSVIG	ZIMPIX
DAKDOI	IBEXES	LOCTUS	PHTTRZ	TOSVUS	ZIWWAD
DAPGAD	IBIGOQ	LOFGUL	PIGHES	TOVWUW	ZIZFET

DAQBIG	ICOQAU	LOFHAS	PIGTIJ	TOVXAD	ZOGSET
DAQBOM	ICOQAU01	LOFHEW	PIGXOS	TUHVAT	ZUFGEO
DAQBUS	ICUJEX	LOKBES	PINYOD	TUJNUJ	ZUGFAK
DAQCAZ	IDUGAP	LOKBOC	PMPBTZ	TUMPAU	ZUGFEO
DATWEA	IDUGET	LOXKAK	PMTSZD	TUQZEK	ZUXTAP
DAXMIB	IDUGIX	LOXKEO	PODQAD	TUXJIF	COYMAH
DEDBOD	IFAKUY	LUPHEK	PODRAE	TUXJIF01	COYMAH01
DEFPUZ	IFALAF	LUPHEK01	POJZOD	UBIWAD	SOZJUP
DEFSAI	IFALEJ	LURJEP	POLQOW	UCOWUF	SOZJUP01
DEGCIC	IFILAL	LUTLER	PONZIC	UFIJUU	WUFRIE
DEJJIL	IFILAL01	LUTLIV	PORWUO	UGAJOB	WUFROH
DELXOI	IFILAL02	LUTLOB	PORXAV	UJEBIV	AGUMEX
DEMYIE	IFILEP	LUTLUH	POSSEW	UQEPIQ	DUMQEK
DEMYOK	IFILIT	LUYGOB	POSSIA	UQETEQ	HUDWUB
DEMYUQ	IFILOZ	MABTRZ	POYVOP	UTIFIO	HUFCUJ
DEMZAX	IFILUF	MADTUI	PPATDZ	UTOGO	HUFXUE
DEMZEB	IGABAV	MAHXEZ	PSBBTZ	UWETAT	HUMVAP
DEMZIF	IHEWUP	MAKNIX	PSBZQI	UXEXOM	HUNDIG
DEMZOL	IHOLOI	MATSTA	PTDZO	UXEXUS	JUPBUU
DENDAC	IIEQUJ	MATSTA10	PTTRZO	UXEYAZ	JUPCAB
DETGOY	IJINUK	MATSTB	PUGJAC	UXEYED	RUPSUT
DETGUE	IJIPAS	MATSTB10	PUGJEG	UXIMIZ	RUPTAA
DEWRIG	IJPEW	MAXVOZ	PUMQIZ	UXOKAU	RUPTEE
DEZFAP	ILOHOI	MAXVUF	PUNLUH	VAFZOT	SUQMOJ
DIBGEC	ILOHUO	MAYTUC	QAHZIJ	VAJFAN	SUQMUP
DIDRUD	ILOLUR	MEGZOO	QAHZOP	VAMFUM	SUQNAW
DIGHOQ	ILOLUR01	MEITZF	QAMPEB	VANMAZ	SUQNEA
DILNER	IMIDOX	MEITZF10	QAPFUL	VAVHUV	SUQNEI
DILNER10	IMIDUD	MENPAW	QELBOY	VAWFIJ	XUFLIW
DISHAP	IMTZBI	MEPTBZ	QEWRES	VAXPIT	
DIZVOZ	INOGIB	MEPZEM	QEXVIB	VAYMUD	
DIZVUF	IPATZL01	METFOR	QEXVOH	VAYNAK	
DIZWAM	IPATZL10	MIETDZ10	QEXZUR	VAYTIZ	

Table 6.2.2. Hits on the CSD containing the following structure:



In bold, structures showing a close contact on the chalcogen atom. In red, structures where the Nu...S-C(1) angle is $> 160^\circ$, in green where the Nu...S-C(2) angle is $> 160^\circ$. In yellow when the structure display both a contact with an Nu...S-C(1) and Nu...S-C(2) angle $> 160^\circ$.

GUCJUM	EDUGIU	IVIPOT	MPHNTH	REFYIN	VERYUP
--------	--------	--------	--------	--------	--------

GUMFUS	EFOTAX	IVIPUZ	MUDKUS	REFYOT	VIGTAG
HOSSIU	EHUXUA	IWUXAA	MUHTUG	REFYUZ	VILBAV
JOXYAZ	EJADOJ	IXOYOL	MUHVUI	REFZAG	VIPPUH
JOZFAI	EKARIT	IXOYUR	MURFUA	REFZEK	VIPQAO
JOZFEM	EKIHAH	IXUWUT	MURGEL	REFZIO	VIPQES
JOZMAP	EKIHIL	IXUXAA	MUWFOZ	RELJIB	VIPQIW
JOZTUQ	EKIHIP	IZEPAE	MUWMAS	RELMED	VIWNUN
JUCHUN	EKOVEH	IZONEQ	NADCUR	REMZIV	VIZDOX
LOYFEN	EKULIH	IZONIU	NALDAF	RENFEX	VIZLIZ
MOVSOI	EMAPOX	IZONOA	NANWEE	REPVUF	VOACGA
MOVTAV	EMAPUD	IZONUG	NATTAD	REQQAG	VOACGA01
NOSSAS	EMCPTP	IZOPAO	NATTOR	REQQEK	VOACGA10
PUHBAY	ENOFUJ	IZOPES	NECFAD	RETROZ	VOJBON
QOWRIG	EPAHIO	IZOPIW	NECFIL	RETYAR	VOJSES
QOXKUM	EPOQUW	IZOPOC	NEJKAQ	REWGEG	VOKGOS
QOXLAT	EQUSAL	JAJGAD	NIDJUF	REWHEJ	VUGKEN
QOZQII	ETIYIR	JANGIP	NIFNIC	REYZEC	VUGKIR
QUCFUS	ETUHUW	JAPLIV	NIJQEE	REZCAA	VUGVID
RUDHEG	ETUJAE	JAQTUQ	NIJQII	RICGIU	VURHUN
RUGMEO	EVIFAR	JATSIJ	NIQFOJ	RICVOP	VUXGUR
SUFXID	EVIXUC	JAWTOT	NISTHD10	RIFQAZ	VUXHAY
VUBBUS	EWEPAZ	JEJVAY	NIVWEX	RIMYIV	VUZMAE
WOSZUC	EWEPON	JEWTOU	NIVWOH	RIQCAY	WACXOQ
XOSWUA	EWEPUT	JEYKOO	NIYBUS	RIQLOT	WACXOQ01
ABAROL	FAFPAP	JEYKUU	NIYNOY	ROBREI	WAFQOK
ABIFAU	FAHYIZ	JJIBIN	NOBFIW	RODHOI	WAMDUL
ABIRIP	FAJPEL	JILVIM	NOBFOC	ROFFEX	WAMPUV
ACPSTP	FAJPOV	JILWEJ	NOBFUI	ROFFOH	WAMRAD
AFINAE	FAJPUB	JIMFUH	NOBGAP	RONQES	WAMRAD01
AGAYAK	FAJRAJ	JIMQEE	NOJFUN	RONQES01	WAMRAD02
AHOPOC	FAKYUO	JIWJEF	NOJQEK	ROQRAQ	WAQNUY
AHUDUC	FANDAZ	JIYKAD	NOJXUH	ROQREU	WAXKIS
AHUDUC01	FAQCUV	JIYKAD01	NOZWAA	ROTLIU	WAXRUK
AJANAC	FAWKIX01	JOBBAD	NSNPBT10	ROTLIY	WAXSAR
AJANEG	FDTURD	JOBZUX	NULRUJ	ROTLIE	WEKVIU
AJOKUH	FEKPOA	JOCBAG	NUPFEJ	ROTMAR	WETYOK
ALUTUW	FESXOR	JOTWAT	NUPFEJ01	ROTMIV	WEVZOO
AMAJUT	FESXUX	JOYFIM	NUQSID	ROTMIZ	WICWUA
AMAKAA	FESYAE	JOYLUG	NUSQEZ	ROTMOF	WIDRUZ
AMENAJ	FEVXOT	JOYMAN	NUYPII	RUDSOA	WIDSAG
AMOLUK	FEVXUZ	JOYMER	NUYPOO	RUDSUG	WIFWUD
ANTHOA	FEVYAG	JOYMIV	OBIQAT	RUDTAN	WIKCAX
APOVUY	FEXFOE	JOYMIV01	OBIQOH	RUDTER	WIKCAX01
AQUJOM	FEYTAG	JOYMOB	OBUGAU	RUDTIV	WITYUV
ARIKER	FIDHUV	JOYMUH	OBUWIR	RUDTOB	WITZAC
ARIKIV	FIFSIY	JUBTAD	OGESOI	RUGCUT	WIYBUC

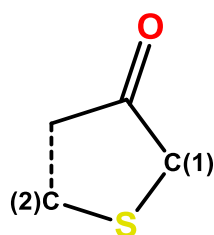
ARUCIA	FIMLOE	JUGTIQ	OGESUO	RUGDAA	WOHLOU
ASINUN	FIMLUK	JUMDEC	OGETAV	RUGDII	WOTKOH
ASIPAV	FIMMAR	JUWNAQ	OHTHPA	RUGDOO	WOTKOH01
ASIPEZ	FIPCAK	KACMUW	OHTHPB	RUKBIJ	WOTKUN
ASIPID	FITXOV	KADJIL	OKUDOO	RUSJIY	WOTKUN01
ASIQAW	FLUTUR10	KAKMOA	OLASID	RUWYUD	WOTLAU
ASUXER	FLUTUR11	KAKMUG	OLASOJ	SACYIF	WOTLAU01
ATEMUH	FMFLTP	KANHAJ	OLASUP	SAKZUB	WOTLEY
AWIWIO	FOBFAD	KAPFIT	OLATAW	SALGUJ	WOTLEY01
AXOZES	FODLAN	KAYKAZ	OPAFOC	SANGAS	WOTLIC
AZAQAT	FODLER	KAZQEH	OPIMUX	SAWDEZ	WOTLIC01
AZEXIO	FODLUH	KAZQEH01	OPINAE	SAZFOQ	WUGKIS
AZEXUA	FODMIW	KAZQIL	OPOBUS	SAZPEQ	XACGAK
AZEYAH	FOLVEI	KAZQIL01	OPOCAZ	SAZPIU	XACGEO
AZOCTA	FOPKEA	KAZQOR	OPHIM	SEBVIF	XACGIS
AZOCTA10	FOSNAC	KEBKIO	OTPLDN	SEDSIG	XACGUE
BASHEK	FOSYAN	KECXEW	OWAYOC	SELDES	XAHLID
BECGOF	FOZQEQ	KEFWOH	OWAYUI	SESDAV	XANQOT
BEHYIX	FOZQIU	KEMDAJ	OWAZIX	SETPUF	XAYBOQ
BEHYOD	FOZQOA	KEMWAB	OXTIND	SEVXUM	XAYBUW
BELGII	FTODEC	KENCOV	OYUPOP	SEWKAI	XAYCAD
BELGII10	FUBYEH	KENROM	OYUPUV	SEWKEM	XAYCEH
BERGAH	FUGYAI	KEPHES	OYUQEG	SEZMIV	XAYRAQ
BETFOV	FUNDEY	KEPHIW	OYUQIK	SICSEE	XEDZIP
BIFVET	FUNDIC	KERYEM	PABDAZ	SIDSEF	XEGDEV
BIGSEQ	FUYBEI	KETXEM	PABDED	SIFLUQ	XELBEW
BIGSIU	FUYBIM	KEVWAM	PABSER	SIHJAU	XELBIA
BIJNEN	GAJRIS	KEYZET	PAGCIL	SIJFID	XELHUR
BIOIND	GAKTAN	KIGZOQ	PASYEP	SIJFOJ	XENDOL
BIOTIN01	GAKTAN01	KIGZUW	PASYIT	SINDIG	XEQYOK
BIOTIN10	GATBIO	KIXHEE	PAYFUR	SINDIG01	XEXRID
BIOTIN12	GATBOU	KOJVAI	PAYGAY	SINDIG02	XEYDOW
BIOTIN13	GAVYEK	KOMNAC	PAYXOF	SINDIG03	XIFDOI
BIOTME10	GEFVAP	KOMNEG	PECMER	SINDIG04	XIHKAC
BIOTME11	GEFVET	KOMNIK	PECNUJ	SINDIG05	XIMXOJ
BIPKES	GEFVIX	KOMNOQ	PECPAR	SINDIG06	XINZAV
BIQYIL	GEVSUG	KOMNUW	PECPEV	SINPOV	XINZAV01
BISYAD	GEGTAN	KOVYUP	PECPIZ	SIWHOW	XIPJEO
BIYVOV	GEGTER	KOWLOZ	PEFCEL	SODSUC	XIWTIJ
BODPOZ	GEPVIG	KOWLUF	PEFDOW	SOJKAD	XIWTOP
BONLOH	GEPVOM	KOWMUG	PEGZUY	SOJROY	XIXGET
BONMUO	GEQZOT	KUBHEU	PEHBEM	SOKRAM	XOHPUF
BONVAB	GESWEI	KUBYUD	PEHBIQ	SOKREQ	XOHQAM
BONVAB01	GEVFOC	KUBZAK	PEHMOF	SONMEP	XOHQEQ
BONVEF	GEXSIL	KUXNOG	PEHTAY	SOQPAP	XOLLUG
BONVIJ	GEXTAE	KUYVIJ	PEQJAW	SOYWEK	XORLEX

BOVYIU	GEYMLJ	KUYVOP	PETQIP	SUBWAN	XOVREH
BOVYOA	GEYMOP	KUYVUV	PHARKA	SUFDII	XOYZIV
BOZPEL	GEYMUU	KUYWEG	PHXTHL	SUFWIB	XUHZIJ
BRYNOL10	GEYNEG	KUZXEI	PIDLIY	SUGCOM	YALBET
BUTHON	GEYNIK	KUZXEI01	PIDLIY01	SUGCUS	YASBAV
BUTHUT	GEYNOQ	KUZXIM	PIDL0D	SUMDAH	YAWVOH
BUZZAZ	GEYNUW	LABJUT	PIFZIQ	SUSWUA	YAZRAV
CACFAQ	GIPQED	LANDIO	PIHCOB	SUVTUZ	YECCIS
CACFEU	GIWPAG	LAPTUU	PIHHIA	TABOCT	YECCOY
CACFIY	GOBFUB	LAWCIW	PIHKEZ	TABOCT01	YECCUE
CACFOE	GONCAN	LAXFAS	PIJDAO	TADWON	YECDAL
CACGAR	GUCYIM	LAXFEW	PIJQOP	TADWUT	YECDEP
CACGEV	GUDMAT	LAXFIA	PIJQUV	TAJFIV	YECDIT
CACGIX	GUFJUM	LEBSUG	PIKWIS	TAQMAB	YEGRIO
CACGIZ	GUFKAT	LEBSUI	PIKWOY	TASSOV	YEGZEQ
CAZDEN	GUMFUQ	LEBTAP	PINYOD	TASSUB	YEGZIU
CAZFEP	GUMTEO	LELYUW	PIRFAZ	TBNUPH	YEGZOA
CAZYOS	GUNYIY	LEMKIA	PIRFED	TEHWAF	YEHHUO
CBIOBT	GUZDIP	LEMKOG	PIVHUX	TEJTEI	YENVET
CESXAZ	HARKUJ	LEMKUM	PIVPFE	TEKNEC	YERDAA
CEVCIR	HAYZUD	LEMLAT	PIYLUE	TELPUY	YERDEE
CEVHUH	HEBRUC	LEMLEX	POCMOM	TEPQUD	YERDOO
CICXAN	HEBSAJ	LEMLIB	PODQOO	TETQOZ	YERDUU
CIGSOD	HEQNUN	LEMLOH	PODQUU	TEVBUR	YERVOJ
CIHGEG	HEQZAG	LEMLUN	POFCIZ	TEVZUP	YETJAI
CIHGIK	HEQZAG01	LEMAU	POJHAX	TEWREV	YETJEM
CIHQOQ	HERSIJ	LEPPEB	POJHEB	TEZBIJ	YEXNAT
CILYUT	HETZCO	LERSEJ	POJHIF	THPHSE	YIDNAA
CIPNAS	HEWSIO	LESQUW	POJNOR	THTHDO	YIHBAS
CIPRUR	HEYNUV	LICYEE	POKDOK	TICQOO	YIHFED
CIVGET	HIDSOF	LICYII	POKNUY	TIKKUW	YIMXUP
CIVGIX	HIDWID	LICYOO	POLVUI	TIPYEY	YIMZIF
CIXYOA	HIDWOJ	LIMQON	POQYUS	TIYDEN	YIZBOB
CIYYIU	HIDWUP	LINVIP	POQZOL	TOCSIN	YIZBOB01
CLCNTP	HIDXAW	LIRWEQ	PORBOQ	TOGGUR	YIZROQ
CODGAD	HIDXEA	LIRWIU	PORPIW	TOKDAA	YOHZIE
COJHUG	HIDXIE	LITCAT	PORPOC	TOKDEE	YOJKEO
COMPEB	HIFNIT	LITCAT01	PORQAP	TOLFIJ	YOJKOY
COSWUD	HIGMIT	LIZJUB	PORQET	TOMLIS	YOJLUF
CUKQAB	HILQEA	LOJKUQ	PORQOD	TOVLUL	YOJPET
CUTRAM	HIMQUS	LOKJAZ	POVHUF	TPIVPF	YOKXAZ
CUTRAM01	HIPVAD	LOKJED	PUDKOO	TPTHFE	YOKXIH
CUYLOX	HITHEZ	LOMPAF	PUDMIM	TPTHFE10	YOMVUS
DABNUS	HIVFOJ	LOMPEJ	PUJVIZ	TRPHGB	YOMWON
DABPAA	HIZSOB	LOVLOX	PUQCIN	TUBVIV	YOPXOR
DABWIO	HIZSUH	LOZDOT	PUQCOT	TUGKUB	YOQGIW

DACZAJ	HIZTAO	LOZDUZ	PUQCUZ	TUJGOU	YOQGOC
DACZAJ01	HIZTES	LOZDUZ01	PUQVAA	TUJGUA	YOQGUI
DACZEN	HMBTQO	LUFLIJ	PUQWAB	TUJGUA01	YOWJAX
DACZEN01	HOCYSL	LUHLEF	PUXVEL	TUJJUF	YOYVAL
DADLOJ	HOCYSL01	LUKGII	QADBIH	TUKFOV	YUGVOM
DADLOJ10	HOCYSL02	LUKGOO	QADKUB	TUPMUM	YURPIM
DAGRAF	HODNAS	LUKGUU	QAJMEU	TUPMUM01	YURQAF
DAGSUA	HOFHUI	LUKHAB	QAKBAG	TUQYAH	YUZJEI
DAKLIN	HOFLOG	LUKHEF	QAPNON	TURIDO	ZAJGAS
DAMKAG	HOKCAL	LUKHJ	QAZRUH	TUXMUU	ZAMFUR
DATHEO	HOKZOZ	LUKHOP	QECPEV	TUZQIO	ZAWLOB
DAWTIE	HOLNII	LUKHUV	QEQQEB	TUZQOU	ZAWLUH
DECKOO	HOLXEL	LUVSEB	QEQQIF	TUZWUG	ZEJLIJ
DEFMIK	HOLXEL01	LUVSIF	QEGXAD	UCAJIR	ZEJVIT
DENWEY	HOPYAN	LUVSOL	QEHQIG	UCIXAG	ZEJVOZ
DENWEY01	HOQDID	LUVSUR	QEPDUN	UCIXAG01	ZEJVUF
DESMIY	HOQLAD	MACQAK	QERBIB	UCIXIO	ZEJWAM
DESNOE	HORMEG	MAGKAJ	QESSAL	UFENUQ	ZICZUJ
DESYEI	HORMIK	MAMVUT	QETWER	UFEWAF	ZIDBEW
DEVMOG	HORMOQ	MANTIF	QETWIV	UFUNUH	ZIDBEW01
DEXXAH	HORXUI	MAYROT	QETWOB	UHJOK	ZIFPEL
DEXXEL	HOVKIM	MBTHFX	QEVFOP	UMAHAT	ZIKXIA
DILBUX	HOWCIH	MCBIOT10	QEZJOU	UROKUJ	ZISYEH
DILNUH	HUHCAP	MEBMUE	QEZJOU01	UROSEB	ZIVMAS
DITNAV	HUHCET	MEDBIG	QEZJOU02	UVEQES	ZOKVAZ
DIYXOZ	HULTUD	MEDBOM	QILWEP	UVIBOR	ZOMQOJ
DIZRUZ	HUTDAB	MEFPIY	QISZUQ	UVIWEC	ZORRON
DMTHIO10	HUWXUU	MEGZEG	QITBAZ	UXOZEN	ZOXNOR
DMTTDO	HUYVIH	MEJZUX	QIWGAE	UXUBIZ	ZOYQUZ
DOGWAX	HXITCA	MENPON	QOBSAE	UXUVOA	ZUBGAG
DOGXAY	ICECEB	MEQDUH	QOGVEP	UYOKOK	ZUCDOS
DOJDAH	IDAKUT	MERBIV	QOGZUI	UZIQIE	ZUCDUY
DOPJOH	IFIVAW	MERBOB	QOVCOV	VACGIR	ZUFWAY
DOPQII	IHOJEW	MERJUO	QOWQOI	VADGIT	ZUFWEC
DOSMIK	IHOJIA	METHPH	QOXTOM	VAGQIE	ZUPTOV
DOSMOQ	IJUHUS	METHPH10	QOYTED	VALLOK	ZUQKED
DOTDIZ	IJUVAK	MIMYOZ	QUBTEO	VALLUQ	ZUSWIT
DOYJUW	IJUVEO	MIMYOZ01	QUBVEQ	VASTAN	ZUSWIT01
DUQBIC	IKODER	MINJOL	QUBWAN	VASWAQ	ZUWLIO
DUQBOI	IKODER01	MINJUR	QUCWOB	VATFOO	ZUWLOU
DUSJEH	IKODIV	MINKUS	QUCWUH	VATLOT	IJADEF
EABMEZ	IKODIV01	MINTSD	QUCXES	VATLUZ	PUFNEM
EADPEE	ILUTEO	MIQSOU	QUCXIW	VATMAG	WUNDAN
EBTHTP	IMSTXP10	MIQSUA	QUCXOC	VATMIO	HUFQIL
ECITAO	IQALAP	MIRHEC	QUCXUI	VATMOU	KUSBAE
EDAGIA01	IQALET	MIRHIG	QUTRAY	VAVZAU	RUSJUN

EDALAY	IQUTUK	MIWWIY	QUTREC	VAVZEY	SUMSOL
EDIMUB	IRIQAB	MIWWOE	RAPJUO	VAVZIC	VUNSAB
EDIQAL	IRIQEF	MIWYAS	RARDEV	VAVZOI	VUNSEF
EDITES	IRIQIJ	MIXTPC	RAXJEG	VAVZUO	ZURYUJ
EDIVEU	IRIQOP	MORKIN	RAYKAF	VAWBAX	ZURZAQ
EDIYIB	IRUYAV	MORMUB	RAYNAG	VEDJET	ZUVSOB
EDUGEQ	IVIPIN	MORNAI	REFXAC	VEQKUA	ZUVSUH

Table 6.2.3. Hits on the CSD containing the following structure:

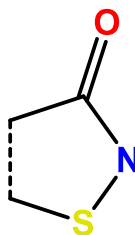


In bold, structures showing a close contact on the chalcogen atom. In red, structures where the Nu...S-C(1) angle is > 160°, in green where the Nu...S-C(2) angle is > 160°. In yellow when the structure display both a contact with an Nu...S-C(1) and Nu...S-C(2) angle > 160°.

JUCHUN	DMTHIO10	JIMQEE	LEMAU	QUBWAN	TUJGOU
QOWRIG	DOJDAH	JOYLUG	LUHLEF	RAXJEG	TUJGUA
RUGMEO	EABMEZ	JOYMAN	MACQAK	REPVUF	TUJGUA01
VUBBUS	ECITAO	JOYMER	MEDBIG	RIMYIV	TUXMUU
AJANAC	EKOVEH	JOYMIV	MEDBOM	ROBREI	VAGQIE
AJANEG	EVIFAR	JOYMIV01	MERBIV	RUGDII	VOACGA
ANTHOA	EWEPAZ	JOYMOB	MERBOB	RUGDOO	VOACGA01
AXOZES	EWEPON	JOYMUH	MINJOL	RUKBIJ	VOACGA10
AZAQAT	EWEPUT	KANHAJ	MINJUR	SEBVIF	WAFQOK
BISYAD	FAPPAF	KEBKIO	MINKUS	SIDSEF	WUGKIS
BODPOZ	FUGYAI	KENCOV	NIFNIC	SINDIG	XAHLID
BUZZAZ	GEQZOT	KEVWAM	NUYPII	SINDIG01	XIPJEO
CESXAZ	GUFJUM	KIGZOQ	NUYPOO	SINDIG02	YAZRAV
COMPEB	GUFKAT	KIGZUW	OBUGAU	SINDIG03	YEGZEQ
DACZAJ	HARKUJ	KOVYUP	OXTIND	SINDIG04	YEGZIU
DACZAJ01	HERSIJ	KUYVIJ	PECNUJ	SINDIG05	YIMXUP
DACZEN	HEYNUV	LEBSUG	PECPAR	SINDIG06	YOKXAZ
DACZEN01	HIZSOB	LELYUW	PECPEV	SIWHOW	YOKXIH
DADLOJ	HIZSUH	LEMKIA	PECPIZ	SUFDII	YUGVOM
DADLOJ10	HIZTAO	LEMKOG	PEHBEM	TAJFIV	ZAMFUR
DAGRAF	HIZTES	LEMKUM	PEHBIQ	TELPUY	ZAWLOB
DAGSUA	HOVKIM	LEMLAT	POKDOK	TEZBIJ	ZAWLUH
DENWEY	HOWCIH	LEMLEX	QEHQIG	THTHDO	ZIVMAS
DENWEY01	HUWXUU	LEMLIB	QOVCOV	TIKKUW	PUFNEM
DEXXAH	JANGIP	LEMLOH	QUBTEO	TOKDAA	KUSBAE

DEXXEL	JAWTOT	LEMLUN	QUBVEQ	TOKDEE	
--------	--------	--------	--------	---------------	--

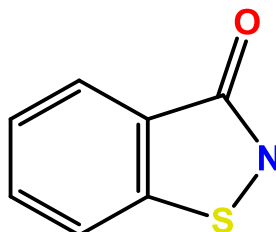
Table 6.2.4. Hits on the CSD containing the following structure:



In bold, structures showing a close contact on the chalcogen atom. In red, structures where the Nu...S-N angle is $> 160^\circ$, in green where the Nu...S-C angle is $> 160^\circ$. In yellow when the structure display both a contact with an Nu...S-N and Nu...S-C angle $> 160^\circ$.

ACIHEA	EMOBAK	KOGYAH	NAJBAB	QOGMOP	TIGXAJ
AXASIB	EMOBEO	KOGYEL	NAJBEB	QOGMUV	TODVAL
AXASOH	EXIJUR	LOCSAA	NAJBEO1	QUFRAM	UCOWUF
AYOREM	FUCFIS	LOCSII	NOKVAK	RAJGER	WIPJOW
AYORIQ	GIYYUJ	LOCSOO	NUNHIN	SENROT	WIPXIE
BIPXEG	GIYZAQ	MIJWAE	OBUZAO	SOKZUO	WIPXOK
BZITHO	HUKGAV	MIJWEI	OCAVUL	SOLBAX	XADPUO
BZITHO01	ICOQAU	MIXQAL	ODILET	SOLBEB	XADQAV
CBTHAZ10	ICOQAU01	MIXQEP	OHALAM	SOLBIF	XIFRIO
CIKCIJ	IGABAV	MIXQIT	OPABAJ	SOLKAG	YINC UW
CIKCOP	IHEWUP	MUQKAK	PIGTIJ	TECVAZ	YINC UW01
COVPEK	JAYWIQ	MUQKAK01	PODRAE	TEYZUS	ZARDED
COWLEH	KEGKOY	MUSPAS	PONZIC	TEZZOP	ZESJOZ
DUQNIO	KOGXOU	MUSPEW	QEWRES	TIBXAF	ZIBVIP

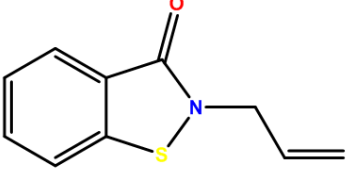
Table 6.2.5. Hits on the CSD containing the following structure:

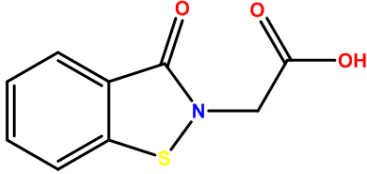


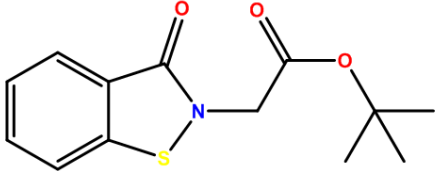
In bold, structures showing a close contact on the chalcogen atom. In red, structures where the Nu...S-N angle is $> 160^\circ$, in green where the Nu...S-C angle is $> 160^\circ$. In yellow when the structure display both a contact with an Nu...S-N and Nu...S-C angle $> 160^\circ$.

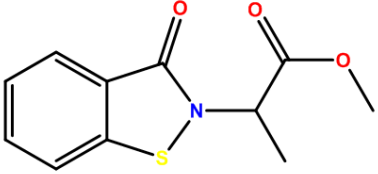
AYOREM	DUQNIO	MIJWAE	MUSPEW	QEWRES	WIPXOK
AYORIQ	EXIJUR	MIJWEI	NAJBAB	RAJGER	ZARDED
BIPXEG	ICOQAU	MIXQAL	NAJBEB	SOLKAG	ZESJOZ

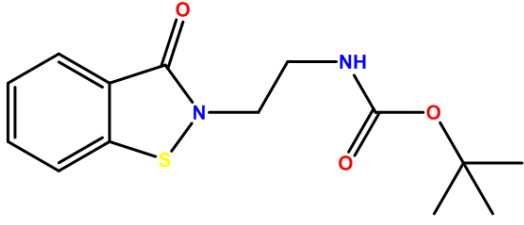
BZITHO	ICOQAU01	MIXQEP	NAJBEF01	TECVAZ	ZIBVIP
BZITHO01	KEGKOY	MIXQIT	OBUZAO	TEZZOP	
CBTHAZ10	LOCSAA	MUQKAK	OCAVUL	TIBXAF	
COVPEK	LOCSII	MUQKAK01	PODRAE	TODVAL	
COWLEH	LOCSOO	MUSPAS	PONZIC	WIPXIE	

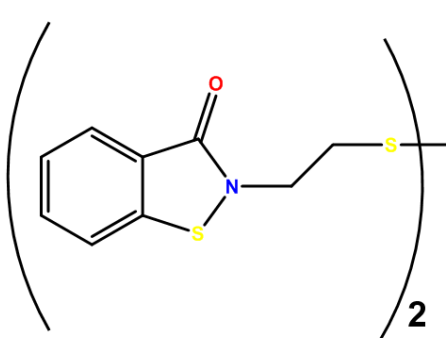
1	Formula: C ₁₀ H ₉ NOS Formula Weight: 191,24 Name: 2-Allylbenzo[d]isothiazol-3(2H)-one	<input checked="" type="checkbox"/> Slow evaporation <input type="checkbox"/> Vapor diffusion <input type="checkbox"/> Solvent layer <input type="checkbox"/> Other		
		Solvent(s)/Other agents: diisopropylether.....		Temperature: 100 K
<input type="checkbox"/> Twinned		a: 11.910 α: 90 b: 6.225 β: 96.76 c: 12.260 γ: 90 Vol: 902.634	R ₁ : 0,0446 System: Monoclinic Space Group: P2 ₁ /c	
<input checked="" type="checkbox"/> IR <input type="checkbox"/> UV		<input checked="" type="checkbox"/> ¹ H-NMR <input checked="" type="checkbox"/> ¹³ C-NMR	<input type="checkbox"/> Other	
Synthesis: A solution of benzisothiazol-3(2H)-one (15.4 g, 100 mmol), 3-bromo-prop-1-ene (100 mmol) in DMF (100 mL) was added dropwise at 0 °C to a slurry of NaH (60% dispersion in mineral oil, 4.8 g, 120 mmol), previously washed in hexanes (3x20 mL) at 0 °C to remove the mineral oil, in DMF (300 mL). The reaction mixture was stirred at the same temperature for 15 min and heated at 80 °C for 1 h. The mixture was poured into a cold saturated NH ₄ Cl solution (200 mL) and extracted with AcOEt (3x100 mL). The combined organics were dried over anhydrous Na ₂ SO ₄ , filtered and evaporated to dryness under reduced pressure to give a residue that was purified by flash chromatography.				
Characterization: ¹ H-NMR (400 MHz, CDCl ₃) δ 8.03 (d, J = 8.2 Hz, 1H), 7.59 (m, 1H), 7.54 (d, J = 8.0 Hz, 1H), 7.39 (dd, J = 7.6, 7.6 Hz, 1H), 5.93 (ddt, J = 17.8, 12.0, 7.4 Hz, 1H), 5.33 (ddt, J = 17.8, 1.1, 1.0 Hz, 1H), 5.30 (ddt, J = 12.0, 1.3, 1.1 Hz, 1H), 4.56 (ddd, J = 7.4, 1.3, 1.0 Hz, 2H). ¹³ C-NMR (100.6 MHz, CDCl ₃) δ 165.3, 140.6, 132.6, 132.0, 126.9, 125.7, 124.9, 120.6, 119.5, 46.4. IR (KBr, ν/cm ⁻¹) 3447, 2918, 1644, 1447, 1334, 1314, 1284, 1240, 1192, 990, 932, 785, 740, 673		Z	4	
		ρ _{calc} / g/cm ³	1.407	
		μ/mm ⁻¹	0.312	
		F(000)	400	
		Radiation	λ = 0.6199	
		Reflections Collected	8468	
		Goodness-of-fit on F ²	0.906	
		Final R indexes [I > 2σ (I)]	R ₁ = 0.1001, wR ₂ = 0.1608	
		Final R indexes (all data)	R ₁ = 0.0446, wR ₂ = 0.1226	

2	Formula: C ₉ H ₇ NO ₃ S Formula Weight: 209.22 Name: methyl 2-[3-oxobenzisothiazol-2(3H)-yl]acetate	<input checked="" type="checkbox"/> Slow evaporation <input type="checkbox"/> Vapor diffusion <input type="checkbox"/> Solvent layer <input type="checkbox"/> Other
		Solvent(s)/Other agents: isopropylether/AcOEt1:1..... <input type="checkbox"/> Twinned Temperature: 100 K
a: 4.778 α: 90 R ₁ : 0.0446 b: 11.295 β: 90 System: Orthorhombic c: 16.149 γ: 90 Space Group: P2 ₁ /c Vol: 871.521		<input checked="" type="checkbox"/> IR <input checked="" type="checkbox"/> ¹ H-NMR <input type="checkbox"/> Other <input type="checkbox"/> UV <input checked="" type="checkbox"/> ¹³ C-NMR
<u>Synthesis:</u> A solution of benzisothiazol-3(2H)-one (15.4 g, 100 mmol), bromomethylacetate (110 mmol) in DMF (100 mL) was added dropwise at 0 °C to a slurry of NaH (60% dispersion in mineral oil, 4.8 g, 120 mmol), previously washed in hexanes (3x20 mL) at 0 °C to remove the mineral oil, in DMF (300 mL). The reaction mixture was stirred at the same temperature for 15 min and heated at 80 °C for 1 h. The mixture was poured into a cold saturated NH ₄ Cl solution (200 mL) and extracted with AcOEt (3x100 mL). The combined organics were dried over anhydrous Na ₂ SO ₄ , filtered and evaporated to dryness under reduced pressure to give a residue that was purified by flash chromatography.		
<u>Characterization:</u>		
¹ H-NMR (400 MHz, CDCl ₃) δ 8.03 (d, J = 7.8 Hz, 1H), 8.02 (d, J = 7.8 Hz, 1H), 7.61 (ddd, J = 8.1, 7.1, 1.1, Hz, 1H), 7.53 (d, J = 8.1 Hz, 1H), 7.38 (ddd, J = 7.8, 7.1, 1.0 Hz, 1H), 4.61 (s, 2H), 3.76 (s, 3H). ¹³ C-NMR (100.6 MHz, CDCl ₃) δ 168.1, 165.7, 140.8, 132.3, 126.9, 125.6, 123.4, 120.4, 52.6, 44.5. IR (KBr, ν/cm ⁻¹) 3383, 2954, 2923, 1745, 1649, 1597, 1445, 1209, 739.	Z	4
	ρ _{calc} / g/cm ³	1.595
	μ/mm ⁻¹	0.329
	F(000)	432
	Radiation	λ = 0.6199
	Reflections Collected	12745
	Goodness-of-fit on F ²	1.110
	Final R indexes [I > 2σ (I)]	R ₁ = 0.0356, wR ₂ = 0.1327
Final R indexes (all data)	R ₁ = 0.0355, wR ₂ = 0.1326	

3	Formula: C ₁₃ H ₁₅ NO ₃ S Formula Weight: 265.32 Name: tert-butyl 2-(3-oxobenzisothiazol-2(3H)-yl)acetate	<input checked="" type="checkbox"/> Slow evaporation <input type="checkbox"/> Vapor diffusion <input type="checkbox"/> Solvent layer <input type="checkbox"/> Other																		
		Solvent(s)/Other agents: EtOH..... <input type="checkbox"/> Twinned Temperature: 100 K																		
		<table border="0" style="width: 100%;"> <tr> <td>a: 18.943</td> <td>α: 90</td> <td>R₁:</td> <td>0.0283</td> </tr> <tr> <td>b: 12.183</td> <td>β: 90</td> <td>System:</td> <td>Orthorhombic</td> </tr> <tr> <td>c: 22.723</td> <td>γ: 90</td> <td>Space Group:</td> <td>Pbca</td> </tr> <tr> <td>Vol: 5244.18</td> <td></td> <td></td> <td></td> </tr> </table>	a: 18.943	α: 90	R ₁ :	0.0283	b: 12.183	β: 90	System:	Orthorhombic	c: 22.723	γ: 90	Space Group:	Pbca	Vol: 5244.18					
a: 18.943	α: 90	R ₁ :	0.0283																	
b: 12.183	β: 90	System:	Orthorhombic																	
c: 22.723	γ: 90	Space Group:	Pbca																	
Vol: 5244.18																				
		<input checked="" type="checkbox"/> IR <input checked="" type="checkbox"/> ¹ H-NMR <input type="checkbox"/> Other <input type="checkbox"/> UV <input checked="" type="checkbox"/> ¹³ C-NMR 																		
<u>Synthesis:</u> A solution of benzisothiazol-3(2H)-one (15.4 g, 100 mmol), bromomethyl-tertbutylacetate (110 mmol) in DMF (100 mL) was added dropwise at 0 °C to a slurry of NaH (60% dispersion in mineral oil, 4.8 g, 120 mmol), previously washed in hexanes (3x20 mL) at 0 °C to remove the mineral oil, in DMF (300 mL). The reaction mixture was stirred at the same temperature for 15 min and heated at 80 °C for 1 h. The mixture was poured into a cold saturated NH ₄ Cl solution (200 mL) and extracted with AcOEt (3x100 mL). The combined organics were dried over anhydrous Na ₂ SO ₄ , filtered and evaporated to dryness under reduced pressure to give a residue that was purified by flash chromatography.																				
<u>Characterization:</u> ¹ H-NMR (400 MHz, CDCl ₃) δ 7.98 (d, J = 7.9 Hz, 1H), 7.54 (d, J = 8.0, 7.9, 1.1 Hz, 1H), 7.54 (d, J = 8.0 Hz, 1H), 7.49 (d, J = 7.9 Hz, 1H), 7.32 (ddd, J = 8.0, 7.9, 1.1 Hz, 1H), 4.46 (s, 2H), 1.43 (s, 9H). ¹³ C-NMR (100.6 MHz, CDCl ₃) δ 166.7, 165.7, 140.9, 132.1, 126.8, 125.4, 123.5, 120.3, 82.8, 45.3, 28.0. IR (KBr, ν/cm ⁻¹) 3368, 2975, 2871, 1739, 1660, 1626, 1444, 1352, 1227, 1149, 1088, 1048, 739.		<table border="1" style="width: 100%; border-collapse: collapse;"> <tr> <td style="text-align: center;">Z</td> <td style="text-align: center;">16</td> </tr> <tr> <td style="text-align: center;">ρ_{calc} / g/cm³</td> <td style="text-align: center;">1.060</td> </tr> <tr> <td style="text-align: center;">μ/mm⁻¹</td> <td style="text-align: center;">0.234</td> </tr> <tr> <td style="text-align: center;">F(000)</td> <td style="text-align: center;">2240</td> </tr> <tr> <td style="text-align: center;">Radiation</td> <td style="text-align: center;">λ = 0.6199</td> </tr> <tr> <td style="text-align: center;">Reflections Collected</td> <td style="text-align: center;">46132</td> </tr> <tr> <td style="text-align: center;">Goodness-of-fit on F²</td> <td style="text-align: center;">0.906</td> </tr> <tr> <td style="text-align: center;">Final R indexes [I > 2σ (I)]</td> <td style="text-align: center;">R₁ = 0.0273, wR₂ = 0.0759</td> </tr> <tr> <td style="text-align: center;">Final R indexes (all data)</td> <td style="text-align: center;">R₁ = 0.0283, wR₂ = 0.0765</td> </tr> </table>	Z	16	ρ_{calc} / g/cm³	1.060	μ/mm⁻¹	0.234	F(000)	2240	Radiation	λ = 0.6199	Reflections Collected	46132	Goodness-of-fit on F²	0.906	Final R indexes [I > 2σ (I)]	R ₁ = 0.0273, wR ₂ = 0.0759	Final R indexes (all data)	R ₁ = 0.0283, wR ₂ = 0.0765
Z	16																			
ρ_{calc} / g/cm³	1.060																			
μ/mm⁻¹	0.234																			
F(000)	2240																			
Radiation	λ = 0.6199																			
Reflections Collected	46132																			
Goodness-of-fit on F²	0.906																			
Final R indexes [I > 2σ (I)]	R ₁ = 0.0273, wR ₂ = 0.0759																			
Final R indexes (all data)	R ₁ = 0.0283, wR ₂ = 0.0765																			

4	Formula: C ₁₁ H ₁₁ NO ₃ S Formula Weight: 237.27 Name: methyl 2-[3-oxobenzisothiazol-2(3H)-yl]propanoate	<input checked="" type="checkbox"/> Slow evaporation <input type="checkbox"/> Vapor diffusion <input type="checkbox"/> Solvent layer <input type="checkbox"/> Other																		
		Solvent(s)/Other agents: diisopropylether..... <input type="checkbox"/> Twinned Temperature: 100 K																		
<p><u>Synthesis:</u></p> <p>A solution of benzisothiazol-3(2H)-one (15.4 g, 100 mmol), methyl 2-bromopropanoate (110 mmol) in DMF (100 mL) was added dropwise at 0 °C to a slurry of NaH (60% dispersion in mineral oil, 4.8 g, 120 mmol), previously washed in hexanes (3x20 mL) at 0 °C to remove the mineral oil, in DMF (300 mL). The reaction mixture was stirred at the same temperature for 15 min and heated at 80 °C for 1 h. The mixture was poured into a cold saturated NH₄Cl solution (200 mL) and extracted with AcOEt (3x100 mL). The combined organics were dried over anhydrous Na₂SO₄, filtered and evaporated to dryness under reduced pressure to give a residue that was purified by flash chromatography.</p>		<table border="1"> <tr> <td>a: 10.545</td> <td>α: 90</td> <td>R₁:</td> <td>0.0438</td> </tr> <tr> <td>b: 11.174</td> <td>β: 91.51</td> <td>System:</td> <td>Monoclinic</td> </tr> <tr> <td>c: 18.402</td> <td>γ: 90</td> <td>Space Group:</td> <td>P2₁/n</td> </tr> <tr> <td>Vol: 2167.6</td> <td></td> <td></td> <td></td> </tr> </table>	a: 10.545	α: 90	R ₁ :	0.0438	b: 11.174	β: 91.51	System:	Monoclinic	c: 18.402	γ: 90	Space Group:	P2 ₁ /n	Vol: 2167.6					
a: 10.545	α: 90	R ₁ :	0.0438																	
b: 11.174	β: 91.51	System:	Monoclinic																	
c: 18.402	γ: 90	Space Group:	P2 ₁ /n																	
Vol: 2167.6																				
<p><u>Characterization:</u></p> <p>¹H-NMR (400 MHz, CDCl₃) δ 8.0 (d, J = 7.6 Hz, 1H), 7.57 (ddd, J = 8.1, 7.9, 1.0, 1H), 7.53 (d, J = 7.9 Hz, 1H), 7.35 (ddd, J = 8.1, 7.6, 1.0 Hz, 1H), 5.42 (q, J = 7.3 Hz, 1H), 3.71 (s, 3H), 1.64 (s, 3H).</p> <p>¹³C-NMR (100.6 MHz, CDCl₃) δ 171.0, 165.6, 140.9, 132.1, 126.7, 125.5, 120.4, 52.7, 51.2, 17.1.</p> <p>IR (KBr, ν/cm⁻¹) 3376, 2972, 2918, 1735, 1504, 1375, 1322, 1258, 1231, 1088, 1047, 739, 575.</p>		<table border="1"> <tr> <td>Z</td> <td>8</td> </tr> <tr> <td>ρ_{calc} / g/cm³</td> <td>1.454</td> </tr> <tr> <td>μ/mm⁻¹</td> <td>0.273</td> </tr> <tr> <td>F(000)</td> <td>992</td> </tr> <tr> <td>Radiation</td> <td>λ = 0.6199</td> </tr> <tr> <td>Reflections Collected</td> <td>28324</td> </tr> <tr> <td>Goodness-of-fit on F²</td> <td>1.048</td> </tr> <tr> <td>Final R indexes [I > 2σ (I)]</td> <td>R₁ = 0.0482, wR₂ = 0.1279</td> </tr> <tr> <td>Final R indexes (all data)</td> <td>R₁ = 0.0438, wR₂ = 0.1229</td> </tr> </table>	Z	8	ρ _{calc} / g/cm ³	1.454	μ/mm ⁻¹	0.273	F(000)	992	Radiation	λ = 0.6199	Reflections Collected	28324	Goodness-of-fit on F ²	1.048	Final R indexes [I > 2σ (I)]	R ₁ = 0.0482, wR ₂ = 0.1279	Final R indexes (all data)	R ₁ = 0.0438, wR ₂ = 0.1229
Z	8																			
ρ _{calc} / g/cm ³	1.454																			
μ/mm ⁻¹	0.273																			
F(000)	992																			
Radiation	λ = 0.6199																			
Reflections Collected	28324																			
Goodness-of-fit on F ²	1.048																			
Final R indexes [I > 2σ (I)]	R ₁ = 0.0482, wR ₂ = 0.1279																			
Final R indexes (all data)	R ₁ = 0.0438, wR ₂ = 0.1229																			
		<input checked="" type="checkbox"/> IR <input checked="" type="checkbox"/> ¹ H-NMR <input type="checkbox"/> Other <input type="checkbox"/> UV <input checked="" type="checkbox"/> ¹³ C-NMR 																		

5	Formula: C ₁₄ H ₁₈ N ₂ O ₃ S Formula Weight: 294.36 Name: methyl 2-(((2-((tert-butoxycarbonyl)amino)ethyl)amino)thio)benzoate	<input checked="" type="checkbox"/> Slow evaporation <input type="checkbox"/> Vapor diffusion <input type="checkbox"/> Solvent layer <input type="checkbox"/> Other																		
		Solvent(s)/Other agents: <input type="checkbox"/> Twinned Temperature: 100 K																		
<p><u>Synthesis:</u></p> <p>To a solution of dimethyl 2,2'-disulfanediyldibenzoate (20.0 g, 60.0 mmol) in CCl₄ (100 mL), neat Br₂ (10.3 g, 66.0 mmol) in CCl₄ (40 mL) was added dropwise in 30 min. The brownish slurry was stirred at RT for 30 min and added dropwise to a solution of tert-butyl (2-aminoethyl)carbamate (72.0 mmol) and Et₃N (72.0 mmol) in CCl₄ (40 mL). The reaction mixture was stirred 1 h at RT and heated at reflux for the suitable amount of time, poured into H₂O (300 mL) and extracted in CHCl₃ (3x100 mL). The combined organic phases were dried over anhydrous Na₂SO₄, filtered and evaporated to dryness under reduced pressure to give a residue that was purified by flash chromatography.</p>		<table border="1" style="width: 100%; border-collapse: collapse;"> <tr> <td>a: 11.840 α: 90</td> <td>R₁: 0.0464</td> </tr> <tr> <td>b: 8.913 β: 104.27</td> <td>System: Monoclinic</td> </tr> <tr> <td>c: 14.023 γ: 90</td> <td>Space Group: P2₁/n</td> </tr> <tr> <td>Vol: 1434.2</td> <td></td> </tr> </table>	a: 11.840 α: 90	R ₁ : 0.0464	b: 8.913 β: 104.27	System: Monoclinic	c: 14.023 γ: 90	Space Group: P2 ₁ /n	Vol: 1434.2											
a: 11.840 α: 90	R ₁ : 0.0464																			
b: 8.913 β: 104.27	System: Monoclinic																			
c: 14.023 γ: 90	Space Group: P2 ₁ /n																			
Vol: 1434.2																				
<p><u>Characterization:</u></p> <p>¹H-NMR (400 MHz, CDCl₃) δ 7.97 (d, J = 8.1 Hz, 1H), 7.87 (d, J = 7.8, 1H), 7.68 (dd, J = 8.1, 7.3 Hz, 1H), 7.43 (dd, J = 7.8, 7.3 Hz, 1H), 6.98 (t, J = 5.0 Hz, 1H), 3.83 (t, J = 5.9 Hz, 2H), 3.23 (dt, J = 5.9, 5.0 Hz, 2H), 1.35 (s, 9H).</p> <p>¹³C-NMR (100.6 MHz, CDCl₃) δ 164.9, 156.1, 141.3, 132.1, 126.0, 125.8, 124.5, 122.2, 78.3, 43.6, 31.1, 28.7.</p> <p>IR (KBr, ν/cm⁻¹) 3327, 2976, 2930, 1697, 1646, 1599, 1519, 1447, 1391, 1365, 1340, 1278, 1249, 1168, 740.</p>		<table border="1" style="width: 100%; border-collapse: collapse;"> <tr> <td style="text-align: center;">Z</td> <td style="text-align: center;">4</td> </tr> <tr> <td style="text-align: center;">ρ_{calc} / g/cm³</td> <td style="text-align: center;">1.363</td> </tr> <tr> <td style="text-align: center;">μ/mm⁻¹</td> <td style="text-align: center;">0.464</td> </tr> <tr> <td style="text-align: center;">F(000)</td> <td style="text-align: center;">624</td> </tr> <tr> <td style="text-align: center;">Radiation</td> <td style="text-align: center;">λ = 0.6199</td> </tr> <tr> <td style="text-align: center;">Reflections Collected</td> <td style="text-align: center;">21573</td> </tr> <tr> <td style="text-align: center;">Goodness-of-fit on F²</td> <td style="text-align: center;">1.022</td> </tr> <tr> <td style="text-align: center;">Final R indexes [I > 2σ (I)]</td> <td style="text-align: center;">R₁ = 0.0464, wR₂ = 0.1065</td> </tr> <tr> <td style="text-align: center;">Final R indexes (all data)</td> <td style="text-align: center;">R₁ = 0.0774, wR₂ = 0.1203</td> </tr> </table>	Z	4	ρ_{calc} / g/cm³	1.363	μ/mm⁻¹	0.464	F(000)	624	Radiation	λ = 0.6199	Reflections Collected	21573	Goodness-of-fit on F²	1.022	Final R indexes [I > 2σ (I)]	R ₁ = 0.0464, wR ₂ = 0.1065	Final R indexes (all data)	R ₁ = 0.0774, wR ₂ = 0.1203
Z	4																			
ρ_{calc} / g/cm³	1.363																			
μ/mm⁻¹	0.464																			
F(000)	624																			
Radiation	λ = 0.6199																			
Reflections Collected	21573																			
Goodness-of-fit on F²	1.022																			
Final R indexes [I > 2σ (I)]	R ₁ = 0.0464, wR ₂ = 0.1065																			
Final R indexes (all data)	R ₁ = 0.0774, wR ₂ = 0.1203																			
<input checked="" type="checkbox"/> IR <input checked="" type="checkbox"/> ¹ H-NMR <input type="checkbox"/> Other <input type="checkbox"/> UV <input checked="" type="checkbox"/> ¹³ C-NMR 																				

6	Formula: C ₁₈ H ₁₆ N ₂ O ₂ S ₄ Formula Weight: 420.57 Name: 2,2'-[disulfanediy]bis[ethane-2,1-diyl]bis(-benzothiazol-3(2H)-one)	<input checked="" type="checkbox"/> Slow evaporation <input type="checkbox"/> Vapor diffusion <input type="checkbox"/> Solvent layer <input type="checkbox"/> Other																		
		Solvent(s)/Other agents: <input type="checkbox"/> Twinned Temperature: 100 K																		
<p>Synthesis:</p> <p>To a solution of dimethyl 2,2'-disulfanediyldibenzoate (20.0 g, 60.0 mmol) in CCl₄(100 mL), neat Br₂(10.3 g, 66.0 mmol) in CCl₄(40 mL) was added dropwise in 30 min. The brownish slurry was stirred at RT for 30 min and added dropwise to a solution of ,2'-disul-fanediyldiethanaminium iodide (72.0 mmol) and Et₃N (72.0 mmol) in CCl₄(40 mL). The reaction mixture was stirred 1 h at RT and heated at reflux for the suitable amount of time, poured into H₂O (300 mL) and extracted in CHCl₃(3x100 mL). The combined organic phases were dried over anhydrous Na₂SO₄, filtered and evaporated to dryness under reduced pressure to give a residue that was purified by flash chromatography.</p>		<table border="1"> <tr> <td>a: 28.589</td> <td>α: 90</td> <td>R₁:</td> <td>0.0323</td> </tr> <tr> <td>b: 5.183</td> <td>β: 107.67</td> <td>System:</td> <td>Monoclinic</td> </tr> <tr> <td>c: 12.842</td> <td>γ: 90</td> <td>Space Group:</td> <td>C 2/c</td> </tr> <tr> <td>Vol: 1813.11</td> <td></td> <td></td> <td></td> </tr> </table>	a: 28.589	α: 90	R ₁ :	0.0323	b: 5.183	β: 107.67	System:	Monoclinic	c: 12.842	γ: 90	Space Group:	C 2/c	Vol: 1813.11					
a: 28.589	α: 90	R ₁ :	0.0323																	
b: 5.183	β: 107.67	System:	Monoclinic																	
c: 12.842	γ: 90	Space Group:	C 2/c																	
Vol: 1813.11																				
<p>Characterization:</p> <p>¹H-NMR (400 MHz, CDCl₃) δ 8.01 (d, J = 7.3 Hz, 2H), 7.57 (dd, J = 7.8, 6.6, 2H), 7.52 (d, J = 7.8 Hz, 2H), 7.37 (dd, J = 7.3, 6.6 Hz, 2H), 4.17 (t, J = 6.3 Hz, 4H), 3.08 (t, J = 6.3 Hz, 4H).</p> <p>¹³C-NMR (100.6 MHz, CDCl₃) δ 165.3, 140.5, 131.9, 126.7, 125.6, 124.2, 120.4, 43.0, 37.1.</p> <p>IR (KBr, ν/cm⁻¹) 3369, 2973, 2900, 1655, 1441, 1424, 1338, 1291, 1248, 1181, 1086, 1049, 874, 734, 668.</p>		<table border="1"> <tr> <td>Z</td> <td>4</td> </tr> <tr> <td>ρ_{calc} / g/cm³</td> <td>1.541</td> </tr> <tr> <td>μ/mm⁻¹</td> <td>0.511</td> </tr> <tr> <td>F(000)</td> <td>872</td> </tr> <tr> <td>Radiation</td> <td>λ = 0.6199</td> </tr> <tr> <td>Reflections Collected</td> <td>12385</td> </tr> <tr> <td>Goodness-of-fit on F²</td> <td>1.090</td> </tr> <tr> <td>Final R indexes [I > 2σ (I)]</td> <td>R₁ = 0.0309, wR₂ = 0.0874</td> </tr> <tr> <td>Final R indexes (all data)</td> <td>R₁ = 0.0323, wR₂ = 0.0879</td> </tr> </table>	Z	4	ρ_{calc} / g/cm³	1.541	μ/mm⁻¹	0.511	F(000)	872	Radiation	λ = 0.6199	Reflections Collected	12385	Goodness-of-fit on F²	1.090	Final R indexes [I > 2σ (I)]	R ₁ = 0.0309, wR ₂ = 0.0874	Final R indexes (all data)	R ₁ = 0.0323, wR ₂ = 0.0879
Z	4																			
ρ_{calc} / g/cm³	1.541																			
μ/mm⁻¹	0.511																			
F(000)	872																			
Radiation	λ = 0.6199																			
Reflections Collected	12385																			
Goodness-of-fit on F²	1.090																			
Final R indexes [I > 2σ (I)]	R ₁ = 0.0309, wR ₂ = 0.0874																			
Final R indexes (all data)	R ₁ = 0.0323, wR ₂ = 0.0879																			

6.2.2. Chalcogen Bond Drives the Packing of Cyanine Crystals.

Materials.

Cyanine halides were purchased from TCI and used without further purification. The synthesis of nitrate and perrhenate salts was performed through salt metathesis described in the following.

Methods.

The single crystal data of **7** and **9** were collected at Bruker SMART APEX II CCD area detector diffractometer at room temperature. Data collection, unit cell refinement and data reduction were performed using Bruker SAINT. The structure was solved by direct methods using SHELXT and refined by full-matrix least-squares on F² with anisotropic displacement parameters for the non-H atoms using SHELXL-2016/6. Absorption correction was performed based on multi-scan procedure using SADABS. Structure analysis was aided by use of the programs PLATON. The hydrogen atoms were calculated in ideal positions with isotropic displacement parameters set to 1.2xU_{eq} of the attached atom.

Data collections for compounds **10-12** were performed at the X-ray diffraction beamline (XRD1) of the Elettra Synchrotron, Trieste (Italy)¹³. The crystals were dipped in NHV oil (Jena Bioscience, Jena, Germany) and mounted on the goniometer head with kapton loops (MiTeGen, Ithaca, USA). Complete datasets were collected at 100 K (nitrogen stream supplied through an Oxford Cryostream 700 - Oxford Cryosystems Ltd., Oxford, United Kingdom) through the rotating crystal method. The diffraction data were indexed and integrated using XDS.¹⁴ The structures were solved by the dual space algorithm implemented in the SHELXT code¹⁵. Fourier analysis and refinement were performed by the full-matrix least-squares methods based on F² implemented in SHELXL (Version 2018/3)¹⁶. The Coot program was used for modeling.¹⁷ Anisotropic thermal motion refinement have been used for all atoms. Geometric restrains (SAME) have been applied on disordered fragments. Hydrogen atoms were included at calculated positions with

¹³ A. Lausi, M. Polentarutti, S. Onesti, J. R. Plaisier, E. Busetto, G. Bais, L. Barba, A. Cassetta, G. Campi, D. Lamba, A. Pifferi, S. C. Mande, D. D. Sarma, S. M. Sharma, G. Paolucci, *Eur. Phys. J. Plus* 2015, 130, 1-8.

¹⁴ W. Kabsch, *Acta Cryst. Section D* 2010, 66(2), 125–132

¹⁵ G. M. Sheldrick, *Acta Cryst. Section A* 2015, 71, 3-8.

¹⁶ G. M. Sheldrick, *Acta Cryst. Section C* 2015, 71, 3-8.

¹⁷ P. Emsley, B. Lohkamp, W. G. Scott, K. Cowtan, *Acta Cryst. Section D* 2010, 66(4), 486–501

isotropic Ufactors = 1.2xUeq or Ufactors = 1.5xUeq for methyl and hydroxyl groups (Ueq being the equivalent isotropic thermal factor of the bonded non hydrogen atom). All the samples showed compact crystal packing without solvent inclusions.

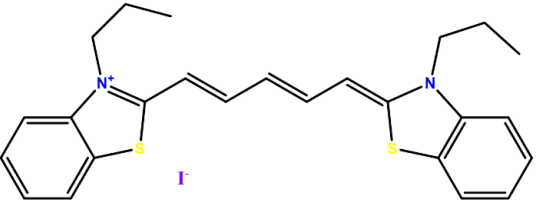
Data collection for **8** and **13** was performed on a Bruker Kappa Apex II diffractometer at 100 K by using a fine-focus sealed Mo-K α tube, $\lambda = 0.71073$ Å. Data collection and reduction was performed by using the program SAINT,¹⁸ and absorption correction, based on multiscan procedure, was achieved by using the program SADABS.¹⁹ Structures were solved with SHELXS²⁰ software and refined on all independent reflections by full-matrix least-squares based on F^2 by using the SHELXL program. Anisotropic thermal motion refinement has been used for all the atoms. Hydrogen atoms were placed in calculated positions and refined by using a riding model. 3D figures were prepared with CCDC Mercury²¹ software.

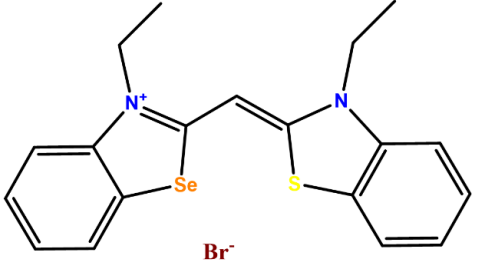
¹⁸ Bruker (2012). SAINT. Bruker AXS Inc., Madison, Wisconsin, USA.

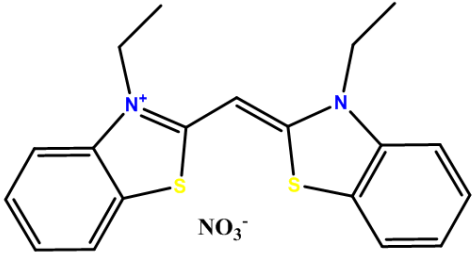
¹⁹ Bruker (2001). SADABS. Bruker AXS Inc., Madison, Wisconsin, USA.

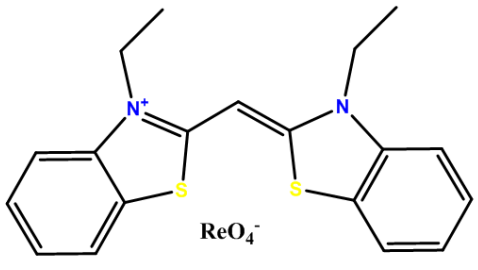
²⁰ G. M. Sheldrick, Acta Cryst. Section A **2008**, *64*, 112–122

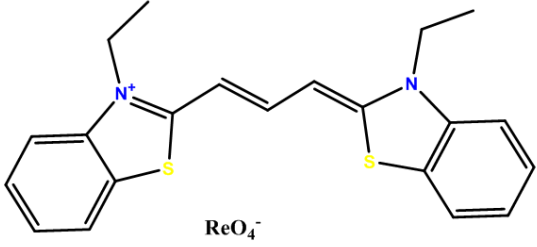
²¹ C. F. Macrae, I. J. Bruno, J. A. Chisholm, P. R. Edgington, P. McCabe, E. Pidcock, L. Rodriguez-Monge, R. Taylor, J. van de Streek, P. A. Wood., *J. Appl. Cryst.* **2008**, *41*, 466-470.

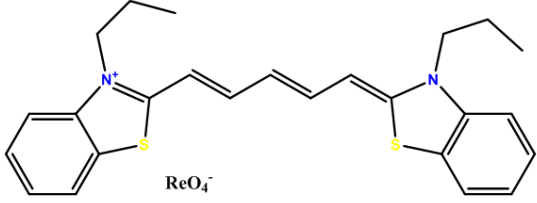
7	Formula: C ₂₆ H ₂₉ S ₂ IN ₂ Formula Weight: 1154.07 Name: 3,3'-dipropylthiadicarbocyanine iodide	<input checked="" type="checkbox"/> Slow evaporation <input type="checkbox"/> Vapor diffusion <input type="checkbox"/> Solvent layer <input type="checkbox"/> Other												
		Solvent(s)/Other agents: EtOH..... <input type="checkbox"/> Twinned Temperature: RT												
<table border="1" style="width: 100%; border-collapse: collapse;"> <tr> <td style="width: 33%;">a: 10.598</td> <td style="width: 33%;">α: 90</td> <td style="width: 33%;">R₁: 0.1055</td> </tr> <tr> <td>b: 21.965</td> <td>β: 112.144</td> <td>System: Monoclinic</td> </tr> <tr> <td>c: 12.686</td> <td>γ: 90</td> <td>Space Group: P₂1</td> </tr> <tr> <td>Vol: 2735.3</td> <td></td> <td></td> </tr> </table>		a: 10.598	α: 90	R ₁ : 0.1055	b: 21.965	β: 112.144	System: Monoclinic	c: 12.686	γ: 90	Space Group: P ₂ 1	Vol: 2735.3			
a: 10.598	α: 90	R ₁ : 0.1055												
b: 21.965	β: 112.144	System: Monoclinic												
c: 12.686	γ: 90	Space Group: P ₂ 1												
Vol: 2735.3														
<input checked="" type="checkbox"/> IR <input type="checkbox"/> ¹ H-NMR <input checked="" type="checkbox"/> Other <input type="checkbox"/> UV <input type="checkbox"/> ¹³ C-NMR melting point...														
<u>Synthesis:</u> The salt was purchased from commercial suppliers and crystallized without further purification.														
<u>Characterization:</u> m.p. (°C): 245 IR (ν/cm ⁻¹): 2957, 1570, 1426, 1316, 1190, 976, 813, 752, 504.														
		Z	2											
		ρ _{calc} / g/cm ³	1.401											
		μ/mm ⁻¹	1.343											
		F(000)	1170											
		Radiation	MoKα (λ = 0.71073)											
		Reflections Collected	34851											
		Goodness-of-fit on F ²	0.945											
		Final R indexes [I > 2σ (I)]	R ₁ = 0.1055, wR ₂ = 0.2745											
		Final R indexes (all data)	R ₁ = 0.2922, wR ₂ = 0.3855											

8	Formula: C ₁₉ H ₁₉ N ₂ SSeBr Formula Weight: 466.29 Name: (2Z)-3-ethyl-2-[(3-ethyl-1,3-benzoselenazol-3-ium-2-yl)methylidene]-1,3-benzothiazole;bromide	<input checked="" type="checkbox"/> Slow evaporation <input type="checkbox"/> Vapor diffusion <input type="checkbox"/> Solvent layer <input type="checkbox"/> Other Solvent(s)/Other agents: Acetonitrile..... <input type="checkbox"/> Twinned Temperature: 100 K																		
		<table border="1" style="width: 100%; border-collapse: collapse;"> <tr> <td>a: 8.0673</td> <td>α: 101.658</td> <td>R₁: 0.0320</td> </tr> <tr> <td>b: 9.8300</td> <td>β: 97.255</td> <td>System: Triclinic</td> </tr> <tr> <td>c: 11.9031</td> <td>γ: 102.756</td> <td>Space Group: P-1</td> </tr> <tr> <td>Vol: 887.10</td> <td></td> <td></td> </tr> </table>	a: 8.0673	α: 101.658	R ₁ : 0.0320	b: 9.8300	β: 97.255	System: Triclinic	c: 11.9031	γ: 102.756	Space Group: P-1	Vol: 887.10								
a: 8.0673	α: 101.658	R ₁ : 0.0320																		
b: 9.8300	β: 97.255	System: Triclinic																		
c: 11.9031	γ: 102.756	Space Group: P-1																		
Vol: 887.10																				
<p><u>Synthesis:</u></p> <p>The salt was purchased from commercial suppliers and crystallized without further purification.</p>																				
<p><u>Characterization:</u></p> <p>m.p. (°C): 300</p> <p>IR (ν/cm⁻¹): 2964, 1511, 1463, 1324, 1224, 1043, 938, 832, 742,</p>		<table border="1" style="width: 100%; border-collapse: collapse;"> <tr> <td style="text-align: center;">Z</td> <td style="text-align: center;">2</td> </tr> <tr> <td style="text-align: center;">ρ_{calc} / g/cm³</td> <td style="text-align: center;">1.746</td> </tr> <tr> <td style="text-align: center;">μ/mm⁻¹</td> <td style="text-align: center;">4.489</td> </tr> <tr> <td style="text-align: center;">F(000)</td> <td style="text-align: center;">464</td> </tr> <tr> <td style="text-align: center;">Radiation</td> <td style="text-align: center;">MoKα (λ = 0.71073)</td> </tr> <tr> <td style="text-align: center;">Reflections Collected</td> <td style="text-align: center;">15271</td> </tr> <tr> <td style="text-align: center;">Goodness-of-fit on F²</td> <td style="text-align: center;">1.003</td> </tr> <tr> <td style="text-align: center;">Final R indexes [I > 2σ (I)]</td> <td style="text-align: center;">R₁ = 0.0320, wR₂ = 0.0518</td> </tr> <tr> <td style="text-align: center;">Final R indexes (all data)</td> <td style="text-align: center;">R₁ = 0.0542, wR₂ = 0.0564</td> </tr> </table>	Z	2	ρ_{calc} / g/cm³	1.746	μ/mm⁻¹	4.489	F(000)	464	Radiation	MoKα (λ = 0.71073)	Reflections Collected	15271	Goodness-of-fit on F²	1.003	Final R indexes [I > 2σ (I)]	R ₁ = 0.0320, wR ₂ = 0.0518	Final R indexes (all data)	R ₁ = 0.0542, wR ₂ = 0.0564
Z	2																			
ρ_{calc} / g/cm³	1.746																			
μ/mm⁻¹	4.489																			
F(000)	464																			
Radiation	MoKα (λ = 0.71073)																			
Reflections Collected	15271																			
Goodness-of-fit on F²	1.003																			
Final R indexes [I > 2σ (I)]	R ₁ = 0.0320, wR ₂ = 0.0518																			
Final R indexes (all data)	R ₁ = 0.0542, wR ₂ = 0.0564																			

9	Formula: C ₁₉ H ₁₉ N ₃ O ₃ S ₂ Formula Weight: 401.49 Name: bis-(3-ethyl-benzothiazol-2-yl)-methinium nitrate	<input checked="" type="checkbox"/> Slow evaporation <input type="checkbox"/> Vapor diffusion <input type="checkbox"/> Solvent layer <input type="checkbox"/> Other																		
		Solvent(s)/Other agents: Acetonitrile..... <input type="checkbox"/> Twinned Temperature: 100 K																		
Synthesis: To a 2 mL acetonitrile solution of bis-(3-ethyl-benzothiazol-2-yl)-methinium iodide (1 mmol) an equimolar amount of AgNO ₃ was added under stirring. Immediately AgI started to precipitate, leaving the desired product in solution. After 12 hours, the reaction crude was filtered off many times into a clear borosilicate vial and left slowly crystallize.		<table border="1" style="width: 100%; border-collapse: collapse;"> <tr> <td>a: 7.416</td> <td>α: 90</td> <td>R₁:</td> <td>0.0703</td> </tr> <tr> <td>b: 26.616</td> <td>β: 91.907</td> <td>System:</td> <td>Triclinic</td> </tr> <tr> <td>c: 9.454</td> <td>γ: 90</td> <td>Space Group:</td> <td>P-1</td> </tr> <tr> <td colspan="2">Vol: 887.10</td> <td colspan="2"></td> </tr> </table>	a: 7.416	α: 90	R ₁ :	0.0703	b: 26.616	β: 91.907	System:	Triclinic	c: 9.454	γ: 90	Space Group:	P-1	Vol: 887.10					
a: 7.416	α: 90	R ₁ :	0.0703																	
b: 26.616	β: 91.907	System:	Triclinic																	
c: 9.454	γ: 90	Space Group:	P-1																	
Vol: 887.10																				
Characterization: m.p. (°C): 315. IR (ν/cm ⁻¹): 2979, 1520, 1313, 1227, 1090, 1048, 945, 832, 748, 699, 544.		<table border="1" style="width: 100%; border-collapse: collapse;"> <tr> <td style="text-align: center;">Z</td> <td style="text-align: center;">4</td> </tr> <tr> <td style="text-align: center;">ρ_{calc} / g/cm³</td> <td style="text-align: center;">1.430</td> </tr> <tr> <td style="text-align: center;">μ/mm⁻¹</td> <td style="text-align: center;">0,311</td> </tr> <tr> <td style="text-align: center;">F(000)</td> <td style="text-align: center;">840</td> </tr> <tr> <td style="text-align: center;">Radiation</td> <td style="text-align: center;">MoKα (λ = 0.71073)</td> </tr> <tr> <td style="text-align: center;">Reflections Collected</td> <td style="text-align: center;">16293</td> </tr> <tr> <td style="text-align: center;">Goodness-of-fit on F²</td> <td style="text-align: center;">1.063</td> </tr> <tr> <td style="text-align: center;">Final R indexes [I > 2σ (I)]</td> <td style="text-align: center;">R₁ = 0.0703, wR₂ = 0.1742</td> </tr> <tr> <td style="text-align: center;">Final R indexes (all data)</td> <td style="text-align: center;">R₁ = 0.1289, wR₂ = 0.2398</td> </tr> </table>	Z	4	ρ_{calc} / g/cm³	1.430	μ/mm⁻¹	0,311	F(000)	840	Radiation	MoKα (λ = 0.71073)	Reflections Collected	16293	Goodness-of-fit on F²	1.063	Final R indexes [I > 2σ (I)]	R ₁ = 0.0703, wR ₂ = 0.1742	Final R indexes (all data)	R ₁ = 0.1289, wR ₂ = 0.2398
Z	4																			
ρ_{calc} / g/cm³	1.430																			
μ/mm⁻¹	0,311																			
F(000)	840																			
Radiation	MoKα (λ = 0.71073)																			
Reflections Collected	16293																			
Goodness-of-fit on F²	1.063																			
Final R indexes [I > 2σ (I)]	R ₁ = 0.0703, wR ₂ = 0.1742																			
Final R indexes (all data)	R ₁ = 0.1289, wR ₂ = 0.2398																			

10	Formula: C ₁₉ H ₁₉ N ₂ O ₄ S ₂ Re Formula Weight: 589.68 Name: bis-(3-ethyl-benzothiazol-2-yl)-methinium perrhenate	<input checked="" type="checkbox"/> Slow evaporation <input type="checkbox"/> Vapor diffusion <input type="checkbox"/> Solvent layer <input type="checkbox"/> Other																		
		Solvent(s)/Other agents: Acetonitrile..... <input type="checkbox"/> Twinned Temperature: 100 K																		
<p><u>Synthesis:</u></p> <p>To a 2 mL acetonitrile solution of bis-(3-ethyl-benzothiazol-2-yl)-methinium iodide (1 mmol) an equimolar amount of AgReO₄ was added under stirring. Immediately AgI started to precipitate, leaving the desired product in solution. After 12 hours, the reaction crude was filtered off many times into a clear borosilicate vial and left slowly crystallize.</p>		<table border="1" style="width: 100%; border-collapse: collapse;"> <tr> <td>a: 7.396</td> <td>α: 76.14</td> <td>R₁:</td> <td>0.0261</td> </tr> <tr> <td>b: 11.583</td> <td>β: 85.66</td> <td>System:</td> <td>Triclinic</td> </tr> <tr> <td>c: 11.779</td> <td>γ: 87.43</td> <td>Space Group:</td> <td>P-1</td> </tr> <tr> <td>Vol: 976.6</td> <td colspan="3"></td> </tr> </table>	a: 7.396	α: 76.14	R ₁ :	0.0261	b: 11.583	β: 85.66	System:	Triclinic	c: 11.779	γ: 87.43	Space Group:	P-1	Vol: 976.6					
a: 7.396	α: 76.14	R ₁ :	0.0261																	
b: 11.583	β: 85.66	System:	Triclinic																	
c: 11.779	γ: 87.43	Space Group:	P-1																	
Vol: 976.6																				
<p><u>Characterization:</u></p> <p>m.p. (°C): 359.</p> <p>IR (ν/cm⁻¹): 3084, 1965, 1515, 1462, 1337, 1260, 1232, 1090, 1048, 895, 744, 715, 543.</p>		<table border="1" style="width: 100%; border-collapse: collapse;"> <tr> <td style="text-align: center;">Z</td> <td style="text-align: center;">2</td> </tr> <tr> <td style="text-align: center;">ρ_{calc} / g/cm³</td> <td style="text-align: center;">2.005</td> </tr> <tr> <td style="text-align: center;">μ/mm⁻¹</td> <td style="text-align: center;">4.501</td> </tr> <tr> <td style="text-align: center;">F(000)</td> <td style="text-align: center;">572</td> </tr> <tr> <td style="text-align: center;">Radiation</td> <td style="text-align: center;">λ = 0.6199</td> </tr> <tr> <td style="text-align: center;">Reflections Collected</td> <td style="text-align: center;">69721</td> </tr> <tr> <td style="text-align: center;">Goodness-of-fit on F²</td> <td style="text-align: center;">1.049</td> </tr> <tr> <td style="text-align: center;">Final R indexes [I > 2σ (I)]</td> <td style="text-align: center;">R₁ = 0.0261, wR₂ = 0.0699</td> </tr> <tr> <td style="text-align: center;">Final R indexes (all data)</td> <td style="text-align: center;">R₁ = 0.0264, wR₂ = 0.0701</td> </tr> </table>	Z	2	ρ_{calc} / g/cm³	2.005	μ/mm⁻¹	4.501	F(000)	572	Radiation	λ = 0.6199	Reflections Collected	69721	Goodness-of-fit on F²	1.049	Final R indexes [I > 2σ (I)]	R ₁ = 0.0261, wR ₂ = 0.0699	Final R indexes (all data)	R ₁ = 0.0264, wR ₂ = 0.0701
Z	2																			
ρ_{calc} / g/cm³	2.005																			
μ/mm⁻¹	4.501																			
F(000)	572																			
Radiation	λ = 0.6199																			
Reflections Collected	69721																			
Goodness-of-fit on F²	1.049																			
Final R indexes [I > 2σ (I)]	R ₁ = 0.0261, wR ₂ = 0.0699																			
Final R indexes (all data)	R ₁ = 0.0264, wR ₂ = 0.0701																			
		<input checked="" type="checkbox"/> IR <input type="checkbox"/> ¹ H-NMR <input checked="" type="checkbox"/> Other <input type="checkbox"/> UV <input type="checkbox"/> ¹³ C-NMR melting point...																		

<h1>11</h1>	Formula: $C_{21}H_{21}N_2O_4S_2Re$ Formula Weight: 615.751 Name: N,N'-diethylthiacarbocyanine perrhenate	<input checked="" type="checkbox"/> Slow evaporation <input type="checkbox"/> Vapor diffusion <input type="checkbox"/> Solvent layer <input type="checkbox"/> Other																			
		Solvent(s)/Other agents: Acetonitrile..... <input type="checkbox"/> Twinned Temperature: 100 K																			
		<table border="0"> <tr> <td>a: 8.258</td> <td>α: 90</td> <td>R_1:</td> <td>0.0459</td> </tr> <tr> <td>b: 17.426</td> <td>β: 97.72</td> <td>System:</td> <td>Monoclinic</td> </tr> <tr> <td>c: 30.800</td> <td>γ: 90</td> <td>Space Group:</td> <td>$P2_1/n$</td> </tr> <tr> <td colspan="4">Vol: 4392.0</td> </tr> </table>		a: 8.258	α : 90	R_1 :	0.0459	b: 17.426	β : 97.72	System:	Monoclinic	c: 30.800	γ : 90	Space Group:	$P2_1/n$	Vol: 4392.0					
		a: 8.258	α : 90	R_1 :	0.0459																
b: 17.426	β : 97.72	System:	Monoclinic																		
c: 30.800	γ : 90	Space Group:	$P2_1/n$																		
Vol: 4392.0																					
<input checked="" type="checkbox"/> IR <input type="checkbox"/> 1H -NMR <input checked="" type="checkbox"/> Other <input type="checkbox"/> UV <input type="checkbox"/> ^{13}C -NMR melting point...																					
<p><u>Synthesis:</u></p> <p>To a 2 mL acetonitrile solution of N,N'-diethylthiacarbocyanine iodide (1 mmol) an equimolar amount of $AgReO_4$ was added under stirring. Immediately AgI started to precipitate, leaving the desired product in solution. After 12 hours, the reaction crude was filtered off many times into a clear borosilicate vial and left slowly crystallize.</p>																					
<p><u>Characterization:</u></p> <p>m.p. ($^{\circ}C$): 309.</p> <p>IR (ν/cm^{-1}): 1550, 1478, 1460, 1423, 1318, 1273, 1208, 1089, 899, 745, 713, 545.</p>		<table border="1"> <tr> <td>Z</td> <td>8</td> </tr> <tr> <td>$\rho_{calc} / g/cm^3$</td> <td>1.890</td> </tr> <tr> <td>μ/mm^{-1}</td> <td>4.009</td> </tr> <tr> <td>F(000)</td> <td>2440</td> </tr> <tr> <td>Radiation</td> <td>$\lambda = 0.6199$</td> </tr> <tr> <td>Reflections Collected</td> <td>106419</td> </tr> <tr> <td>Goodness-of-fit on F^2</td> <td>0.967</td> </tr> <tr> <td>Final R indexes [$I > 2\sigma(I)$]</td> <td>$R_1 = 0.0459, wR_2 = 0.1183$</td> </tr> <tr> <td>Final R indexes (all data)</td> <td>$R_1 = 0.0954, wR_2 = 0.1413$</td> </tr> </table>		Z	8	$\rho_{calc} / g/cm^3$	1.890	μ/mm^{-1}	4.009	F(000)	2440	Radiation	$\lambda = 0.6199$	Reflections Collected	106419	Goodness-of-fit on F^2	0.967	Final R indexes [$I > 2\sigma(I)$]	$R_1 = 0.0459, wR_2 = 0.1183$	Final R indexes (all data)	$R_1 = 0.0954, wR_2 = 0.1413$
Z	8																				
$\rho_{calc} / g/cm^3$	1.890																				
μ/mm^{-1}	4.009																				
F(000)	2440																				
Radiation	$\lambda = 0.6199$																				
Reflections Collected	106419																				
Goodness-of-fit on F^2	0.967																				
Final R indexes [$I > 2\sigma(I)$]	$R_1 = 0.0459, wR_2 = 0.1183$																				
Final R indexes (all data)	$R_1 = 0.0954, wR_2 = 0.1413$																				

12	Formula: C ₂₅ H ₂₇ N ₂ O ₄ S ₂ Re Formula Weight: 669.80 Name: 3,3'-dipropylthiadicarbocyanine perrhenate	<input checked="" type="checkbox"/> Slow evaporation <input type="checkbox"/> Vapor diffusion <input type="checkbox"/> Solvent layer <input type="checkbox"/> Other																		
		Solvent(s)/Other agents: Acetonitrile..... <input type="checkbox"/> Twinned Temperature: RT																		
<p><u>Synthesis:</u></p> <p>To a 2 mL acetonitrile solution of 3,3'-dipropylthiadicarbocyanine iodide (1 mmol) an equimolar amount of AgReO₄ was added under stirring. Immediately AgI started to precipitate, leaving the desired product in solution. After 12 hours, the reaction crude was filtered off many times into a clear borosilicate vial and left slowly crystallize.</p>		<table border="1" style="width: 100%; border-collapse: collapse;"> <tr> <td>a: 7.7870</td> <td>α: 90</td> <td>R₁:</td> <td>0.0203</td> </tr> <tr> <td>b: 13.774</td> <td>β: 95.24</td> <td>System:</td> <td>Monoclinic</td> </tr> <tr> <td>c: 22.837</td> <td>γ: 90</td> <td>Space Group:</td> <td>P2₁/c</td> </tr> <tr> <td>Vol: 2439.2</td> <td></td> <td></td> <td></td> </tr> </table>	a: 7.7870	α: 90	R ₁ :	0.0203	b: 13.774	β: 95.24	System:	Monoclinic	c: 22.837	γ: 90	Space Group:	P2 ₁ /c	Vol: 2439.2					
a: 7.7870	α: 90	R ₁ :	0.0203																	
b: 13.774	β: 95.24	System:	Monoclinic																	
c: 22.837	γ: 90	Space Group:	P2 ₁ /c																	
Vol: 2439.2																				
<p><u>Characterization:</u></p> <p>m.p. (°C): 337.</p> <p>IR (ν/cm⁻¹): 1567, 1431, 1316, 1250, 1103, 971, 889, 817, 740.</p>		<table border="1" style="width: 100%; border-collapse: collapse;"> <tr> <td style="text-align: center;">Z</td> <td style="text-align: center;">4</td> </tr> <tr> <td style="text-align: center;">ρ_{calc} / g/cm³</td> <td style="text-align: center;">1.824</td> </tr> <tr> <td style="text-align: center;">μ/mm⁻¹</td> <td style="text-align: center;">3.614</td> </tr> <tr> <td style="text-align: center;">F(000)</td> <td style="text-align: center;">1320</td> </tr> <tr> <td style="text-align: center;">Radiation</td> <td style="text-align: center;">λ = 0.6199</td> </tr> <tr> <td style="text-align: center;">Reflections Collected</td> <td style="text-align: center;">58467</td> </tr> <tr> <td style="text-align: center;">Goodness-of-fit on F²</td> <td style="text-align: center;">1.035</td> </tr> <tr> <td style="text-align: center;">Final R indexes [I > 2σ (I)]</td> <td style="text-align: center;">R₁ = 0.0370, wR₂ = 0.0695</td> </tr> <tr> <td style="text-align: center;">Final R indexes (all data)</td> <td style="text-align: center;">R₁ = 0.0567, wR₂ = 0.0754</td> </tr> </table>	Z	4	ρ_{calc} / g/cm³	1.824	μ/mm⁻¹	3.614	F(000)	1320	Radiation	λ = 0.6199	Reflections Collected	58467	Goodness-of-fit on F²	1.035	Final R indexes [I > 2σ (I)]	R ₁ = 0.0370, wR ₂ = 0.0695	Final R indexes (all data)	R ₁ = 0.0567, wR ₂ = 0.0754
Z	4																			
ρ_{calc} / g/cm³	1.824																			
μ/mm⁻¹	3.614																			
F(000)	1320																			
Radiation	λ = 0.6199																			
Reflections Collected	58467																			
Goodness-of-fit on F²	1.035																			
Final R indexes [I > 2σ (I)]	R ₁ = 0.0370, wR ₂ = 0.0695																			
Final R indexes (all data)	R ₁ = 0.0567, wR ₂ = 0.0754																			
		<input checked="" type="checkbox"/> IR <input type="checkbox"/> ¹ H-NMR <input checked="" type="checkbox"/> Other <input type="checkbox"/> UV <input type="checkbox"/> ¹³ C-NMR melting point...																		

13	Formula: C ₁₉ H ₁₉ N ₂ O ₄ ReSe Formula Weight: 636.58 Name: (2Z)-3-ethyl-2-[(3-ethyl-1,3-benzoselenazol-3-ium-2-yl)methylidene]-1,3-benzothiazole perrhenate	<input checked="" type="checkbox"/> Slow evaporation <input type="checkbox"/> Vapor diffusion <input type="checkbox"/> Solvent layer <input type="checkbox"/> Other																		
		Solvent(s)/Other agents: Acetonitrile..... <input type="checkbox"/> Twinned Temperature: 100 K																		
<p>Synthesis:</p> <p>To a 2 mL acetonitrile solution of (2Z)-3-ethyl-2-[(3-ethyl-1,3-benzoselenazol-3-ium-2-yl)methylidene]-1,3-benzothiazole bromide (1 mmol) an equimolar amount of AgReO₄ was added under stirring. Immediately AgBr started to precipitate, leaving the desired product in solution. After 12 hours, the reaction crude was filtered off many times into a clear borosilicate vial and left slowly crystallize.</p>		<table border="1"> <tr> <td>a: 7.812</td> <td>α: 90</td> <td>R₁:</td> <td>0.0385</td> </tr> <tr> <td>b: 11.997</td> <td>β: 91.68</td> <td>System:</td> <td>Monoclinic</td> </tr> <tr> <td>c: 21.182</td> <td>γ: 90</td> <td>Space Group:</td> <td>P2₁/n</td> </tr> <tr> <td>Vol: 1984.0</td> <td></td> <td></td> <td></td> </tr> </table>	a: 7.812	α: 90	R ₁ :	0.0385	b: 11.997	β: 91.68	System:	Monoclinic	c: 21.182	γ: 90	Space Group:	P2 ₁ /n	Vol: 1984.0					
a: 7.812	α: 90	R ₁ :	0.0385																	
b: 11.997	β: 91.68	System:	Monoclinic																	
c: 21.182	γ: 90	Space Group:	P2 ₁ /n																	
Vol: 1984.0																				
<p>Characterization:</p> <p>m.p. (°C): 367.</p> <p>IR (ν/cm⁻¹): 1583, 1511, 1463, 1261, 1168, 892, 742, 706, 507.</p>		<table border="1"> <tr> <td>Z</td> <td>4</td> </tr> <tr> <td>ρ_{calc} / g/cm³</td> <td>2.131</td> </tr> <tr> <td>μ/mm⁻¹</td> <td>8.092</td> </tr> <tr> <td>F(000)</td> <td>1216</td> </tr> <tr> <td>Radiation</td> <td>MoKα (λ = 0.71073)</td> </tr> <tr> <td>Reflections Collected</td> <td>37903</td> </tr> <tr> <td>Goodness-of-fit on F²</td> <td>1.045</td> </tr> <tr> <td>Final R indexes [I > 2σ (I)]</td> <td>R₁ = 0.0385, wR₂ = 0.0722</td> </tr> <tr> <td>Final R indexes (all data)</td> <td>R₁ = 0.0845, wR₂ = 0.0835</td> </tr> </table>	Z	4	ρ _{calc} / g/cm ³	2.131	μ/mm ⁻¹	8.092	F(000)	1216	Radiation	MoKα (λ = 0.71073)	Reflections Collected	37903	Goodness-of-fit on F ²	1.045	Final R indexes [I > 2σ (I)]	R ₁ = 0.0385, wR ₂ = 0.0722	Final R indexes (all data)	R ₁ = 0.0845, wR ₂ = 0.0835
Z	4																			
ρ _{calc} / g/cm ³	2.131																			
μ/mm ⁻¹	8.092																			
F(000)	1216																			
Radiation	MoKα (λ = 0.71073)																			
Reflections Collected	37903																			
Goodness-of-fit on F ²	1.045																			
Final R indexes [I > 2σ (I)]	R ₁ = 0.0385, wR ₂ = 0.0722																			
Final R indexes (all data)	R ₁ = 0.0845, wR ₂ = 0.0835																			
<input checked="" type="checkbox"/> IR <input type="checkbox"/> ¹ H-NMR <input checked="" type="checkbox"/> Other <input type="checkbox"/> UV <input type="checkbox"/> ¹³ C-NMR melting point...																				

6.3. The Tetrel Bond at Work.

Contributions:

6.3.1. The N-methylammonium moiety: a tetrel bond donor site.

GR designed the experiments.

AD and AP performed the experiments.

GT and TP oversaw the crystallographic characterization.

EW and AG performed and interpreted the calculations.

AD and AP interpreted the results and performed CSD surveys.

6.3.2. Bis(pyridinium)methylene salts as $-C(sp^3)H_2$ -Tetrel Bond Donors.

GR designed the experiments.

AD and MU performed the synthesis of the compounds, characterization and crystallization.

ND performed synchrotron experiments and structure refinement on **6**.

Structure **7** was solved and refined by Rigaku's laboratories.

Structure **8** was solved and refined by Bruker's laboratories.

6.3.3. Tetrel Bonds in Choline and Betaine derivatives.

AD and GR designed the experiments.

AD, MC and GC performed the methathesis and crystallizations.

GT oversaw the crystallographic characterization.

ND performed occasional synchrotron experiments and structure refinement on **9, 10, 14**.

6.3.1. The N-methylammonium moiety: a tetrel bond donor site.

Materials.

Compounds and solvents were purchased from Sigma Aldrich and TCI and used without further purification.

Methods.

The single crystal data of all the structures displayed in this work were collected at Bruker SMART APEX II CCD area detector diffractometer at 100 K. Data collection, unit cell refinement and data reduction were performed using Bruker SAINT. The structure was solved by direct methods using SHELXT and refined by full-matrix least-squares on F^2 with anisotropic displacement parameters for the non-H atoms using SHELXL-2016/6. Absorption correction was performed based on multi-scan procedure using SADABS. Structure analysis was aided by use of the programs PLATON. The hydrogen atoms were calculated in ideal positions with isotropic displacement parameters set to 1.2xUeq of the attached atom, or determined by HAR.

Fundamentals of Hirshfeld Atom Refinement (HAR).

The Hirshfeld atom refinement (HAR) is a self-consistent refinement procedure based on the following steps.

1. Quantum chemical calculation on a system that at least corresponds to the asymmetric unit of the target crystal structure. The starting geometry is usually the one that is obtained from the preliminary IAM refinement.
2. Subdivision of the obtained electron density $\rho_0(\mathbf{r})$ (associated with the quantum chemical calculation at point 1) into atomic contributions using the Hirshfeld stockholder partitioning technique. According to this method, the atomic density distribution for each atom is given by

$$\rho_A(\mathbf{r}) = w_A(\mathbf{r}) \rho_0(\mathbf{r})$$

where $w_A(\mathbf{r})$ is the Hirshfeld weight function provided by the ration between the spherically-averaged atomic density of the atom under consideration (ρ_A°) and the

promolecular density, which is the sum of the spherically-averaged atomic densities of all the atoms forming the investigated system:

$$w_A(\mathbf{r}) = \frac{\rho_A^o(\mathbf{r})}{\sum_{B=1}^{N_{atoms}} \rho_B^o(\mathbf{r})}$$

3. Calculation of the atomic form factors through Fourier transformation of the atomic densities obtained at point 2.
4. Calculation of the global structure factors $\{F_{\mathbf{h}}^{calc}\}$ as sum of the atomic form factors resulting from point 3.
5. Least-squares minimization of the χ^2 statistical agreement between experimental and calculated structure factor amplitudes with respect to the scale factor η , atomic coordinates and ADPs. The χ^2 statistical agreement is given by the following relation:

$$\chi^2 = \frac{1}{N_r - N_p} \sum_{\mathbf{h}} \frac{(\eta |F_{\mathbf{h}}^{calc}| - |F_{\mathbf{h}}^{exp}|)^2}{\sigma_{\mathbf{h}}^2}$$

with N_r as the number of reflections, N_p as the number of parameters in the model, $|F_{\mathbf{h}}^{calc}|$ and $|F_{\mathbf{h}}^{exp}|$ as the calculated and experimental structure factor amplitudes, respectively, for the reflection corresponding to the Miller indices triplet $\mathbf{h} = (h, k, l)$, $\sigma_{\mathbf{h}}$ as the experimental error associated with the experimental structure factor amplitude $|F_{\mathbf{h}}^{exp}|$, and η as an overall (\mathbf{h} -independent) factor that puts $|F_{\mathbf{h}}^{calc}|$ on the same scale of $|F_{\mathbf{h}}^{exp}|$.

6. Check of convergence on the atomic structural parameters (i.e., atomic coordinates and ADPs). When convergence is achieved, the iterative procedure ends, and electronic properties of the system may be calculated exploiting the wave function / electron density corresponding to the converged structure. Otherwise, the new geometry is exploited to start a new iteration and, particularly, to carry out a new quantum chemical calculation (see point 1).

As already mentioned in the main text, it is worth noting that, in order to properly account for the crystal field effects, the quantum mechanical computations at point 1 can be also performed by embedding the reference system through a cluster of point charges and dipoles. They are generally placed on all those atoms of the surrounding moieties of the crystal that have at least one atom at a distance lower than 8 Å from the reference system considered for the quantum chemical calculations.

CSD Surveys.

Table 6.3.1. Hexamethonium (1,6-bis-(trimethyl ammonium) hexane) structures present on the CSD. In bold structures that present a short contact between one of the methyl's carbons and an electron rich atom (atoms considered N, P, O, S, Se, F, Cl, Br, I) establishing a $N^+-C\cdots Nu$ angle comprised between 160 and 180°. In bold and red entries where the contact is shorter than the sum of their respective vdW radii, in bold and black contacts where the contact is shorter than the sum plus 0.2 Å.

DIQBIQ	HMENAM01	NUTTAY	URUBUF
DIQBOW	HMTMAC	NUTTAY01	XEPDEB
DIQBUC	HMTMAC01	SOFYER	YEPGOQ
FUGGET	MUXSUT	TIBROL	PUPBEK
HMACQM	NUTSOL	URUBIT	VUGNUJ
HMENAM	NUTSUR	URUBOZ	VUGNUJ01

Table 6.3.2. Octamethonium (1,8-bis-(trimethyl ammonium) octane) structures present on the CSD. In bold structures that present a short contact between one of the methyl's carbons and an electron rich atom (atoms considered N, P, O, S, Se, F, Cl, Br, I) establishing a $N^+-C\cdots Nu$ angle comprised between 160 and 180°. In bold and red entries where the contact is shorter than the sum of their respective vdW radii, in bold and black contacts where the contact is shorter than the sum plus 0.2 Å.

XOTZOW	XOTZUC	ZIHXOG	
---------------	--------	--------	--

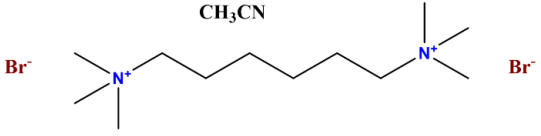
Table 6.3.3. Decamethonium (1,10-bis(trimethylammonium) decane) structures present on the CSD. In bold structures that present a short contact between one of the methyl's carbons and an electron rich atom (atoms considered N, P, O, S, Se, F, Cl, Br, I) establishing a $N^+-C\cdots Nu$ angle comprised between 160 and 180°. In bold and red entries where the contact is shorter than the sum of their respective vdW radii, in bold and black contacts where the contact is shorter than the sum plus 0.2 Å.

DIMENAM	SIHYOZ	XOVBAM	
SIHFAQ	SIHYUF	XOVBEQ	
SIHYIT	WESLAK	XOVBIU	

1	Formula: C ₁₂ H ₃₀ Br ₂ N ₂ Formula Weight: 362.20 Name: Hexamethonium Bromide	<input checked="" type="checkbox"/> Slow evaporation <input type="checkbox"/> Vapor diffusion <input type="checkbox"/> Solvent layer <input type="checkbox"/> Other																		
		Solvent(s)/Other agents: CH ₂ Cl ₂ <input type="checkbox"/> Twinned Temperature: 100 K	a: 5.4796 α: 90 R ₁ : 0.0235 b: 13.1109 β: 93.580 System: Monoclinic c: 11.5815 γ: 90 Space Group: P2 ₁ /c Vol: 830.42																	
<input checked="" type="checkbox"/> IR <input checked="" type="checkbox"/> ¹ H-NMR <input type="checkbox"/> Other <input type="checkbox"/> UV <input checked="" type="checkbox"/> ¹³ C-NMR 																				
<u>Synthesis:</u> The salt was purchased from commercial suppliers and crystallized without further purification.																				
<u>Characterization:</u> FTIR (ν /cm ⁻¹) 3485, 2945, 1630, 1482, 1413, 1061, 971, 946, 915, 817. ¹ H-NMR (400 MHz, D ₂ O) δ 1.43 (m, 4H), 1.80 (m, 4H), 3.30 (m, 4H), 3.10 (s, 18H). ¹³ C-NMR (100.6 MHz, D ₂ O) δ 22 (N ⁺ -CH ₂ -CH ₂ -CH ₂ -), 25 (N ⁺ -CH ₂ -CH ₂ -CH ₂ -), 53 (CH ₃ -N ⁺) 66 (N ⁺ -CH ₂ -CH ₂ -CH ₂ -).		<table border="1"> <tr> <td style="text-align: center;">Z</td> <td style="text-align: center;">2</td> </tr> <tr> <td style="text-align: center;">ρ_{calc} / g/cm³</td> <td style="text-align: center;">1.449</td> </tr> <tr> <td style="text-align: center;">μ/mm⁻¹</td> <td style="text-align: center;">4.864</td> </tr> <tr> <td style="text-align: center;">F(000)</td> <td style="text-align: center;">3720</td> </tr> <tr> <td style="text-align: center;">Radiation</td> <td style="text-align: center;">MoKα (λ = 0.71073)</td> </tr> <tr> <td style="text-align: center;">Reflections Collected</td> <td style="text-align: center;">13885</td> </tr> <tr> <td style="text-align: center;">Goodness-of-fit on F²</td> <td style="text-align: center;">1.005</td> </tr> <tr> <td style="text-align: center;">Final R indexes [I > 2σ (I)]</td> <td style="text-align: center;">R₁ = 0.0235, wR₂ = 0.0441</td> </tr> <tr> <td style="text-align: center;">Final R indexes (all data)</td> <td style="text-align: center;">R₁ = 0.0408, wR₂ = 0.0481</td> </tr> </table>	Z	2	ρ_{calc} / g/cm³	1.449	μ/mm⁻¹	4.864	F(000)	3720	Radiation	MoKα (λ = 0.71073)	Reflections Collected	13885	Goodness-of-fit on F²	1.005	Final R indexes [I > 2σ (I)]	R ₁ = 0.0235, wR ₂ = 0.0441	Final R indexes (all data)	R ₁ = 0.0408, wR ₂ = 0.0481
Z	2																			
ρ_{calc} / g/cm³	1.449																			
μ/mm⁻¹	4.864																			
F(000)	3720																			
Radiation	MoKα (λ = 0.71073)																			
Reflections Collected	13885																			
Goodness-of-fit on F²	1.005																			
Final R indexes [I > 2σ (I)]	R ₁ = 0.0235, wR ₂ = 0.0441																			
Final R indexes (all data)	R ₁ = 0.0408, wR ₂ = 0.0481																			

2	Formula: C ₁₂ H ₃₄ Br ₂ N ₂ O ₂ Formula Weight: 398.22 Name: Hexamethonium Bromide water solvate	<input checked="" type="checkbox"/> Slow evaporation <input type="checkbox"/> Vapor diffusion <input type="checkbox"/> Solvent layer <input type="checkbox"/> Other																		
		Solvent(s)/Other agents: H ₂ O..... <input type="checkbox"/> Twinned Temperature: 100 K																		
<u>Synthesis:</u> Crystallization in specific solvent afforded the solvate adduct		<table border="1" style="width: 100%; border-collapse: collapse;"> <tr> <td>a: 7.3339</td> <td>α: 90</td> <td>R₁:</td> <td>0.0172</td> </tr> <tr> <td>b: 18.292</td> <td>β: 108.824</td> <td>System:</td> <td>Monoclinic</td> </tr> <tr> <td>c: 7.0915</td> <td>γ: 90</td> <td>Space Group:</td> <td>P2₁/c</td> </tr> <tr> <td>Vol: 900.43</td> <td></td> <td></td> <td></td> </tr> </table>	a: 7.3339	α: 90	R ₁ :	0.0172	b: 18.292	β: 108.824	System:	Monoclinic	c: 7.0915	γ: 90	Space Group:	P2 ₁ /c	Vol: 900.43					
a: 7.3339	α: 90	R ₁ :	0.0172																	
b: 18.292	β: 108.824	System:	Monoclinic																	
c: 7.0915	γ: 90	Space Group:	P2 ₁ /c																	
Vol: 900.43																				
<u>Characterization:</u> FTIR (ν /cm ⁻¹) 3484, 2947, 1629, 1595, 1482, 1411, 1060, 971, 946, 918, 814. ¹ H-NMR (400 MHz, D ₂ O) δ 1.42 (m, 4H), 1.81 (m, 4H), 3.10 (m, 4H), 3.33 (s, 18H), 4.80 (s, H ₂ O). ¹³ C-NMR (100.6 MHz, D ₂ O) δ 22 (N ⁺ -CH ₂ -CH ₂ -CH ₂ -), 25 (N ⁺ -CH ₂ -CH ₂ -CH ₂ -), 53 (CH ₃ -N ⁺) 67 (N ⁺ -CH ₂ -CH ₂ -CH ₂ -).		<table border="1" style="width: 100%; border-collapse: collapse;"> <tr> <td style="text-align: center;">Z</td> <td style="text-align: center;">2</td> </tr> <tr> <td style="text-align: center;">ρ_{calc} / g/cm³</td> <td style="text-align: center;">1.4687</td> </tr> <tr> <td style="text-align: center;">μ/mm⁻¹</td> <td style="text-align: center;">4.500</td> </tr> <tr> <td style="text-align: center;">F(000)</td> <td style="text-align: center;">311.1</td> </tr> <tr> <td style="text-align: center;">Radiation</td> <td style="text-align: center;">MoKα (λ = 0.71073)</td> </tr> <tr> <td style="text-align: center;">Reflections Collected</td> <td style="text-align: center;">30774</td> </tr> <tr> <td style="text-align: center;">Goodness-of-fit on F²</td> <td style="text-align: center;">1.040</td> </tr> <tr> <td style="text-align: center;">Final R indexes [I > 2σ (I)]</td> <td style="text-align: center;">R₁ = 0.0172, wR₂ = 0.0424</td> </tr> <tr> <td style="text-align: center;">Final R indexes (all data)</td> <td style="text-align: center;">R₁ = 0.0200, wR₂ = 0.0439</td> </tr> </table>	Z	2	ρ_{calc} / g/cm³	1.4687	μ/mm⁻¹	4.500	F(000)	311.1	Radiation	MoKα (λ = 0.71073)	Reflections Collected	30774	Goodness-of-fit on F²	1.040	Final R indexes [I > 2σ (I)]	R ₁ = 0.0172, wR ₂ = 0.0424	Final R indexes (all data)	R ₁ = 0.0200, wR ₂ = 0.0439
Z	2																			
ρ_{calc} / g/cm³	1.4687																			
μ/mm⁻¹	4.500																			
F(000)	311.1																			
Radiation	MoKα (λ = 0.71073)																			
Reflections Collected	30774																			
Goodness-of-fit on F²	1.040																			
Final R indexes [I > 2σ (I)]	R ₁ = 0.0172, wR ₂ = 0.0424																			
Final R indexes (all data)	R ₁ = 0.0200, wR ₂ = 0.0439																			

3	Formula: C ₁₃ H ₃₄ Br ₂ N ₂ O Formula Weight: 394.24 Name: Hexamethonium Bromide Methanol Solvate	<input checked="" type="checkbox"/> Slow evaporation <input type="checkbox"/> Vapor diffusion <input type="checkbox"/> Solvent layer <input type="checkbox"/> Other																		
		Solvent(s)/Other agents: CH ₃ OH..... <input type="checkbox"/> Twinned Temperature: 100 K																		
<p><u>Synthesis:</u></p> <p>Crystallization in specific solvent afforded the solvate adduct</p>		<table border="1" style="width: 100%; border-collapse: collapse;"> <tr> <td>a: 9.270</td> <td>α: 90</td> <td>R₁:</td> <td>0.0503</td> </tr> <tr> <td>b: 11.720</td> <td>β: 92.20</td> <td>System:</td> <td>Monoclinic</td> </tr> <tr> <td>c: 16.537</td> <td>γ: 90</td> <td>Space Group:</td> <td>P2₁/n</td> </tr> <tr> <td>Vol: 1795.3</td> <td></td> <td></td> <td></td> </tr> </table>	a: 9.270	α: 90	R ₁ :	0.0503	b: 11.720	β: 92.20	System:	Monoclinic	c: 16.537	γ: 90	Space Group:	P2 ₁ /n	Vol: 1795.3					
a: 9.270	α: 90	R ₁ :	0.0503																	
b: 11.720	β: 92.20	System:	Monoclinic																	
c: 16.537	γ: 90	Space Group:	P2 ₁ /n																	
Vol: 1795.3																				
<p><u>Characterization:</u></p> <p>FTIR (ν /cm⁻¹) 3485, 2945, 2833, 2522, 2046, 1630, 1482, 1413, 1116, 1061, 971, 946, 915, 817.</p> <p>¹H-NMR (400 MHz, D₂O) δ 1.42 (m, 4H), 1.80 (m, 4H), 3.09 (m, 4H), 3.33 (s, 18H), 3.41 (s, 3H, CH₃OH).</p> <p>¹³C-NMR (100.6 MHz, D₂O) δ 22 (N⁺-CH₂-CH₂-CH₂-), 25 (N⁺-CH₂-CH₂-CH₂-), 49 (methanol), 53 (CH₃-N⁺) 66 (N⁺-CH₂-CH₂-CH₂-).</p>		<table border="1" style="width: 100%; border-collapse: collapse;"> <tr> <td style="text-align: center;">Z</td> <td style="text-align: center;">4</td> </tr> <tr> <td style="text-align: center;">ρ_{calc} / g/cm³</td> <td style="text-align: center;">1.459</td> </tr> <tr> <td style="text-align: center;">μ/mm⁻¹</td> <td style="text-align: center;">4.510</td> </tr> <tr> <td style="text-align: center;">F(000)</td> <td style="text-align: center;">816.0</td> </tr> <tr> <td style="text-align: center;">Radiation</td> <td style="text-align: center;">MoKα (λ = 0.71073)</td> </tr> <tr> <td style="text-align: center;">Reflections Collected</td> <td style="text-align: center;">14875</td> </tr> <tr> <td style="text-align: center;">Goodness-of-fit on F²</td> <td style="text-align: center;">0.953</td> </tr> <tr> <td style="text-align: center;">Final R indexes [I > 2σ (I)]</td> <td style="text-align: center;">R₁ = 0.0503, wR₂ = 0.0894</td> </tr> <tr> <td style="text-align: center;">Final R indexes (all data)</td> <td style="text-align: center;">R₁ = 0.1293, wR₂ = 0.1117</td> </tr> </table>	Z	4	ρ_{calc} / g/cm³	1.459	μ/mm⁻¹	4.510	F(000)	816.0	Radiation	MoKα (λ = 0.71073)	Reflections Collected	14875	Goodness-of-fit on F²	0.953	Final R indexes [I > 2σ (I)]	R ₁ = 0.0503, wR ₂ = 0.0894	Final R indexes (all data)	R ₁ = 0.1293, wR ₂ = 0.1117
Z	4																			
ρ_{calc} / g/cm³	1.459																			
μ/mm⁻¹	4.510																			
F(000)	816.0																			
Radiation	MoKα (λ = 0.71073)																			
Reflections Collected	14875																			
Goodness-of-fit on F²	0.953																			
Final R indexes [I > 2σ (I)]	R ₁ = 0.0503, wR ₂ = 0.0894																			
Final R indexes (all data)	R ₁ = 0.1293, wR ₂ = 0.1117																			

4	Formula: C ₁₄ H ₃₃ Br ₂ N ₃ Formula Weight: 403.25 Name: Hexamethonium Bromide Acetonitrile Solvate	<input checked="" type="checkbox"/> Slow evaporation <input type="checkbox"/> Vapor diffusion <input type="checkbox"/> Solvent layer <input type="checkbox"/> Other																		
		Solvent(s)/Other agents: CH ₂ CN..... <input type="checkbox"/> Twinned Temperature: 100 K																		
<p><u>Synthesis:</u></p> <p>Crystallization in specific solvent afforded the solvate adduct</p>		<table border="1" style="width: 100%;"> <tr> <td>a: 12.4309</td> <td>α: 90</td> <td>R₁:</td> <td>0.0503</td> </tr> <tr> <td>b: 9.5074</td> <td>β: 94.584</td> <td>System:</td> <td>Monoclinic</td> </tr> <tr> <td>c: 15.9984</td> <td>γ: 90</td> <td>Space Group:</td> <td>P2₁/c</td> </tr> <tr> <td>Vol: 1884.7</td> <td></td> <td></td> <td></td> </tr> </table>	a: 12.4309	α: 90	R ₁ :	0.0503	b: 9.5074	β: 94.584	System:	Monoclinic	c: 15.9984	γ: 90	Space Group:	P2 ₁ /c	Vol: 1884.7					
a: 12.4309	α: 90	R ₁ :	0.0503																	
b: 9.5074	β: 94.584	System:	Monoclinic																	
c: 15.9984	γ: 90	Space Group:	P2 ₁ /c																	
Vol: 1884.7																				
<p><u>Characterization:</u></p> <p>FTIR (ν /cm⁻¹) 3485, 2945, 2293, 1630, 1482, 1445, 1413, 1181, 1061, 971, 946, 915, 817.</p> <p>¹H-NMR (400 MHz, D₂O) δ 1.42 (m, 4H), 1.79 (m, 4H), 2.05 (s, 3H, acetonitrile), 3.10 (m, 4H), 3.31 (s, 18H).</p> <p>¹³C-NMR (100.6 MHz, D₂O) δ 5 (acetonitrile, CH₃), 22 (N⁺-CH₂-CH₂-CH₂-), 25 (N⁺-CH₂-CH₂-CH₂-), 53 (CH₃-N⁺) 66 (N⁺-CH₂-CH₂-CH₂-) 120 (acetonitrile, CN).</p>		<table border="1" style="width: 100%;"> <tr> <td>Z</td> <td>4</td> </tr> <tr> <td>ρ_{calc} / g/cm³</td> <td>1.421</td> </tr> <tr> <td>μ/mm⁻¹</td> <td>4.296</td> </tr> <tr> <td>F(000)</td> <td>832.0</td> </tr> <tr> <td>Radiation</td> <td>MoKα (λ = 0.71073)</td> </tr> <tr> <td>Reflections Collected</td> <td>44615</td> </tr> <tr> <td>Goodness-of-fit on F²</td> <td>1.112</td> </tr> <tr> <td>Final R indexes [I > 2σ (I)]</td> <td>R₁ = 0.0503, wR₂ = 0.1438</td> </tr> <tr> <td>Final R indexes (all data)</td> <td>R₁ = 0.0684, wR₂ = 0.1519</td> </tr> </table>	Z	4	ρ _{calc} / g/cm ³	1.421	μ/mm ⁻¹	4.296	F(000)	832.0	Radiation	MoKα (λ = 0.71073)	Reflections Collected	44615	Goodness-of-fit on F ²	1.112	Final R indexes [I > 2σ (I)]	R ₁ = 0.0503, wR ₂ = 0.1438	Final R indexes (all data)	R ₁ = 0.0684, wR ₂ = 0.1519
Z	4																			
ρ _{calc} / g/cm ³	1.421																			
μ/mm ⁻¹	4.296																			
F(000)	832.0																			
Radiation	MoKα (λ = 0.71073)																			
Reflections Collected	44615																			
Goodness-of-fit on F ²	1.112																			
Final R indexes [I > 2σ (I)]	R ₁ = 0.0503, wR ₂ = 0.1438																			
Final R indexes (all data)	R ₁ = 0.0684, wR ₂ = 0.1519																			

5	Formula: C ₁₄ H ₃₃ I ₂ N ₃ Formula Weight: 403.25 Name: Hexamethonium Iodide Acetonitrile Solvate	<input checked="" type="checkbox"/> Slow evaporation <input type="checkbox"/> Vapor diffusion <input type="checkbox"/> Solvent layer <input type="checkbox"/> Other																		
		Solvent(s)/Other agents: CH ₂ CN..... <input type="checkbox"/> Twinned Temperature: 100 K																		
<p><u>Synthesis:</u></p> <p>Crystallization in specific solvent afforded the solvate adduct</p>		<table border="1"> <tr> <td>a: 9.920</td> <td>α: 90</td> <td>R₁:</td> <td>0.0372</td> </tr> <tr> <td>b: 12.776</td> <td>β: 96.07</td> <td>System:</td> <td>Monoclinic</td> </tr> <tr> <td>c: 16.440</td> <td>γ: 90</td> <td>Space Group:</td> <td>P2₁/n</td> </tr> <tr> <td>Vol: 2071.9</td> <td></td> <td></td> <td></td> </tr> </table>	a: 9.920	α: 90	R ₁ :	0.0372	b: 12.776	β: 96.07	System:	Monoclinic	c: 16.440	γ: 90	Space Group:	P2 ₁ /n	Vol: 2071.9					
a: 9.920	α: 90	R ₁ :	0.0372																	
b: 12.776	β: 96.07	System:	Monoclinic																	
c: 16.440	γ: 90	Space Group:	P2 ₁ /n																	
Vol: 2071.9																				
<p><u>Characterization:</u></p> <p>FTIR (ν /cm⁻¹) 3485, 2945, 2293, 1630, 1482, 1445, 1413, 1181, 1061, 971, 946, 915, 817.</p> <p>¹H-NMR (400 MHz, D₂O) δ 1.43 (m, 4H), 1.82 (m, 4H), 2.06 (s, 3H, acetonitrile), 3.10 (m, 4H), 3.32 (s, 18H).</p> <p>¹³C-NMR (100.6 MHz, D₂O) δ 5 (acetonitrile, CH₃), 22 (N⁺-CH₂-CH₂-CH₂-), 25 (N⁺-CH₂-CH₂-CH₂-CH₂-), 53 (CH₃-N⁺) 67 (N⁺-CH₂-CH₂-CH₂-) 120 (acetonitrile, CN).</p>		<table border="1"> <tr> <td>Z</td> <td>4</td> </tr> <tr> <td>ρ_{calc} / g/cm³</td> <td>1.594</td> </tr> <tr> <td>μ/mm⁻¹</td> <td>3.031</td> </tr> <tr> <td>F(000)</td> <td>976.0</td> </tr> <tr> <td>Radiation</td> <td>MoKα (λ = 0.71073)</td> </tr> <tr> <td>Reflections Collected</td> <td>21599</td> </tr> <tr> <td>Goodness-of-fit on F²</td> <td>0.973</td> </tr> <tr> <td>Final R indexes [I > 2σ (I)]</td> <td>R₁ = 0.0372, wR₂ = 0.0607</td> </tr> <tr> <td>Final R indexes (all data)</td> <td>R₁ = 0.0703, wR₂ = 0.0686</td> </tr> </table>	Z	4	ρ _{calc} / g/cm ³	1.594	μ/mm ⁻¹	3.031	F(000)	976.0	Radiation	MoKα (λ = 0.71073)	Reflections Collected	21599	Goodness-of-fit on F ²	0.973	Final R indexes [I > 2σ (I)]	R ₁ = 0.0372, wR ₂ = 0.0607	Final R indexes (all data)	R ₁ = 0.0703, wR ₂ = 0.0686
Z	4																			
ρ _{calc} / g/cm ³	1.594																			
μ/mm ⁻¹	3.031																			
F(000)	976.0																			
Radiation	MoKα (λ = 0.71073)																			
Reflections Collected	21599																			
Goodness-of-fit on F ²	0.973																			
Final R indexes [I > 2σ (I)]	R ₁ = 0.0372, wR ₂ = 0.0607																			
Final R indexes (all data)	R ₁ = 0.0703, wR ₂ = 0.0686																			
<input checked="" type="checkbox"/> IR <input checked="" type="checkbox"/> ¹ H-NMR <input type="checkbox"/> Other <input type="checkbox"/> UV <input checked="" type="checkbox"/> ¹³ C-NMR 																				

6.3.2. Bis(pyridinium)methylene salts as $-\text{C}(\text{sp}^3)\text{H}_2$ -Tetrel Bond Donors.

Materials.

Compounds and solvents were purchased from Sigma Aldrich and TCI and used without further purification.

Methods.

Data collections for compound **6** was performed at the X-ray diffraction beamline (XRD1) of the Elettra Synchrotron, Trieste (Italy)²². The crystals were dipped in NHV oil (Jena Bioscience, Jena, Germany) and mounted on the goniometer head with kapton loops (MiTeGen, Ithaca, USA). Complete datasets were collected at 100 K (nitrogen stream supplied through an Oxford Cryostream 700 - Oxford Cryosystems Ltd., Oxford, United Kingdom) through the rotating crystal method. The diffraction data were indexed and integrated using XDS.²³ The structures were solved by the dual space algorithm implemented in the SHELXT code.²⁴ Fourier analysis and refinement were performed by the full-matrix least-squares methods based on F^2 implemented in SHELXL (Version 2018/3)²⁵. The Coot program was used for modeling.²⁶ Anisotropic thermal motion refinement has been used for all atoms. Geometric restrains (SAME) have been applied on disordered fragments of d. Hydrogen atoms were included at calculated positions with isotropic Ufactors = $1.2 \times U_{\text{eq}}$ or Ufactors = $1.5 \times U_{\text{eq}}$ for methyl and hydroxyl groups (U_{eq} being the equivalent isotropic thermal factor of the bonded non hydrogen atom).

A suitable crystal of **7** was selected and mounted on a XtaLAB Synergy, Dualflex, HyPix diffractometer. The crystal was kept at 100.00(11) K during data collection. Using Olex2²⁷, the structure was solved with the SHELXS structure solution program using Direct Methods and refined with the SHELXL refinement package using Least Squares minimisation.

²² A. Lausi, M. Polentarutti, S. Onesti, J. R. Plaisier, E. Busetto, G. Bais, L. Barba, A. Cassetta, G. Campi, D. Lamba, A. Pifferi, S. C. Mande, D. D. Sarma, S. M. Sharma, G. Paolucci, *Eur. Phys. J. Plus* **2015**, *130*, 1-8.

²³ W. Kabsch, *Acta Cryst. Section D* **2010**, *66(2)*, 125–132.

²⁴ G. M. Sheldrick, *Acta Cryst. Section A* **2015**, *71*, 3-8.

²⁵ G. M. Sheldrick, *Acta Cryst. Section C* **2015**, *71*, 3-8.

²⁶ P. Emsley, B. Lohkamp, W. G. Scott, K. Cowtan, *Acta Cryst. Section D* **2010**, *66(4)*, 486–501.

²⁷ Dolomanov, O.V., Bourhis, L.J., Gildea, R.J., Howard, J.A.K., Puschmann, H., *J. Appl. Cryst.* **2009** *42*, 339-341.

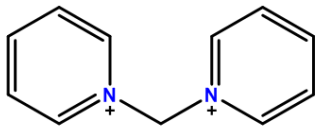
A specimen of **8**, approximate dimensions 0.112 mm x 0.185 mm x 0.212 mm, was used for the X-ray crystallographic analysis. The X-ray intensity data were measured ($\lambda = 1.54178 \text{ \AA}$). A total of 3854 frames were collected. The total exposure time was 0.75 hours. The frames were integrated with the Bruker SAINT software package using a narrow-frame algorithm. The integration of the data using a monoclinic unit cell yielded a total of 38489 reflections to a maximum θ angle of 74.39° (0.80 \AA resolution), of which 3107 were independent (average redundancy 12.388, completeness = 99.5%, $R_{\text{int}} = 2.89\%$, $R_{\text{sig}} = 1.75\%$) and 3030 (97.52%) were greater than $2\sigma(F^2)$. The final cell constants of $a = 13.2862(9) \text{ \AA}$, $b = 6.7076(5) \text{ \AA}$, $c = 18.0470(12) \text{ \AA}$, $\beta = 108.697(2)^\circ$, volume = $1523.45(18) \text{ \AA}^3$, are based upon the refinement of the XYZ-centroids of 9871 reflections above $20 \sigma(I)$ with $7.266^\circ < 2\theta < 148.7^\circ$. Data were corrected for absorption effects using the Numerical Mu Calculated method (SADABS). The ratio of minimum to maximum apparent transmission was 0.494. The calculated minimum and maximum transmission coefficients (based on crystal size) are 0.3722 and 0.7538. The structure was solved and refined using the Bruker SHELXTL Software Package, using the space group $P 1 21/c 1$, with $Z = 4$. The final anisotropic full-matrix least-squares refinement on F2 with 212 variables converged at $R_1 = 2.55\%$, for the observed data and $wR_2 = 7.34\%$ for all data. The goodness-of-fit was 1.326. The largest peak in the final difference electron density synthesis was $0.632 \text{ e}/\text{\AA}^3$ and the largest hole was $-0.630 \text{ e}/\text{\AA}^3$ with an RMS deviation of $0.185 \text{ e}/\text{\AA}^3$. On the basis of the final model, the calculated density was $1.669 \text{ g}/\text{cm}^3$ and $F(000)$, 760 e^- .

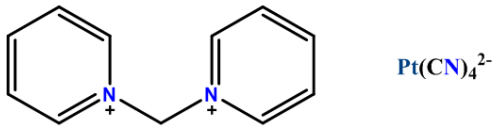
CSD Surveys.

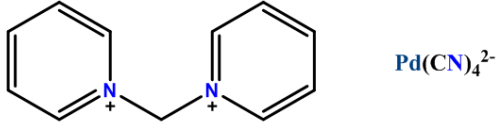
Table 6.3.4. Dipyrindyl methylene structures present on the CSD. In bold structures that present a short contact between the methylene carbon and an electron rich atom (atoms considered N, P, O, S, Se, F, Cl, Br, I). In bold and red entries where the contact is shorter than the sum of their respective vdW radii, in bold and black contacts where the contact is shorter than the sum plus 0.2 \AA . In yellow structures where the nucleophile is a nitrile.

BECSIN	NEKTIG	USEZAU
BECSOT	NELBUB	USEZEY
CIWKIC	NEYJIK	UZALEN
COGKUF	NIDCUY	UZALIR
DEHKEG	NIDDAF	VABBEG
DEHKEG01	NIDDEJ	WERPIV
DOVLAD	NILVOT	XAZPET
DOWVAM	NIRWIU	XUDLAL
ENOPED	NOYRIC	YODFIG
FOQMAZ	NOYROI	YODFOM
GIXWUF	NOYRUO	YOWMOM

GOYCIG	NOYTIE	YUHRIC
GOYCIG01	NUQXED	YUHROI
GOYCIG02	NUQXED01	YUSDIB
HEVDAN	PUBHAV	YUSPEJ
HIFHOT	PUZCIW	YUSPEJ01
HIFHUZ	PUZCOC	ZAHGUK
HIFYEA	RACQAN	ZAVCEE
HIWWEF	RAGSUN	ZAVCII
JAFQEM	RAGTAU	ZAVCOO
JUHQOU	RAHZUX	ZELZAR
LEZBAT	TOPTUN	ZELZEV
LUJCIC	TOPVAV	ZELZIZ
MAKFUZ	TOPVEZ	ZUYYUN
MAYLIH	TOSHIU	
NEKTEC	TOSHOA	

6	Formula: C ₁₁ H ₁₄ I ₂ N ₂ O Formula Weight: 444.04 Name: dipyridyl methylene iodide water solvate	<input checked="" type="checkbox"/> Slow evaporation <input type="checkbox"/> Vapor diffusion <input type="checkbox"/> Solvent layer <input type="checkbox"/> Other		
	 2I, H₂O	Solvent(s)/Other agents: H ₂ O.....		<input type="checkbox"/> Twinned Temperature: 100 K
a: 17.381 α: 90 b: 19.484 β: 90 c: 8.523 γ: 90 Vol: 2886.3		R ₁ : 0.0402 System: Orthorhombic Space Group: Fdd2		
<input checked="" type="checkbox"/> IR <input checked="" type="checkbox"/> ¹ H-NMR <input type="checkbox"/> Other <input type="checkbox"/> UV <input checked="" type="checkbox"/> ¹³ C-NMR 				
<u>Synthesis:</u> The synthesis of dipyridyl methylene iodide is described here: N. A. Tcyrulnikov, R. Varadharajan, A. A. Tikhomorova, M. Pattabiraman, V. Ramamurthy, <i>J. Org. Chem</i> 2019 , 84, 8759-8765.				
<u>Characterization:</u> FTIR (ν /cm ⁻¹): 3062, 1634, 1490, 1182, 830, 672, 561. ¹ H-NMR (400 MHz, D ₂ O) δ 7.43 (2, 2H), 8.29 (m, 4H), 8.82 (t, 2H), 9.31 (m, 4H). ¹³ C-NMR (100.6 MHz, D ₂ O) δ 78, 129, 145, 150		Z	8	
		ρ_{calc} / g/cm³	2.044	
		μ/mm⁻¹	2.967	
		F(000)	1664.0	
		Radiation	MoKα (λ = 0.71073)	
		Reflections Collected	16928	
		Goodness-of-fit on F²	0.995	
		Final R indexes [I > 2σ (I)]	R ₁ = 0.0402, wR ₂ = 0.0928	
		Final R indexes (all data)	R ₁ = 0.0626, wR ₂ = 0.1013	

7	Formula: C ₁₅ H ₁₂ N ₆ Pd Formula Weight: 382.71 Name: dipyriddy methylene tetracyanoplatinate	<input checked="" type="checkbox"/> Slow evaporation <input type="checkbox"/> Vapor diffusion <input type="checkbox"/> Solvent layer <input type="checkbox"/> Other																		
		Solvent(s)/Other agents: H ₂ O..... <input type="checkbox"/> Twinned Temperature: 100 K																		
Synthesis: The synthesis of dipyriddy methylene chloride is described here: A. R. Rudine, M. G. Walker, C. C. Wamser, J. Org. Chem. 2010, 75, 4292–4295. Equimolar dipyriddy methylene chloride and potassium tetracyanoplatinate are dissolved in methanol. The product immediately precipitates from the solution as an amorphous powder. It is filtered off and then redissolved in water to crystallize		<table border="1"> <tr> <td>a: 13.286</td> <td>α: 90</td> <td>R₁:</td> <td>0.0255</td> </tr> <tr> <td>b: 6.7076</td> <td>β: 108.69</td> <td>System:</td> <td>Monoclinic</td> </tr> <tr> <td>c: 18.047</td> <td>γ: 90</td> <td>Space Group:</td> <td>P2₁/c</td> </tr> <tr> <td>Vol: 1523.45</td> <td></td> <td></td> <td></td> </tr> </table>	a: 13.286	α: 90	R ₁ :	0.0255	b: 6.7076	β: 108.69	System:	Monoclinic	c: 18.047	γ: 90	Space Group:	P2 ₁ /c	Vol: 1523.45					
a: 13.286	α: 90	R ₁ :	0.0255																	
b: 6.7076	β: 108.69	System:	Monoclinic																	
c: 18.047	γ: 90	Space Group:	P2 ₁ /c																	
Vol: 1523.45																				
Characterization: FTIR (ν /cm ⁻¹): 3062, 2124, 1634, 1490, 1182, 830, 672, 561. ¹ H-NMR (400 MHz, D ₂ O) δ 7.45 (2, 2H), 8.28 (m, 4H), 8.80 (t, 2H), 9.29 (m, 4H). ¹³ C-NMR (100.6 MHz, D ₂ O) δ 78, 112, 129, 145, 150		<table border="1"> <tr> <td>Z</td> <td>4</td> </tr> <tr> <td>ρ_{calc} / g/cm³</td> <td>1.669</td> </tr> <tr> <td>μ/mm⁻¹</td> <td>9.871</td> </tr> <tr> <td>F(000)</td> <td>760.0</td> </tr> <tr> <td>Radiation</td> <td>MoKα (λ = 0.71073)</td> </tr> <tr> <td>Reflections Collected</td> <td>38489</td> </tr> <tr> <td>Goodness-of-fit on F²</td> <td>1.326</td> </tr> <tr> <td>Final R indexes [I > 2σ (I)]</td> <td>R₁ = 0.0255, wR₂ = 0.0730</td> </tr> <tr> <td>Final R indexes (all data)</td> <td>R₁ = 0.0259, wR₂ = 0.0734</td> </tr> </table>	Z	4	ρ_{calc} / g/cm³	1.669	μ/mm⁻¹	9.871	F(000)	760.0	Radiation	MoKα (λ = 0.71073)	Reflections Collected	38489	Goodness-of-fit on F²	1.326	Final R indexes [I > 2σ (I)]	R ₁ = 0.0255, wR ₂ = 0.0730	Final R indexes (all data)	R ₁ = 0.0259, wR ₂ = 0.0734
Z	4																			
ρ_{calc} / g/cm³	1.669																			
μ/mm⁻¹	9.871																			
F(000)	760.0																			
Radiation	MoKα (λ = 0.71073)																			
Reflections Collected	38489																			
Goodness-of-fit on F²	1.326																			
Final R indexes [I > 2σ (I)]	R ₁ = 0.0255, wR ₂ = 0.0730																			
Final R indexes (all data)	R ₁ = 0.0259, wR ₂ = 0.0734																			

8	Formula: $C_{60}H_{48}N_{24}Pt_4$ Formula Weight: 1885.58 Name: dipyriddy methylene tetracyanopalladiate	<input checked="" type="checkbox"/> Slow evaporation <input type="checkbox"/> Vapor diffusion <input type="checkbox"/> Solvent layer <input type="checkbox"/> Other Solvent(s)/Other agents: H ₂ O..... <input type="checkbox"/> Twinned Temperature: 100 K											
		<table border="1" style="width: 100%; border-collapse: collapse;"> <tr> <td style="padding: 2px;">a: 13.304</td> <td style="padding: 2px;">α: 90</td> <td style="padding: 2px;">R₁: 0.0187</td> </tr> <tr> <td style="padding: 2px;">b: 6.7123</td> <td style="padding: 2px;">β: 138.273</td> <td style="padding: 2px;">System: Monoclinic</td> </tr> <tr> <td style="padding: 2px;">c: 25.6217</td> <td style="padding: 2px;">γ: 90</td> <td style="padding: 2px;">Space Group: P2₁/n</td> </tr> <tr> <td style="padding: 2px;">Vol: 1522.89</td> <td></td> <td></td> </tr> </table>	a: 13.304	α: 90	R ₁ : 0.0187	b: 6.7123	β: 138.273	System: Monoclinic	c: 25.6217	γ: 90	Space Group: P2 ₁ /n	Vol: 1522.89	
a: 13.304	α: 90	R ₁ : 0.0187											
b: 6.7123	β: 138.273	System: Monoclinic											
c: 25.6217	γ: 90	Space Group: P2 ₁ /n											
Vol: 1522.89													
<p><u>Synthesis:</u></p> <p>The synthesis of dipyriddy methylene chloride is described here: A. R. Rudine, M. G. Walker, C. C. Wamser, J. Org. Chem. 2010, 75, 4292–4295.</p> <p>Equimolar dipyriddy methylene chloride and potassium tetracyanopalladiate are dissolved in methanol. The product immediately precipitates from the solution as an amorphous powder. It is filtered off and then redissolved in water to crystallize</p>													
<p><u>Characterization:</u></p> <p>FTIR (ν /cm⁻¹): 3062, 2124, 1634, 1490, 1182, 830, 672, 561.</p> <p>¹H-NMR (400 MHz, D₂O) δ 7.42 (2, 2H), 8.30 (m, 4H), 8.82 (t, 2H), 9.30 (m, 4H).</p> <p>¹³C-NMR (100.6 MHz, D₂O) δ 78, 112, 129, 145, 150</p>													
		Z	1										
		$\rho_{\text{calc}} / \text{g/cm}^3$	2.056										
		μ / mm^{-1}	17.281										
		F(000)	888.0										
		Radiation	MoKα ($\lambda = 0.71073$)										
		Reflections Collected	32558										
		Goodness-of-fit on F ²	1.117										
		Final R indexes [I > 2σ (I)]	R ₁ = 0.0187, wR ₂ = 0.0543										
		Final R indexes (all data)	R ₁ = 0.0203, wR ₂ = 0.0561										

6.3.3. Tetrel Bonds in Choline and Betaine derivatives.

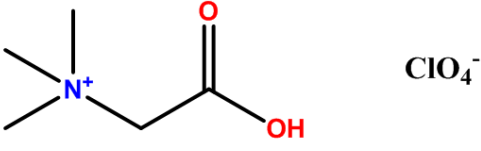
Materials.

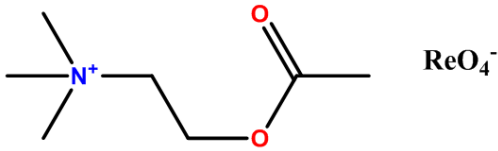
Compounds and solvents were purchased from Sigma Aldrich and TCI and used without further purification.

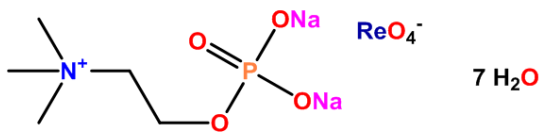
Methods.

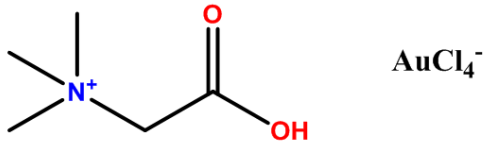
Data collections for compounds **9**, **10** and **14** were performed at the X-ray diffraction beamline (XRD1) of the Elettra Synchrotron, Trieste (Italy). The crystals were dipped in NHV oil (Jena Bioscience, Jena, Germany) and mounted on the goniometer head with kapton loops (MiTeGen, Ithaca, USA). Complete datasets were collected at 100 K (nitrogen stream supplied through an Oxford Cryostream 700 - Oxford Cryosystems Ltd., Oxford, United Kingdom) through the rotating crystal method. The diffraction data were indexed and integrated using XDS. The structures were solved by the dual space algorithm implemented in the SHELXT code. Fourier analysis and refinement were performed by the full-matrix least-squares methods based on F^2 implemented in SHELXL (Version 2018/3). The Coot program was used for modeling. Anisotropic thermal motion refinement has been used for all atoms. Geometric restrains (SAME) have been applied on disordered fragments of d. Hydrogen atoms were included at calculated positions with isotropic Ufactors = $1.2 \times U_{eq}$ or Ufactors = $1.5 \times U_{eq}$ for methyl and hydroxyl groups (U_{eq} being the equivalent isotropic thermal factor of the bonded non hydrogen atom).

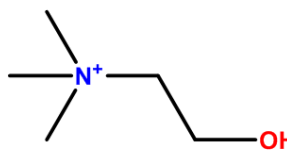
The single crystal data of all the remaining structures displayed in this work were collected at Bruker SMART APEX II CCD area detector diffractometer at 100 K. Data collection, unit cell refinement and data reduction were performed using Bruker SAINT. The structure was solved by direct methods using SHELXT and refined by full-matrix least-squares on F^2 with anisotropic displacement parameters for the non-H atoms using SHELXL-2016/6. Absorption correction was performed based on multi-scan procedure using SADABS. Structure analysis was aided by use of the programs PLATON. The hydrogen atoms were calculated in ideal positions with isotropic displacement parameters set to $1.2 \times U_{eq}$ of the attached atom.

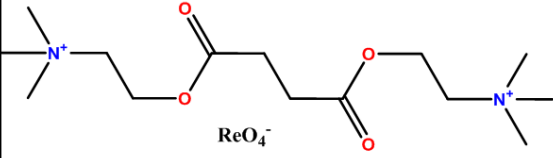
9	Formula: C ₅ H ₁₄ ClNO ₆ Formula Weight: 235.62 Name: Betaine perchlorate	<input checked="" type="checkbox"/> Slow evaporation <input type="checkbox"/> Vapor diffusion <input type="checkbox"/> Solvent layer <input type="checkbox"/> Other																		
		Solvent(s)/Other agents: i-PrOH.....	<input type="checkbox"/> Twinned Temperature: 100 K																	
a: 9.6760 α: 90 b: 9.1950 β: 110.53 c: 12.011 γ: 90 Vol: 1000.84		R ₁ : 0.0378 System: Monoclinic Space Group: P2 ₁ /c																		
<input checked="" type="checkbox"/> IR <input checked="" type="checkbox"/> ¹ H-NMR <input type="checkbox"/> Other <input type="checkbox"/> UV <input checked="" type="checkbox"/> ¹³ C-NMR 																				
<u>Synthesis:</u> 0.1 mmol of betaine are dissolved in 3 mL of isopropanol. To this solution an equimolar quantity of HClO ₄ is added. The solution is let slowly evaporate over a period of weeks.																				
<u>Characterization:</u> FTIR (ν /cm ⁻¹) 1718, 1637, 1476, 1377, 1107, 1079, 993, 846. ¹ H-NMR (400 MHz, D ₂ O) δ 3.22 (s, 9H), 3.85 (s, 2H). ¹³ C-NMR (100.6 MHz, D ₂ O) δ 53, 66, 169.		<table border="1" style="width: 100%; border-collapse: collapse;"> <tr> <td style="text-align: center;">Z</td> <td style="text-align: center;">4</td> </tr> <tr> <td style="text-align: center;">ρ_{calc} / g/cm³</td> <td style="text-align: center;">1.564</td> </tr> <tr> <td style="text-align: center;">μ/mm⁻¹</td> <td style="text-align: center;">0.271</td> </tr> <tr> <td style="text-align: center;">F(000)</td> <td style="text-align: center;">496.0</td> </tr> <tr> <td style="text-align: center;">Radiation</td> <td style="text-align: center;">MoKα (λ = 0.71073)</td> </tr> <tr> <td style="text-align: center;">Reflections Collected</td> <td style="text-align: center;">18487</td> </tr> <tr> <td style="text-align: center;">Goodness-of-fit on F²</td> <td style="text-align: center;">1.037</td> </tr> <tr> <td style="text-align: center;">Final R indexes [I > 2σ (I)]</td> <td style="text-align: center;">R₁ = 0.0378, wR₂ = 0.1004</td> </tr> <tr> <td style="text-align: center;">Final R indexes (all data)</td> <td style="text-align: center;">R₁ = 0.0395, wR₂ = 0.1019</td> </tr> </table>	Z	4	ρ_{calc} / g/cm³	1.564	μ/mm⁻¹	0.271	F(000)	496.0	Radiation	MoKα (λ = 0.71073)	Reflections Collected	18487	Goodness-of-fit on F²	1.037	Final R indexes [I > 2σ (I)]	R ₁ = 0.0378, wR ₂ = 0.1004	Final R indexes (all data)	R ₁ = 0.0395, wR ₂ = 0.1019
Z	4																			
ρ_{calc} / g/cm³	1.564																			
μ/mm⁻¹	0.271																			
F(000)	496.0																			
Radiation	MoKα (λ = 0.71073)																			
Reflections Collected	18487																			
Goodness-of-fit on F²	1.037																			
Final R indexes [I > 2σ (I)]	R ₁ = 0.0378, wR ₂ = 0.1004																			
Final R indexes (all data)	R ₁ = 0.0395, wR ₂ = 0.1019																			

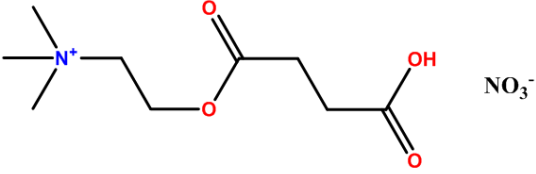
10	Formula: $C_7H_{16}NO_6Re$ Formula Weight: 396.41 Name: acetylcholine perrhenate	<input checked="" type="checkbox"/> Slow evaporation <input type="checkbox"/> Vapor diffusion <input type="checkbox"/> Solvent layer <input type="checkbox"/> Other Solvent(s)/Other agents: i-PrOH..... <input type="checkbox"/> Twinned Temperature: 100 K																		
		a: 7.4570 α: 79.60 R ₁ : 0.0163 b: 8.8910 β: 81.71 System: Triclinic c: 18.993 γ: 67.84 Space Group: P-1 Vol: 1143.05																		
Synthesis: To 0.1 mmol of acetylcholine chloride in 3 mL of isopropanol an equimolar amount of AgReO ₄ is added. A whitish-gray precipitate readily forms and is filtered out. The filtered solution is then let slowly evaporate over a period of weeks.																				
Characterization: FTIR (ν / cm^{-1}) 1732, 1475, 1229, 1052, 893, 608. ¹ H-NMR (400 MHz, D ₂ O) δ 2.13 (s, 3H), 3.20 (s, 9H), 3.72 (m, 2H), 4.53 (m, 2H). ¹³ C-NMR (100.6 MHz, D ₂ O) δ 20, 54, 58, 65, 173.		<table border="1" style="width: 100%; border-collapse: collapse;"> <tr> <td style="text-align: center;">Z</td> <td style="text-align: center;">4</td> </tr> <tr> <td style="text-align: center;">$\rho_{\text{calc}} / \text{g/cm}^3$</td> <td style="text-align: center;">2.304</td> </tr> <tr> <td style="text-align: center;">μ / mm^{-1}</td> <td style="text-align: center;">7.418</td> </tr> <tr> <td style="text-align: center;">F(000)</td> <td style="text-align: center;">752.0</td> </tr> <tr> <td style="text-align: center;">Radiation</td> <td style="text-align: center;">MoKα ($\lambda = 0.71073$)</td> </tr> <tr> <td style="text-align: center;">Reflections Collected</td> <td style="text-align: center;">51377</td> </tr> <tr> <td style="text-align: center;">Goodness-of-fit on F²</td> <td style="text-align: center;">1.082</td> </tr> <tr> <td style="text-align: center;">Final R indexes [I > 2σ (I)]</td> <td style="text-align: center;">R₁ = 0.0163, wR₂ = 0.0408</td> </tr> <tr> <td style="text-align: center;">Final R indexes (all data)</td> <td style="text-align: center;">R₁ = 0.0166, wR₂ = 0.0410</td> </tr> </table>	Z	4	$\rho_{\text{calc}} / \text{g/cm}^3$	2.304	μ / mm^{-1}	7.418	F(000)	752.0	Radiation	MoK α ($\lambda = 0.71073$)	Reflections Collected	51377	Goodness-of-fit on F²	1.082	Final R indexes [I > 2σ (I)]	R ₁ = 0.0163, wR ₂ = 0.0408	Final R indexes (all data)	R ₁ = 0.0166, wR ₂ = 0.0410
Z	4																			
$\rho_{\text{calc}} / \text{g/cm}^3$	2.304																			
μ / mm^{-1}	7.418																			
F(000)	752.0																			
Radiation	MoK α ($\lambda = 0.71073$)																			
Reflections Collected	51377																			
Goodness-of-fit on F²	1.082																			
Final R indexes [I > 2σ (I)]	R ₁ = 0.0163, wR ₂ = 0.0408																			
Final R indexes (all data)	R ₁ = 0.0166, wR ₂ = 0.0410																			

11	Formula: $C_5H_{15}NO_8PReNa_{0.5}Ag_{0.5}Cl_{1.5}$ Formula Weight: 532.51 Name: phosphocholine perrhenate sodium oxide	<input checked="" type="checkbox"/> Slow evaporation <input type="checkbox"/> Vapor diffusion <input type="checkbox"/> Solvent layer <input type="checkbox"/> Other Solvent(s)/Other agents: i-PrOH.....																		
		<input type="checkbox"/> Twinned Temperature: 100 K a: 6.4011 α : 89.629 R_1 : 0.0381 b: 8.7029 β : 84.275 System: Triclinic c: 18.0549 γ : 85.507 Space Group: P1 Vol: 997.716																		
<u>Synthesis:</u> To 0.1 mmol of phosphocholine chloride sodium salt in 3 mL of isopropanol an equimolar amount of $AgReO_4$ is added. A withish-gray precipitate readily forms and is filtered out. The filtered solution is then let sloly evaporate over a period of weeks.																				
<u>Characterization:</u> FTIR (ν / cm^{-1}) 1650, 1477, 1087, 955, 897, 747. 1H -NMR (400 MHz, D_2O) δ 3.18 (s, 9H), 3.56 (m, 2H), 4.11 (m, 2H). ^{13}C -NMR (100.6 MHz, D_2O) δ 54, 58, 67.		<table border="1" style="width: 100%; border-collapse: collapse;"> <tr> <td style="text-align: center;">Z</td> <td style="text-align: center;">4</td> </tr> <tr> <td style="text-align: center;">$\rho_{calc} / g/cm^3$</td> <td style="text-align: center;">3.681</td> </tr> <tr> <td style="text-align: center;">μ/mm^{-1}</td> <td style="text-align: center;">13.756</td> </tr> <tr> <td style="text-align: center;">F(000)</td> <td style="text-align: center;">1042.0</td> </tr> <tr> <td style="text-align: center;">Radiation</td> <td style="text-align: center;">MoKα ($\lambda = 0.71073$)</td> </tr> <tr> <td style="text-align: center;">Reflections Collected</td> <td style="text-align: center;">22696</td> </tr> <tr> <td style="text-align: center;">Goodness-of-fit on F²</td> <td style="text-align: center;">1.070</td> </tr> <tr> <td style="text-align: center;">Final R indexes [I > 2σ (I)]</td> <td style="text-align: center;">$R_1 = 0.0381, wR_2 = 0.1194$</td> </tr> <tr> <td style="text-align: center;">Final R indexes (all data)</td> <td style="text-align: center;">$R_1 = 0.0488, wR_2 = 0.1432$</td> </tr> </table>	Z	4	$\rho_{calc} / g/cm^3$	3.681	μ/mm^{-1}	13.756	F(000)	1042.0	Radiation	MoK α ($\lambda = 0.71073$)	Reflections Collected	22696	Goodness-of-fit on F²	1.070	Final R indexes [I > 2σ (I)]	$R_1 = 0.0381, wR_2 = 0.1194$	Final R indexes (all data)	$R_1 = 0.0488, wR_2 = 0.1432$
Z	4																			
$\rho_{calc} / g/cm^3$	3.681																			
μ/mm^{-1}	13.756																			
F(000)	1042.0																			
Radiation	MoK α ($\lambda = 0.71073$)																			
Reflections Collected	22696																			
Goodness-of-fit on F²	1.070																			
Final R indexes [I > 2σ (I)]	$R_1 = 0.0381, wR_2 = 0.1194$																			
Final R indexes (all data)	$R_1 = 0.0488, wR_2 = 0.1432$																			

12	Formula: C ₅ H ₁₁ NO ₂ AuCl ₄ Formula Weight: 400.24 Name: betaine tetrachlorido aurate	<input checked="" type="checkbox"/> Slow evaporation <input type="checkbox"/> Vapor diffusion <input type="checkbox"/> Solvent layer <input type="checkbox"/> Other																	
		Solvent(s)/Other agents: H ₂ O <input type="checkbox"/> Twinned Temperature: 298 K	a: 15.3561 α: 101.465 R ₁ : 0.0563 b: 15.9569 β: 107.769 System: Triclinic c: 20.2908 γ: 94.263 Space Group: P-1 Vol: 4591.5																
<input checked="" type="checkbox"/> IR <input checked="" type="checkbox"/> ¹ H-NMR <input type="checkbox"/> Other <input type="checkbox"/> UV <input checked="" type="checkbox"/> ¹³ C-NMR 																			
<u>Synthesis:</u> 0.1 mmol of betaine are dissolved in 3 mL of water. To this solution an equimolar quantity of HAuCl ₄ is added. The solution is let slowly evaporate over a period of weeks.																			
<u>Characterization:</u> FTIR (ν /cm ⁻¹) 1727, 1632, 1470, 1224, 953, 882. ¹ H-NMR (400 MHz, D ₂ O) δ 3.21 (s, 9H), 3.84 (s, 2H). ¹³ C-NMR (100.6 MHz, D ₂ O) δ 53, 66, 169.		<table border="1" style="width: 100%; border-collapse: collapse;"> <tr> <td style="text-align: center;">Z</td> <td style="text-align: center;">15</td> </tr> <tr> <td style="text-align: center;">ρ_{calc} / g/cm³</td> <td style="text-align: center;">2.171</td> </tr> <tr> <td style="text-align: center;">μ/mm⁻¹</td> <td style="text-align: center;">10.303</td> </tr> <tr> <td style="text-align: center;">F(000)</td> <td style="text-align: center;">2820.0</td> </tr> <tr> <td style="text-align: center;">Radiation</td> <td style="text-align: center;">MoKα (λ = 0.71073)</td> </tr> <tr> <td style="text-align: center;">Reflections Collected</td> <td style="text-align: center;">60025</td> </tr> <tr> <td style="text-align: center;">Goodness-of-fit on F²</td> <td style="text-align: center;">1.052</td> </tr> <tr> <td style="text-align: center;">Final R indexes [I > 2σ (I)]</td> <td style="text-align: center;">R₁ = 0.0563, wR₂ = 0.1513</td> </tr> <tr> <td style="text-align: center;">Final R indexes (all data)</td> <td style="text-align: center;">R₁ = 0.1123, wR₂ = 0.2080</td> </tr> </table>	Z	15	ρ_{calc} / g/cm³	2.171	μ/mm⁻¹	10.303	F(000)	2820.0	Radiation	MoKα (λ = 0.71073)	Reflections Collected	60025	Goodness-of-fit on F²	1.052	Final R indexes [I > 2σ (I)]	R ₁ = 0.0563, wR ₂ = 0.1513	Final R indexes (all data)
Z	15																		
ρ_{calc} / g/cm³	2.171																		
μ/mm⁻¹	10.303																		
F(000)	2820.0																		
Radiation	MoKα (λ = 0.71073)																		
Reflections Collected	60025																		
Goodness-of-fit on F²	1.052																		
Final R indexes [I > 2σ (I)]	R ₁ = 0.0563, wR ₂ = 0.1513																		
Final R indexes (all data)	R ₁ = 0.1123, wR ₂ = 0.2080																		

13	Formula: C ₅ H ₁₃ ONAuCl ₄ Formula Weight: 442.76 Name: Choline tetrachloridoaurate	<input checked="" type="checkbox"/> Slow evaporation <input type="checkbox"/> Vapor diffusion <input type="checkbox"/> Solvent layer <input type="checkbox"/> Other Solvent(s)/Other agents: i H ₂ O																		
	 AuCl₄⁻	<input type="checkbox"/> Twinned Temperature: 100 K <hr/> <table style="width: 100%; border-collapse: collapse;"> <tr> <td style="width: 33%;">a: 11.3912</td> <td style="width: 33%;">α: 101.91</td> <td style="width: 33%;">R₁: 0.0324</td> </tr> <tr> <td>b: 16.1886</td> <td>β: 98.588</td> <td>System: Triclinic</td> </tr> <tr> <td>c: 20.281</td> <td>γ: 91.047</td> <td>Space Group: P-1</td> </tr> <tr> <td>Vol: 2071.9</td> <td></td> <td></td> </tr> </table> <hr/> <input checked="" type="checkbox"/> IR <input checked="" type="checkbox"/> ¹ H-NMR <input type="checkbox"/> Other <input type="checkbox"/> UV <input checked="" type="checkbox"/> ¹³ C-NMR 	a: 11.3912	α: 101.91	R ₁ : 0.0324	b: 16.1886	β: 98.588	System: Triclinic	c: 20.281	γ: 91.047	Space Group: P-1	Vol: 2071.9								
a: 11.3912	α: 101.91	R ₁ : 0.0324																		
b: 16.1886	β: 98.588	System: Triclinic																		
c: 20.281	γ: 91.047	Space Group: P-1																		
Vol: 2071.9																				
<u>Synthesis:</u> 0.1 mmol of choline chloride are dissolved in 3 mL of water. To this solution an equimolar quantity of HAuCl ₄ is added. The solution is let slowly evaporate over a period of weeks.																				
<u>Characterization:</u> FTIR (ν /cm ⁻¹) 1726, 1633, 1471, 1241, 1080, 949, 965. ¹ H-NMR (400 MHz, D ₂ O) δ 3.17 (s, 9H), 3.50 (m, 2H), 4.05 (m, 2H). ¹³ C-NMR (100.6 MHz, D ₂ O) δ 54, 56, 67.		<table border="1" style="width: 100%; border-collapse: collapse;"> <tr> <td style="text-align: center;">Z</td> <td style="text-align: center;">12</td> </tr> <tr> <td style="text-align: center;">ρ_{calc} / g/cm³</td> <td style="text-align: center;">2.441</td> </tr> <tr> <td style="text-align: center;">μ/mm⁻¹</td> <td style="text-align: center;">13.060</td> </tr> <tr> <td style="text-align: center;">F(000)</td> <td style="text-align: center;">2470.0</td> </tr> <tr> <td style="text-align: center;">Radiation</td> <td style="text-align: center;">MoKα (λ = 0.71073)</td> </tr> <tr> <td style="text-align: center;">Reflections Collected</td> <td style="text-align: center;">61235</td> </tr> <tr> <td style="text-align: center;">Goodness-of-fit on F²</td> <td style="text-align: center;">1.082</td> </tr> <tr> <td style="text-align: center;">Final R indexes [I > 2σ (I)]</td> <td style="text-align: center;">R₁ = 0.0324, wR₂ = 0.0584</td> </tr> <tr> <td style="text-align: center;">Final R indexes (all data)</td> <td style="text-align: center;">R₁ = 0.0540, wR₂ = 0.0651</td> </tr> </table>	Z	12	ρ_{calc} / g/cm³	2.441	μ/mm⁻¹	13.060	F(000)	2470.0	Radiation	MoKα (λ = 0.71073)	Reflections Collected	61235	Goodness-of-fit on F²	1.082	Final R indexes [I > 2σ (I)]	R ₁ = 0.0324, wR ₂ = 0.0584	Final R indexes (all data)	R ₁ = 0.0540, wR ₂ = 0.0651
Z	12																			
ρ_{calc} / g/cm³	2.441																			
μ/mm⁻¹	13.060																			
F(000)	2470.0																			
Radiation	MoKα (λ = 0.71073)																			
Reflections Collected	61235																			
Goodness-of-fit on F²	1.082																			
Final R indexes [I > 2σ (I)]	R ₁ = 0.0324, wR ₂ = 0.0584																			
Final R indexes (all data)	R ₁ = 0.0540, wR ₂ = 0.0651																			

14	Formula: $C_{14}H_{30}N_2O_{12}Re_2$ Formula Weight: 790.80 Name: Succinylcholine perrhenate	<input checked="" type="checkbox"/> Slow evaporation <input type="checkbox"/> Vapor diffusion <input type="checkbox"/> Solvent layer <input type="checkbox"/> Other																		
		Solvent(s)/Other agents: i-PrOH..... <input type="checkbox"/> Twinned Temperature: 100 K																		
		<table border="0" style="width: 100%;"> <tr> <td>a: 6.5700</td> <td>α: 90</td> <td style="border-left: 1px dashed black;">R₁: 0.0617</td> </tr> <tr> <td>b: 12.050</td> <td>β: 90.05</td> <td style="border-left: 1px dashed black;">System: Monoclinic</td> </tr> <tr> <td>c: 14.342</td> <td>γ: 90</td> <td style="border-left: 1px dashed black;">Space Group: P2₁/c</td> </tr> <tr> <td colspan="2">Vol: 1135.4</td> <td style="border-left: 1px dashed black;"></td> </tr> </table>	a: 6.5700	α : 90	R ₁ : 0.0617	b: 12.050	β : 90.05	System: Monoclinic	c: 14.342	γ : 90	Space Group: P2 ₁ /c	Vol: 1135.4								
a: 6.5700	α : 90	R ₁ : 0.0617																		
b: 12.050	β : 90.05	System: Monoclinic																		
c: 14.342	γ : 90	Space Group: P2 ₁ /c																		
Vol: 1135.4																				
		<input checked="" type="checkbox"/> IR <input checked="" type="checkbox"/> ¹ H-NMR <input type="checkbox"/> Other <input type="checkbox"/> UV <input checked="" type="checkbox"/> ¹³ C-NMR 																		
<u>Synthesis:</u> To 0.1 mmol of succinylcholine chloride in 3 mL of isopropanol an equimolar amount of AgReO ₄ is added. A whitish-gray precipitate readily forms and is filtered out. The filtered solution is then slowly evaporated over a period of weeks.																				
<u>Characterization:</u> FTIR (ν /cm ⁻¹) 1722, 1477, 1312, 1160, 900, 797. ¹ H-NMR (400 MHz, D ₂ O) δ 2.76 (s, 4H), 3.20 (s, 18H), 3.73 (m, 4H), 4.58 (m, 4H). ¹³ C-NMR (100.6 MHz, D ₂ O) δ 29, 54, 59, 65, 174.		<table border="1" style="width: 100%; border-collapse: collapse;"> <tr> <td style="text-align: center;">Z</td> <td style="text-align: center;">2</td> </tr> <tr> <td style="text-align: center;">ρ_{calc} / g/cm³</td> <td style="text-align: center;">2.313</td> </tr> <tr> <td style="text-align: center;">μ/mm⁻¹</td> <td style="text-align: center;">7.467</td> </tr> <tr> <td style="text-align: center;">F(000)</td> <td style="text-align: center;">748.0</td> </tr> <tr> <td style="text-align: center;">Radiation</td> <td style="text-align: center;">MoKα (λ = 0.71073)</td> </tr> <tr> <td style="text-align: center;">Reflections Collected</td> <td style="text-align: center;">23225</td> </tr> <tr> <td style="text-align: center;">Goodness-of-fit on F²</td> <td style="text-align: center;">1.232</td> </tr> <tr> <td style="text-align: center;">Final R indexes [I > 2σ (I)]</td> <td style="text-align: center;">R₁ = 0.0617, wR₂ = 0.1865</td> </tr> <tr> <td style="text-align: center;">Final R indexes (all data)</td> <td style="text-align: center;">R₁ = 0.0697, wR₂ = 0.1916</td> </tr> </table>	Z	2	ρ_{calc} / g/cm³	2.313	μ/mm⁻¹	7.467	F(000)	748.0	Radiation	MoK α (λ = 0.71073)	Reflections Collected	23225	Goodness-of-fit on F²	1.232	Final R indexes [I > 2σ (I)]	R ₁ = 0.0617, wR ₂ = 0.1865	Final R indexes (all data)	R ₁ = 0.0697, wR ₂ = 0.1916
Z	2																			
ρ_{calc} / g/cm³	2.313																			
μ/mm⁻¹	7.467																			
F(000)	748.0																			
Radiation	MoK α (λ = 0.71073)																			
Reflections Collected	23225																			
Goodness-of-fit on F²	1.232																			
Final R indexes [I > 2σ (I)]	R ₁ = 0.0617, wR ₂ = 0.1865																			
Final R indexes (all data)	R ₁ = 0.0697, wR ₂ = 0.1916																			

15	Formula: C ₉ H ₁₈ N ₂ O ₇ Formula Weight: 266.25 Name: succinylmonocholine nitrate	<input checked="" type="checkbox"/> Slow evaporation <input type="checkbox"/> Vapor diffusion <input type="checkbox"/> Solvent layer <input type="checkbox"/> Other Solvent(s)/Other agents: i-PrOH..... <input type="checkbox"/> Twinned Temperature: 100 K																			
		a: 8.701 α: 90 b: 14.128 β: 98.97 c: 10.250 γ: 90 Vol: 1245.2	R ₁ : 0.0408 System: Monoclinic Space Group: P2 ₁ /c																		
Synthesis: To 0.1 mmol of succinylcholine chloride in 3 mL of isopropanol an equimolar amount of silver nitrate is added. A whitish-gray precipitate readily forms and is filtered out. The filtered solution is then let slowly evaporate over a period of weeks.																					
Characterization: FTIR (ν /cm ⁻¹) 1679, 1408, 1304, 1197, 1175, 907, 635. ¹ H-NMR (400 MHz, D ₂ O) δ 2.61 (m, 2H), 2.78 (m, 2H), 3.20 (s, 9H), 3.73 (m, 2H), 4.54 (m, 2H). ¹³ C-NMR (100.6 MHz, D ₂ O) δ 29, 55, 60, 66, 172, 174.		<table border="1"> <tr> <td style="text-align: center;">Z</td> <td style="text-align: center;">2</td> </tr> <tr> <td style="text-align: center;">ρ_{calc} / g/cm³</td> <td style="text-align: center;">1.421</td> </tr> <tr> <td style="text-align: center;">μ/mm⁻¹</td> <td style="text-align: center;">0.123</td> </tr> <tr> <td style="text-align: center;">F(000)</td> <td style="text-align: center;">568.0</td> </tr> <tr> <td style="text-align: center;">Radiation</td> <td style="text-align: center;">MoKα (λ = 0.71073)</td> </tr> <tr> <td style="text-align: center;">Reflections Collected</td> <td style="text-align: center;">6577</td> </tr> <tr> <td style="text-align: center;">Goodness-of-fit on F²</td> <td style="text-align: center;">0.946</td> </tr> <tr> <td style="text-align: center;">Final R indexes [I > 2σ (I)]</td> <td style="text-align: center;">R₁ = 0.0408, wR₂ = 0.0769</td> </tr> <tr> <td style="text-align: center;">Final R indexes (all data)</td> <td style="text-align: center;">R₁ = 0.0703, wR₂ = 0.0863</td> </tr> </table>		Z	2	ρ_{calc} / g/cm³	1.421	μ/mm⁻¹	0.123	F(000)	568.0	Radiation	MoKα (λ = 0.71073)	Reflections Collected	6577	Goodness-of-fit on F²	0.946	Final R indexes [I > 2σ (I)]	R ₁ = 0.0408, wR ₂ = 0.0769	Final R indexes (all data)	R ₁ = 0.0703, wR ₂ = 0.0863
Z	2																				
ρ_{calc} / g/cm³	1.421																				
μ/mm⁻¹	0.123																				
F(000)	568.0																				
Radiation	MoKα (λ = 0.71073)																				
Reflections Collected	6577																				
Goodness-of-fit on F²	0.946																				
Final R indexes [I > 2σ (I)]	R ₁ = 0.0408, wR ₂ = 0.0769																				
Final R indexes (all data)	R ₁ = 0.0703, wR ₂ = 0.0863																				

6.4. Beyond the *p* Block.

Contributions:

6.4.1. Tetrachloridoaurate as an Effective Anion...Anion Coinage Bond Donor.

AD, AP and GR designed the experiments.

AD, AP and MU performed the crystallizations and characterization.

AD solved and refined the X-ray structures.

GT oversaw the crystallographic characterization.

AF performed and interpreted the calculations.

AD, AP and GR interpreted the results and performed CSD surveys.

All the above mentioned authors contributed to the manuscript.

6.4.2. The fringe behaviour of Group VIII atoms in the higher oxidation state.

GR designed the experiments.

AD, AP and MC performed the experiments and spectroscopic characterization.

AD solved and refined the X-ray structures.

GT oversaw the crystallographic characterization.

SB performed SS-NMR.

AF performed and interpreted the calculations.

AD, AP, MC and GR interpreted the results and performed CSD surveys.

All the above mentioned authors contributed to the manuscript.

6.4.1. Tetrachloridoaurate as an Effective Anion...Anion Coinage Bond Donor.

Materials.

Compounds and solvents were purchased from Sigma Aldrich and TCI and used without further purification.

CSD Survey.

Table 6.4.1. Number of structures in the CSD containing gold(III) anions.

Anion	Structures in CSD ^a	Hits displaying close contact (percentage) ^b
AuCl ₄ ⁻	354	103 (29%)
AuBr ₄ ⁻	71	12 (17%)
AuCN ₄ ⁻	56	19 (34%)

^a Total number of structures in the CSD containing the respective anion. ^b Number of structures displaying a π -hole CiB, namely an Au...Nu close contact between the gold atom and a nucleophile (Nu = N, P, O, S, Se, F, Cl, Br, I. Cl/Br/C–Au...Nu angles spanning the range 80-100°). The van der Waals radius for Gold(III) used for this survey is assumed 210 pm^[4]. The percentage of total structures displaying a close contact is indicated in brackets.

Table 6.4.2. REFCODEs of CSD structure containing the AuCl₄⁻ anion. In bold, the structures displaying an Au...Nu CiB (Nu=N, P, O, S, Se, F, Cl, Br, I; Cl–Au...Nu angles in the range 80-100°).

AZOREO01	BIHXIC18	GALGEI	KUDNUS	PPOHAU01	UKAZUD
KOVVOJ	BIJBUU	GAZSEH	KUFMUU	PUHYIB	UKUXEF
ROQQAR01	BOFSEV	GEGNEL	KUQFOS	PUYVUC	UKUXIJ
ROQQEV01	BOGBIJ	GEHSOB	LAWFIY	QAFYII	ULIYUL
ZUKTEH	BOKFIS	GEHSOB01	LAWLUT	QAFYOO	UPEWES
ZUKTIL	BOKQOK	GEJVOI	LAYQAF	QAFYOO01	UQIBAY
AFOWAV	BONFEQ	GEJVUO	LAYQAF01	QAFYUU	UQIBIG
AHIWEV	BTURAN	GIFBEC	LIHHIT	QAFZAB	VAJMOK
AHIYEX	BUHZUB	GINHAP	LOBZEI	QAFZIJ	VAQHOM
AHODUY	BUVVEU	GOGDIQ	LONBEY	QAFZUV	VEJSAE

AHOFOU	BUXDAA	GOLLUP	LONBOI	QEKGUI	VEPMUA
AHOGEL	BUYMUD	GOLRIJ	LUFXER	QEKHAP	VEVGAE
AHOGOUB	CAWVON	GOLSEG	LUHFEB	QINQUZ	VEVGAE01
AHOGOVB	CEMVEY	GOQSOU	LUHFEB01	QIXVEA	VIMFUS
AHOGUB	CERMOD	GOXCEB	MAMHAL	QOCVUB	VIWKOB
ALEMUA	CESMUJ	GUBJIY	MBIAUC	QOCWAI	VUFXAW
ALIPIV	CESNAQ	HDMAAU	MEDDAA	QOTHOX	VUFXEA
ASABAX	CETWUT	HDMAAU01	MEXVOC	QOTKAM	VUNZAH
ASABEB	CEWREC	HESWOU	MEXVUI	QQQHDV	VUXPOT
ASABIF	CICBIZ	HEWTUZ	MIHSOL	QQQHDY	VUYREM
ASABOL	CISZAF	HEYVEN	MIYYIF	QUQMUK	WAVKEM
ASACAY	CITKIA	HOFZAD	MUJHII	QUQNOF	WIYJEW
ASACEC	CITKOG	HORVIV	MUPHAH	QUQNOF01	WOMXAY
ASACIG	CITKUM	HYPXAM	MUPHIP	QUQNUL	WONREZ
ASACOM	COGBIJ	IBESIT	MUPHOV	QUQPAT	WUNZAI
AVAVAV	CUZSOF	ICOMIX	NENNIE	QUQPEX	WUNZEM
AXEPEZ	DEDKUS	IDAQIO	NEYHAA	QUQPEX01	XACRIF
AYATEB	DILJIR	IJUCOH	NIBWEB	QUQPIB	XEMBEX
AZOHII	DIWXEP	IVIJEC	NIYTAS	QUQPOH	XIYSIJ
AZOHOO	DIWYOA	IVIJIG	NOKREM	RADLEN	XIYSOP
AZOHOO01	DIWYUG	IVOMOX	NUBJID	RAZBAX	XIZDIW
AZOREO	DONYOU	IVOMUD	NUBJID01	RAZBEB	XIZXEL
AZUZOM	DUBVUT	JADVOC	NUWRIG	RENHAT	XUNBAJ
BAFKEA	DULFAS	JEBGUS	NUWRIG01	RIWZAB	YEDMUR
BALGUQ	DULFEW	JEFFAC	NUWRIG02	RIXCOQ	YEDZOZ
BALGUQ10	DUMGIC	JEYDEZ	OBUHAX	ROQQAR	YEDZUF
BAMWUK	DUYCUV	JEYVOY	OCUSAI	ROQQEV	YEFBAP
BECSOT	EBOZIF	JEYVUE	OCUSOW	SETLOT	YEYCIR
BENYAU	EBOZOL	JIFREV	OHEJIV	SEWYEA	YEYDAK
BEQQUL	EBOZUR	JOTQOY	OHEJOB	SEWYIE	YIHHUU
BEQRAS	EGOWOO	JOTQOY01	OKALUH	SEWYOK	YIHJEG
BIHXIC	EKIPEU	JOTQOY02	OWIPER	SOKBOM	YIHJOQ
BIHXIC01	EPECOS	JOTQOY03	OWIPOB	SOKBUS	ZAKXIS
BIHXIC02	EPECUY	JOTQUE	OWIQES	SOKCAZ	ZARDUU
BIHXIC03	EQICAJ	JOTQUE01	OWIZIF	SOQXOL	ZATHUX
BIHXIC04	EREGIT	KAJSIA	OWIZOL	SOXYUA	ZELLEJ
BIHXIC05	EREGOZ	KAMPIZ	OWIZUR	SOZFUI	ZEQPES
BIHXIC06	EYIDEV	KAQXIK	OWOBEJ	SUWVIR	ZUBDEF
BIHXIC07	FEDVAN	KAVMUS	OXOGOZ02	TARHAW	ZZZDXA
BIHXIC08	FEDVER	KECJOR	OYOJIX	TEFBAH	ZZZQOQ
BIHXIC09	FOGXIK	KEJVEC	OYOJUJ	TEMMED	ZZZTWY
BIHXIC10	FOGXOQ	KEJVIG	PAHWAW	TETSUI	ZZZTWY01
BIHXIC11	FUGGOE	KESBIV	PAHWEA	TETTAP	LUNKAJ
BIHXIC12	FUFJEV	KIKYOU	PANBOY	TIDLUQ	MUGJOQ
BIHXIC13	FUSTAP	KIKYUA	PANCEP	TIGMON	NUJCED
BIHXIC14	GAFJEF	KILFIV	PEFDEL	TIRMAL	NUJCIH

BIHXIC15	GAFQEM	KIYVUK	PIFXEJ	TIRMEP	NUJCON
BIHXIC16	GAFXET	KOHVOS	POFGOH	TPASAU	NUJCUT
BIHXIC17	GAGXUH	KOYCUW	PPOHAU	UGACUB	WUJLAR

Table 6.4.3. REFCODEs of CSD structure containing the AuBr₄⁻ anion. In bold, the structures displaying an Au...Nu CiB (Nu=N, P, O, S, Se, F, Cl, Br, I; Cl–Au...Nu angles in the range 80-100°).

AHIYAT	BENBEC	IJUMEH	ODAXAU	QOCXOX	XEMBIB
AHOFAG	BOKNOH	IVONAK	OKALOB	SAQVEM	XEMCAU
AHOFIO	BUJBEP	IVONEO	OWIPIV	TACGEJ	XEMCEY
AHOFUA	BUJBUF	IVONIS	OWIPUH	UCILOI	XEMCEY01
AHOGIP	COQHUL	IVONNOY	OWIQAQ	UYOLAX	YEGDOD
AHOHAI	DIWXUF	IVONUE	OWIQIW	VAYZEA	YEYCOX
ALAMOR	ECUXAB	JARLEW	OWIQOC	VUGDUW	YEYDEO
ALAZIY	EPAXOJ	LEYNOS	OWIQUI	VUWKEF	YIHJAC
ALENOW	GEVHAR	LONBUO	OWOBAF	WIMFUW	YIHJIK
AXECCO	HEDJEF	NOKRUC	OYOJOD	WOQMEU	YIHJUW
AZUQET	HEVFET	ODAWAT	PIFWUY	WOQMIY	ZUYLEM
BADSUU	IJUMAD	ODAWOH	QOCXIR	WOQMOE	

Table 6.4.4. REFCODEs of CSD structure containing the Au(CN)₄⁻ anion. In bold, the structures displaying an Au...Nu CiB (Nu=N, P, O, S, Se, F, Cl, Br, I; Cl–Au...Nu angles in the range 80-100°).

CIKYUR	GOXCOL	OBUTEN	OVAMII	VIKSIS01	YEBZAI
CIKYUR01	IHOPOK	OTEVUF	OVAMOO	VIKSIS02	YINXUP
CIKZAY	IHOPUQ	OTEWAM	OVAMUU	VIKSOY	YINYAW
CIKZAY01	IHOQAX	OTEWEQ	OVANAB	VIKSOY01	YINYEA
DONYUA	IHOQEB	OTEWIU	OVANEF	VIKSUE	YINYIE
EVIMED	IHOQIF	OTEWOA	SEGKIZ	VIKSUE01	YIRZIJ
GASBAG	LIRZUI	OTEWUG	SEKOF	VIKTAL	
GEFROZ	LISBAR	OTEXAN	TUKHOX	VIKTAL01	
GEFROZ01	MUXXOS	OTEXER	VAZWOJ	VUZDEZ	
GOXCIF	OBUTAJ	OTEXIV	VIKSIS	XIZCOY	

Theoretical Methods.

General Remarks: The energetic features of the adducts analyzed in this work were calculated at the PBE0²⁸-D3²⁹/def2-TZVP³⁰ level of theory using the crystallographic coordinates. The GAUSSIAN-16 program has been used for the energetic calculations and NBO analysis.³¹ The basis set superposition error for the calculation of interaction energies has been corrected using the counterpoise method.³² Molecular electrostatic potential (MEP) surfaces have been computed at the same level of theory and represented using several isovalues of electron density to map the electrostatic potential. The QTAIM analysis³³ has been performed using the AIMAll program at the same level of theory.³⁴

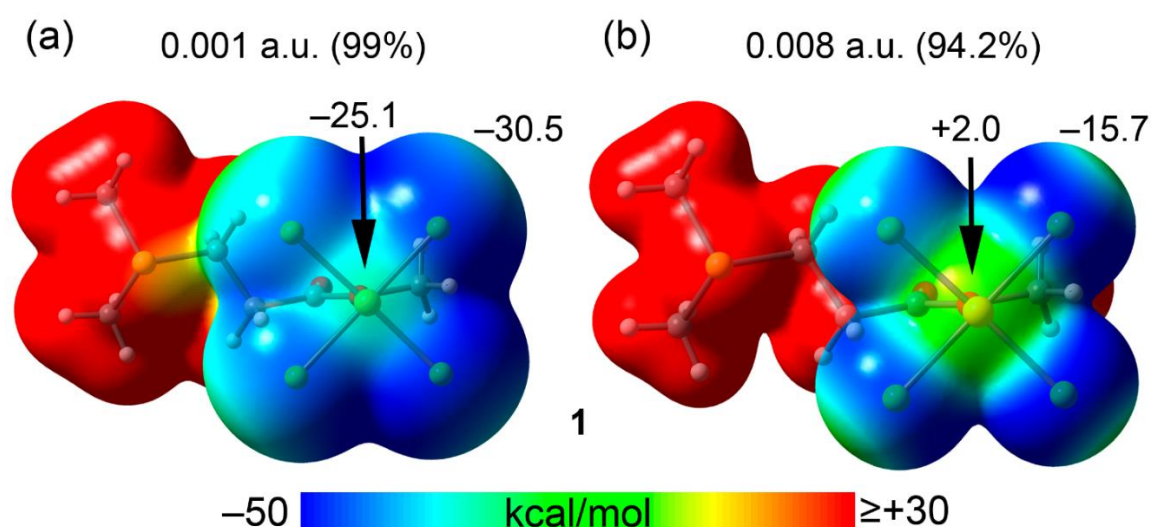


Figure 6.4.1. MEP surfaces of compound **1** using 0.001 a.u. (a) and 0.008 a.u. (b) isovalues at the PBE0-D3/def2-TZVP level of theory. The values at some points of the surface are given in kcal·mol⁻¹.

²⁸ C. Adamo, V. Barone, *J. Chem. Phys.* **1999**, *110*, 6158-6170.

²⁹ F. Weigend, *Phys. Chem. Chem. Phys.* **2006**, *8*, 1057-1065.

³⁰ S. Grimme, J. Antony, S. Ehrlich, H. Krieg, *J. Chem. Phys.* **2010**, *132*, 154104.

³¹ M. J. Frisch, G. W. Trucks, H. B. Schlegel, G. E. Scuseria, M. A. Robb, J. R. Cheeseman, G. Scalmani, V. Barone, G. A. Petersson, H. Nakatsuji, X. Li, M. Caricato, A. V. Marenich, J. Bloino, B. G. Janesko, R. Gomperts, B. Mennucci, H. P. Hratchian, J. V. Ortiz, A. F. Izmaylov, J. L. Sonnenberg, Williams, F. Ding, F. Lipparini, F. Egidi, J. Goings, B. Peng, A. Petrone, T. Henderson, D. Ranasinghe, V. G. Zakrzewski, J. Gao, N. Rega, G. Zheng, W. Liang, M. Hada, M. Ehara, K. Toyota, R. Fukuda, J. Hasegawa, M. Ishida, T. Nakajima, Y. Honda, O. Kitao, H. Nakai, T. Vreven, K. Throssell, J. A. Montgomery Jr., J. E. Peralta, F. Ogliaro, M. J. Bearpark, J. J. Heyd, E. N. Brothers, K. N. Kudin, V. N. Staroverov, T. A. Keith, R. Kobayashi, J. Normand, K. Raghavachari, A. P. Rendell, J. C. Burant, S. S. Iyengar, J. Tomasi, M. Cossi, J. M. Millam, M. Klene, C. Adamo, R. Cammi, J. W. Ochterski, R. L. Martin, K. Morokuma, O. Farkas, J. B. Foresman, D. J. Fox, Wallingford, CT, **2016**.

³² S. F. Boys, F. Bernardi, *Mol. Phys.* **1970**, *19*, 553-566.

³³ R. F. W. Bader, *Chem. Rev.* **1991**, *91*, 893-928.

³⁴ T. A. Keith, TK Gristmill Software, OverlandPark KS, USA **2019**.

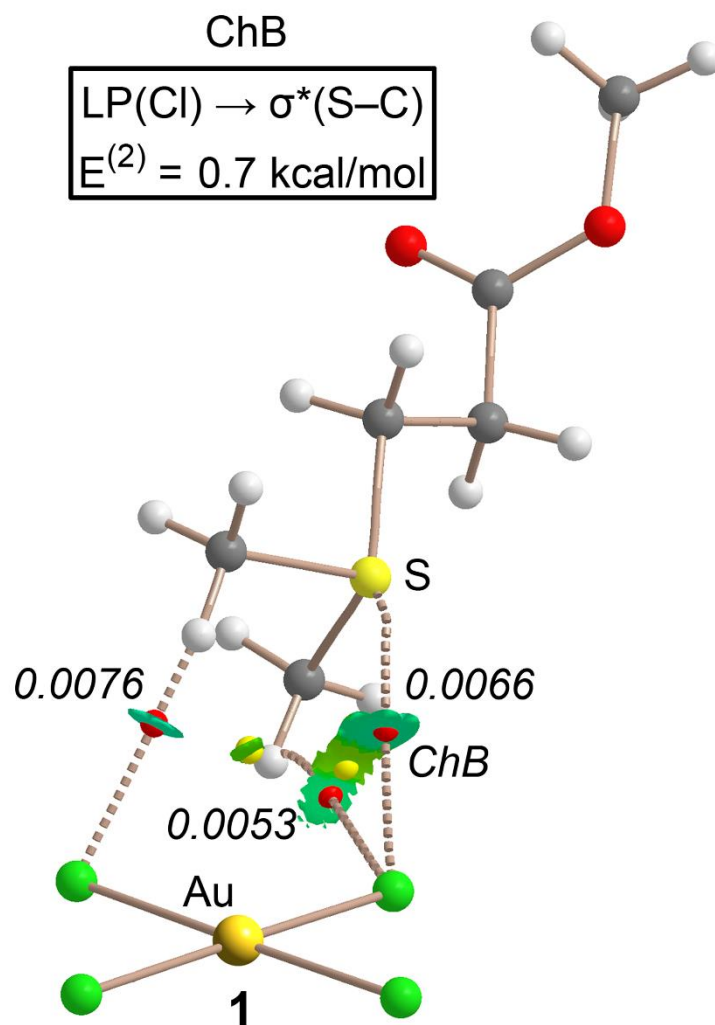
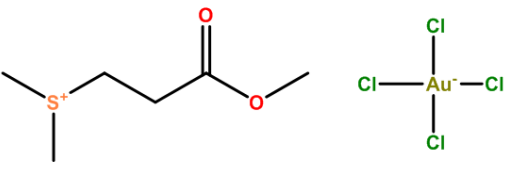
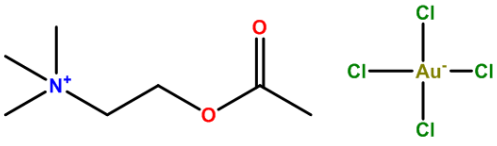


Figure 6.4.2. QTAIM distribution of intermolecular bond and ring critical points (red and yellow spheres, respectively) and bond paths for the binding of AuCl_4^- anion with the sulfonium moiety in compound **1**. The density at the bond CPs that characterize the HBs and the ChB are given in italics (a.u.) The superimposed NCIplot isosurface (RDG isovalue = 0.4 a.u.) is shown. The cut-off $\rho = 0.04$ a.u. has been used. Color range $-0.02 \text{ a.u.} \leq (\text{sign}\lambda_2)\rho \leq 0.02$. Level of theory: PBE0-D3/def2-TZVP.

1	Formula: C ₆ H ₁₃ AuCl ₄ O ₂ S Formula Weight: 487.99 Name: 3-(Dimethylsulfonio) methylpropionate tetrachloroaurate	<input checked="" type="checkbox"/> Slow evaporation <input type="checkbox"/> Vapor diffusion <input type="checkbox"/> Solvent layer <input type="checkbox"/> Other																		
		Solvent(s)/Other agents: H ₂ O..... <input type="checkbox"/> Twinned Temperature: 100 K																		
<p><u>Synthesis:</u></p> <p>A solution of HAuCl₄ (0.3 mmol) in 5 mL of water was added to a 5 mL solution of an equimolar amount of methyl 3-(dimethylsulfonio)propionate chloride in the same solvent. The mixture was stirred for two hours at room temperature in a clear borosilicate vial. Slow isothermal evaporation of the solvent afforded yellow/golden single crystals suitable for X-Ray diffraction after four days.</p>		<table border="1" style="width: 100%; border-collapse: collapse;"> <tr> <td>a: 7.8771</td> <td>α: 90</td> <td>R₁: 0.0218</td> </tr> <tr> <td>b: 8.6445</td> <td>β: 90</td> <td>System: Orthorhombic</td> </tr> <tr> <td>c: 19.740</td> <td>γ: 90</td> <td>Space Group: P2₁2₁2₁</td> </tr> <tr> <td>Vol: 1344.2</td> <td></td> <td></td> </tr> </table>	a: 7.8771	α: 90	R ₁ : 0.0218	b: 8.6445	β: 90	System: Orthorhombic	c: 19.740	γ: 90	Space Group: P2 ₁ 2 ₁ 2 ₁	Vol: 1344.2								
a: 7.8771	α: 90	R ₁ : 0.0218																		
b: 8.6445	β: 90	System: Orthorhombic																		
c: 19.740	γ: 90	Space Group: P2 ₁ 2 ₁ 2 ₁																		
Vol: 1344.2																				
<p><u>Characterization:</u></p> <p>IR (selected bands, cm⁻¹): 1726, 1470, 1420, 1379, 1241, 1081, 1046, 1000, 948, 872, 643, 607.</p> <p>¹H NMR (400 MHz, D₂O): δ 2.89 (s, 6H S+-CH₃), 2.97 (t, 2H, 3J = 6.3 Hz), 3.51 (t, 2H, 3J = 6.2 Hz), 3.70 (s, O-CH₃).</p> <p>¹³C NMR (101 MHz, D₂O): δ 172.04 (C=O), 52.8 (O-CH₃), 38.6 (CH₂-C=O), 28.4 (S+-CH₂), 25.1 (CH₃-S+).</p>		<table border="1" style="width: 100%; border-collapse: collapse;"> <tr> <td style="text-align: center;">Z</td> <td style="text-align: center;">4</td> </tr> <tr> <td style="text-align: center;">ρ_{calc} / g/cm³</td> <td style="text-align: center;">2.411</td> </tr> <tr> <td style="text-align: center;">μ/mm⁻¹</td> <td style="text-align: center;">11.869</td> </tr> <tr> <td style="text-align: center;">F(000)</td> <td style="text-align: center;">912.0</td> </tr> <tr> <td style="text-align: center;">Radiation</td> <td style="text-align: center;">MoKα (λ = 0.71073)</td> </tr> <tr> <td style="text-align: center;">Reflections Collected</td> <td style="text-align: center;">27994</td> </tr> <tr> <td style="text-align: center;">Goodness-of-fit on F²</td> <td style="text-align: center;">1.015</td> </tr> <tr> <td style="text-align: center;">Final R indexes [I > 2σ (I)]</td> <td style="text-align: center;">R₁ = 0.0218, wR₂ = 0.0376</td> </tr> <tr> <td style="text-align: center;">Final R indexes (all data)</td> <td style="text-align: center;">R₁ = 0.0257, wR₂ = 0.0388</td> </tr> </table>	Z	4	ρ_{calc} / g/cm³	2.411	μ/mm⁻¹	11.869	F(000)	912.0	Radiation	MoKα (λ = 0.71073)	Reflections Collected	27994	Goodness-of-fit on F²	1.015	Final R indexes [I > 2σ (I)]	R ₁ = 0.0218, wR ₂ = 0.0376	Final R indexes (all data)	R ₁ = 0.0257, wR ₂ = 0.0388
Z	4																			
ρ_{calc} / g/cm³	2.411																			
μ/mm⁻¹	11.869																			
F(000)	912.0																			
Radiation	MoKα (λ = 0.71073)																			
Reflections Collected	27994																			
Goodness-of-fit on F²	1.015																			
Final R indexes [I > 2σ (I)]	R ₁ = 0.0218, wR ₂ = 0.0376																			
Final R indexes (all data)	R ₁ = 0.0257, wR ₂ = 0.0388																			

2	Formula: $C_{21}H_{24}F_{22}I_3KO_6$ Formula Weight: 484.97 Name: Acetylcholine tetrachloroaurate	<input checked="" type="checkbox"/> Slow evaporation <input type="checkbox"/> Vapor diffusion <input type="checkbox"/> Solvent layer <input type="checkbox"/> Other																		
		Solvent(s)/Other agents: H ₂ O..... <input type="checkbox"/> Twinned Temperature: 100 K																		
<p><u>Synthesis:</u></p> <p>A solution of HAuCl₄ (0.3 mmol) in 5 mL of water was added to a 5 mL solution of an equimolar amount of acetylcholine chloride in the same solvent. The mixture was stirred for two hours at room temperature in a clear borosilicate vial. Slow isothermal evaporation of the solvent afforded yellow/golden single crystals suitable for X-Ray diffraction after four days.</p>		<table border="1" style="width: 100%; border-collapse: collapse;"> <tr> <td>a: 7.7321</td> <td>α: 90</td> <td>R₁:</td> <td>0.0281</td> </tr> <tr> <td>b: 21.1258</td> <td>β: 90</td> <td>System:</td> <td>Monoclinic</td> </tr> <tr> <td>c: 8.6805</td> <td>γ: 120</td> <td>Space Group:</td> <td>P2₁2₁2₁</td> </tr> <tr> <td>Vol: 1408.49</td> <td></td> <td></td> <td></td> </tr> </table>	a: 7.7321	α: 90	R ₁ :	0.0281	b: 21.1258	β: 90	System:	Monoclinic	c: 8.6805	γ: 120	Space Group:	P2 ₁ 2 ₁ 2 ₁	Vol: 1408.49					
a: 7.7321	α: 90	R ₁ :	0.0281																	
b: 21.1258	β: 90	System:	Monoclinic																	
c: 8.6805	γ: 120	Space Group:	P2 ₁ 2 ₁ 2 ₁																	
Vol: 1408.49																				
<p><u>Characterization:</u></p> <p>IR (selected bands, cm⁻¹): 1726, 1483, 1471, 1380, 1242, 1046, 944, 874, 812, 643, 607.</p> <p>¹H NMR (400 MHz, D₂O): δ 2.05 (s, CH₃-C=O), 3.16 (s, 9H, N⁺-CH₃), 3.49 (brt, 2H, N⁺-CH₂), 4.02 (brt, 2H, CH₂-O),</p> <p>¹³C NMR (101 MHz, D₂O): δ 176.6 (C=O), 67.4 (N⁺-CH₂), 55.7 (CH₂-O), 54.0 (N⁺-CH₃), 20.4 (CH₃-C=O).</p>		<table border="1" style="width: 100%; border-collapse: collapse;"> <tr> <td style="text-align: center;">Z</td> <td style="text-align: center;">4</td> </tr> <tr> <td style="text-align: center;">ρ_{calc} / g/cm³</td> <td style="text-align: center;">2.287</td> </tr> <tr> <td style="text-align: center;">μ/mm⁻¹</td> <td style="text-align: center;">11.186</td> </tr> <tr> <td style="text-align: center;">F(000)</td> <td style="text-align: center;">912.0</td> </tr> <tr> <td style="text-align: center;">Radiation</td> <td style="text-align: center;">MoKα (λ = 0.71073)</td> </tr> <tr> <td style="text-align: center;">Reflections Collected</td> <td style="text-align: center;">17266</td> </tr> <tr> <td style="text-align: center;">Goodness-of-fit on F²</td> <td style="text-align: center;">0.999</td> </tr> <tr> <td style="text-align: center;">Final R indexes [I > 2σ (I)]</td> <td style="text-align: center;">R₁ = 0.0281, wR₂ = 0.0430</td> </tr> <tr> <td style="text-align: center;">Final R indexes (all data)</td> <td style="text-align: center;">R₁ = 0.0443, wR₂ = 0.0464</td> </tr> </table>	Z	4	ρ_{calc} / g/cm³	2.287	μ/mm⁻¹	11.186	F(000)	912.0	Radiation	MoKα (λ = 0.71073)	Reflections Collected	17266	Goodness-of-fit on F²	0.999	Final R indexes [I > 2σ (I)]	R ₁ = 0.0281, wR ₂ = 0.0430	Final R indexes (all data)	R ₁ = 0.0443, wR ₂ = 0.0464
Z	4																			
ρ_{calc} / g/cm³	2.287																			
μ/mm⁻¹	11.186																			
F(000)	912.0																			
Radiation	MoKα (λ = 0.71073)																			
Reflections Collected	17266																			
Goodness-of-fit on F²	0.999																			
Final R indexes [I > 2σ (I)]	R ₁ = 0.0281, wR ₂ = 0.0430																			
Final R indexes (all data)	R ₁ = 0.0443, wR ₂ = 0.0464																			
		<input checked="" type="checkbox"/> IR <input checked="" type="checkbox"/> ¹ H-NMR <input type="checkbox"/> Other <input type="checkbox"/> UV <input checked="" type="checkbox"/> ¹³ C-NMR 																		

6.4.2. The fringe behaviour of Group VIII atoms in the higher oxidation state.

Methods.

^1H and ^{13}C NMR spectra in solution were recorded at ambient temperature on Nuclear Magnetic Resonance Spectrometer AVANCE III, Bruker-BioSpin (400 MHz). The Larmor frequency for ^1H and ^{13}C on those instruments were 400.13 and 100.61 MHz, respectively. All the chemical shifts are given in ppm and the coupling constants in Hz. CDCl_3 was used as both solvent and internal standard (as residual CHCl_3) in ^1H NMR spectra and in ^{13}C . SSNMR spectra were recorded at room temperature using a Jeol ECZR 600 spectrometer operating at 150.91 and 60.81 MHz for ^{13}C and ^{15}N nuclei, respectively. Zirconia rotors (volume 60 μL , diameter 3.2 mm) were filled with sample powders. ^{13}C CPMAS spectra were obtained with a 20 kHz rotation speed, ramp cross-polarization pulse sequence, 3.5 ms contact time, a 2.0 μs ^1H pulse at 90° , optimized recycle time of 13.6 s (256 scans) or 15 s (256 scans). ^{15}N CPMAS spectra were obtained with a 12 kHz rotation speed, ramp cross-polarization pulse sequence, 7 ms contact time, a 2.0 μs ^1H pulse at 90° , optimized recycle time of 13.6 s (5140 scans) or 15 s (9400 scans). In all spectra the two-pulse phase modulation (TPPM) decoupling scheme was used with a 108.5 kHz radio frequency field. Glycine methylene and glycine signals ($\delta= 43.7$ ppm and $\delta= 33.4$ ppm relative to NH_3) were used as external standards for ^{13}C and ^{15}N chemical shifts. FT-IR spectra for solids were obtained using a Nicolet Nexus FT-IR spectrometer equipped with UATR unit. Solution IR spectra were obtained using a demountable liquid cell kit mounted on the same instrument and equipped with PTFE O-ring and CaF_2 windows (round, 32 mm, Sigma Aldrich).

Single Crystal X-Ray Determination.

The single crystal data of the compounds were collected at 100 K using a Bruker SMART APEX II CCD area detector diffractometer. Data collection, unit cell refinement and data reduction were performed using Bruker SAINT. Structures were solved by direct methods using SHELXT and refined by full-matrix least-squares on F^2 with anisotropic displacement parameters for the non-H atoms using SHELXL-2016/6. Absorption correction was performed based on multi-scan procedure using SADABS. Structure analysis was aided by use of the programs PLATON. The hydrogen atoms were calculated in ideal positions with isotropic displacement parameters set to 1.2xUeq of the bonded atom.

Computational Details.

The energetic features of the adducts analyzed in this work were calculated at the PBE0-D3/def2-TZVP level of theory using the crystallographic coordinates for the X-ray adducts and fully optimizations for the complexes. For osmium, the inner shell electrons are

modelled by ECPs (ECP-60 scheme), which also accounts for scalar relativistic effects. The GAUSSIAN-16 program has been used for the energetic calculations and NBO analysis. The basis set superposition error for the calculation of interaction energies has been corrected using the counterpoise method. Molecular electrostatic potential (MEP) surfaces have been computed at the same level of theory and represented using several isovalues of electron density to map the electrostatic potential. The QTAIM analysis has been performed using the AIMAll program at the same level of theory.

General synthetic procedure.

1 mL of a CH₂Cl₂ solution containing 0.11 mmol of osmium tetroxide are added dropwise under stirring to 4 mL of a solution of the Lewis base, containing 0.10 mmol of electron donor site, in the same solvent in a borosilicate glass flask. The resulting colorless solution instantaneously turns to yellow/brown. The solvent is removed over 1~3 hours under a gentle stream of anhydrous nitrogen gas. Brownish crystals, suitable for X-Ray diffraction for adducts **3-5**, are formed on the walls and at the bottom of the flask in nearly quantitative yields. Crystals are collected and characterized.

Synthesis and Characterization of **3**.

The brown co-crystals of **3** were synthesized following the general procedure starting from 0.11 mmol of OsO₄ and 0.05 mmol of 4,4'-bipyridine, respectively. FTIR (solid, cm⁻¹) 1605, 1409, 1215, 906, 812, 630, 470. ¹H NMR (400.13 MHz, CDCl₃) δ 8.72 (d, J = 4.6 Hz, 4H), 7.56 (d, J = 5.2 Hz, 4H). ¹³C NMR (100.61 MHz, CDCl₃) δ 149.9 (s, NC), 146.1 (s, NCCC), 121.9 (s, NCC).

Synthesis and Characterization of **4**.

The brown co-crystals of **4** were synthesized following the general procedure starting from 0.11 mmol of OsO₄ and 0.05 mmol and 1,2-di(pyridin-4-yl)ethane. FTIR (solid, cm⁻¹) 1613, 1428, 1201, 902, 829, 539. ¹H NMR (400.13 MHz, CDCl₃) δ 8.50 (dd, J = 5.4, 1.6 Hz, 4H), 7.07 (d, J = 5.2, 1.6 Hz, 4H), 2.95 (s, 4H). ¹³C NMR (100.61 MHz, CDCl₃) δ 150.2 (s, NCCC), 149.2 (s, NC) 124.2 (s, NCC), 35.7 (s, CH₂).

Synthesis and Characterization of **5**.

The brown co-crystals of **5** were synthesized following the general procedure starting from 0.11 mmol of OsO₄ and 0.05 mmol of [4,4'-bipyridine] 1,1'-dioxide polyhydrate. FTIR (solid, cm⁻¹) 1470, 1207, 1172, 909, 823, 548. ¹H NMR (400.13 MHz, CDCl₃) δ 8.28 (dd, J = 5.4, 2.0 Hz, 4H), 7.49 (dd, J = 5.3, 2.0 Hz, 4H). ¹³C NMR (100.61 MHz, CDCl₃) δ 140.1 (s, NC), 133.0 (s, NCCC), 123.1 (s, NCC). [4,4'-bipyridine] 1,1'-dioxide dihydrated^[4] was prepared through crystallization of [4,4'-bipyridine] 1,1'-dioxide polyhydrate from non-anhydrous CH₂Cl₂. [4,4'-bipyridine] 1,1'-dioxide is hygroscopic; on storage in an open flask in the air the water content of the sample increases as shown by ¹H NMR analyses. Different batches were obtained containing 3-6 water molecules per dioxide molecule ([4,4'-bipyridine] 1,1'-dioxide polyhydrate). When OsO₄ and different batches of [4,4'-bipyridine] 1,1'-dioxide polyhydrate were crystallized using the general synthetic procedure described

above, **5** was exclusively isolated (yields >85%) as shown by IR (solid and solution), ¹H NMR analyses, and single crystal X-ray analyses.

Synthesis and Characterization of **6**.

The brown powder of co-crystal **6** was synthesized following the general procedure starting from 0.11 mmol of OsO₄ and 0.05 mmol of 1,3-di(pyridin-4-yl)propane. FTIR (solid, cm⁻¹) 1612, 1424, 901, 819, 621, 512. ¹H NMR (400.13 MHz, CDCl₃) δ 8.41 (*d*, J = 5.6 Hz, 4H), 7.06 (*d*, J = 5.6 Hz, 4H), 2.59 (*t*, J = 8.0 Hz, 4H), 1.92 (*m*, J = 8.0 Hz, 2H). ¹³C NMR (100.61 MHz, CDCl₃) δ 151.3 (NCCC), 143.7 (NCC), 124.15 (NC), 34.5 (CH₂CH₂CH₂), 30.5 (CH₂CH₂CH₂).

32.4 mg Of the brown powder of **6** were dissolved in 0.5 mL of CDCl₃ containing 6.3 mg of 1,2,4,5-tetrafluorobenzene as internal standard for ¹H NMR signals integration. The ratio of the areas of NCH and NCHCH doublets of the reagent and the area of the quintuplet of 1,2,4,5-tetrafluorobenzene revealed that the 1,3-di(pyridin-4-yl)propane/OsO₄ ratio in **6** is 1:2.

Synthesis and Characterization of **7**.

The brown powder of co-crystal **7** was synthesized following the general procedure starting from 0.11 mmol of OsO₄ and 0.10 mmol of 4-methoxypyridine 1-oxide hydrated, Sigma Aldrich). FTIR (solid, cm⁻¹) 1630, 1494, 1198, 906, 754, 557. ¹H NMR (400.13 MHz, CDCl₃) δ 8.06 (*d*, J = 8.0 Hz, 2H), 6.78 (*d*, J = 7.2 Hz, 2H), 3.82 (*s*, 3H). ¹³C NMR (100.61 MHz, CDCl₃) δ 159.3 (NCHCHC), 140.7 (NCHCH), 111.7 (NCH), 56.2 (CH₃). Crystallization of commercially available 4-methoxypyridine 1-oxide hydrated from non-anhydrous CH₂Cl₂ afforded the monohydrated pyridine 1-oxide wherein water was hydrogen bonded to N-oxide oxygen (Tables S19-24, Figure S19). When monohydrated pyridine 1-oxide and OsO₄ were crystallized following the general procedure, **7** was isolated in nearly quantitative yields.

26.2 mg Of the brown powder of **7** were dissolved in 0.5 mL of CDCl₃ containing 6.3 mg of 1,2,4,5-tetrafluorobenzene as internal standard for ¹H NMR signals integration. The ratio of the areas of NCH and NCHCH doublets of the reagent and the area of the quintuplet of 1,2,4,5-tetrafluorobenzene revealed that the 4-methoxypyridine 1-oxide /OsO₄ ratio in **7** is 1:1.

Synthesis and Characterization of **8**.

The brown powder of co-crystal **8** was synthesized following the general procedure starting from 0.108 mmol of OsO₄ and 0.100 mmol of isoquinoline 1-oxide. FTIR (solid, cm⁻¹) 1613, 1428, 1207, 1022, 900, 820, 750, 539. ¹H NMR (400.13 MHz, CDCl₃) δ 8.70 (*s*, 1H), 8.07 (*dd*, J = 7.2, 1.6 Hz, 1H), 7.71 (*dd*, J = 7.6, 1.52, Hz, 2H), 7.60 (*d*, J = 6.8 Hz, 1H), 7.55 (*m*, J = 7.2 Hz, 1H). ¹³C NMR (100.61 MHz, CDCl₃) δ 136.9 (NCH), 136.3 (NCH), 129.5 (NCHC), 129.1 (NCHC), 126.7 (NCHCCH), 125.0 (NCHCCH), 124.2 (NCHCCHCH). Crystallization of commercially available isoquinoline 1-oxide (Sigma Aldrich) from non-anhydrous CH₂Cl₂ afforded hydrated isoquinoline 1-oxide as visible from the following IR spectrum. When hydrated isoquinoline 1-oxide and OsO₄ were crystallized following the general procedure, **8** was isolated in nearly quantitative yields.

24.9 mg of the brown powder of **8** were dissolved in 0.5 mL of CDCl₃ containing 6.3 mg of 1,2,4,5-tetrafluorobenzene as internal standard for ¹H NMR signals integration. The ratio of the areas of signals of isoquinoline 1-oxide and the area of the quintuplet of 1,2,4,5-tetrafluorobenzene revealed that the isoquinoline 1-oxide /OsO₄ ratio in **8** is 1:1.

¹H and ¹³C NMR spectra of pure reagents are very similar to those reported above for corresponding adducts for the cocrystals.

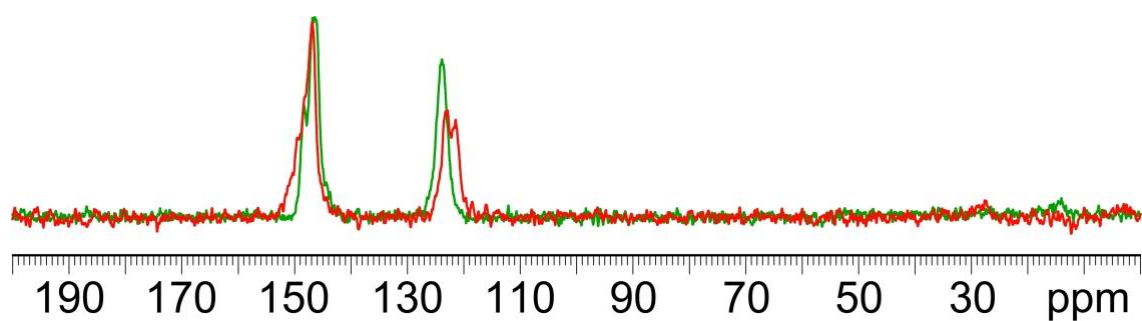


Figure 6.4.3. ^{13}C SSNMR spectra of: pure 4,4'-bipyridine, red line (121.4 and 122.9, NCHCH ; 146.9, NCH and NCHCHC); cocrystal **3**, green line (123.8, NCHCH ; 146.4, NCH ; 148.3, NCHCHC).

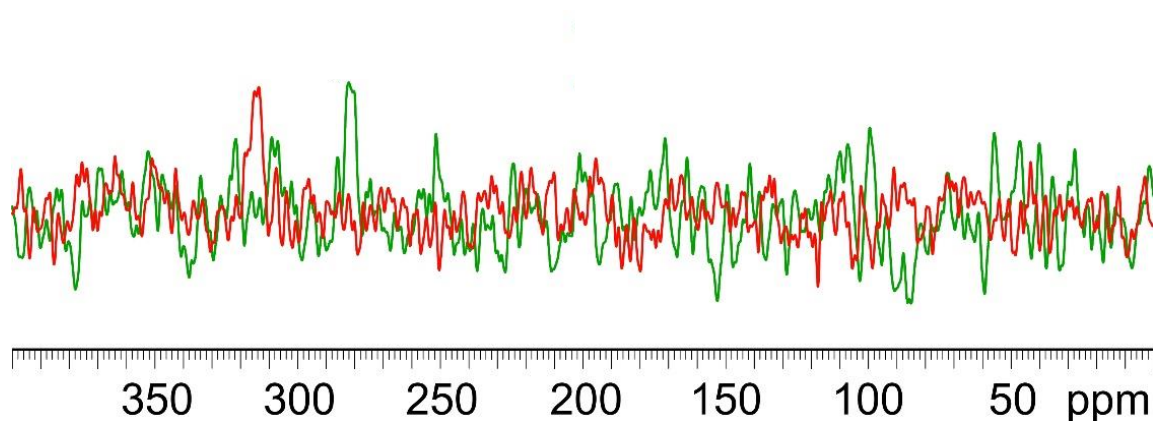


Figure 6.4.4. ^{15}N SSNMR spectra of: pure 4,4'-bipyridine, red line (313.7); cocrystal **3**, green line (282.0).

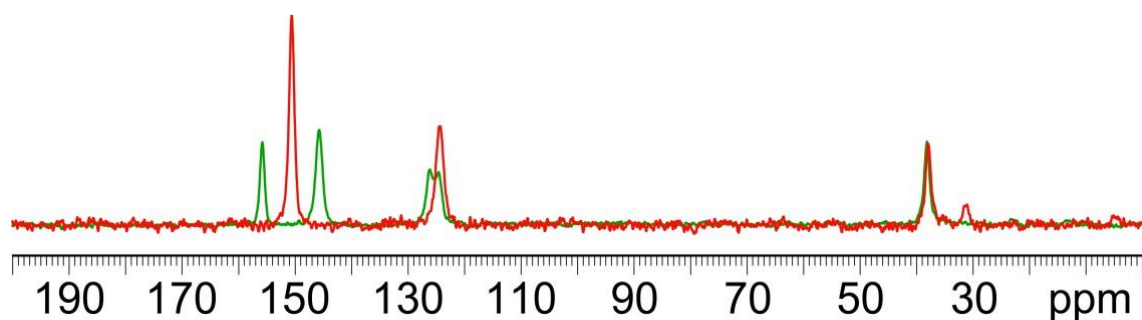


Figure 6.4.5. ^{13}C SSNMR spectra of: pure 1,2-di(pyridin-4-yl)ethane, red line (38.0, CH_2 ; 124.6 and 126.2, NCHCH ; 150.6, NCH and NCHCHC); cocrystal **4**, green line (38.2, CH_2 ; 123.8, NCHCH ; 145.6, NCH ; 155.8, NCHCHC).

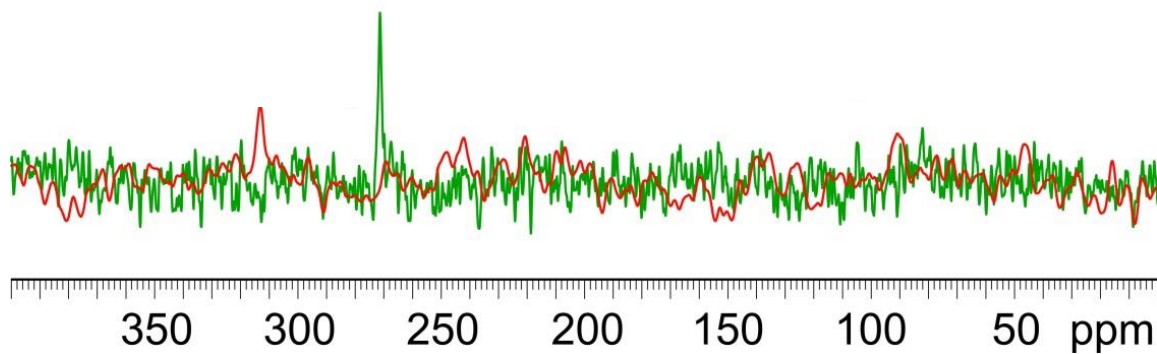


Figure 6.4.6. ^{15}N SSNMR spectra of: pure 1,2-di(pyridin-4-yl)ethane, red line (313.0); cocrystal **4**, green line (271.3).

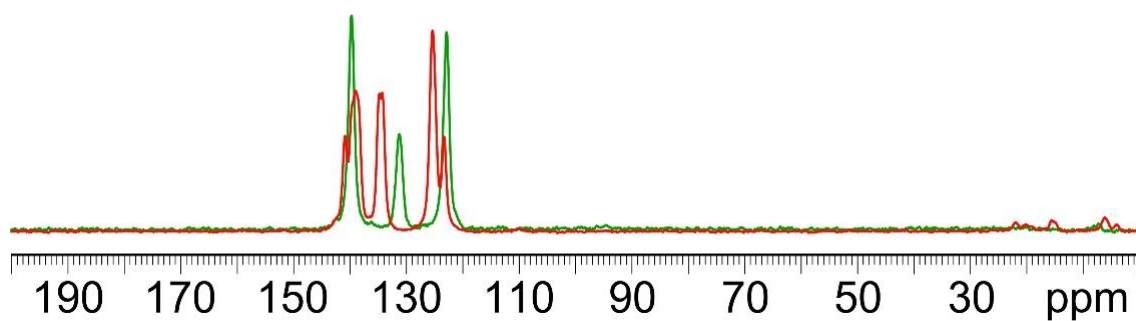


Figure 6.4.7. ^{13}C SSNMR spectra of: [4,4'-bipyridine] 1,1'-dioxide, red line (123.5 and 125.5, $\text{NCH}\underline{\text{C}}\text{H}$; 134.5 and 134.9, $\text{NCHCH}\underline{\text{C}}$; 139.2, 139.9 and 141.1, NCH); **5**, green line (122.9, $\text{NCH}\underline{\text{C}}\text{H}$; 131.3, $\text{NCHCH}\underline{\text{C}}$; 139.7, NCH).

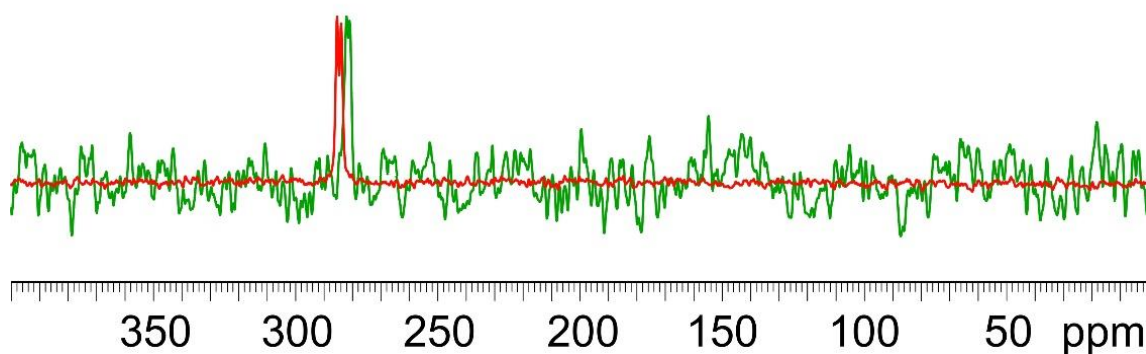


Figure 6.4.8. ^{15}N SSNMR spectra of: [4,4'-bipyridine] 1,1'-dioxide, red line (283.8 and 285.3); **5**, green line (280.9 and 282.0).

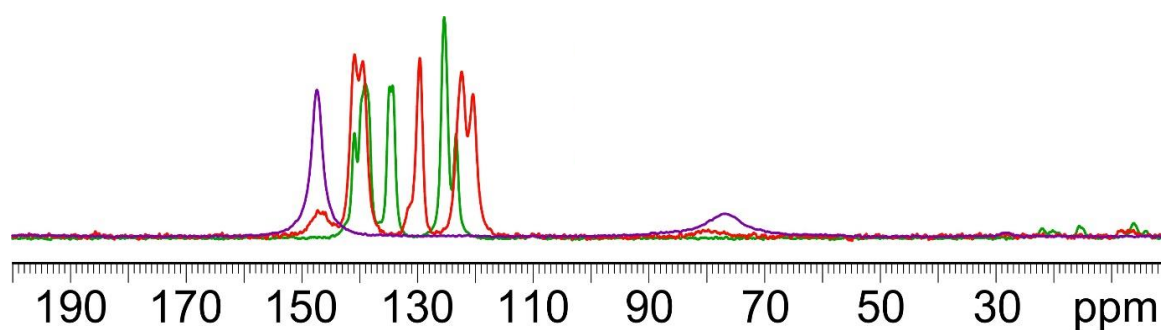


Figure 6.4.9. ^{13}C SSNMR spectra of: [4,4'-bipyridine] 1,1'-dioxide hydrated, green line (141.1, 139.9 and 139.2, NCH ; 134.9 and 134.5, NCHCHC ; 125.5 and 123.5, NCHCH); Diiodotetrafluorobenzene, violet line (147.4, CF ; 76.8, CI); [4,4'-bipyridine] 1,1'-dioxide·Diiodotetrafluorobenzene, red line (~147, CF ; 141.1 and 139.9, NCH ; 129.7 NCHCHC ; 122.3 and 120.4, NCHCH ; ~80, CI).

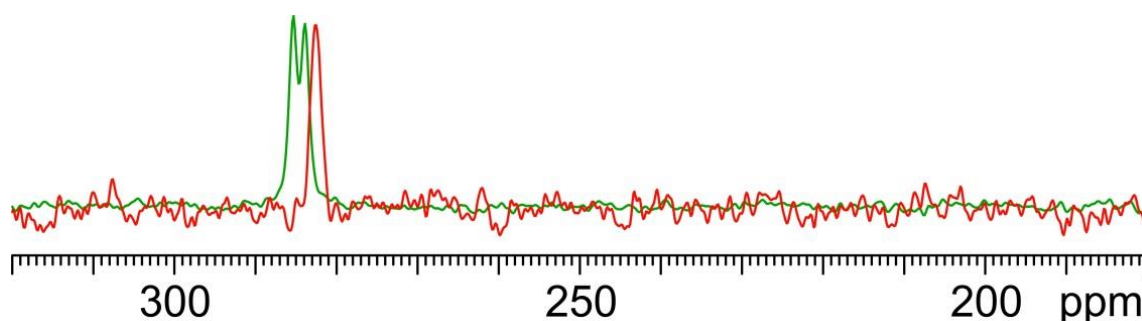


Figure 6.4.10. ^{15}N SSNMR spectra of: [4,4'-bipyridine] 1,1'-dioxide hydrated, green line (285.3 and 283.8); [4,4'-bipyridine] 1,1'-dioxide·Diiodotetrafluorobenzene, red line (282.5).

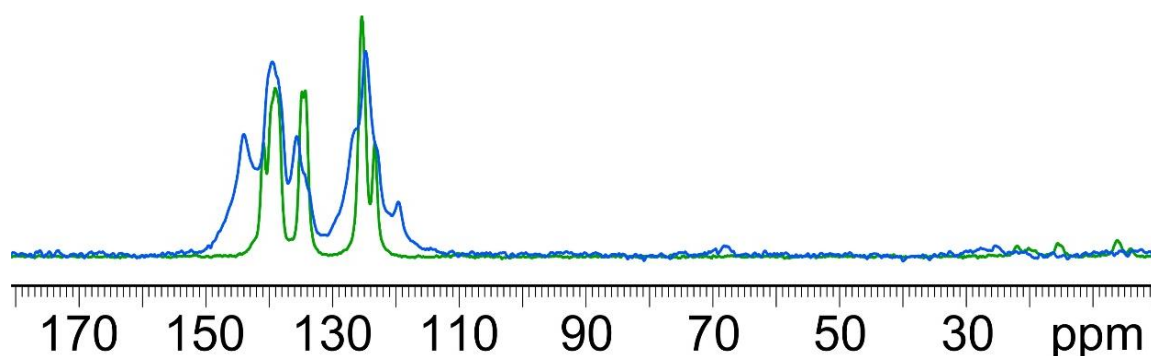


Figure 6.4.11. ^{13}C SSNMR spectra of: [4,4'-bipyridine] 1,1'-dioxide hydrated, green line (123.5 and 125.5, NCHCH ; 134.5 and 134.9, NCHCHC ; 139.2, 139.9 and 141.1, NCH); [4,4'-bipyridine] 1,1'-dioxide· SbF_3 , blue line (traces of starting [4,4'-bipyridine] 1,1'-dioxide hydrated are present in the sample) (126.7, 124.7 and 119.7, NCHCH ; 135.6, NCHCHC ; 143.9 and 139.7, NCH).

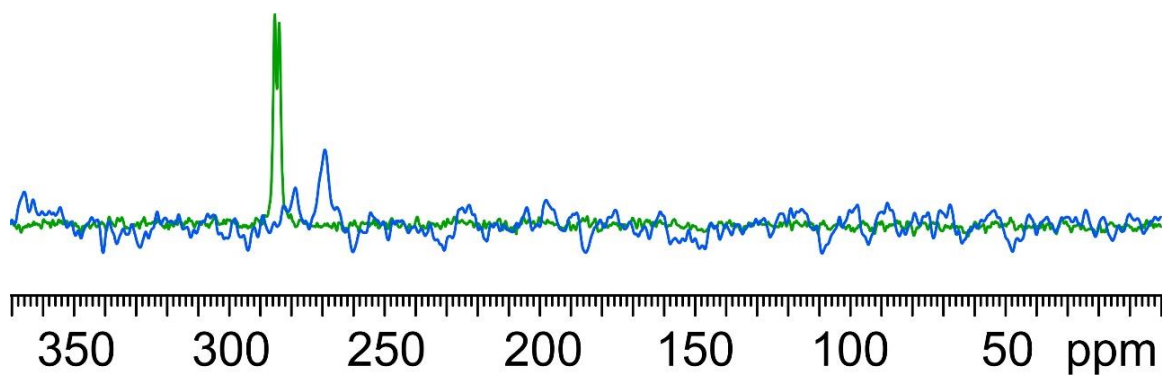


Figure 6.4.12. ^{15}N SSNMR spectra of: [4,4'-bipyridine] 1,1'-dioxide hydrated, green line (285.3 and 283.8); [4,4'-bipyridine] 1,1'-dioxide \cdot SbF_3 , blue line (269.1).

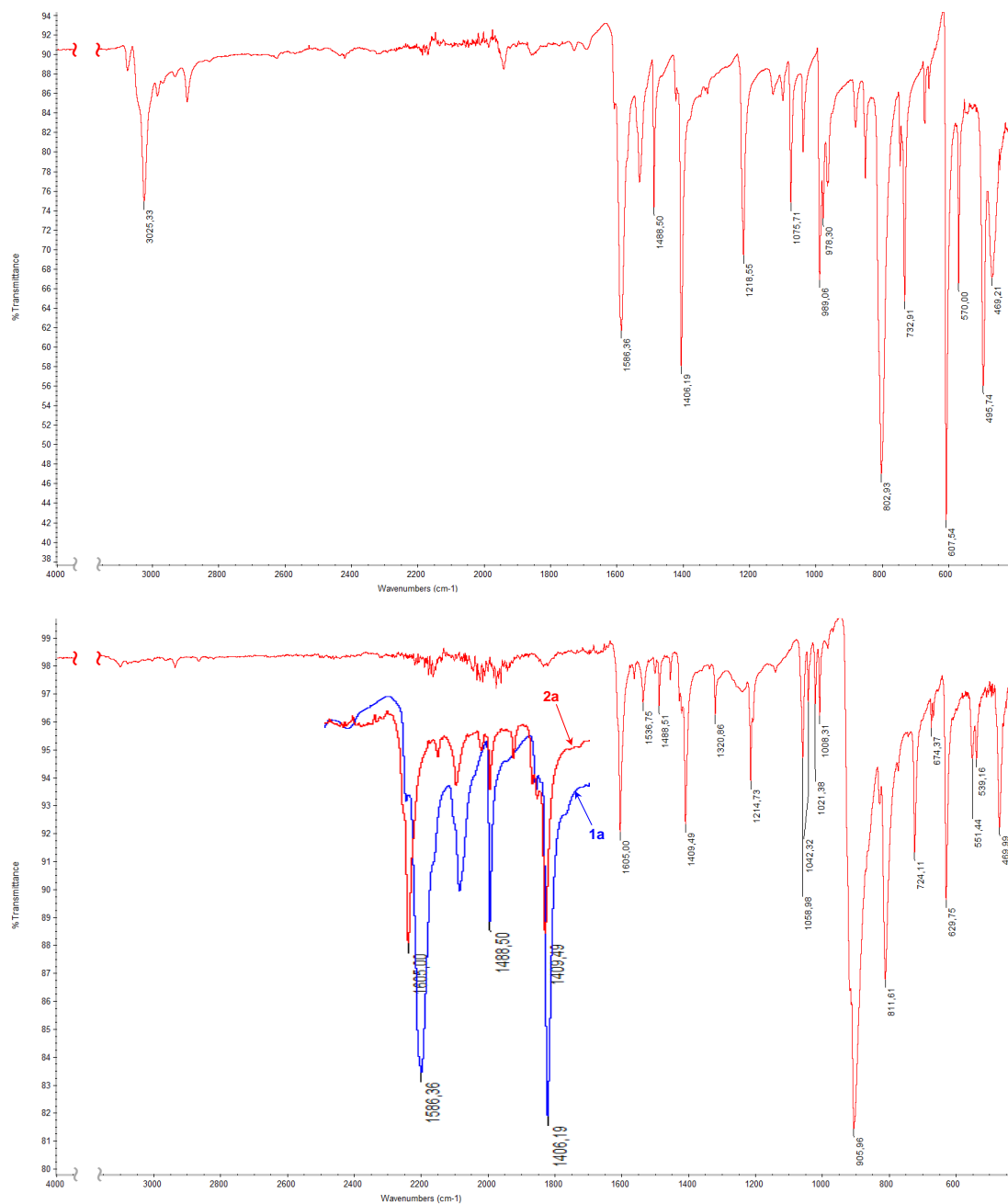


Figure 6.4.13. IR spectra (solid) of pure 4,4'-bipyridine (top) and of corresponding cocystal **3** (bottom). The insert in the bottom spectrum is zooming on overlapped spectra in the region of breathing vibrations.

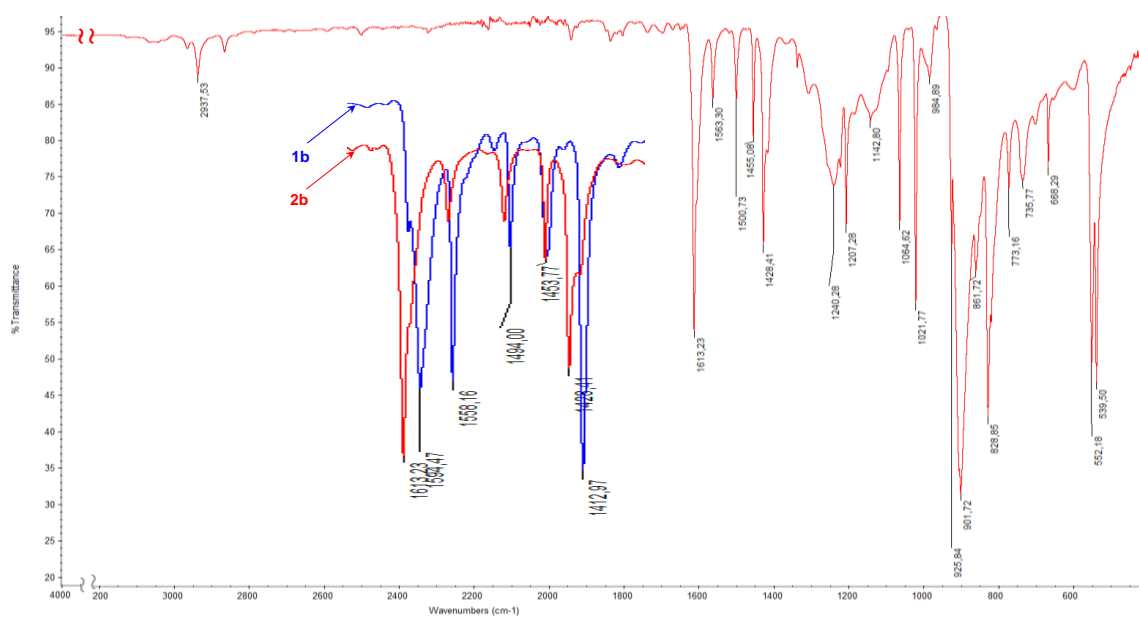
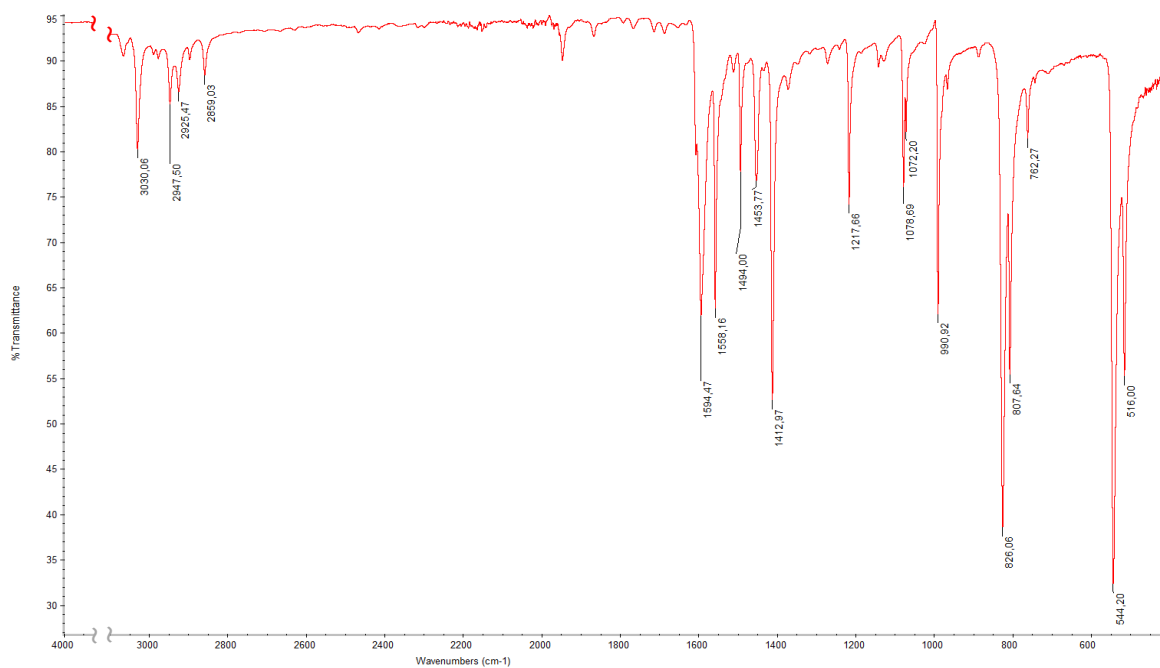


Figure 6.4.14. IR spectra (solid) of pure 1,2-di(pyridin-4-yl)ethane (top) and of corresponding cocystal **4** (bottom). The insert in the bottom spectrum is zooming on overlapped spectra in the region of breathing vibrations.

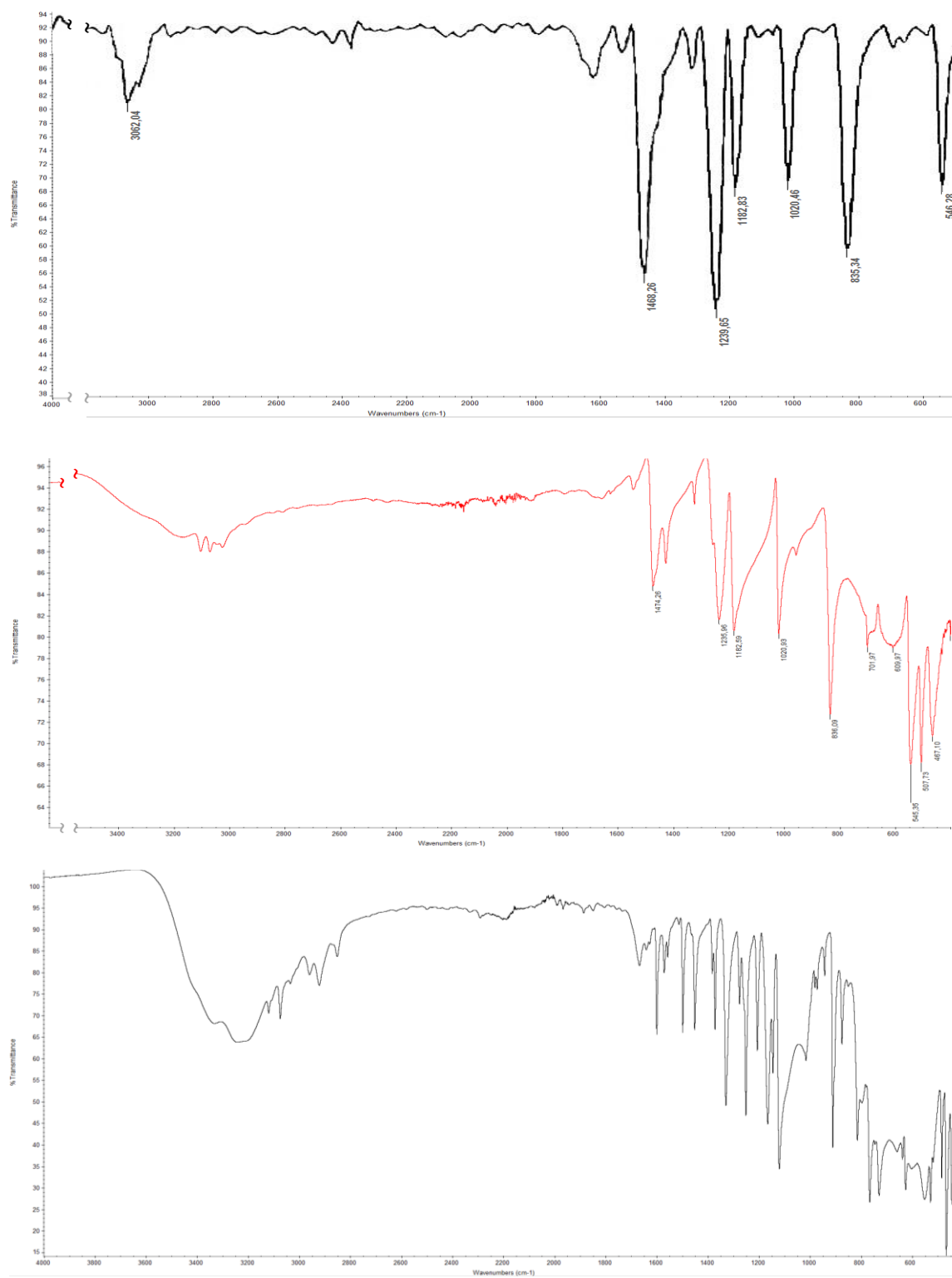


Figure 6.4.15. IR spectra (solid) of [4,4'-bipyridine] 1,1'-dioxide (top), [4,4'-bipyridine] 1,1'-dioxide polyhydrate (mid), isoquinoline 2-oxide hydrated (bottom).

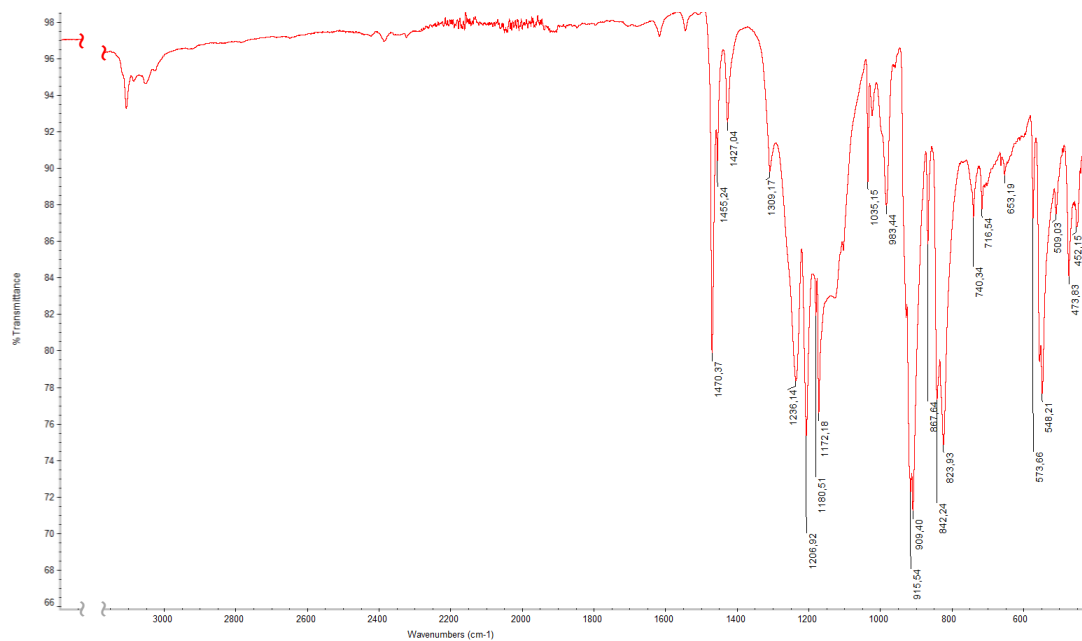


Figure 6.4.16. IR spectrum (solid) of the cocrystal **5**.

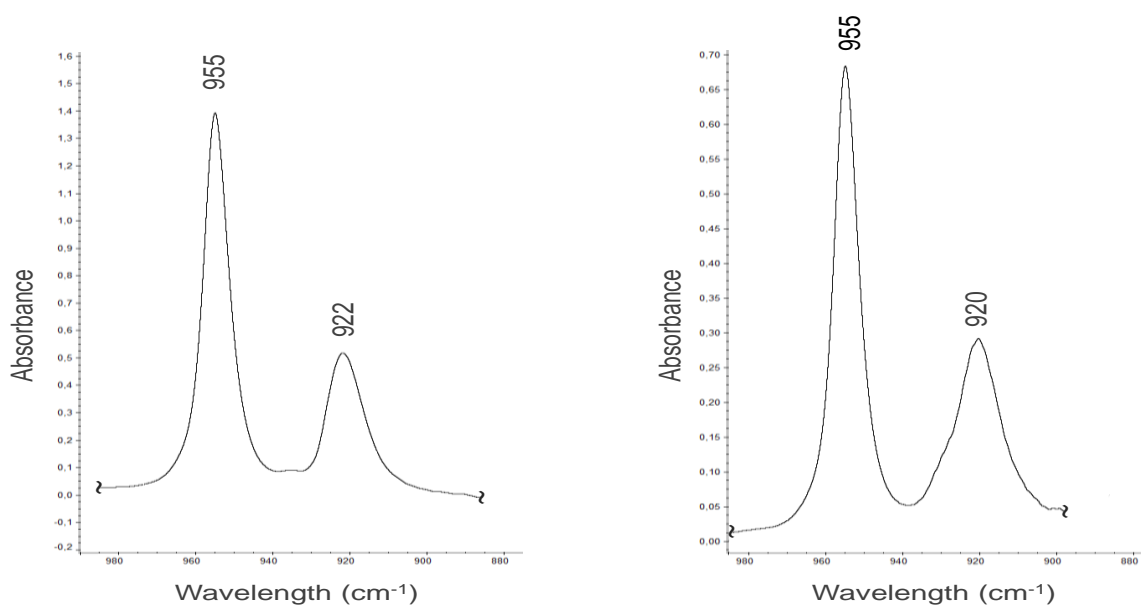


Figure 6.4.17. IR spectra (CHCl_3 solution) of cocrystals **3** (left) and **4** (right) in the region of ν_3 band of OsO_4 .

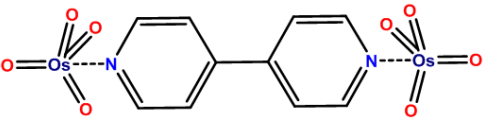
Cartesian Coordinates Of the Optimized Adducts

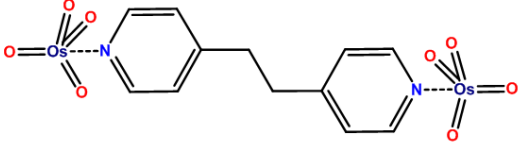
O₄Fe...NCCH₃				44	-1.041984	-0.000016	-0.000023
8	0.780801	-1.239925	-0.776666	6	3.357546	0.000128	0.000178
8	0.818659	-0.038833	1.472691	7	2.209596	0.000378	0.000552
8	2.887048	-0.047238	-0.003172	6	4.806059	-0.000196	-0.000287
8	0.851208	1.307973	-0.692556	1	5.179228	-1.007747	0.189339
26	1.324840	-0.004162	0.000072	1	5.179154	0.339122	-0.967776
6	-3.228630	0.023265	-0.000418	1	5.179789	0.667786	0.777208
7	-2.081017	0.072178	-0.001275				
6	-4.676367	-0.038301	0.000707	O₄Ru...NC₅H₅			
1	-5.013514	-0.905002	0.571338	7	0.165369	1.259685	0.000000
1	-5.088907	0.864713	0.453281	6	1.408575	1.726598	0.000000
1	-5.048043	-0.122338	-1.021673	1	2.198627	0.981433	0.000000
O₄Fe...NC₅H₅				6	1.700870	3.080350	0.000000
7	0.107946	1.312980	0.000000	1	2.730762	3.415149	0.000000
6	1.338846	1.811240	0.000000	6	0.648496	3.982697	0.000000
1	2.148943	1.085615	0.000000	8	-1.754679	-0.751176	0.000000
6	1.613904	3.170998	0.000000	8	0.648496	-1.104659	1.389053
1	2.639742	3.521045	0.000000	6	-0.649070	3.497116	0.000000
6	0.549890	4.058753	0.000000	1	-1.501150	4.165523	0.000000
8	-1.652716	-1.289726	0.000000	6	-0.840957	2.124276	0.000000
8	0.549890	-1.529816	1.276914	1	-1.836608	1.690836	0.000000
6	-0.739227	3.549564	0.000000	8	-0.470548	-3.065646	0.000000
1	-1.603350	4.203884	0.000000	8	0.648496	-1.104659	-1.389053
6	-0.904854	2.172276	0.000000	1	0.837789	5.050141	0.000000
1	-1.901096	1.736762	0.000000	44	-0.222014	-1.417681	0.000000
8	-0.408543	-3.500632	0.000000	O₄Os...NCCH₃			
8	0.549890	-1.529816	-1.276914	8	-0.976541	-1.281547	-0.237662
1	0.722336	5.129118	0.000000	8	1.596613	-0.208030	-0.246189
26	-0.239297	-1.947859	0.000000	8	-0.000648	-0.017659	-2.455910
O₄Ru...NCCH₃				8	-0.619678	1.483594	-0.257377
8	-0.520006	-0.369924	1.534970	6	0.000375	0.025984	3.524918
8	-0.519461	-1.144249	-1.087781	7	0.000670	0.017008	2.377527
8	-2.708110	-0.000205	-0.000320	6	0.000009	0.037288	4.973028
8	-0.519881	1.514293	-0.446988	1	0.483601	-0.863883	5.352963
				1	0.541028	0.911122	5.339129

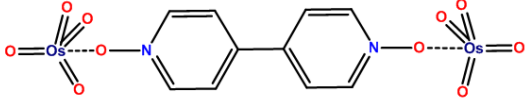
1	-1.024915	0.073348	5.345258	6	0.346966	-4.192418	0.000000
76	-0.000062	-0.005660	-0.764350	8	1.594486	0.854483	0.000000
O₄Os...NC₅H₅				8	-0.888598	0.574819	1.423439
76	-0.096163	1.061652	0.000000	6	1.493247	-3.415325	0.000000
7	0.175689	-1.437002	0.000000	1	2.479008	-3.863049	0.000000
6	-0.926313	-2.181030	0.000000	6	1.360029	-2.036511	0.000000
1	-1.866546	-1.640193	0.000000	1	2.220894	-1.376705	0.000000
6	-0.888598	-3.563418	0.000000	8	-0.276056	2.744686	0.000000
1	-1.810814	-4.130526	0.000000	8	-0.888598	0.574819	-1.423439
				1	0.414164	-5.274282	0.000000

Table 6.4.5. Refcodes of structures present on the Cambridge Structural Database (CSD) containing OsO₄ engaging in OmB with nucleophiles. The CSD search was made assuming that the Nu may be N, P, O, S, Se, F, Cl, Br, I. Relevant distances, Ncs and angles are reported. Batsanov van der Waals radii were used to calculate Ncs.

REFCODE	Nu	Os...Nu distance (Nc)	Most linear O=Os...Nu angle(s)	Reference
COTTEK	Cl ⁻	2759 (0.72)	179.00°	R. Weber, K. Dehnicke, U. Muller, D. Fenske, Z. Anorg. Allg. Chem. 1984, 516, 214.
NOLTIR	O ⁻	2304 (0.64)	175.09°	A. J. Bailey, M. G. Bhowon, W. P. Griffith, A. G. F. Shoair, A. J. P. White, D. J. Williams, J. Chem. Soc., Dalton Trans. 1997, 3245
NOLTOX	N	2441 (0.68)	177.74°	A. J. Bailey, M. G. Bhowon, W. P. Griffith, A. G. F. Shoair, A. J. P. White, D. J. Williams, J. Chem. Soc., Dalton Trans. 1997, 3245.
RICTOM	N	2318 (0.64)	179.31°	D. W. Nelson, A. Gypser, P. T. Ho, H. C. Kolb, T. Kondo, H.-L. Kwong, D. V. McGrath, A. E. Rubin, P.-O.Norrby, K. P. Gable, K. B. Sharpless, J.Am.Chem.Soc. 1997, 119, 1840.
RICTUS	N	2419 (0.67)	178.82°	D. W. Nelson, A. Gypser, P. T. Ho, H. C. Kolb, T. Kondo, H.-L. Kwong, D. V. McGrath, A. E. Rubin, P.-O.Norrby, K. P. Gable, K. B. Sharpless, J.Am.Chem.Soc. 1997, 119, 1840.
RICVAA	N	2453 (0.68)	178.61°	D. W. Nelson, A. Gypser, P. T. Ho, H. C. Kolb, T. Kondo, H.-L. Kwong, D. V. McGrath, A. E. Rubin, P.-O.Norrby, K. P. Gable, K. B. Sharpless, J.Am.Chem.Soc. 1997, 119, 1840.
SARDUK	N	2478 (0.68)	179.23	J.S.Svendsen, I.Marko, E.N.Jacobsen, C.P.Rao, S.Bott, K.B.Sharpless, J.Org.Chem. (1989), 54, 2263. DOI: 10.1021/jo00271a002. SUKJOX E. J. Corey, M. C. Noe, S. Sarshar, J. Am. Chem. Soc. 1993, 115, 3828.
SUKJOX01	N; N	2.403 (0.67); 2458 (0.68)	176.25°; 175.38°	R. E. Marsh, Acta Crystallogr., Sect. B: Struct. Sci. 1999, 55, 931.
TIXXAZ	N; N	2.329 (0.65); 2.334 (0.65)	167.35°; 165.79°	E. J. Corey, S. Sarshar, M. D. Azimioara, R. C. Newbold, M. C. Noe, J. Am. Chem. Soc. 1996, 118, 7851.
XAKBUG	F ⁻	2075 (0.59)	156.89°	M. Gerken, D. A. Dixon, G. J. Schrobilgen, Inorg. Chem. 2000, 39, 4244-4255.
ZATKEK	N	2437 (0.68)	178.35°	W. P. Griffith, T. Y. Koh, A. J. P. White, D. J. Williams, Polyhedron 1995, 14, 2019.

3	Formula: C ₁₀ H ₈ N ₂ O ₈ Os ₂ Formula Weight: 664.58 Name: Osmium tetroxide · 4,4' dipyridyl	<input checked="" type="checkbox"/> Slow evaporation <input type="checkbox"/> Vapor diffusion <input type="checkbox"/> Solvent layer <input type="checkbox"/> Other																
		Solvent(s)/Other agents: CH ₂ Cl ₂																
		<input type="checkbox"/> Twinned Temperature: 100 K																
		<table border="0" style="width: 100%;"> <tr> <td>a: 14.4805</td> <td>α: 90</td> <td>R₁:</td> <td>0.0196</td> </tr> <tr> <td>b: 14.4805</td> <td>β: 90</td> <td>System:</td> <td>Tetragonal</td> </tr> <tr> <td>c: 6.4815</td> <td>γ: 90</td> <td>Space Group:</td> <td>P4₂/mbc</td> </tr> <tr> <td>Vol: 1359.1</td> <td></td> <td></td> <td></td> </tr> </table>	a: 14.4805	α: 90	R ₁ :	0.0196	b: 14.4805	β: 90	System:	Tetragonal	c: 6.4815	γ: 90	Space Group:	P4 ₂ /mbc	Vol: 1359.1			
a: 14.4805	α: 90	R ₁ :	0.0196															
b: 14.4805	β: 90	System:	Tetragonal															
c: 6.4815	γ: 90	Space Group:	P4 ₂ /mbc															
Vol: 1359.1																		
		<input checked="" type="checkbox"/> IR <input checked="" type="checkbox"/> ¹ H-NMR <input type="checkbox"/> Other <input type="checkbox"/> UV <input checked="" type="checkbox"/> ¹³ C-NMR 																
<u>Synthesis:</u> 1 mL of a CH ₂ Cl ₂ solution containing 0.1 mmol of osmium tetroxide are added dropwise to 4 mL of an equimolar solution of 4,4' dipyridyl in the same solvent. The resulting solution instantaneously changed color from colorless to yellow/brown. The solvent was then removed over an hour period under a gentle stream of nitrogen gas. The resulting solid, in the form of crystals suitable for X-Ray diffraction, was collected at the bottom and walls of the vial and characterized.																		
<u>Characterization:</u>																		
FTIR (cm ⁻¹) 1605, 1409, 1215, 906, 812, 630, 470.	Z	2																
¹ H NMR (400 MHz, Chloroform-d) δ 8.72 (d, J = 4.6 Hz, 4H), 7.56 (d, J = 5.2 Hz, 4H).	ρ_{calc} / g/cm³	3.248																
¹³ C NMR (101 MHz, Chloroform-d) δ 149.9 (s, NC, 4C), 146.1 (s, NCCC, 2C), 121.9 (s, NCC, 4C).	μ/mm⁻¹	18.724																
	F(000)	1192.0																
	Radiation	MoKα (λ = 0.71073)																
	Reflections Collected	22626																
	Goodness-of-fit on F²	0.817																
	Final R indexes [I > 2σ (I)]	R ₁ = 0.0196, wR ₂ = 0.0560																
	Final R indexes (all data)	R ₁ = 0.0283, wR ₂ = 0.0603																

4	Formula: C ₁₂ H ₁₂ N ₂ O ₈ Os ₂ Formula Weight: 692.64 Name: Osmium tetroxide · bis(4-pyridyl) ethane	<input checked="" type="checkbox"/> Slow evaporation <input type="checkbox"/> Vapor diffusion <input type="checkbox"/> Solvent layer <input type="checkbox"/> Other																		
		Solvent(s)/Other agents: H ₂ O..... <input type="checkbox"/> Twinned Temperature: 100 K																		
<p><u>Synthesis:</u></p> <p>1 mL of a CH₂Cl₂ solution containing 0.1 mmol of osmium tetroxide are added dropwise to 4 mL of an equimolar solution of bis(4-pyridyl) ethane in the same solvent. The resulting solution instantaneously changed color from colorless to yellow/brown. The solvent was then removed over an hour period under a gentle stream of nitrogen gas. The resulting solid, in the form of crystals suitable for X-Ray diffraction, was collected at the bottom and walls of the vial and characterized.</p>		a: 8.3593 α: 90 R ₁ : 0.0271 b: 12.0646 β: 114.514 System: Monoclinic c: 8.8811 γ: 90 Space Group: P2 ₁ /c Vol: 1408.49																		
<p><u>Characterization:</u></p> <p>FTIR (cm⁻¹) 1613, 1428, 1201, 902, 829, 539.</p> <p>¹H NMR (400 MHz, Chloroform-d) δ 8.50 (dd, J = 5.40, 1.6 Hz, 4H), 7.07 (d, J = 5.20, 1.6 Hz, 4H), 2.95 (s, 4H).</p> <p>¹³C NMR (101 MHz, Chloroform-d) δ 150.2 (s, NCCC, 2C), 149.2 (s, NC, 4C) 124.2 (s, NCC, 4C), 35.7 (s, CH₂, 2C).</p>		<input checked="" type="checkbox"/> IR <input checked="" type="checkbox"/> ¹ H-NMR <input type="checkbox"/> Other <input type="checkbox"/> UV <input checked="" type="checkbox"/> ¹³ C-NMR 																		
		<table border="1" style="width: 100%; border-collapse: collapse;"> <tr> <td style="text-align: center;">Z</td> <td style="text-align: center;">2</td> </tr> <tr> <td style="text-align: center;">ρ_{calc} / g/cm³</td> <td style="text-align: center;">2.823</td> </tr> <tr> <td style="text-align: center;">μ/mm⁻¹</td> <td style="text-align: center;">15.620</td> </tr> <tr> <td style="text-align: center;">F(000)</td> <td style="text-align: center;">628.0</td> </tr> <tr> <td style="text-align: center;">Radiation</td> <td style="text-align: center;">MoKα (λ = 0.71073)</td> </tr> <tr> <td style="text-align: center;">Reflections Collected</td> <td style="text-align: center;">14445</td> </tr> <tr> <td style="text-align: center;">Goodness-of-fit on F²</td> <td style="text-align: center;">1.027</td> </tr> <tr> <td style="text-align: center;">Final R indexes [I > 2σ (I)]</td> <td style="text-align: center;">R₁ = 0.0271, wR₂ = 0.0576</td> </tr> <tr> <td style="text-align: center;">Final R indexes (all data)</td> <td style="text-align: center;">R₁ = 0.0431, wR₂ = 0.0634</td> </tr> </table>	Z	2	ρ_{calc} / g/cm³	2.823	μ/mm⁻¹	15.620	F(000)	628.0	Radiation	MoKα (λ = 0.71073)	Reflections Collected	14445	Goodness-of-fit on F²	1.027	Final R indexes [I > 2σ (I)]	R ₁ = 0.0271, wR ₂ = 0.0576	Final R indexes (all data)	R ₁ = 0.0431, wR ₂ = 0.0634
Z	2																			
ρ_{calc} / g/cm³	2.823																			
μ/mm⁻¹	15.620																			
F(000)	628.0																			
Radiation	MoKα (λ = 0.71073)																			
Reflections Collected	14445																			
Goodness-of-fit on F²	1.027																			
Final R indexes [I > 2σ (I)]	R ₁ = 0.0271, wR ₂ = 0.0576																			
Final R indexes (all data)	R ₁ = 0.0431, wR ₂ = 0.0634																			

5	Formula: C ₁₀ H ₈ N ₂ O ₁₀ Os ₂ Formula Weight: 696.58 Name: Acetylcholine tetrachloroaurate	<input checked="" type="checkbox"/> Slow evaporation <input type="checkbox"/> Vapor diffusion <input type="checkbox"/> Solvent layer <input type="checkbox"/> Other																		
		Solvent(s)/Other agents: H ₂ O..... <input type="checkbox"/> Twinned Temperature: 100 K																		
<p>Synthesis:</p> <p>1 mL of a CH₂Cl₂ solution containing 0.1 mmol of osmium tetroxide are added dropwise to 4 mL of an equimolar solution of 4,4' dipyridyl n-oxide in the same solvent. The resulting solution instantaneously changed color from colorless to yellow/brown. The solvent was then removed over an hour period under a gentle stream of nitrogen gas. The resulting solid, in the form of crystals suitable for X-Ray diffraction, was collected at the bottom and walls of the vial and characterized.</p>		<table border="1" style="width: 100%; border-collapse: collapse;"> <tr> <td>a: 136.2536</td> <td>α: 90</td> <td>R₁:</td> <td>0.0316</td> </tr> <tr> <td>b: 7.5785</td> <td>β: 112.724</td> <td>System:</td> <td>Monoclinic</td> </tr> <tr> <td>c: 15.7024</td> <td>γ: 90</td> <td>Space Group:</td> <td>P2₁/n</td> </tr> <tr> <td>Vol: 1454.8</td> <td></td> <td></td> <td></td> </tr> </table>	a: 136.2536	α: 90	R ₁ :	0.0316	b: 7.5785	β: 112.724	System:	Monoclinic	c: 15.7024	γ: 90	Space Group:	P2 ₁ /n	Vol: 1454.8					
a: 136.2536	α: 90	R ₁ :	0.0316																	
b: 7.5785	β: 112.724	System:	Monoclinic																	
c: 15.7024	γ: 90	Space Group:	P2 ₁ /n																	
Vol: 1454.8																				
<p>Characterization:</p> <p>FTIR (cm⁻¹) 1470, 1207, 1172, 909, 823, 548.</p> <p>¹H NMR (400 MHz, CDCl₃) ¹H NMR (400 MHz, Chloroform-d) δ 8.28 (dd, J = 5.40, 1.92, 4H), 7.49 (dd, J = 5.30, 2.04, 4H).</p> <p>¹³C NMR (101 MHz, Chloroform-d) δ 140.1 (s, NC, 4C), 133.0 (s, NCCC, 2C), 123.1 (s, NCC, 4C).</p>		<table border="1" style="width: 100%; border-collapse: collapse;"> <tr> <td style="text-align: center;">Z</td> <td style="text-align: center;">4</td> </tr> <tr> <td style="text-align: center;">ρ_{calc} / g/cm³</td> <td style="text-align: center;">3.180</td> </tr> <tr> <td style="text-align: center;">μ/mm⁻¹</td> <td style="text-align: center;">17.511</td> </tr> <tr> <td style="text-align: center;">F(000)</td> <td style="text-align: center;">1256.0</td> </tr> <tr> <td style="text-align: center;">Radiation</td> <td style="text-align: center;">MoKα (λ = 0.71073)</td> </tr> <tr> <td style="text-align: center;">Reflections Collected</td> <td style="text-align: center;">13650</td> </tr> <tr> <td style="text-align: center;">Goodness-of-fit on F²</td> <td style="text-align: center;">1.013</td> </tr> <tr> <td style="text-align: center;">Final R indexes [I > 2σ (I)]</td> <td style="text-align: center;">R₁ = 0.0316, wR₂ = 0.0497</td> </tr> <tr> <td style="text-align: center;">Final R indexes (all data)</td> <td style="text-align: center;">R₁ = 0.0523, wR₂ = 0.0542</td> </tr> </table>	Z	4	ρ_{calc} / g/cm³	3.180	μ/mm⁻¹	17.511	F(000)	1256.0	Radiation	MoKα (λ = 0.71073)	Reflections Collected	13650	Goodness-of-fit on F²	1.013	Final R indexes [I > 2σ (I)]	R ₁ = 0.0316, wR ₂ = 0.0497	Final R indexes (all data)	R ₁ = 0.0523, wR ₂ = 0.0542
Z	4																			
ρ_{calc} / g/cm³	3.180																			
μ/mm⁻¹	17.511																			
F(000)	1256.0																			
Radiation	MoKα (λ = 0.71073)																			
Reflections Collected	13650																			
Goodness-of-fit on F²	1.013																			
Final R indexes [I > 2σ (I)]	R ₁ = 0.0316, wR ₂ = 0.0497																			
Final R indexes (all data)	R ₁ = 0.0523, wR ₂ = 0.0542																			

7. Conclusions.

*“Scientist alone is true poet
he gives us the moon
he promises the stars
he’ll make us a new universe
if it comes to that.”*

- Allen Ginsberg

The present thesis analyses the interactional landscape of a number of different systems under the new lens offered by the mindset introduced by Peter Politzer in the nineteen nineties. This lens can be holistically described as the anisotropic distribution of the electron density which occurs in a wide diversity of bonded atoms. This anisotropic distribution is related to, and is a consequence of, the covalent bonds formed by the atoms and affects and/or determines the non-covalent bonds the atoms give rise to.

Both computational and experimental approaches have been employed to investigate the attractive interactions directing and/or controlling recognition and self-assembly processes in systems wherein elements of groups 17, 16, 14, 11, and 8 are the electrophilic site. Some heuristic principles for designing and preparing cocrystals were identified moving from the stereoelectronic features affecting the σ -holes, π -holes, $V_{s,max}$, $V_{s,min}$, etc., (namely affecting the localization, surface, and electrostatic potential at the areas of depleted or excess electron density). These principles guided the investigations reported in this thesis. They allowed for the obtainment of some peculiar crystal architectures, e.g., the systems assembled under control of the halogen bond (HaB, chapter 2) wherein the fluoride anion functions as the electron donor. More important, they allowed for the successful obtainment of several and different systems wherein the electrophilic atom span over various groups of the periodic table so that their generality is confirmed.

The systems showing the presence of chalcogen bonds (ChBs) and tetrel bonds (TtBs) (chapters 3 and 4, respectively) proved the direct relevance of these interactions to compounds of biomedical and industrial importance. While this thesis does not discuss the direct impact of these interactions on functionally useful features of any system, the above-mentioned relevance may foreshadow a likely bright future for these interactions in applicative fields (e.g., medicinal and material chemistry).

It has been shown that the adopted mindset can be usefully employed for the design and rationalization of adducts formed by elements not only of the p block but also of the d block of the periodic table. The reported examples of systems wherein metals of the 8 group and 11 group function as electrophiles (coinage bond (CiB) and osme bond (OmB), chapter 5) testify the robustness of the approach and extend the set of elements having an interactional landscape consistent with it. The adopted mindset thus appears as a powerful tool providing a satisfactory and “periodic” model for many different interactions between bonded atoms.

7.1. Acknowledgments.

I am much honored to state that this work would not have been possible without the help of many great colleagues, scientists, and people. Prof. Resnati played a profound role in shaping my vision of chemistry and research as a whole. Importantly, while providing the necessary guidelines for me to move in a laboratory and in a work environment, he gave me room to perform the chemistry I like, the way I like it. Prof. Terraneo was a great teacher in crystallography, and to this day the person I refer to when encountering a problem involving the subject. Dr. Pizzi is a treasured laboratory partner, careful listener of my ravings about the subject at hand and a rare individual who shares my dedication for the research. His contribution to this work was inestimable.

At Politecnico di Milano I've met many colleagues that I dare to define my friends. I would like to thank in particular Mr. Marchetti, an admirable combination of an untiring worker, a sharp intellect, and an empathetic person. Perhaps unknowingly, Mss. Calabrese provided vital contributions to the quality of the laboratory environment of my work.

COVID-19 precluded me from moving abroad for a relevant period. Nevertheless, I've been able to work on different projects with many great scientists, that were not always explicitly mentioned in the thesis. I would like to thank Prof.s Bryce, Famulari, Frontera, Genoni, Murray, Politzer and Rissanen and, by extension, their collaborators. Their mindset and commitment have been instrumental for the development of this work.

My friends and family deserve credit for the development for this thesis, from simply providing much needed relief to giving me useful advices and guidance when I felt lost.

A special thanks goes to my parents, especially my mother, who relentlessly insisted for me to get back in academia. As stubborn as I was, I'm now adamant it was the best decision I have made.

These three years went by in a blink. Thank you.

7.2. List of Publications.

Anion... anion Interactions Involving σ -Holes of Perrhenate, Pertechnetate and Permanganate Anions.

A. Daolio, A. Pizzi, G. Terraneo, A. Frontera, G. Resnati
ChemPhysChem **2021**, *22*, 22, 2281-2285.

Molecular electrostatic potential and noncovalent interactions in derivatives of group 8 elements.

A. Daolio, A. Pizzi, M. Calabrese, G. Terraneo, S. Bordignon, A. Frontera, G. Resnati
Angew. Chem. Int. Ed. **2021**, *133*, 38, 20891-20895.

Chalcogen Bonds in Selenocysteine Seleninic Acid, a Functional GPx Constituent, and in Other Seleninic or Sulfinic Acid Derivatives.

A. Tripathi, A. Daolio, A. Pizzi, Z. Guo, D. R. Turner, A. Baggioli, A. Famulari, G. B. Deacon, G. Resnati, H. B. Singh
Chem, - Asian J. **2021**, *16*, 2351-2360.

Anion...Anion Coinage Bond: the Case of Tetrachloridoaurate.

A. Daolio, A. Pizzi, G. Terraneo, M. Ursini, A. Frontera, G. Resnati
Angew. Chem. Int. Ed., **2021**, *60*, 26, 14385-14389.

Tetrel and Pnictogen Bonds Complement Hydrogen and Halogen Bonds in Framing the Interactional Landscape of Barbituric Acids.

V. Kumar, P. Scilabra, P. Politzer, G. Terraneo, A. Daolio, F. Palacio, J. S. Murray, G. Resnati
Cryst. Growth Des. **2021**, *21*, 642-652.

Binding motif of ebselen in solution: chalcogen and hydrogen bonds team up.

A. Daolio, P. Scilabra, M.E. Di Pietro, C. Resnati, K. Rissanen, G. Resnati
New J. Chem. **2020**, *44*, 20697-20703.

The Relevance of Size Matching in Self-assembly: Impact on Regio-and Chemoselective Cocrystallizations.

J. X. Lin, A. Daolio, P. Scilabra, G. Terraneo, H. Li, G. Resnati, R. Cao
Chem. - Eur J. **2020**, *26*, 11701-11704.

C (sp³) atoms as tetrel bond donors: A crystallographic survey.

A. Daolio, P. Scilabra, G. Terraneo, G. Resnati
Coord. Chem. Rev. **2020**, *413*, 213265.

4,4'-Dipyridyl Dioxide-SbF₃ Cocrystal: Pnictogen Bond Prevails over Halogen and Hydrogen Bonds in Driving Self-Assembly.

P Scilabra, G Terraneo, A Daolio, A Baggioli, A Famulari, C Leroy, D. L. Bryce, G. Resnati
Cryst. Growth & Des. **2020**, *20*, 916-922.